

Magnetic properties of the kagome staircase mixed system $(\text{Co}_x\text{Ni}_{1-x})_3\text{V}_2\text{O}_8$

Dem Fachbereich Material- und Geowissenschaften
der Technischen Universität Darmstadt



zur Erlangung des akademischen Grades eines
Doktors der Naturwissenschaften (Dr. rer. nat.)
genehmigte Dissertation

vorgelegt von
Dipl. - Ing. Navid Qureshi
aus Raunheim

Referent:	Prof. Dr.-Ing. Dr. h.c. H. Fueß
Korreferent:	Prof. Dr. rer. nat. L. Alff
Tag der Einreichung:	11. August 2008
Tag der mündlichen Prüfung:	26. September 2008

Darmstadt, April 2009
D17

Diese Arbeit wurde in der Zeit von Oktober 2005 bis August 2008 am Institut für Materialwissenschaft der Technischen Universität Darmstadt unter der Leitung von Herrn Prof. Dr.-Ing. Dr. h.c. H. Fueß und Priv-Doz. Dr. rer. nat. Helmut Ehrenberg sowie am Institut Max von Laue-Paul Langevin in Grenoble unter der Leitung von Dr. T. C. Hansen und Prof. Dr. Juan Rodríguez-Carvajal durchgeführt. Finanziell wurde diese Arbeit unterstützt von der Deutschen Forschungsgemeinschaft im Rahmen des Schwerpunktprogramms 1178.

Danksagung

Ich möchte mich an dieser Stelle bei Herrn Prof. Dr.-Ing. Dr. h.c. Hartmut Fueß für die Vergabe der Doktorarbeit, die Betreuung und die Bereitstellung der dafür benötigten Arbeitsmittel bedanken. Sein Interesse an meiner Arbeit hat viel zu meiner Motivation beigetragen. Weiterhin bin ich sehr dankbar, dass ich aufgrund seiner Initiative weltweit Kontakte knüpfen, nette Kollegen kennenlernen und schöne Orte erkunden konnte.

Ich bedanke mich bei Herrn Prof. Dr. rer. nat. Lambert Alff für seine Bereitschaft zum Korreferent dieser Arbeit.

Ich danke Helmut Ehrenberg für seine stetige Diskussionsbereitschaft und hilfreiche fachliche Beratung.

Ich bedanke mich bei Thomas Hansen für die Betreuung und Unterstützung in allen Fragen während meiner Zeit am ILL.

Je remercie Juan Rodríguez-Carvajal pour sa patience pendant les nombreuses discussions qui m'ont été d'un grand bénéfice.

J'adresse des remerciements à tous les collègues de l'ILL qui ont contribué à la réussite de cette thèse, soit par leur support pendant les manips, soit par les nombreuses discussions. Je remercie en particulier Bachir Ouladdiaf, Eric Ressouche, Clemens Ritter, Anne Stunault et Mohamed Zbiri.

Je remercie Béatrice Gillon et Arsen Gukasov pour leur aide pendant mon séjour au Laboratoire Léon Brillouin.

I want to thank Prof. Jozef Kožíšek, Lucia Perašínová and Marek Fronc for their hospitality and support at the Slovak University of Technology.

Many thanks go to Yoshiharu Sakurai, Masayoshi Ito, Saeed Kamali and Ignace Jarrige for welcoming and helping me that much at SPring-8.

Der Deutschen Forschungsgemeinschaft danke ich für die finanzielle Unterstützung und Förderung dieser Arbeit.

El último agradecimiento, pero quizás el más importante, está dedicado a Lola Ruiz Martín que me ha ayudado y apoyado tanto sobre todo durante los últimos meses de este trabajo.

Magnetische Eigenschaften der Orthooxovanadate $(\text{Co}_x\text{Ni}_{1-x})_3\text{V}_2\text{O}_8$

Zusammenfassung

Die Orthooxovanadate der 3d Übergangsmetalle $\text{M}_3\text{V}_2\text{O}_8$, deren Kristallstruktur als *kagome staircase* bekannt ist, weisen gerade aufgrund dieser bemerkenswerten Struktur interessante magnetische Eigenschaften auf. Obwohl diese Verbindungen für $\text{M}=\text{Co}$, Ni , Mn , Cu isostrukturell zueinander sind, weichen sie in Bezug auf ihre magnetischen Phasenumwandlungen und Magnetstrukturen deutlich voneinander ab. Da die magnetischen Ionen auf den Eckpunkten von eckverknüpften Dreiecken liegen, spielt geometrische Frustration in diesem System eine große Rolle. Dies beschränkt sich nicht nur darauf, dass die antiferromagnetischen Strukturen verringerte geordnete magnetische Momente aufweisen, sondern anscheinend auch auf die ferromagnetische Struktur des $\text{Co}_3\text{V}_2\text{O}_8$, da sie mit 1.54 Bohrschen Magnetonen ein stark vermindertes Cobalt-Moment aufweist.

Im Rahmen dieser Arbeit wurde eben jene ferromagnetische Struktur im Detail untersucht, und es konnte gezeigt werden, dass das verhältnismäßig schwache magnetische Moment nicht Folge der Frustration ist, sondern auf die starke Hybridisierung zwischen Cobalt- und Sauerstofforbitalen zurückzuführen ist. Der ausgeprägte kovalente Charakter jenes Cobalt-Ions führt auch dazu, dass die Sauerstoffionen infolge des Ladungstransfers mit Anlegen eines externen Magnetfelds signifikant zur Magnetisierung beitragen.

Im zweiten Teil dieser Arbeit wurde die Mischreihe $(\text{Co}_x\text{Ni}_{1-x})_3\text{V}_2\text{O}_8$ systematisch untersucht. Es konnte ein detailliertes Phasendiagramm aufgestellt werden, in das die magnetischen Phasenumwandlungen in Abhängigkeit der Temperatur und der Zusammensetzung eingetragen wurden. Weiterhin konnte an einer ausgewählten Zusammensetzung von $x=0.5$ eine interessante Magnetstruktur beobachtet werden, die sich stark von denen der Endglieder unterscheidet.

Magnetic properties of the kagome staircase mixed system $(\text{Co}_x\text{Ni}_{1-x})_3\text{V}_2\text{O}_8$

Abstract

The orthooxovanadates of the 3d transition metals $\text{M}_3\text{V}_2\text{O}_8$, known as *kagome staircase* systems, reveal interesting magnetic properties due to their crystal structure. Although these compounds are isostructural for $\text{M}=\text{Co}, \text{Ni}, \text{Mn}, \text{Cu}$, they differ considerably with respect to their magnetic phase transitions and magnetic structures. As the magnetic ions are situated on corners of corner-sharing triangles, geometric frustration plays an important role in this system. This is not only confined to the fact, that the antiferromagnetic structures exhibit reduced magnetic moments, but apparently also to the ferromagnetic structure of $\text{Co}_3\text{V}_2\text{O}_8$, which exhibits a strongly reduced Co moment of 1.54 Bohr magnetons.

Within this work precisely this ferromagnetic structure has been investigated in detail and it could be shown that the relatively weak magnetic moment does not result from frustration, but is a consequence of the strong hybridization effects between the cobalt and oxygen orbitals. The pronounced covalent character of this Co ion leads to the fact that due to the charge transfer the oxygen ions significantly contribute to the bulk magnetization when applying an external magnetic field.

The second part of the presented work deals with the systematic investigation of the mixed system $(\text{Co}_x\text{Ni}_{1-x})_3\text{V}_2\text{O}_8$. A detailed magnetic phase diagram could be drawn, in which the temperature and composition dependent magnetic phase transitions have been pinpointed. Furthermore, an interesting magnetic structure of a chosen composition of $x=0.5$ has been observed, which differs considerably from those of the end members.

Contents

1. Introduction	1
1.1. Aims of the thesis work	3
2. Special methodology and theory	5
2.1. Polarized neutron diffraction	5
2.2. Magnetic Compton Scattering	8
2.2.1. Introduction to X-ray Compton Scattering	8
2.2.2. Basic formulae	8
2.2.3. Magnetic Compton Profile	11
2.2.4. Experimental set-up	12
2.3. Group theory	14
2.3.1. Definition of a group	14
2.3.2. Subgroups	15
2.3.3. Cosets and coset decomposition	16
2.3.4. Conjugate elements or classes	16
2.3.5. Representations of a group	17
2.3.6. Characters	19
2.3.6.1. Construction of character tables	21
2.3.7. Basis functions and projection operators	23
2.3.8. Application to the magnetic structures of $(\text{Co}_x\text{Ni}_{1-x})_3\text{V}_2\text{O}_8$	24
2.3.8.1. Space group Cmca and atomic positions	24
2.3.8.2. Propagation vectors	24
2.3.8.3. Irreducible matrix representations	25
2.3.8.4. Transformation-induced matrix representations and reduction	26
2.3.8.5. Deduction of the magnetic modes	31
2.4. Extinction	36
2.4.1. The Becker-Coppens model	38
2.4.2. The extinction model implemented in FullProf	44
2.5. Molecular orbitals and basis sets	46

3. Sample preparation and characterization	49
4. Results	51
4.1. $\text{Co}_3\text{V}_2\text{O}_8$	51
4.1.1. Nuclear structure within the paramagnetic phase	51
4.1.2. Nuclear structure in the ferromagnetic phase	56
4.1.3. Ab initio calculations using the GAMESS code	59
4.1.4. Magnetization density in real space	64
4.1.5. Spin density in momentum space	68
4.1.6. Correlated refinement in both spaces	74
4.2. $(\text{Co}_x\text{Ni}_{1-x})_3\text{V}_2\text{O}_8$	79
4.2.1. The dependence of \mathbf{k} on the composition parameter x	79
4.2.2. Magnetic composition-temperature phase diagram	85
4.3. $(\text{Co}_{0.5}\text{Ni}_{0.5})_3\text{V}_2\text{O}_8$	94
4.3.1. Nuclear structure	95
4.3.2. Magnetic phase transition temperature	97
4.3.3. Propagation vector	99
4.3.4. Magnetic structure	99
5. Summary	103
Appendices	111
A. Group theory	111
A.1. Derivations	111
A.1.1. The orthogonality theorem	111
A.1.2. Equality of characters for equivalent representations	113
A.1.3. Constancy of characters within classes	113
A.1.4. Second orthogonality theorem for classes	114
A.1.5. Sum of characters over representations	115
A.2. Calculations	117
A.2.1. Compatibility of symmetry elements with propagation vectors	117
A.2.2. Reduction of the permutation representation	118
A.2.3. Reduction of the axial vector representation	122
A.2.4. Reduction of some direct products	124
A.2.5. Deduction of the basis vectors	147
B. Ab initio calculations	159
B.1. Orbital exponents and contraction parameters	159

B.2. Calculation output	160
B.2.1. Co_eO_6 cluster	161
B.2.2. Co_sO_6 cluster	164
Bibliography	169

1. Introduction

The transition metal orthooxovanadates $M_3V_2O_8$ (MVO) ($M = Ni, Co, Cu, Mn$) have recently attracted the interest of the scientific community due to their complex magnetic and ferroelectric properties. Especially the compounds $Co_3V_2O_8$ (CVO) and $Ni_3V_2O_8$ (NVO) have been in the focus of international research groups. The crystal structure of these isostructural compounds is known for almost 40 years and has first been published by Fuess et al. in 1970 [1]¹ and three years later confirmed by Sauerbrei et al. [2]. The MVO compounds crystallize in the orthorhombic space group $Cmca$ and are characterized by edge-sharing MO_6 octahedra separated by VO_4 tetrahedra (Fig. 1.1). This geometry is interesting with respect to the magnetic properties as the magnetic ions form buckled planes of corner-sharing isosceles triangles (Fig. 1.2) representing an anisotropic variation of the ideal kagome net [3]. Within these buckled planes, the kagome staircases, M1 ions on crystallographic (4a) sites, denoted as cross-tie (c) ions in the literature, link the linear chains of M2 or so called spine (s) ions on (8e) sites, which are situated above and below the M1 plane.

If a crystal lattice imposes a triangular arrangement of magnetic ions, an incompatibility of their antiferromagnetic nearest neighbour interactions occurs, which is known as geometrical frustration and has been subject of recent intensive experimental and theoretical work. Highly frustrated systems like the spin- $\frac{1}{2}$ two-dimensional kagome net possess an infinitely large number of classical ground states and remain disordered spin liquids down to 0 K [4, 5]. Due to the zig-zag geometry of the kagome staircases, two inequivalent magnetic sites and slightly different distances between them, the exchange interactions between different nearest neighbours become anisotropic as well as supplementary important interaction pathways occur, which relieve the frustration and lead to long-range ordered magnetic structures and interesting magnetic phase diagrams. The magnetic coupling is mainly effectuated via a nearly 90° superexchange pathway between M_c - M_s and M_s - M_s nearest neighbours, but further more complex intra- and interlayer coupling pathways exist, which play an important role for the temperature dependence of the magnetic properties [6].

¹Reference [1] uses a different notation for labeling the axes; space group $Abam$ was used, so the a and c axes are swapped.

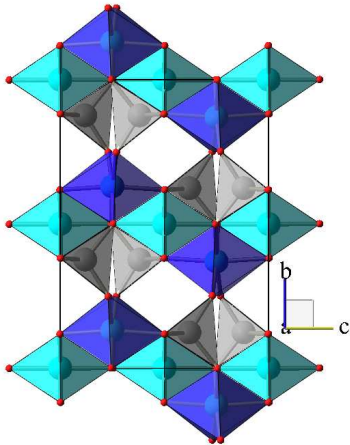


Figure 1.1.: Visualization of the buckled planes of edge sharing MO_6 octahedra (M_cO_6 light blue, M_sO_6 dark blue) isolated by non-magnetic VO_4 tetrahedra (grey).

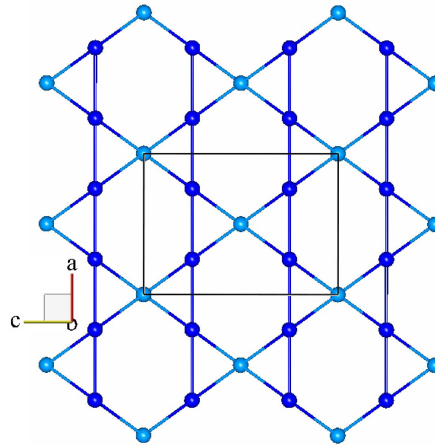


Figure 1.2.: A single kagome staircase viewed along the b axis only showing the magnetic ions on both crystallographic sites (M_c light blue, M_s dark blue) revealing the corner-sharing isosceles triangles.

First results concerning the magnetic structure have been published before 1982 [1, 7], but despite this interesting crystal structure it was only in 2002 that Rogado et al. continued to focus on the magnetic properties of these materials [8, 9]. Magnetization measurements showed that, despite their isostructurality, these compounds exhibit quite different sequences of magnetic phase transitions [6, 10–14]. Thus, $\text{Cu}_3\text{V}_2\text{O}_8$ undergoes one magnetic phase transition [9], but much more complex behaviour can be observed for NVO and CVO with a sequence of four [15] and five [6] magnetic phase transitions in absence of an applied external magnetic field. Field dependent studies on single-crystals [11–13, 15, 16] revealed highly anisotropic magnetic phase diagrams. It has to be stressed once again that although these compounds are isostructural, the magnetic phase diagrams differ considerably depending on the spin state of the magnetic ion reflecting the sensitive balance between the many competitive magnetic interactions, which are possible in the kagome staircase lattice. Recent work on $\text{Mn}_3\text{V}_2\text{O}_8$ [17] revealed two magnetic phase transitions at zero field and a rich magnetic phase diagram with seven different phases.

Partially substituting one type of magnetic ions with another, again leads to new magnetic properties, which differ from those of either end member. So it could be shown in [11] for powder samples of the mixed system $(\text{Co}_x\text{Ni}_{1-x})_3\text{V}_2\text{O}_8$ (CNVO) with $x=0.25$,

0.5 and 0.75 that only one magnetic phase transition occurs, which was revealed by magnetization measurements. Not less interesting is the fact that the magnetic structures differ substantially despite their isostructurality. CVO reveals a ferromagnetic ground state with intermediate antiferromagnetic phases modulated by a propagation vector with a b^* component [6, 13, 18], while NVO exhibits four different antiferromagnetic structures modulated along a^* [15, 19].

Further studies on the magnetic properties of CVO by implanted muons [20] and inelastic neutron scattering [21] have been reported, while considerable work has been done concerning the multiferroic properties of NVO [22–25].

1.1. Aims of the thesis work

One part of this thesis work is motivated by the discovery made in [11] concerning the differing magnetic properties of the mixed system CNVO. In addition to the magnetization experiments, neutron diffraction data have already been collected on a $(\text{Co}_{0.5}\text{Ni}_{0.5})_3\text{V}_2\text{O}_8$ powder sample. An a^* modulation has been deduced, but the exact modulation and magnetic structure have not been understood. In this matter further neutron powder and single crystal diffraction experiments will be performed.

The existence of only one magnetic phase transition has been deduced in [11] by magnetization measurements and neutron powder diffractograms at three different temperatures. This will be completed by heat capacity measurements, which will be done in cooperation with Dr. Thomas Wolf from Research Center Karlsruhe (Institute of Solid State Physics).

It has already been observed in [11] that the Néel temperature varies as a function of composition. This observation will be extended to the whole range of the mixed system CNVO. In this concern, more powder samples with shorter steps in the composition parameter x will be prepared and investigated. Heat capacity experiments on the whole range using single crystals will again be carried out with Dr. Thomas Wolf.

In order to elucidate the mechanism of the superexchange coupling in the kagome staircase compounds, magnetization density maps will be deduced by measuring precise magnetic structure factors using a single crystal of the pure Co compound. Due to its ferromagnetic ground state it is suited to be investigated by the polarized neutron technique. The accuracy of this method will permit to draw a detailed magnetization density map as a two-dimensional projection. Directly from such a map information about the superexchange and possibly supersuperexchange pathways, which would be manifest by magnetization

1. Introduction

on the V and O sites, could be deduced. The Co-O-Co superexchange coupling mechanism will be investigated by performing an aspheric refinement on the observed magnetic structure factors, which should yield the orbital occupations of the t_g and e_{2g} states.

A second approach to the magnetization density will be attempted by the Magnetic Compton Scattering method. This method, which is sensitive to only the spin of the magnetic moment, yields the spin density in momentum space as a one-dimensional projection on the scattering vector. By measuring different directions the two-dimensional momentum spin density will be reconstructed and correlated with the magnetization density obtained by the polarized neutron method.

Additionally, ab initio calculations will be performed, which will be done in cooperation with Dr. Mohamed Zbiri from the Institut Laue-Langevin. The calculation will furnish system-specific electron wave functions for the different Co3d orbitals. As the square of a wave function, which is occupied by an unpaired electron, represents the magnetization density, this is an appropriate way to compare the observations with theoretical predictions.

2. Special methodology and theory

2.1. Polarized neutron diffraction

The basis of classical polarized neutron diffraction (PND) is the determination of precise magnetic structure factors, which can be used to map the distribution of unpaired spins in magnetic materials. The fact that the strength of the interaction between neutron and condensed matter is dependent on the orientation of the neutron spin is the principle idea of polarizing neutron beams. The nuclear interaction is only neutron spin dependent, if the scattering nucleus itself has a spin and if the spins of the nuclei are ordered, which only applies to extreme conditions like very low temperatures in the mK region or very high magnetic fields. Therefore, nuclear diffraction can be considered as spin independent. In contrast, electron spins are much more easily ordered leading to an important neutron spin dependence of the magnetic scattering.

The scattering cross-section of a spin polarized neutron beam contains an interference term between the nuclear and the magnetic scattering, which changes sign when the neutron spin direction is flipped. This interference already implies an important criterion for the investigated materials: the nuclear and magnetic scattering have to contribute to the same Bragg reflection, which is the case for ferromagnets and ferrimagnets, where the nuclear and magnetic scattering densities have the same periodicity. But also the investigation of paramagnetic materials is possible as soon as a magnetization has been induced by an external magnetic field. The observed intensity of the diffracted neutrons with spin-up or spin-down for a given Bragg reflection is proportional to the square of the sum or difference, respectively, of its nuclear structure factor (F_N) and magnetic interaction vector (\mathbf{Q}_M) (Eq. 2.1)

$$I^\pm \sim (F_N \pm |\mathbf{Q}_M|)^2 = F_N^2 \pm 2p^\pm F_N Q_M^z + Q_M^2, \quad (2.1)$$

where $2p^\pm F_N Q_M^z$ is the aforementioned interference term with the polarization p^\pm of the spin-up and spin-down beam, respectively. The magnetic interaction vector \mathbf{Q}_M (Eq. 2.2) expresses the component of the magnetic structure factor, which is perpendicular to the scattering vector \mathbf{k} and therefore is effective in magnetic scattering.

$$\mathbf{Q}_M = \frac{\mathbf{k}}{|\mathbf{k}|} \times \mathbf{F}_M \times \frac{\mathbf{k}}{|\mathbf{k}|} \quad (2.2)$$

\mathbf{Q}_M^z , the component of \mathbf{Q}_M along the magnetization direction, is the quantity which is effective with respect to the neutron polarization. The geometry of the introduced vectors can be seen in Figure 2.1.

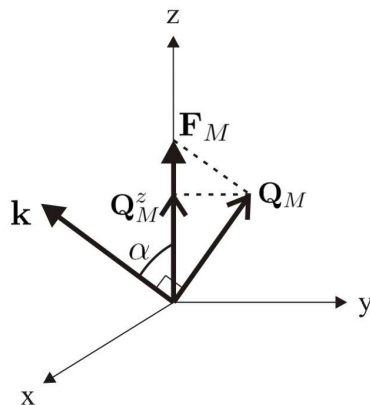


Figure 2.1.: Geometrical definition of the vectors \mathbf{F}_M , \mathbf{Q}_M , \mathbf{Q}_M^z , \mathbf{k} and the angle α .

By measuring the *flipping ratio* R , which is the ratio between the spin-up and spin-down intensity, one is able to express the magnetic structure factor as a fraction of the nuclear one (Eq. 2.3) with the help of the geometrical relations $Q_M = qF_M$ and $Q_M^z = qQ_M = q^2F_M$ ($q = \sin \alpha$) according to Fig. 2.1.

$$R = \frac{I^+}{I^-} = \frac{F_N^2 + 2p^+ F_N F_M q^2 + F_M^2 q^2}{F_N^2 - 2p^- F_N F_M q^2 + F_M^2 q^2} = \frac{1 + 2p^+ q^2 \gamma + q^2 \gamma^2}{1 - 2p^- q^2 \gamma + q^2 \gamma^2}, \text{ with } \gamma = \frac{F_M}{F_N} \quad (2.3)$$

As the magnetic structure factors are obtained by a simple ratio measurement, many of the systematic errors which have to be taken into account for absolute measurements cancel out. Another great advantage of this method is the sensitivity for small magnetic moments, which can be emphasized by a simple example. Considering an in-plane reflection with $q=1$ and a magnetic structure factor which is a tenth of the value of the nuclear structure factor i.e. $\gamma = 0.1$, the observed intensity using unpolarized neutrons would be

$$I \sim F_N^2 + F_M^2 = F_N^2 + 0.01F_N^2 = 1.01F_N^2.$$

In contrast, for polarized neutrons the intensity of e.g. the spin-up neutrons is much higher due to the interference term:

$$I^+ \sim (F_N + F_M)^2 = F_N^2 + 0.2F_N^2 + 0.01F_N^2 = 1.21F_N^2$$

This fact also allows a more precise measurement of weak magnetic reflections in higher $\sin \theta/\lambda$ regions.

A simple schematic arrangement of a polarized neutron diffractometer is depicted in Fig. 2.2. Neutrons from a reactor source are monochromated and polarized by a mag-

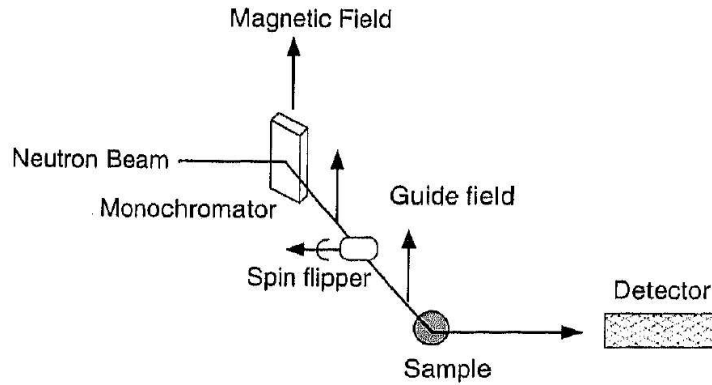


Figure 2.2.: Simple schematic arrangement of a polarized neutron diffractometer [26].

netized crystal. Therefore, the monochromating crystal needs to possess a Bragg reflection, for which the nuclear structure factor is equal to the magnetic interaction vector. In this case the intensity of neutrons whose spins are polarized parallel to \mathbf{Q}_M will be proportional to $2F_N$, while the intensity of the ones with antiparallel spins will be zero. The monochromated and polarized beam passes through magnetic guide fields in order to avoid depolarization by stray fields. A *spin flipper* is inserted between the monochromator and the sample, which, when activated, reverses the direction of the neutron spins. The sample is mounted on a two-circle diffractometer, which offers the possibility of applying a vertical magnetic field. The measurement of flipping ratios is performed by positioning the sample in a way that it diffracts the maximum intensity of a given Bragg reflection. By turning the spin flipper on and off with a frequency of about 1 Hz fluctuations of the neutron beam flux are compensated and the ratio between the intensities can be built after correcting them for the background.

Further information can be found in [27] and [28].

2.2. Magnetic Compton Scattering

2.2.1. Introduction to X-ray Compton Scattering

The well known Compton effect is an inelastic scattering process of a photon with an electron and obviously shows the partial-like behaviour of radiation (Fig. 2.3). The electron taking part in the collision may gain or lose momentum after the transfer, which results in a Compton shifted line in the spectrum. This line is Doppler-broadened along the direction of momentum transfer, which is the scattering vector, due to the initial motion of the electron. The observed quantity in a Compton scattering experiment is therefore a one-dimensional projection of the momentum component along the scattering vector. Direct three-dimensional information is only accessible by detecting the recoil electron as well as the scattered photon in a complicated experiment, which is still in the development stage. An indirect method, which allows to gain three-dimensional information is the reconstruction of many one-dimensional projections obtained by different crystal orientations with respect to the incident beam. As Compton scattering is an incoherent interaction, the perfection of the single crystal is not critical, i.e. extinction effects, which plague single crystal diffraction experiments, do not have to be considered.

Compton profile studies involve measuring changes in photon energy implying the need of an incident beam with well-defined energy. Because of the weakness of the cross-section, high flux is necessary. Furthermore, higher energies than the ones supplied by X-ray tubes are necessary to overcome intensity losses due to photoelectrical absorption, coherent diffraction and incoherent scattering. All these requirements are perfectly fulfilled by synchrotron radiation. An absolute imperative for synchrotron radiation, however, is the need of circularly polarized radiation in order to investigate spin densities, which will be described in detail in Sec. 2.2.3, when dealing with Magnetic Compton Scattering (MCS).

For further information the interested reader is referred to [29] and [30].

2.2.2. Basic formulae

The basic formula for the Compton shift for a stationary target electron, which can be derived by the application of conservation of momentum and energy, is given in Eq. 2.4

$$\Delta\lambda = \frac{2h}{mc} \sin^2\left(\frac{\phi}{2}\right) = \frac{h}{mc}(1 - \cos\phi), \quad (2.4)$$

where $\Delta\lambda$ is the wavelength shift of the scattered photon and ϕ is the scattering angle.

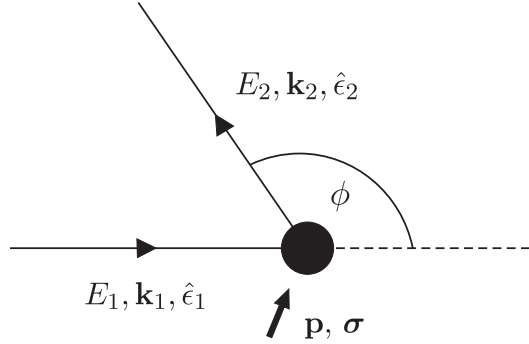


Figure 2.3.: Schematic diagram of the Compton scattering interaction. The indices 1 and 2 refer to the photon properties (E energy, \mathbf{k} wave vector, $\hat{\epsilon}$ polarization) before and after the scattering process, respectively. \mathbf{p} and $\boldsymbol{\sigma}$ denote the electron's momentum and spin.

The symbol ϕ has been chosen instead of θ to clearly distinguish between the Compton scattering angle and the Bragg angle. In situations where incoherent and coherent scattering may occur $\phi = 2\theta$. The remaining symbols have their usual meaning. For the purposes of X-ray Compton scattering it is more useful to write Eq. 2.4 in terms of the energies of the incoming and scattered photons, E_1 and E_2 ,

$$E_2 = \frac{E_1}{1 + (E_1/mc^2)(1 - \cos \phi)}. \quad (2.5)$$

From this equation one can understand the powerful energy loss mechanism of the Compton scattering process as for backscattering ($\phi = 180^\circ$) the energy of the scattered photon beam never exceeds $\frac{1}{2}mc^2$ whatever the incident beam energy.

According to Fig. 2.3 the photon energy shift, i.e. the transferred energy to the electron with initial momentum \mathbf{p} , can be written as

$$\begin{aligned} E_2 - E_1 = \hbar\omega &= \frac{1}{2m} [\mathbf{p} + \hbar(\mathbf{k}_1 - \mathbf{k}_2)]^2 - \frac{|\mathbf{p}|^2}{2m} \\ &= \frac{\hbar^2 \mathbf{q}^2}{2m} + \frac{\hbar \mathbf{q} \cdot \mathbf{p}}{m} \end{aligned} \quad (2.6)$$

by using the energy and momentum conservation. The first term is simply the fixed Compton shift and the second term is a Doppler shift that depends on the component of the electron momentum along the direction of momentum transfer, i.e. the scattering vector \mathbf{q} . If this direction shall be referred to as the z -axis, the *Compton profile*, $J(p_z)$, can be

defined as

$$J(p_z) = \int \int \rho(p_x, p_y, p_z) dp_x dp_y, \quad (2.7)$$

which is a one-dimensional projection of the probability distribution of the electron momenta onto the z -axis, i.e. \mathbf{q} . The probability function $\rho(\mathbf{p})$ can be normalized by the requirement that

$$\int J(p_z) dp_z = \int \rho(\mathbf{p}) d\mathbf{p} = Z, \quad (2.8)$$

where Z is the number of electrons per formula unit. Now $\rho(\mathbf{p})$ is a probability density just like $\rho(\mathbf{r})$, so the Fourier transform of the first can be defined as

$$B(\mathbf{r}) = \int \rho(\mathbf{p}) \exp(i\mathbf{p} \cdot \mathbf{r}/\hbar) d\mathbf{p}, \quad (2.9)$$

which is called the reciprocal form factor [31, 32] and is the counterpart of the familiar X-ray form factor. Similarly, this quantity is to be deduced by a Compton scattering experiment. The accessibility of this three-dimensional function becomes clear by combining Eqs. 2.7 and 2.9 to

$$B(z) = \int J(p_z) \exp(ip_z z/\hbar) dp_z. \quad (2.10)$$

Eq. 2.10 states that the Fourier transform of a Compton profile represents a line through the three-dimensional function $B(\mathbf{r})$, i.e. this function can be reconstructed by measuring a large number of directional Compton profiles. This procedure is called the direct Fourier-transform method and was reported to be one of the most useful to reconstruct momentum densities [33, 34]. Due to the finite number of values of Compton profiles an approximate $B(\mathbf{r})$ is obtained by interpolation at fine mesh points in position space. Finally, the momentum space density can be deduced by the inverse Fourier transform of $B(\mathbf{r})$:

$$\rho(\mathbf{p}) = (1/2\pi\hbar)^3 \int B(\mathbf{r}) \exp(-i\mathbf{p} \cdot \mathbf{r}/\hbar) d\mathbf{r} \quad (2.11)$$

A fundamental concept of Compton scattering is the so called *impulse approximation*, which requires that the transferred energy $\hbar\omega$ is large compared with characteristic energies $\hbar\omega_c$ of the system [35]. The essence of the impulse approximation is that the scattering

process is assumed to be so fast that the scattering atom has no time to rearrange itself. As a consequence the transferred energy and momentum are so large that the recoil electron can be considered as free. Within the impulse approximation the double differential scattering cross-section (DDSCS) simplifies to

$$\frac{d^2\sigma}{d\Omega d\omega_2} = \left(\frac{d\sigma}{d\Omega}\right)_{Th} \frac{m}{\hbar q} J(p_z), \quad (2.12)$$

where ω_2 is the scattered photon frequency, Ω is the scattered solid angle and $\left(\frac{d\sigma}{d\Omega}\right)_{Th}$ is the Thomson scattering cross-section arising from charge scattering.

2.2.3. Magnetic Compton Profile

In the case of MCS the magnetic field associated with the incident electromagnetic wave interacts with the magnetic moment of the electron, which leads to a magnetic contribution to the charge scattering [35, 36]. The DDSCS is therefore extended by a magnetic cross-section term (Eq. 2.13), which interferes with the charge cross-section term and stems from only the spin part of the magnetic moment as the orbital part cancels out.

$$\frac{d^2\sigma}{d\Omega d\omega_2} \propto |A(\hat{\epsilon}_1, \hat{\epsilon}_2)|^2 J(p_z) + 2i\{A^*(\hat{\epsilon}_1, \hat{\epsilon}_2)B(\hat{\epsilon}_1, \hat{\epsilon}_2, \mathbf{k}_1, \mathbf{k}_2, \boldsymbol{\sigma})\} J_{mag}(p_z) \quad (2.13)$$

A and B stand for the amplitudes of charge and magnetic scattering, respectively, whose squares correspond to their differential cross-section. The purely magnetic scattering amplitude is about a factor of $(\hbar\omega/mc^2)$ smaller than the charge scattering amplitude, i.e. the detected intensity of the purely magnetic scattering will be of at least four orders smaller when using photons of 10 keV (additionally, the ratio of unpaired to total electron number and the size of the magnetic moment have to be accounted for). The imaginary part of the interference term denotes the different polarization behaviour of the charge and magnetic scattering. Because of the factor i the magnetic contribution to the Compton scattering will only be found experimentally if the polarization factors connected with the magnetic scattering amplitude are complex or if the structure is non-centrosymmetric. Complex polarization factors will occur, if the incident photon beam is circularly polarized.

A further important term in the cross-section of magnetic scattering is the spin-direction with respect to the scattering geometry, which is

$$\frac{d^2\sigma_{mag}}{d\Omega d\omega_2} \propto \boldsymbol{\sigma} \cdot (\mathbf{k}_1 \cos \phi + \mathbf{k}_2). \quad (2.14)$$

For a backscattering geometry this means that the magnetic signal will be maximal, if the sample is magnetized along the beam direction. The fact that the interference term is proportional to the momentum density of unpaired-spin electrons $[\rho_{\uparrow}(\mathbf{p}) - \rho_{\downarrow}(\mathbf{p})]$ is exploited in order to obtain a difference in the DDSCS on reversing the direction of the sample magnetization, which only reverses the sign of the interference term. In doing so, the Compton profiles of the respective sample magnetization states are subtracted from each other yielding the Magnetic Compton Profile (MCP), which is defined as

$$J_{mag}(p_z) = \int \int |\chi_{\uparrow}(\mathbf{p})|^2 - |\chi_{\downarrow}(\mathbf{p})|^2 = \int \int \rho_{mag}(\mathbf{p}) dp_x dp_y \quad (2.15)$$

with $\chi_{\uparrow(\downarrow)}(\mathbf{p})$ denoting the momentum wave function of an occupied majority (minority) spin state. Similar to the charge Compton profile the MCP is normalized to the spin moment per formula unit:

$$\int J_{mag}(p_z) dp_z = \int \rho_{mag}(\mathbf{p}) d\mathbf{p} = \mu_S \quad (2.16)$$

The relative contribution of the MCP to the total Compton profile is expressed by the *magnetic effect*

$$M_0 = \frac{I^+ - I^-}{I^+ + I^-} \cdot 100\%, \quad (2.17)$$

where I^+ and I^- denote the intensity of the total Compton scattering with the magnetization of the sample being parallel and antiparallel, respectively, to the scattering vector.

2.2.4. Experimental set-up

Figure 2.4 shows the experimental set-up for the determination of magnetic Compton profiles. An insertion device called Elliptic Multipole Wiggler (EMPW) (a) is placed in a straight section of the electron orbit between two bending magnets. An EMPW consists of a well defined arrangement of periodic permanent magnets creating horizontal and vertical magnetic fields. The resulting magnetic field on the beam axis causes the electrons to follow an elliptic trajectory, which tangentially emit elliptically polarized radiation. The doubly bent monochromator (b) selects a specified photon energy and focuses the beam onto the sample (d), which is mounted between the poles of a C-shaped electromagnet (e) and is magnetized along the incident beam direction in order to maximize the scattering cross-section. By reversing the direction of the electromagnet's current the reversal of the

sample magnetization is effected. In order to reduce the background due to air scattering, the sample is held inside vacuum, while an ion chamber (c) monitors the beam intensity. A detector (f) usually placed at a scattering angle of almost 180° consists of several elements circularly arranged around the diffracted beam. The experimental procedure consists

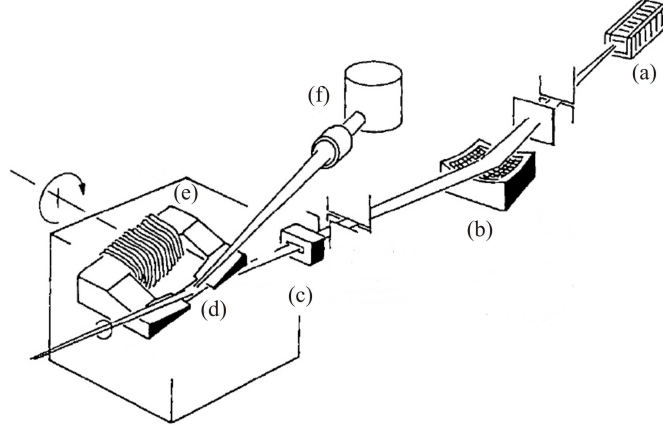


Figure 2.4.: Schematic diagram of a magnetic Compton profile measurement [29]. (a) The insertion device (EMPW), (b) doubly bent focusing monochromator, (c) ion chamber, (d) sample, (e) C-shaped electromagnet, (f) multi-element detector.

in recording the Compton profiles, i.e. to analyze the energy of the diffracted photons, measured with the sample magnetization parallel and antiparallel to the beam direction. The difference between these profiles yields one directional magnetic Compton profile. For reconstructing the two-dimensional spin momentum density in a desired crystallographic plane several directional magnetic Compton profiles have to be measured by rotating the sample about a vertical axis. Beam decay and fluctuations are accounted for by switching the magnetization in short intervals (few seconds) with a repetition of the cycle such as $[+ - - +]$ and monitoring the diffracted photon intensity by detecting a fluorescence and/or elastic peak from an element in the sample. It must be ensured that the sample does not move when switching the polarization of the magnet, so that the photons impinge on exactly the same position.

2.3. Group theory

Physical systems like e.g. crystal and magnetic structures are provided with a certain symmetry, which needs to be reflected correctly in a mathematical way. In this regard group theory has become a central mathematical tool for dealing with symmetry, and its applications in physics have led to rich and fruitful consequences. In connection to solving magnetic structures, group theory or representation analysis is used to obtain magnetic configurations that are symmetry compatible rather than using the trial-and-error method, which can be difficult and misleading especially for complex magnetic structures with a large number of magnetic moments in the primitive cell.

The content of this chapter will be elucidated by using the space group $Cmca$ as an example in every subsection as it is the space group in which the $(Co_xNi_{1-x})_3V_2O_8$ compounds crystallize in. For a complete description of group theory and its application to magnetic structures see [37] and [38].

2.3.1. Definition of a group

A *group* G is a set of distinct *elements* g_1, g_2, \dots, g_n , which are the symmetry operators in the case of space groups. Any two elements g_i and g_j combined by an operation called the group multiplication (\circ) should satisfy the following four axioms:

- The set G is closed under multiplication: For any two elements g_i and g_j of G , their unique product $g_j \circ g_i$ also belongs to G .

- The associative law holds:

$$g_k \circ (g_j \circ g_i) = (g_k \circ g_j) \circ g_i.$$

- There exists in G an element E which satisfies

$$E \circ g = g \circ E = g$$

for any element $g \in G$. Such an element E is called the *identity element*.

- For any element $g \in G$, there exists an element g^{-1} which satisfies

$$g^{-1} \circ g = g \circ g^{-1} = E,$$

where g^{-1} is the *inverse element* of g .

Groups containing an infinite number of elements are called *infinite*, while *finite groups* have a finite number of elements, where the total number of elements corresponds the *order* of the group.

The commutative law does not necessarily hold, but:

- If any two elements g_i and g_j of a given group G commute, i.e., if

$$g_j \circ g_i = g_i \circ g_j$$

holds, then such a group G is said to be *Abelian*.

The space group Cmca contains eight symmetry operators for the $(000)^+$ set [39], hence $G = \{E, 2_{1,z}, 2_{1,y}, 2_x, \bar{1}, b_{xy}, c_{xz}, m_{yz}\}$. The symmetry operators correspond to the identity element, a two-fold screw axis along z , a two-fold screw axis along y , a two-fold rotational axis along x , an inversion center, a glide plane perpendicular to z with a translation along b , a glide plane perpendicular to y with a translation along c and a mirror plane perpendicular to x . The existence of the identity is trivial and the inverse element to any element is the element itself, because $g_i^2 = E$. The fulfillment of the associative and commutative can be deduced from the *multiplication table* (Tab. 2.1).

Table 2.1.: Multiplication table of space group Cmca.

	E	$2_{1,z}$	$2_{1,y}$	2_x	$\bar{1}$	b_{xy}	c_{xz}	m_{yz}
E	E	$2_{1,z}$	$2_{1,y}$	2_x	$\bar{1}$	b_{xy}	c_{xz}	m_{yz}
$2_{1,z}$	$2_{1,z}$	E	2_x	$2_{1,y}$	b_{xy}	$\bar{1}$	m_{yz}	c_{xz}
$2_{1,y}$	$2_{1,y}$	2_x	E	$2_{1,z}$	c_{xz}	m_{yz}	$\bar{1}$	b_{xy}
2_x	2_x	$2_{1,y}$	$2_{1,z}$	E	m_{yz}	c_{xz}	b_{xy}	$\bar{1}$
$\bar{1}$	$\bar{1}$	b_{xy}	c_{xz}	m_{yz}	E	$2_{1,z}$	$2_{1,y}$	2_x
b_{xy}	b_{xy}	$\bar{1}$	m_{yz}	c_{xz}	$2_{1,z}$	E	2_x	$2_{1,y}$
c_{xz}	c_{xz}	m_{yz}	$\bar{1}$	b_{xy}	$2_{1,y}$	2_x	E	$2_{1,z}$
m_{yz}	m_{yz}	c_{xz}	b_{xy}	$\bar{1}$	2_x	$2_{1,y}$	$2_{1,z}$	E

The multiplication table of space group Cmca is diagonally symmetric, which directly shows that it is an Abelian group.

2.3.2. Subgroups

H is a *subgroup* of G , if it is a group itself under the four axioms mentioned in the previous section and if all elements h_i are elements of G . Both the single element $\{E\}$ and the group G itself are trivial subgroups of G . All other subgroups are called *proper subgroups*. The space group Cmca has the following 14 proper subgroups:

$$\{E, 2_{1,z}\}, \{E, 2_{1,y}\}, \{E, 2_x\}, \{E, \bar{1}\}, \{E, b_{xy}\}, \{E, c_{xz}\}, \{E, m_{yz}\},$$

$$\{E, 2_{1,z}, 2_{1,y}, 2_x\}, \{E, 2_{1,z}, \bar{1}, b_{xy}\}, \{E, 2_{1,z}, c_{xz}, m_{yz}\},$$

$$\{E, 2_{1,y}, \bar{1}, c_{xz}\}, \{E, 2_{1,y}, b_{xy}, m_{yz}\}, \{E, 2_x, \bar{1}, m_{yz}\}, \{E, 2_x, b_{xy}, c_{xz}\}.$$

2.3.3. Cosets and coset decomposition

From every set of elements one can obtain a *coset* by multiplying it by a scalar or an element not in the specific set. E.g., if the elements of the subgroup $H = \{1, 2_{1,z}\}$ are multiplied by $2_{1,y}$ on the right side, one obtains

$$H2_{1,y} = \{1, 2_{1,z}\}2_{1,y} = \{2_{1,y}, 2_x\},$$

which is the *right coset* of H (the group multiplication symbol is omitted from this section onwards). Similarly, the elements of H can be multiplied on the right side by $\bar{1}$ and c_{xz} , which yields the right cosets $\{\bar{1}, b_{xy}\}$ and $\{c_{xz}, m_{yz}\}$. One can see that all elements of space group Cmca can be generated by right cosets, hence there exists a *right coset decomposition* of Cmca with respect to the subgroup H :

$$\text{Cmca} = H + H2_{1,y} + H\bar{1} + Hc_{xz}, \text{ with } H = \{1, 2_{1,z}\}.$$

As Cmca is an Abelian group the *left coset decomposition* is equivalent.

2.3.4. Conjugate elements or classes

Group elements, which are *conjugate* to each other can be classified into *classes*. An element b is conjugate to a if there is a group element g so that

$$b = gag^{-1}. \tag{2.18}$$

With the help of the multiplication table (Tab. 2.1) one can evaluate Eq. 2.18 for every combination of elements a and g , which is given in Tab. 2.2.

As every line consists of exactly one element, there exist no conjugate elements in space group Cmca, i.e. every single element builds a class by itself resulting in eight classes. As a consequence every subgroup H of Cmca is composed by classes, which is a characteristic of *invariant* subgroups, because it satisfies the relation

$$gHg^{-1} = H \tag{2.19}$$

for all elements $g \in \text{Cmca}$.

Table 2.2.: Calculation of Eq. 2.18.

	E	2 _{1,z}	2 _{1,y}	2 _x	$\bar{1}$	b _{xy}	c _{xz}	m _{yz}
E	E	E	E	E	E	E	E	E
2 _{1,z}	2 _{1,z}	2 _{1,z}	2 _{1,z}	2 _{1,z}	2 _{1,z}	2 _{1,z}	2 _{1,z}	2 _{1,z}
2 _{1,y}	2 _{1,y}	2 _{1,y}	2 _{1,y}	2 _{1,y}	2 _{1,y}	2 _{1,y}	2 _{1,y}	2 _{1,y}
2 _x	2 _x	2 _x	2 _x	2 _x	2 _x	2 _x	2 _x	2 _x
$\bar{1}$	$\bar{1}$	$\bar{1}$	$\bar{1}$	$\bar{1}$	$\bar{1}$	$\bar{1}$	$\bar{1}$	$\bar{1}$
b _{xy}	b _{xy}	b _{xy}	b _{xy}	b _{xy}	b _{xy}	b _{xy}	b _{xy}	b _{xy}
c _{xz}	c _{xz}	c _{xz}	c _{xz}	c _{xz}	c _{xz}	c _{xz}	c _{xz}	c _{xz}
m _{yz}	m _{yz}	m _{yz}	m _{yz}	m _{yz}	m _{yz}	m _{yz}	m _{yz}	m _{yz}

2.3.5. Representations of a group

Group G shall be a finite group of order n_G consisting of the elements $g_1 (= E), g_2, \dots, g_n$ and $\Gamma(g_i)$ are square matrices associated with each group element g_i . If the matrices satisfy the homomorphism rule

$$\Gamma(g_j)\Gamma(g_i) = \Gamma(g_k) \quad (2.20)$$

for the corresponding relation of the group elements

$$g_j g_i = g_k, \quad (2.21)$$

then the set of matrices $\Gamma(g_1), \Gamma(g_2), \dots, \Gamma(g_n)$ is called a *representation* of the group G . To every Γ there exists an Ω with

$$\Omega(g) = \mathbf{P}^{-1}\Gamma(g)\mathbf{P}, \quad (2.22)$$

where \mathbf{P} is a permutation matrix, then Γ and Ω are said to be equivalent. The individual matrices are called representation matrices and the size of the matrices is the *dimension* d of the representation, which can also be expressed as

$$d = \text{Tr}[\Gamma(E)] = \sum_i \Gamma_{i,i}(E). \quad (2.23)$$

From two representations Γ^1 and Γ^2 of group G one can construct a representation of

larger dimension, which results from the direct sum of Γ^1 and Γ^2

$$\Gamma(g) = \Gamma^1(g) \oplus \Gamma^2(g) = \begin{pmatrix} \Gamma^1(g) & 0 \\ 0 & \Gamma^2(g) \end{pmatrix} \quad (2.24)$$

with the dimension being $d_\Gamma = d_{\Gamma^1} + d_{\Gamma^2}$. A representation with a structure like the one in Eq. 2.24 is called *reducible*, which can be *reduced* or *decomposed* into Γ^1 and Γ^2 . The reduction can also be achieved due to an equivalence transformation. If no equivalence transformation can achieve such a block-diagonalization like in Eq. 2.24, the presentation is called *irreducible*.

A special reducible representation is the *regular representation*, which is defined by the matrices

$$(\Gamma^{reg}(g))_{i,j} = \delta(g_i^{-1}gg_j), \quad (2.25)$$

where $\delta(g)$ is 1, if g is the unit element and 0 otherwise. The rows and columns of the matrices are specified by the numbers i and j attached to the group elements and only those matrix elements i, j are nonzero for which $g_i = gg_j$ holds. The dimension of the representation is equal to the order of the group. The explicit form of the regular representation matrices can easily be deduced from the multiplication table by replacing the elements in the first row with their inverse elements. The matrix $\Gamma^{reg}(g)$ is then obtained by replacing all g in the table with 1 and filling the rest with 0. As the inverse elements of space group Cmca are the elements themselves the multiplication table does not change. Hence, e.g. $\Gamma^{reg}(2_{1,z})$ would be

$$\Gamma^{reg}(2_{1,z}) = \begin{pmatrix} 0 & 1 & 0 & 0 & 0 & 0 & 0 & 0 \\ 1 & 0 & 0 & 0 & 0 & 0 & 0 & 0 \\ 0 & 0 & 0 & 1 & 0 & 0 & 0 & 0 \\ 0 & 0 & 1 & 0 & 0 & 0 & 0 & 0 \\ 0 & 0 & 0 & 0 & 0 & 1 & 0 & 0 \\ 0 & 0 & 0 & 0 & 1 & 0 & 0 & 0 \\ 0 & 0 & 0 & 0 & 0 & 0 & 0 & 1 \\ 0 & 0 & 0 & 0 & 0 & 0 & 1 & 0 \end{pmatrix}. \quad (2.26)$$

Every presentation can be brought into a unitary form by means of an equivalence transformation. An important property of a unitary matrix is that its inverse is equal to its conjugate transpose

$$(\mathbf{A}^{-1})_{i,j} = (\mathbf{A}^*)_{j,i}, \quad (2.27)$$

which simplifies calculations. Therefore, from now on every representation should be considered as unitary.

From the *Schür lemmas* important equations can be deduced, which are necessary to construct irreducible representations.

- Schür's first lemma

If Γ^U and Γ^V are two irreducible matrix representations of orders d_U and d_V of a group G , \mathbf{A} is a matrix of order $d_U \times d_V$ and

$$\Gamma^U(g)\mathbf{A} = \mathbf{A}\Gamma^V(g) \quad \forall g \in G \quad (2.28)$$

is fulfilled, then \mathbf{A} is either the zero matrix or a square matrix ($U = V$) and the two matrix representations are equivalent.

- Schür's second lemma

If Γ^U is an irreducible matrix representation of order d_U and \mathbf{A} is a matrix of order $d_U \times d_U$ such that

$$\Gamma^U(g)\mathbf{A} = \mathbf{A}\Gamma^U(g) \quad \forall g \in G, \quad (2.29)$$

then \mathbf{A} is either the null matrix or a (complex) multiple of the unit matrix of order $d_U \times d_U$.

An outcome of the Schür lemmas is the *orthogonality theorem* (see Appendix A.1.1 for the proof)

$$\sum_{g \in G} \Gamma_{j,l}^U(g) (\Gamma_{n,m}^V(g))^* = \frac{n_G}{d_U} \delta_{UV} \delta_{jn} \delta_{lm}, \quad (2.30)$$

where $\delta_{\alpha\beta}$ is the Kronecker symbol ($\delta_{\alpha\beta} = 1$ if and only if $\alpha = \beta$ and 0 otherwise).

2.3.6. Characters

A very important concept attached to any matrix representation $\Gamma(g)$ is its character, which is

$$\chi(g) = \text{Tr}[\Gamma(g)] = \sum_i \Gamma_{i,i}(g). \quad (2.31)$$

As the trace is invariant under circular permutation of matrices it is well suited to show that two equivalent matrix representation have the same character and two matrix representations with the same character are equivalent (see Appendix A.1.2). A second fundamental property is that the values of the characters $\chi(g)$ are common to all the conjugate elements (see Appendix A.1.3).

The sum of $\chi(g)$ over the irreducible presentations yields important relations (see Appendix A.1.5 for the proof) like

$$\sum_U d_U \chi^U(g) = 0, \text{ for } g \neq E \quad (2.32)$$

and

$$\sum_U d_U^2 = n_G, \text{ for } g = E. \quad (2.33)$$

From the orthogonality theorem (Eq. 2.30) the first orthogonality of characters (Eq. 2.34) can easily be deduced by putting $j = l$, $n = m$ and summing over j and n .

$$\sum_{g \in G} \chi^U(g) (\chi^V(g))^* = n_G \delta_{UV} \quad (2.34)$$

As the character is equal for every element g_e in the class C_e one can write χ_e and sum over the classes:

$$\sum_{e=1}^{n_{cl}} n(C_e) \chi_e^U (\chi_e^V)^* = n_G \delta_{UV}, \quad (2.35)$$

with n_{cl} being the number of classes and $n(C_e)$ the number of elements in the respective class.

A second orthogonality theorem of characters can be deduced (see Appendix A.1.4), which can be expressed by

$$\sum_U \chi_e^U (\chi_f^U)^* = \frac{n_G}{n(C_e)} \delta_{ef}. \quad (2.36)$$

If one defines a vector according to

$$\begin{pmatrix} \sqrt{n(C_1)}\chi_1^U(g) \\ \sqrt{n(C_2)}\chi_2^U(g) \\ \vdots \\ \sqrt{n(C_{n_{cl}})}\chi_{n_{cl}}^U(g) \end{pmatrix} \quad (2.37)$$

then the scalar product of such vectors is simply the left-side of Eq. 2.35. As an n_{cl} -dimensional vector space can have at most n_{cl} mutually orthogonal vectors, the number of vectors n_r , i.e. the number of representations, must not exceed the dimension n_{cl} :

$$n_r \leq n_{cl}.$$

Similarly, a vector in n_r dimensions can be constructed:

$$\begin{pmatrix} \chi_e^1(g) \\ \chi_e^2(g) \\ \vdots \\ \chi_e^{n_r}(g) \end{pmatrix} \quad (2.38)$$

The orthogonality of such vectors is expressed by Eq. 2.36 implying that the number of vectors n_{cl} does not exceed the dimension n_r :

$$n_{cl} \leq n_r.$$

From these two requirements the important result

$$n_r = n_{cl} \quad (2.39)$$

can be obtained, which means that the number n_r of inequivalent irreducible representations is equal to the number n_{cl} of classes.

2.3.6.1. Construction of character tables

All relations necessary to determine the characters of irreducible representations have been derived:

1. The number of inequivalent irreducible representations n_r is equal to the number of classes n_{cl} (Eq. 2.39):

$$n_r = n_{cl}.$$

2. Special methodology and theory

2. The sum of squares of the dimensions of inequivalent irreducible representations is equal to the order n_G of the group (Eq. 2.33):

$$\sum_U d_U^2 = n_G.$$

3. First orthogonality of characters (Eq. 2.34):

$$\sum_{g \in G} \chi^U(g) (\chi^V(g))^* = n_G \delta_{UV}.$$

4. Second orthogonality of characters (Eq. 2.36):

$$\sum_U \chi_e^U (\chi_f^U)^* = \frac{n_G}{n(C_e)} \delta_{ef}.$$

5. Relation for characters resulting from class multiplication (Eq. A.26):

$$n(C_e)n(C_f)\chi_e^U(g)\chi_f^U(g) = d_U \sum_w c_{ef}^w n(C_w)\chi_w^U(g).$$

In many cases the first three rules suffice to create the character table. Group Cmca consists of eight classes (see Sec. 2.3.4), which using (1) leads to eight inequivalent irreducible representations. The order of group Cmca is $n_G = 8$, so it can easily be deduced from the second rule, that eight one-dimensional irreducible representations exist containing the identity representation with $\chi^1(g) = 1$. At this point an intermediate character table can be constructed, which contains the so far deduced characters written in red colour (Tab. 2.3). As $g^2=E$ for every element g , all characters must hold $(\chi^U(g))^2 = 1$ or $\chi^U(g) = \pm 1$. From (3) with $U \neq V$ it follows that each row of the character table contains four times 1 and four times -1. Respecting mutual orthogonality the character table can be completed.

Table 2.3.: Character table of space group Cmca.

	E	2 _{1,z}	2 _{1,y}	2 _x	$\bar{1}$	b _{xy}	c _{xz}	m _{yz}
Γ^1	1	1	1	1	1	1	1	1
Γ^2	1	1	1	1	-1	-1	-1	-1
Γ^3	1	1	-1	-1	1	1	-1	-1
Γ^4	1	1	-1	-1	-1	-1	1	1
Γ^5	1	-1	1	-1	1	-1	1	-1
Γ^6	1	-1	1	-1	-1	1	-1	1
Γ^7	1	-1	-1	1	1	-1	-1	1
Γ^8	1	-1	-1	1	-1	1	1	-1

2.3.7. Basis functions and projection operators

A set of functions $\{\psi_1, \psi_2, \dots, \psi_{d_U}\}$ is called a *basis* for a representation Γ^U , if

$$g_k \psi_j = \sum_{i=1}^{d_U} \psi_i \Gamma_{i,j}^U(g_k) \quad (2.40)$$

holds, i.e., if the basis is closed within itself under the operations $g \in G$. Individual members of the basis are called *basis functions* or *basis vectors*, which are symmetry-adapted functions or vectors.

Such basis functions, which transform according to a unitary matrix $\Gamma^U(g)$ of an irreducible representation, can be constructed by the method of *projection operators*. An arbitrary function f contains, in general, components of various irreducible representations, which allows the decomposition

$$f = \sum_U \sum_j c_j^U \psi_j^U, \quad (2.41)$$

where the c_i^U are the coefficients of the expansion. When a projection operator defined by

$$O_{P_{i,j}^U} = \frac{d_U}{n_G} \sum_{g \in G} (\Gamma_{i,j}^U(g))^* g \quad (2.42)$$

is applied to the above function f , it picks up the symmetry-adapted function ψ_i^U :

$$O_{P_{i,j}^U} f = c_j^U \psi_i^U \quad (2.43)$$

Thus, if the function f contains an irreducible component ψ_j^U , operation of the above projection operator on f generates ψ_i^U . If not, Eq. 2.43 is zero. $O_{P_{i,i}}$ is the diagonal projection operator that either gives a basis vector or nothing, while $O_{P_{i,j \neq i}}$ is a shift operator that from a basis vector helps to generate the other basis vectors.

2.3.8. Application to the magnetic structures of $(\text{Co}_x\text{Ni}_{1-x})_3\text{V}_2\text{O}_8$

For solving a magnetic structure it is absolutely necessary to know the crystal structure of the investigated compound, i.e. the space group, in order to apply the techniques deduced by group theory analysis. As a second step the periodicity of the magnetic structure expressed by the propagation vector \mathbf{k} has to be determined, because the group G or little group $G_{\mathbf{k}}$ (magnetic subgroup of G) under consideration is dependent on the type of \mathbf{k} . With the help of the derived rules of Sec. 2.3.6.1 the character table can be built, from which the irreducible matrix representations can be deduced. From the direct product of the permutation representation $\mathbf{\Gamma}^{perm}$ and the axial vector representation $\mathbf{\Gamma}^{vect}$, representing the permutation of magnetic atoms and the orientation of their magnetic moments due to the symmetry elements, respectively, one obtains the transformation-induced matrix representations. These will then be decomposed again into a direct sum of irreducible representations. Applying the projection operator technique on the irreducible representations with respect to a given starting function yields the basis vectors, i.e. the symmetry adapted vectors, which describe the magnetic modes.

2.3.8.1. Space group Cmca and atomic positions

As mentioned above the space group Cmca contains eight symmetry operators, which are $G = \{E, 2_{1,z}, 2_{1,y}, 2_x, \bar{1}, b_{xy}, c_{xz}, m_{yz}\}$. The magnetic ions M^{2+} occupy the Wyckoff sites 4a and 8e (Tab. 2.4).

2.3.8.2. Propagation vectors

For $(\text{Co}_x\text{Ni}_{1-x})_3\text{V}_2\text{O}_8$ three different types of propagation vectors have been observed, which are $\mathbf{k}_1 = 0$, $\mathbf{k}_2 = (k_{a^*}, 0, 0)$ and $\mathbf{k}_3 = (0, k_{b^*}, 0)$. For \mathbf{k}_1 all eight symmetry operators are compatible, hence $G_{\mathbf{k}_1} = G$. If the propagation is nonzero, $G_{\mathbf{k}}$ may be a proper subgroup of G , i.e. certain symmetry elements are not compatible with the propagation vector. The condition for compatibility of a symmetry element $g = \{\alpha | \mathbf{t}_\alpha + \mathbf{R}_n\}$, where α denotes the rotational part (proper or improper) and \mathbf{t}_α , \mathbf{R}_n its translational part, is that it leaves the propagation vector invariant modulo a reciprocal lattice vector \mathbf{K}_p , which writes as

Table 2.4.: Reference atoms for the Wyckoff sites 4a and 8e. To every position (x, y, z) the position $(x + \frac{1}{2}, y + \frac{1}{2}, z)$ exists due to the C-centering.

Site j	Atom s	x, y, z -Coordinates
(4a)	1	(0,0,0)
	2	$(0, \frac{1}{2}, \frac{1}{2})$
(8e)	1	$(\frac{1}{4}, \bar{y}, \frac{1}{4})$
	2	$(\frac{3}{4}, \bar{y} + \frac{1}{2}, \frac{3}{4})$
	3	$(\frac{3}{4}, \bar{y}, \frac{3}{4})$
	4	$(\frac{1}{4}, \bar{y} + \frac{1}{2}, \frac{1}{4})$

$$\alpha^* \mathbf{k} = \mathbf{k} + \mathbf{K}_p. \quad (2.44)$$

Using Eq. 2.44 with all symmetry elements in combination with \mathbf{k}_2 and \mathbf{k}_3 yields the little groups $G_{\mathbf{k}_2}$ and $G_{\mathbf{k}_3}$ (see Appendix A.2.1 for the individual calculations):

$$G_{\mathbf{k}_2} = \{E, 2_x, b_{xy}, c_{xz}\} \quad G_{\mathbf{k}_3} = \{E, 2_{1,y}, b_{xy}, m_{yz}\} \quad (2.45)$$

2.3.8.3. Irreducible matrix representations

Using the derived relations, which are summarized in Sec. 2.3.6.1, the character tables for the different little groups can be built. Tab. 2.3 already represents the character table of the vector group $G_{\mathbf{k}_1}$ with $\mathbf{k}_1=0$ describing the ferromagnetic structure of $\text{Co}_3\text{V}_2\text{O}_8$. Since the irreducible representations $\Gamma^{\mathbf{k},U}$ are all 1-dimensional, they coincide with their characters.

The character table for $G_{\mathbf{k}_2}$ can be constructed as easily as for $G_{\mathbf{k}_1}$ and is shown in Tab. 2.5. In the case of $G_{\mathbf{k}_3}$ it has to be considered, that the symmetry elements $2_{1,y}$

Table 2.5.: Character table of the little group $G_{\mathbf{k}_2}$.

	E	2_x	b_{xy}	c_{xz}
$\Gamma^{\mathbf{k}_2,1}$	1	1	1	1
$\Gamma^{\mathbf{k}_2,2}$	1	1	-1	-1
$\Gamma^{\mathbf{k}_2,3}$	1	-1	1	-1
$\Gamma^{\mathbf{k}_2,4}$	1	-1	-1	1

and b_{xy} possess a translational part of $(0\frac{1}{2}0)$, which coincides with the direction of the propagation vector. This fact is accounted for by applying a phase factor, which describes the modulation of the magnetic moments along the direction of propagation (Eq. 2.46).

$$\mathbf{m}_{ljs} = \sum_{\{k\}} \mathbf{S}_{\mathbf{k}js} \exp(2\pi i \mathbf{k} \mathbf{R}_l) \quad (2.46)$$

\mathbf{m}_{ljs} denotes the magnetic moment at a lattice point l of sublattice s of Wyckoff site j , $\{k\}$ is the star of \mathbf{k} consisting of all vectors $\alpha_i \mathbf{k}$ not differing by a reciprocal lattice vector, $\mathbf{S}_{\mathbf{k}js}$ is the Fourier coefficient and the exponential term containing the propagation vector \mathbf{k} and a lattice vector \mathbf{R}_l represents the phase shift. The phase factor, with which the irreducible representations $\Gamma^{\mathbf{k}_3,U}(2_{1,y})$ and $\Gamma^{\mathbf{k}_3,U}(b_{xy})$, hence the characters $\chi^{\mathbf{k}_3,U}(2_{1,y})$ and $\chi^{\mathbf{k}_3,U}(b_{xy})$, have to be multiplied calculates as

$$\varphi = \exp(2\pi i \mathbf{k} \mathbf{R}_l) = \exp \left[2\pi i \begin{pmatrix} 0 \\ k_{b^*} \\ 0 \end{pmatrix} \begin{pmatrix} \frac{1}{2} \\ \frac{1}{2} \\ 0 \end{pmatrix} \right] = \exp(\pi i k_{b^*}) \quad (2.47)$$

Tab. 2.6 shows the character table for $G_{\mathbf{k}_3}$ containing the phase shifts for the special symmetry operators.

Table 2.6.: Character table of the little group $G_{\mathbf{k}_3}$.

	E	2_{1y}	b_{xy}	m_{yz}
$\Gamma^{\mathbf{k}_3,1}$	1	$\exp(\pi i k_{b^*})$	$-\exp(\pi i k_{b^*})$	-1
$\Gamma^{\mathbf{k}_3,2}$	1	$\exp(\pi i k_{b^*})$	$\exp(\pi i k_{b^*})$	1
$\Gamma^{\mathbf{k}_3,3}$	1	$-\exp(\pi i k_{b^*})$	$-\exp(\pi i k_{b^*})$	1
$\Gamma^{\mathbf{k}_3,4}$	1	$-\exp(\pi i k_{b^*})$	$\exp(\pi i k_{b^*})$	-1

2.3.8.4. Transformation-induced matrix representations and reduction

As mentioned above the transformation-induced matrix representations for the different sites are obtained by

$$\Gamma_j^{\mathbf{k}} = \Gamma^{\mathbf{k},vect} \otimes \Gamma_j^{\mathbf{k},perm}. \quad (2.48)$$

The two and four reference atoms (Tab. 2.4) for the magnetic sites 4a and 8e, respectively,

are the only ones required to uniquely define the magnetic structure. All the others are related to these by the primitive translations of the C-centered lattice. The reference atoms form a basis for the permutation representations $\Gamma_{4a}^{\mathbf{k},perm}$ and $\Gamma_{8e}^{\mathbf{k},perm}$, which are of dimension 2 and 4, respectively. Atomic positions are polar vectors, which are transformed by a symmetry operator according to

$$\mathbf{x}' = \alpha\mathbf{x} + \mathbf{t}_\alpha. \quad (2.49)$$

The transformation properties are shown in Tab. 2.7. It can easily be deduced that the

Table 2.7.: Transformation of the positions for the magnetic sites 4a and 8e.

	4a		8e			
	1	2	1	2	3	4
E	1	2	1	2	3	4
$2_{1,z}$	2	1	2	1	4	3
$2_{1,y}$	2	1	1	2	3	4
2_x	1	2	2	1	4	3
$\bar{1}$	1	2	3	4	1	2
b_{xy}	2	1	4	3	2	1
c_{xz}	2	1	3	4	1	2
m_{yz}	1	2	4	3	2	1

only nonzero traces of $\Gamma_{4a}^{\mathbf{k}_1,perm}$ are for $E, 2_x, \bar{1}$ and m_{yz} , while $\Gamma_{8e}^{\mathbf{k}_1,perm}$ contains nonzero diagonal elements only for E and $2_{1,y}$:

$$\chi_{4a}^{\mathbf{k}_1,perm}(E) = \chi_{4a}^{\mathbf{k}_1,perm}(2_x) = \chi_{4a}^{\mathbf{k}_1,perm}(\bar{1}) = \chi_{4a}^{\mathbf{k}_1,perm}(m_{yz}) = 2 \quad (2.50)$$

$$\chi_{8e}^{\mathbf{k}_1,perm}(E) = \chi_{8e}^{\mathbf{k}_1,perm}(2_{1,y}) = 4. \quad (2.51)$$

The derived transformation properties and characters are also valid for $G_{\mathbf{k}_2}$ with the exception that the symmetry elements not in the little group simply vanish. In the special case of $G_{\mathbf{k}_3}$, where the remaining symmetry elements do not generate the entire cell, the M2 8e site splits into two orbits (orbit 1: atom 1 and 4, orbit 2: atom 2 and 3), i.e. the permutation representations for the two orbits of 8e are of dimension 2. The transformation properties of the two orbits are shown in Tab. 2.8. The atoms marked

2. Special methodology and theory

by an asterisk are those, which are equal in the crystallographic point of view, but have been translated by the C-centering translation vector after application of the symmetry operator.

Table 2.8.: Transformation of the positions for the two orbits of the magnetic site 8e.

	o_1	1	4	o_2	2	3
E		1	4		2	3
$2_{1,y}$		1*	4*		2*	3*
b_{xy}		4	1		3	2
m_{yz}		4*	1*		3*	2*

Bearing in mind the phase factor the nonzero characters are

$$\chi^{\mathbf{k}_3,perm}(E) = 2 \quad \text{and} \quad \chi^{\mathbf{k}_3,perm}(2_{1,y}) = 2 \exp(\pi i k_b^*). \quad (2.52)$$

The permutation representations will now be decomposed into the irreducible representations according to

$$\Gamma_j^{\mathbf{k},perm}(g) = \bigoplus_U n_{\mathbf{k},U} \Gamma^{\mathbf{k},U}(g) \quad \text{with} \quad n_{\mathbf{k},U} = \frac{1}{n_{G_{\mathbf{k}}}} \sum_{g \in G_{\mathbf{k}}} \chi_j^{\mathbf{k},perm}(g) \left(\chi^{\mathbf{k},U}(g) \right)^*. \quad (2.53)$$

Using the obtained permutation characters (Eq. 2.51) and the character table (Tab. 2.3) the coefficients $n_{\mathbf{k},U}$ can be calculated (see Appendix A.2.2) indicating how many times $\Gamma^{\mathbf{k},U}$ is contained in $\Gamma_j^{\mathbf{k},perm}$. For \mathbf{k}_1 one obtains for the different sites:

$$\Gamma_{4a}^{\mathbf{k}_1,perm} = \Gamma^{\mathbf{k}_1,1} \oplus \Gamma^{\mathbf{k}_1,7}, \quad (2.54)$$

$$\Gamma_{8e}^{\mathbf{k}_1,perm} = \Gamma^{\mathbf{k}_1,1} \oplus \Gamma^{\mathbf{k}_1,2} \oplus \Gamma^{\mathbf{k}_1,5} \oplus \Gamma^{\mathbf{k}_1,6}. \quad (2.55)$$

The direct sums of the irreducible representations give back the representations of dimension 2 and 4 as expected. It can be checked in Appendix A.2.2 that the reductions for $G_{\mathbf{k}_2}$ and $G_{\mathbf{k}_3}$ are

$$\Gamma_{4a}^{k_2,perm} = \Gamma^{k_2,1} \oplus \Gamma^{k_2,2} \quad (2.56)$$

$$\Gamma_{8e}^{k_2,perm} = \Gamma^{k_2,1} \oplus \Gamma^{k_2,2} \oplus \Gamma^{k_2,3} \oplus \Gamma^{k_2,4} \quad (2.57)$$

$$\Gamma_{4a}^{k_3,perm} = \Gamma^{k_3,2} \oplus \Gamma^{k_3,3} \quad (2.58)$$

$$\Gamma_{o_1}^{k_3,perm} = \Gamma_{o_2}^{k_3,perm} = \Gamma^{k_3,1} \oplus \Gamma^{k_3,2} \quad (2.59)$$

Now the transformation of the magnetic moments is taken into account. As the magnetic moment is an axial vector, it transforms as a polar vector under rotation, but remains invariant under the inversion. This is expressed by

$$\mathbf{S}' = \eta(\alpha)\alpha\mathbf{S} = \mathbf{\Gamma}^{vect}(g)\mathbf{S}, \quad (2.60)$$

where $\eta(\alpha)$ is the determinant of α . The transformation properties of magnetic moments are depicted in Fig. 2.5 and listed for the symmetry operators of space group Cmca in Tab. 2.9.

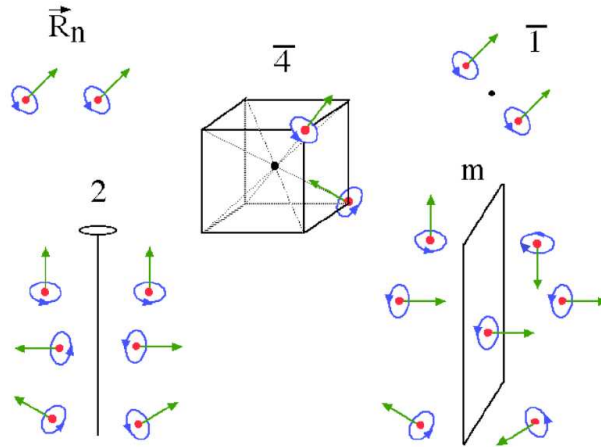


Figure 2.5.: Symmetry operators acting on axial vectors.

2. Special methodology and theory

Table 2.9.: Transformation of the components S_x , S_y and S_z of a magnetic moment \mathbf{S} .

E	$2_{1,z}$	$2_{1,y}$	2_x	$\bar{1}$	b_{xy}	c_{xz}	m_{yz}
S_x	$-S_x$	$-S_x$	S_x	S_x	$-S_x$	$-S_x$	S_x
S_y	$-S_y$	S_y	$-S_y$	S_y	$-S_y$	S_y	$-S_y$
S_z	S_z	$-S_z$	$-S_z$	S_z	S_z	$-S_z$	$-S_z$

Reductions of $\Gamma^{\mathbf{k},vect}$ over the irreducible representations $\Gamma^{\mathbf{k},U}$ yield

$$\Gamma^{\mathbf{k}_1,vect} = \Gamma^{\mathbf{k}_1,3} \oplus \Gamma^{\mathbf{k}_1,5} \oplus \Gamma^{\mathbf{k}_1,7} \quad (2.61)$$

$$\Gamma^{\mathbf{k}_2,vect} = \Gamma^{\mathbf{k}_2,2} \oplus \Gamma^{\mathbf{k}_2,3} \oplus \Gamma^{\mathbf{k}_2,4} \quad (2.62)$$

$$\Gamma^{\mathbf{k}_3,vect} = \Gamma^{\mathbf{k}_3,1} \oplus \Gamma^{\mathbf{k}_3,3} \oplus \Gamma^{\mathbf{k}_3,4} \quad (2.63)$$

which is verified in Appendix A.2.3.

Finally, the transformation-induced matrix representations are obtained with the help of further direct product reductions (see Appendix A.2.4):

$$\Gamma_{4a}^{\mathbf{k}_1} = (\Gamma^{\mathbf{k}_1,3} \oplus \Gamma^{\mathbf{k}_1,5} \oplus \Gamma^{\mathbf{k}_1,7}) \otimes (\Gamma^{\mathbf{k}_1,1} \oplus \Gamma^{\mathbf{k}_1,7}) = \Gamma^{\mathbf{k}_1,1} \oplus 2\Gamma^{\mathbf{k}_1,3} \oplus 2\Gamma^{\mathbf{k}_1,5} \oplus \Gamma^{\mathbf{k}_1,7} \quad (2.64)$$

$$\begin{aligned} \Gamma_{8e}^{\mathbf{k}_1} &= (\Gamma^{\mathbf{k}_1,3} \oplus \Gamma^{\mathbf{k}_1,5} \oplus \Gamma^{\mathbf{k}_1,7}) \otimes (\Gamma^{\mathbf{k}_1,1} \oplus \Gamma^{\mathbf{k}_1,2} \oplus \Gamma^{\mathbf{k}_1,5} \oplus \Gamma^{\mathbf{k}_1,6}) \\ &= \Gamma^{\mathbf{k}_1,1} \oplus \Gamma^{\mathbf{k}_1,2} \oplus 2\Gamma^{\mathbf{k}_1,3} \oplus 2\Gamma^{\mathbf{k}_1,4} \oplus \Gamma^{\mathbf{k}_1,5} \oplus \Gamma^{\mathbf{k}_1,6} \oplus 2\Gamma^{\mathbf{k}_1,7} \oplus 2\Gamma^{\mathbf{k}_1,8} \end{aligned} \quad (2.65)$$

From Eq. 2.64 one can conclude that the basis functions for the irreducible representations $\Gamma^{\mathbf{k}_1,2}$, $\Gamma^{\mathbf{k}_1,4}$, $\Gamma^{\mathbf{k}_1,6}$ and $\Gamma^{\mathbf{k}_1,8}$, which are not contained in the reduction of $\Gamma_{4a}^{\mathbf{k}_1}$, are necessarily zero. For all irreducible representation that appear twice in the reduction two different sets of linearly independent basis vectors will have to be built.

Analogously the reduction of the transformation-induced matrix representations over the irreducible matrix representations of the little groups $G_{\mathbf{k}_2}$ and $G_{\mathbf{k}_3}$ are

$$\begin{aligned} \Gamma_{4a}^{\mathbf{k}_2} &= (\Gamma^{\mathbf{k}_2,2} \oplus \Gamma^{\mathbf{k}_2,3} \oplus \Gamma^{\mathbf{k}_2,4}) \otimes (\Gamma^{\mathbf{k}_2,1} \oplus \Gamma^{\mathbf{k}_2,2}) \\ &= \Gamma^{\mathbf{k}_2,1} \oplus \Gamma^{\mathbf{k}_2,2} \oplus 2\Gamma^{\mathbf{k}_2,3} \oplus 2\Gamma^{\mathbf{k}_2,4} \end{aligned} \quad (2.66)$$

$$\begin{aligned}\Gamma_{8e}^{\mathbf{k}_2} &= (\Gamma^{\mathbf{k}_2,2} \oplus \Gamma^{\mathbf{k}_2,3} \oplus \Gamma^{\mathbf{k}_2,4}) \otimes (\Gamma^{\mathbf{k}_2,1} \oplus \Gamma^{\mathbf{k}_2,2} \oplus \Gamma^{\mathbf{k}_2,3} \oplus \Gamma^{\mathbf{k}_2,4}) \\ &= 3\Gamma^{\mathbf{k}_2,1} \oplus 3\Gamma^{\mathbf{k}_2,2} \oplus 3\Gamma^{\mathbf{k}_2,3} \oplus 3\Gamma^{\mathbf{k}_2,4}\end{aligned}\quad (2.67)$$

$$\begin{aligned}\Gamma_{4a}^{\mathbf{k}_3} &= (\Gamma^{\mathbf{k}_3,1} \oplus \Gamma^{\mathbf{k}_3,3} \oplus \Gamma^{\mathbf{k}_3,4}) \otimes (\Gamma^{\mathbf{k}_3,2} \oplus \Gamma^{\mathbf{k}_3,3}) \\ &= 2\Gamma^{\mathbf{k}_3,1} \oplus \Gamma^{\mathbf{k}_3,2} \oplus \Gamma^{\mathbf{k}_3,3} \oplus 2\Gamma^{\mathbf{k}_3,4}\end{aligned}\quad (2.68)$$

$$\begin{aligned}\Gamma_{o1}^{\mathbf{k}_3} = \Gamma_{o2}^{\mathbf{k}_3} &= (\Gamma^{\mathbf{k}_3,1} \oplus \Gamma^{\mathbf{k}_3,3} \oplus \Gamma^{\mathbf{k}_3,4}) \otimes (\Gamma^{\mathbf{k}_3,1} \oplus \Gamma^{\mathbf{k}_3,2}) \\ &= \Gamma^{\mathbf{k}_3,1} \oplus \Gamma^{\mathbf{k}_3,2} \oplus 2\Gamma^{\mathbf{k}_3,3} \oplus 2\Gamma^{\mathbf{k}_3,4}\end{aligned}\quad (2.69)$$

2.3.8.5. Deduction of the magnetic modes

The magnetic modes, which are the basis vectors for the irreducible representations, are obtained by the projection operator technique. The basis vectors for each site are deduced as

$$\psi_{i,j}^{\mathbf{k},U} = O_{P_{i,j}^{\mathbf{k},U}} \psi = \frac{d_U}{n_G} \sum_{g \in G} \left(\Gamma_{i,j}^{\mathbf{k},U}(g) \right)^* g \psi \quad (2.70)$$

from a trial magnetic moment $\psi = \mathbf{S} = (S_{1x} \ S_{1y} \ S_{1z})^T$. Since all the irreducible representations are one-dimensional only the calculation of $\psi_{1,1}^{\mathbf{k},U}$ is necessary. Using the respective transformation properties of the 4a positions and spin components from Tab. 2.7 and Tab. 2.9 one obtains

$$\begin{aligned}\psi_{1,1}^{\mathbf{k}_1,1} &= \frac{1}{8} \left[1 \cdot \begin{pmatrix} S_{1x} \\ S_{1y} \\ S_{1z} \end{pmatrix} + 1 \cdot \begin{pmatrix} -S_{2x} \\ -S_{2y} \\ S_{2z} \end{pmatrix} + 1 \cdot \begin{pmatrix} -S_{2x} \\ S_{2y} \\ -S_{2z} \end{pmatrix} + 1 \cdot \begin{pmatrix} S_{1x} \\ -S_{1y} \\ -S_{1z} \end{pmatrix} \right] \\ &+ \frac{1}{8} \left[1 \cdot \begin{pmatrix} S_{1x} \\ S_{1y} \\ S_{1z} \end{pmatrix} + 1 \cdot \begin{pmatrix} -S_{2x} \\ -S_{2y} \\ S_{2z} \end{pmatrix} + 1 \cdot \begin{pmatrix} -S_{2x} \\ S_{2y} \\ -S_{2z} \end{pmatrix} + 1 \cdot \begin{pmatrix} S_{1x} \\ -S_{1y} \\ -S_{1z} \end{pmatrix} \right] \\ &= \frac{1}{2} \left[\begin{pmatrix} S_{1x} \\ 0 \\ 0 \end{pmatrix} - \begin{pmatrix} S_{2x} \\ 0 \\ 0 \end{pmatrix} \right].\end{aligned}\quad (2.71)$$

Disregarding the prefactor, which anyway will be the refined parameter in the magnetic structure refinement, the essential result for the basis vectors of irreducible representation

2. Special methodology and theory

$\Gamma^{\mathbf{k}_1,1}$ is an antiferromagnetic coupling along the x direction of atom 1 at (000) and atom 2 at $(0\frac{1}{2}\frac{1}{2})$, while the y and z components are zero. The same calculation for the 8e site yields an antiferromagnetic G -mode for the y component (see Wollan-Köhler-Bertaut notation [40] below):

$$\begin{aligned}
\psi_{1,1}^{\mathbf{k}_1,1} &= \frac{1}{8} \left[1 \cdot \begin{pmatrix} S_{1x} \\ S_{1y} \\ S_{1z} \end{pmatrix} + 1 \cdot \begin{pmatrix} -S_{2x} \\ -S_{2y} \\ S_{2z} \end{pmatrix} + 1 \cdot \begin{pmatrix} -S_{1x} \\ S_{1y} \\ -S_{1z} \end{pmatrix} + 1 \cdot \begin{pmatrix} S_{2x} \\ -S_{2y} \\ -S_{2z} \end{pmatrix} \right] \\
&+ \frac{1}{8} \left[1 \cdot \begin{pmatrix} S_{3x} \\ S_{3y} \\ S_{3z} \end{pmatrix} + 1 \cdot \begin{pmatrix} -S_{4x} \\ -S_{4y} \\ S_{4z} \end{pmatrix} + 1 \cdot \begin{pmatrix} -S_{3x} \\ S_{3y} \\ -S_{3z} \end{pmatrix} + 1 \cdot \begin{pmatrix} S_{4x} \\ -S_{4y} \\ -S_{4z} \end{pmatrix} \right] \\
&= \frac{1}{4} \left[\begin{pmatrix} 0 \\ S_{1y} \\ 0 \end{pmatrix} - \begin{pmatrix} 0 \\ S_{2y} \\ 0 \end{pmatrix} + \begin{pmatrix} 0 \\ S_{3y} \\ 0 \end{pmatrix} - \begin{pmatrix} 0 \\ S_{4y} \\ 0 \end{pmatrix} \right]. \tag{2.72}
\end{aligned}$$

$$\begin{aligned}
\mathbf{G} &= \mathbf{S}_1 - \mathbf{S}_2 + \mathbf{S}_3 - \mathbf{S}_4 \quad (G\text{-mode}), \\
\mathbf{A} &= \mathbf{S}_1 - \mathbf{S}_2 - \mathbf{S}_3 + \mathbf{S}_4 \quad (A\text{-mode}), \\
\mathbf{C} &= \mathbf{S}_1 + \mathbf{S}_2 - \mathbf{S}_3 - \mathbf{S}_4 \quad (C\text{-mode}), \\
\mathbf{F} &= \mathbf{S}_1 + \mathbf{S}_2 + \mathbf{S}_3 + \mathbf{S}_4 \quad (F\text{-mode}).
\end{aligned}$$

The n sets of basis vectors of all the respective irreducible matrix representations obtained by the projection operator technique are listed in Tab. 2.10 (see Appendix A.2.5 for the respective calculations) and as mentioned above all the irreducible representations appearing twice in the reduction possess two sets of linearly independent basis vectors.

Table 2.10.: Basis vectors of the irreducible matrix representations of $G_{\mathbf{k}_1}$.

	4a			8e		
$\Gamma^{\mathbf{k}_1,1}$	$S_{1x} - S_{2x}$	0	0	0	G_y	0
$\Gamma^{\mathbf{k}_1,2}$	0	0	0	0	A_y	0
$\Gamma^{\mathbf{k}_1,3}$	0	$S_{1y} - S_{2y}$	$S_{1z} + S_{2z}$	G_x	0	F_z
$\Gamma^{\mathbf{k}_1,4}$	0	0	0	A_x	0	C_z
$\Gamma^{\mathbf{k}_1,5}$	0	$S_{1y} + S_{2y}$	$S_{1z} - S_{2z}$	0	F_y	0
$\Gamma^{\mathbf{k}_1,6}$	0	0	0	0	C_y	0
$\Gamma^{\mathbf{k}_1,7}$	$S_{1x} + S_{2x}$	0	0	F_x	0	G_z
$\Gamma^{\mathbf{k}_1,8}$	0	0	0	C_x	0	A_z

The fundamental hypothesis of representation analysis is that the vectorial Fourier coefficients $\mathbf{S}_{\mathbf{k}j_s}$ are linear combinations of basis vectors, which is in a simplified form:

$$\mathbf{S}_{\mathbf{k}j} = \sum_n C_n \psi_{i,j}^{\mathbf{k},U,n}. \quad (2.73)$$

The coefficients C_n , which can be complex, are the refined parameters in the calculation of the magnetic moments according to Eq. 2.46, which e.g. for $\Gamma^{\mathbf{k}_1,7}$ would be

$$\begin{aligned} \mathbf{m}_{l,4a} &= \sum_{\{\mathbf{k}\}} \mathbf{S}_{\mathbf{k},4a} \exp(-2\pi i \mathbf{k} \mathbf{R}_l) = \mathbf{S}_{\mathbf{k},4a} \exp(-2\pi i \mathbf{k} \mathbf{R}_l) + \mathbf{S}_{\mathbf{k},4a}^* \exp(2\pi i \mathbf{k} \mathbf{R}_l) \\ &= 2\mathbf{S}_{\mathbf{k},4a} = 2 \sum_n C_n \psi_{1,1}^{\mathbf{k}_1,7,n} = 2C_1(S_{1x} + S_{2x}) \end{aligned} \quad (2.74)$$

and

$$\mathbf{m}_{l,8e} = 2[C_2(F_x) + C_3(G_z)]. \quad (2.75)$$

The basis vectors for the irreducible matrix representations of $G_{\mathbf{k}_2}$ and $G_{\mathbf{k}_3}$ are shown in Tab. 2.11 and Tab. 2.12. The reference atoms 2 and 3 of the 8e site shall now be $2' = 2 + \mathbf{t}$ and $3' = 3 + \mathbf{t}$, where \mathbf{t} denotes the translation vector $(\frac{1}{2}, \frac{1}{2}, 0)$. The renumbering is done in order to have all the reference atoms at the same x -value, i.e. in phase.

It could be shown in the preceding chapters that a purely mathematical treatment based on symmetry properties yields a manageable number of magnetic structure models, which

2. Special methodology and theory

have to be tested separately with the observed data. Due to the symmetry relations between equivalent magnetic moments the number of refinable parameters is reduced significantly.

Table 2.11.: Basis vectors of the irreducible matrix representations of $G_{\mathbf{k}_2}$.

	4a			8e		
$\Gamma^{\mathbf{k}_2,1}$	$S_{1x} - S_{2x}$	0	0	C_x	G_y	A_z
$\Gamma^{\mathbf{k}_2,2}$	$S_{1x} + S_{2x}$	0	0	F_x	A_y	G_z
$\Gamma^{\mathbf{k}_2,3}$	0	$S_{1y} - S_{2y}$	$S_{1z} + S_{2z}$	G_x	C_y	F_z
$\Gamma^{\mathbf{k}_2,4}$	0	$S_{1y} + S_{2y}$	$S_{1z} - S_{2z}$	A_x	F_y	C_z

Table 2.12.: Basis vectors of the irreducible matrix representations of $G_{\mathbf{k}_3}$.

	4a			$o_{1(2)}$		
$\Gamma^{\mathbf{k}_3,1}$	0	$S_{1y} + aS_{2y}$	$S_{1z} - aS_{2z}$	0	$S_{1(2)y} + aS_{4(3)y}$	0
$\Gamma^{\mathbf{k}_3,2}$	$S_{1x} - aS_{2x}$	0	0	0	$S_{1(2)y} + aS_{4(3)y}$	0
$\Gamma^{\mathbf{k}_3,3}$	$S_{1x} + aS_{2x}$	0	0	$S_{1(2)x} + aS_{4(3)x}$	0	$S_{1(2)z} - aS_{4(3)z}$
$\Gamma^{\mathbf{k}_3,4}$	0	$S_{1y} - aS_{2y}$	$S_{1z} + aS_{2z}$	$S_{1(2)x} - aS_{4(3)x}$	0	$S_{1(2)z} + aS_{4(3)z}$

2.4. Extinction

The complex phenomena of extinction is an effect, which severely plagues single crystal diffraction experiments, because the application of its correction is connected to idealized crystal models and to a compromise between different diffraction theories. The kinematical theory [41], which is derived from interference calculations for the waves scattered by individual atoms, assumes that the diffracted amplitude is always small so the interaction between the incident and the scattered waves can be neglected. This case cannot be applied to perfect crystals, whose lattices are coherent over a large region. The diffraction of perfect crystals is described by the dynamical theory [42–47], while its application is rather restricted. Therefore, as pointed out by Zachariasen [48], a general theory for extinction needs to contain both theories as limiting cases.

The extinction effect itself is the attenuation of the incident as well as the diffracted beam inside the crystal due to successive interaction between both. Within a perfect domain of the crystal the scattered and transmitted beams act themselves as incident beams, which are scattered or transmitted again. Accordingly, the beam S_p in Figure 2.6 can be thought of as a superposition of the transmitted part of beam S_{p-1} through plane p and the scattered part of T_p at the same plane. The incident beam, which has already lost intensity through scattering is thus further reduced in amplitude by the doubly diffracted beam, which has a phase shift of π radians. This phenomena is called *primary extinction* and leads to a much stronger attenuation compared to what would be expected by the kinematic theory even taking into account ordinary absorption. Primary extinction becomes negligibly small when the mosaic blocks or the structure factor are very small.

In the case of a real crystal, which can be understood with the highly oversimplified concept of an ideally imperfect crystal as depicted in Figure 2.7, the perfect domains extend only to very small blocks. These blocks possess a mean radius and a distributed orientation so that when one block is in the reflection position only a fraction of the others are oriented likewise. The attenuation of the beam like for primary extinction is now effectuated by whole blocks, which is called *secondary extinction*. But contrarily the intensity and not the amplitude is reduced as the blocks do not scatter coherently because of being slightly rotated and not necessarily distant by a lattice vector. Secondary extinction becomes negligibly small when the misorientation of the blocks becomes sufficiently large or again if the reflection is very weak.

In the two following sections the extinction models, which are implemented in the Cambridge Crystallographic Subroutine Library (CCSL) [49] and in FullProf [50], will be elu-

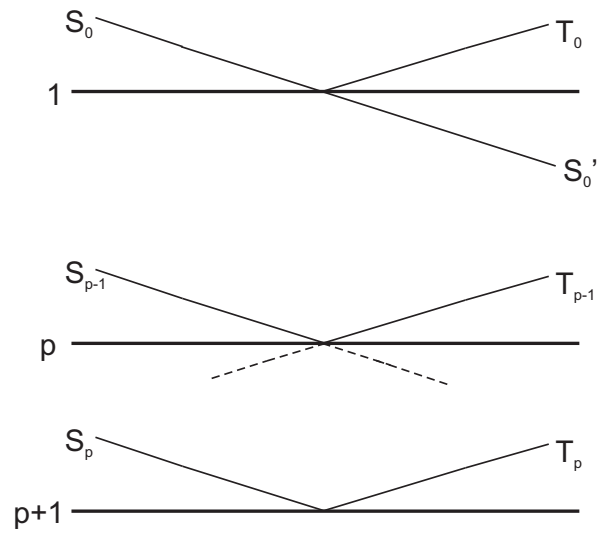


Figure 2.6.: Scattering and transmission of respective beams S at planes p .

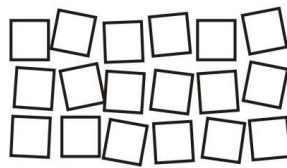


Figure 2.7.: Illustration of an ideally imperfect crystal by a distribution of slightly misaligned blocks.

dated.

2.4.1. The Becker-Coppens model

The widely accepted and applied model for extinction correction is the one developed by Pierre J. Becker and Philip Coppens, which has been published in a tripartite publication [51–53]. Their theory is based on Darwin’s transfer equations for the manifold energy exchange between the incident and diffracted beams inside the crystal:

$$\begin{aligned}\frac{\partial I_0}{\partial x_1} &= -\sigma(I_0 - I) \\ \frac{\partial I}{\partial x_2} &= -\sigma(I - I_0) \\ \frac{\partial I_0}{\partial x_1} + \frac{\partial I}{\partial x_2} &= 0\end{aligned}\tag{2.76}$$

with the boundary conditions

$$\begin{aligned}I_0(M_1^0) &= \mathcal{I}_0 \\ I(M_2^0) &= 0.\end{aligned}\tag{2.77}$$

I_0 and I represent the intensity of the incident and diffracted beam at a certain point $M(x_1, x_2)$ inside the crystal related to an external coordinate system after having been rescattered at $N(u_1, u_2)$ (see Fig. 2.8), \mathcal{I}_0 is the incident intensity before the beam enters the crystal. σ defines the diffraction cross-section per unit volume and unit intensity, which is given by

$$\sigma(\epsilon_1) = \mathcal{I}_0^{-1} v^{-1} P_k(\epsilon_1) = \mathcal{I}_0^{-1} v^{-1} R_0^2 \iint I_k(\epsilon) d\epsilon_2 d\epsilon_3,\tag{2.78}$$

where $P_k(\epsilon_1)$ and $I_k(\epsilon)$ are the detected power and intensity at a distance R_0 in the kinematical approach in dependence on the primary (ϵ_1) and secondary (ϵ_2, ϵ_3) divergence. Finally, I_k writes as

$$I_k(\epsilon) = \mathcal{I}_0 \left| \frac{FK}{R_0} \right|^2 \left| \sum_L \exp(2\pi i \lambda^{-1} \epsilon \cdot \mathbf{L}) \right|^2\tag{2.79}$$

with the structure factor F , the polarization factor K , the wavelength λ and a lattice

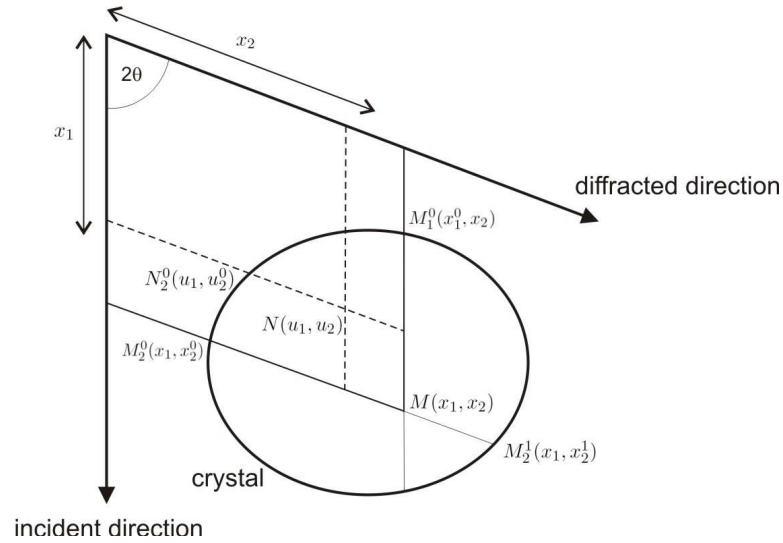


Figure 2.8.: Section of the crystal in the diffraction plane indicating a point $M(x_1|x_2)$ inside the crystal.

vector \mathbf{L} . $\sigma(\epsilon_1)$ is considered to be constant over the crystal volume and only dependent on the average domain size and shape. The quantity Q , the average cross-section per unit volume, is obtained by integrating $\sigma(\epsilon_1)$ over ϵ_1 , which results in

$$Q = \left| \frac{FK}{V} \right|^2 \lambda^3 / \sin(2\theta). \quad (2.80)$$

The kinematical integrated intensity \mathcal{P}_k is:

$$\mathcal{P}_k = \int P_k(\epsilon_1) d\epsilon_1 = \mathcal{I}_0 v Q. \quad (2.81)$$

So if extinction effects are present, the observed integrated intensity \mathcal{P} reduces to

$$\mathcal{P} = \mathcal{P}_k \cdot y \quad (2.82)$$

with y being the extinction factor, which needs to be calculated. By solving the transfer equations with an ansatz of the form $I(x_1, x_2) = a(x_1, x_2) \exp(-\sigma x_2)$ or $I_0(x_1, x_2) = b(x_1, x_2) \exp(-\sigma x_1)$ one can express the diffracted beam intensity at point $M(x_1|x_2)$ after the beam has been rescattered at $N(u_1|u_2)$ (Appendix A of [51]):

$$I_0(x_1, x_2) = \mathcal{I}_0 \exp[-\sigma(x_1 - x_1^0)] + \sigma^2 \{ \exp[-\sigma(x_1 + x_2)] \int_{x_1^0}^{x_1} du_1 \int_{u_2^0}^{x_2} I_0(u_1, u_2) \exp[\sigma(u_1 + u_2)] du_2 \} \quad (2.83)$$

Using 2.78 with $I_0(x_1, x_2)$ and the beam path length $\overline{MM_2^1}$ the power of the diffracted beam writes as

$$P(\epsilon_1) = \sigma \int_v I_0(x_1, x_2) \exp[-\sigma(x_2^1 - x_2)] dv. \quad (2.84)$$

One can define a function $\varphi(\sigma)$ so that

$$P(\epsilon_1) = \mathcal{I}_0 v \sigma \varphi(\sigma) = P_k(\epsilon_1) \varphi(\sigma). \quad (2.85)$$

Integrating Eq. 2.85 over ϵ_1 with the help of

$$\int f(x)g[h(x)]dx = \int f(x)dx \frac{\int h(x)g[h(x)]}{\int h(x)dx} \quad (2.86)$$

yields with Eq. 2.82

$$y = Q^{-1} \int \sigma \varphi(\sigma) d\epsilon_1. \quad (2.87)$$

Therefore, the extinction factor is dependent on the functions $\varphi(\sigma)$, which describes the manifold rescattering before point M is reached, and $\sigma(\epsilon_1)$, which has to be evaluated for different crystal shapes in dependence on the mean domain radius and mosaicity. The function $\varphi(\sigma)$ can be obtained by using Eq. 2.83 p iterative times, which accounts for $2p$ -fold energy exchange between the incident and the diffracted beam. As Eq. 2.83 contains a quadratic term in σ each iteration adds a term in which the power in σ is increased by 2. Hence, $\varphi(\sigma)$ can be expressed as a power series in σ (Appendix B of [51]):

$$\varphi(\sigma) = 1 - \sigma t^{(1)} + \frac{\sigma^2}{2!} t^{(2)} + \dots + (-1)^n \frac{\sigma^n}{n!} t^{(n)} + \dots \quad (2.88)$$

with the total beam path length

$$t^{(n)} = \sum_{j=0}^n \binom{n}{j}^2 v^{-1} \int_v dv t_1^j t_2'^{n-j}, \quad (2.89)$$

where t_1 and t'_2 represent the distances $\overline{M_1^0 M}$ and $\overline{M M_2^1}$, respectively. Assuming a crystal with a convex limiting surface the diffracting cross section $\sigma(\epsilon_1)$ can be expressed as (Appendix C [51])

$$\sigma(\epsilon_1) = Qv^{-1} \int_v dv \cdot \alpha \cdot \frac{\sin^2(\pi\epsilon_1\alpha)}{(\pi\epsilon_1\alpha)^2}, \quad (2.90)$$

where

$$\alpha = l \sin(2\theta/\lambda) \quad (2.91)$$

with l being the thickness of the crystal parallel to the diffracted beam. In order to include secondary extinction effects the misorientation angle η of the various crystallites has to be taken into account. Hence, the deviation of the ideal Bragg angle is now $(\epsilon_1 + \eta)$ and the diffracting cross-section becomes

$$\bar{\sigma}(\epsilon_1) = \int \sigma(\epsilon_1 + \eta) W(\eta) d\eta, \quad (2.92)$$

where $W(\eta)$ is the angular distribution of the misorientation. Eq. 2.92 corresponds to a convolution of σ and W and represents two broadening effects on the reflection curve, which are the mean particle size \bar{t} and the mean angular misorientation g , respectively. As Eqs. 2.76 describe the transfer of intensity they are physically more realistic for treating secondary extinction, where the diffraction is incoherent due to the misorientation of the crystallites. In the case of primary extinction, which is characterized by the interference of coherently scattered beams, they are, however, a reasonable approximation. In practice, the complicated Eq. 2.87 is reduced to an analytical expression by fitting Eq. 2.93 to the numerically obtained values.

$$y_i = \left\{ 1 + 2x_i + \frac{A_i(\theta)x_i^2}{1 + B_i(\theta)x_i} \right\}^{-1/2} \quad (2.93)$$

The index i is p or s for primary or secondary extinction, respectively. The functions x_i , $A_i(\theta)$ and $B_i(\theta)$ are given below [$\bar{\alpha}$ is the mean value of α (Eq. 2.91), G and L stand for Gaussian or Lorentzian crystallite distributions, \bar{T} is the mean path length through the whole crystal].

$$x_p = \frac{2}{3} Q \bar{\alpha} \bar{t} \quad (2.94)$$

$$x_s = \frac{2}{3}Q\alpha_{G,L}\bar{T} \quad (2.95)$$

$$\alpha_G = \bar{\alpha} / \left(1 + \frac{\bar{\alpha}^2}{2g^2}\right)^{1/2} \quad (2.96)$$

$$\alpha_L = \bar{\alpha} / \left(1 + \frac{2\bar{\alpha}}{3g}\right)^{1/2} \quad (2.97)$$

$$A_p(\theta) = 0.2 + 0.45 \cos 2\theta \quad (2.98)$$

$$B_p(\theta) = 0.22 - 0.12(0.5 - \cos 2\theta)^2 \quad (2.99)$$

$$A_{s,G}(\theta) = 0.58 + 0.48 \cos 2\theta + 0.24 \cos^2 2\theta \quad (2.100)$$

$$B_{s,G}(\theta) = 0.02 - 0.025 \cos 2\theta \quad (2.101)$$

$$A_{s,L}(\theta) = 0.025 + 0.285 \cos 2\theta \quad (2.102)$$

$$B_{s,L}(\theta) = 0.15 - 0.2(0.75 - \cos 2\theta)^2 \quad \text{if } \cos 2\theta > 0 \quad (2.103)$$

$$\bar{B}_{s,L}(\theta) = -0.45 \cos 2\theta \quad \text{if } \cos 2\theta < 0 \quad (2.104)$$

The final approximation for the extinction factor y is

$$y \simeq y_p \cdot y_s. \quad (2.105)$$

An application of the Becker and Coppens model to the treatment of flipping ratios has been reviewed in [54]. The transfer equations (Eqs. 2.76) for the intensities of the two different spin states [55] can be expressed as

$$\begin{aligned} \frac{\partial I_0^+}{\partial x_1} &= -\bar{\sigma}^+ I_0^+ + \bar{\sigma}^{++} I^+ + \bar{\sigma}^{-+} I^- \\ \frac{\partial I^+}{\partial x_2} &= -\bar{\sigma}^+ I^+ + \bar{\sigma}^{++} I_0^+ + \bar{\sigma}^{-+} I_0^- \\ \frac{\partial I_0^-}{\partial x_1} &= -\bar{\sigma}^- I_0^- + \bar{\sigma}^{--} I^- + \bar{\sigma}^{+-} I^+ \\ \frac{\partial I^-}{\partial x_2} &= -\bar{\sigma}^- I^- + \bar{\sigma}^{--} I_0^- + \bar{\sigma}^{+-} I_0^+, \end{aligned} \quad (2.106)$$

using the Becker and Coppens notation, where again I_0^\pm and I^\pm refer to the incident and diffracted intensities, + and - indicates the spin state of the neutrons. Here $\bar{\sigma}^{ij}$ denotes the diffracting cross-section for an incident neutron in spin state i to be diffracted in spin

state j . $\bar{\sigma}^+$ and $\bar{\sigma}^-$ represent the total diffraction cross-section for incident neutrons in a given spin state according to

$$\begin{aligned}\bar{\sigma}^+ &= \bar{\sigma}^{++} + \bar{\sigma}^{+-} \\ \bar{\sigma}^- &= \bar{\sigma}^{--} + \bar{\sigma}^{-+}.\end{aligned}\tag{2.107}$$

In contrast to the unpolarized neutron case the diffraction cross-sections $\bar{\sigma}^{ij}$ differ from each other by $|F^{ij}|$:

$$\begin{aligned}\bar{\sigma}^{++}(\epsilon_1) &= \chi(\epsilon_1)|F^{++}|^2 = \chi(\epsilon_1)|F_N + q^2 F_M|^2 \\ \bar{\sigma}^{--}(\epsilon_1) &= \chi(\epsilon_1)|F^{--}|^2 = \chi(\epsilon_1)|F_N - q^2 F_M|^2 \\ \bar{\sigma}^{+-}(\epsilon_1) &= \bar{\sigma}^{-+}(\epsilon_1) = \chi(\epsilon_1)|F^{+-}|^2 = \chi(\epsilon_1)|F_M|^2 q^2 (1 - q^2),\end{aligned}\tag{2.108}$$

where $\chi(\epsilon_1)$ is a Lorentzian or Gaussian function of ϵ_1 and q is the geometrical factor described in Sec. 2.1. Generally, the cross-section $\bar{\sigma}^{+-}$ is very small and the values of q^2 are close to 1, so that if $\bar{\sigma}^{+-}$ is assumed as zero, Eqs. 2.108 reduce to Eqs. 2.76 and a solution can be found in the same manner like for the unpolarized case. If the perturbing effect of the spin-flip term is too big, it can be corrected by a method described in the Appendix of [55], where the intensities I^+ and I^- are expressed as Taylor-series expansions around $x = 0$ only keeping terms up to second order.

Finally, the observed flipping ratio R can be calculated by correcting the kinematical flipping ratio R_k according to

$$R = R_k \frac{y^+}{y^-},\tag{2.109}$$

where both y^+ and y^- fulfill the assumption of Eq. 2.105. The correction factor of secondary extinction for a Lorentzian distribution of crystallites, which is commonly the case, is given by

$$y_s^\pm = \sum_{n=0}^{\infty} \left(-\frac{Q\alpha_L y_p}{3} \right)^n \binom{2n}{n} \frac{\overline{T^{(n)}}}{n!} \quad \text{with } \alpha_L = \left(\frac{\lambda}{t \sin 2\theta} + \frac{2}{3g} \right)^{-1}\tag{2.110}$$

The different correction factors for the two spin states originate from the different values of Q , which contains the structure factor (see Eq. 2.80). The correction factor y_p^\pm for primary extinction remains the one given in Eq. 2.93.

2.4.2. The extinction model implemented in FullProf

The extinction model used in FullProf is an empirical model and represents a compromise to cover both primary and secondary extinction. It is also implemented in the Shelx program [56] and has shown to work well in practice, although the expression for the extinction factor does not correspond to any of those in the literature. The extinction factor, which is most similar to the treatment in [57], is given by

$$y = \left(1 + \frac{0.001x F_c^2 \lambda^3}{4 \sin(2\theta) (\sin \theta / \lambda)^2} \right)^{-\frac{1}{2}}, \quad (2.111)$$

where x is the refinable isotropic extinction parameter and F_c is the calculated structure factor.

FullProf is complemented by an anisotropic extinction model, where the isotropic parameter x is replaced by x_{aniso} , a tensor acting subsequently on the scattering vector (hkl):

$$x_{aniso} = \left[\begin{pmatrix} x_{11} & x_{12} & x_{13} \\ 0 & x_{22} & x_{23} \\ 0 & 0 & x_{33} \end{pmatrix} \begin{pmatrix} h \\ k \\ l \end{pmatrix} \right] \begin{pmatrix} h \\ k \\ l \end{pmatrix} = x_{11}h^2 + x_{22}k^2 + x_{33}l^2 + x_{12}hk + x_{13}hl + x_{23}kl. \quad (2.112)$$

By applying this formalism and refining the parameters x_{ij} one can empirically correct extinction effects, which can vary considerably for different families of (hkl) reflections.

The extinction correction for flipping ratios used in FullProf is based on the formalism presented in [54]. The observed flipping ratio for centrosymmetric crystal structures (real structure factors) is written as

$$R = \frac{(F_N^2 + q^2 F_M^2) p_p^+ + 2q^2 F_N F_M p_m^+ + (1 - q^2) q^2 F_M^2 y_{pm}}{(F_N^2 + q^2 F_M^2) p_p^- + 2q^2 F_N F_M p_m^- + (1 - q^2) q^2 F_M^2 y_{pm}} \quad (2.113)$$

with the correction terms

$$p_p^\pm = \frac{1}{2} \left[(1 \pm p) \left(1 + \frac{0.001 I^+ \lambda^3 x_{aniso}}{4 \sin^2(\theta/\lambda) \sin(2\theta)} \right)^{-1/2} + (1 \mp p) \left(1 + \frac{0.001 I^- \lambda^3 x_{aniso}}{4 \sin^2(\theta/\lambda) \sin(2\theta)} \right)^{-1/2} \right] \quad (2.114)$$

$$p_m^\pm = \frac{1}{2} \left[(1 \pm p) \left(1 + \frac{0.001 I^+ \lambda^3 x_{aniso}}{4 \sin^2(\theta/\lambda) \sin(2\theta)} \right)^{-1/2} - (1 \mp p) \left(1 + \frac{0.001 I^- \lambda^3 x_{aniso}}{4 \sin^2(\theta/\lambda) \sin(2\theta)} \right)^{-1/2} \right] \quad (2.115)$$

$$y_{pm} = \left(1 + \frac{0.001(1 - q^2)q^2 F_M \lambda^3 r}{4 \sin^2(\theta/\lambda) \sin(2\theta)}\right)^{-1/2}, \quad (2.116)$$

where p is the beam polarization and I^\pm are the uncorrected intensities for a spin-up and spin-down beam, respectively (see Eq. 2.1).

2.5. Molecular orbitals and basis sets

For describing the electronic properties of a molecule or an isolated cluster it is not sufficient just to consider atomic orbitals (AOs) as bonding effects play a considerably large role in the deformation of valence orbitals due to hybridization. Thus it is more reasonable to use molecular orbitals $\psi(\mathbf{r})$ (MO), which are the linear combination of basis functions $\phi(\mathbf{r})$ emerging from the AO wave functions with respect to a certain basis set:

$$\psi_i(\mathbf{r}) = \sum_j c_j \phi_j(\mathbf{r}) \quad (2.117)$$

In principle, any set of mathematical functions can be used, since the coefficients c_j of the basis functions in the final MO are selected by the variation function to minimize the self-consistent field (SCF) energy, i.e. inadequate basis functions will simply appear with small or zero coefficients. However, the choice of the basis set will depend on the atoms and properties to be studied. The first basis sets were developed by J. C. Slater, who used Slater-type orbitals (STOs) [58], whose general expression is given as

$$s = N \exp(-\zeta r). \quad (2.118)$$

STOs are quite accurate, but very tedious in calculation. S. F. Boys came up with an alternative when he developed the Gaussian-type orbital (GTO) [59]:

$$g = N \exp(-\alpha r^2) \quad (2.119)$$

The difference between the GTO and the STO lies in the radial dependence. The GTO squares the radius so that the product of two Gaussians is another Gaussian (Gaussian Product Theorem), which makes the equations easy to handle and reduces computational effort. The loss of accuracy is compensated by combining several Gaussian equations.

The general equation for a GTO g is given by

$$g(x, y, z, \alpha) = N x^m y^n z^o \exp(-\alpha[x^2 + y^2 + z^2]), \quad (2.120)$$

where N is a normalization factor and α is the orbital exponent. The variables x , y and z are cartesian coordinates. The quantities m , n and o are not quantum numbers but simply integral exponents at cartesian coordinates. When $m + n + o = 0$, then g is said to be a s-type Gaussian function; when $m + n + o = 1$, then g is a p-type Gaussian; and

when $m + n + o = 2$, then g is a d-type Gaussian.

Minimum basis sets simply consist of one basis function for every AO under consideration, thus this concept is not very suited to describe molecular charge distributions. The smallest basis set, which should be used to account for bonding effects, is a *Split Valence Basis* (SVB). In this set the inner shell atomic orbitals are built by a single contracted Gaussian-type orbital (CGTO), while the valence shell is described by two basis functions. This concept bears the advantage of a more accurate representation of the actual orbital due to increased flexibility. Widely used SVB sets are the 3-21G [60–62] and the 6-21G [62–64] basis sets for elements up to Ar and Xe, respectively. If higher accuracy is required than attainable with a SVB, then a *Triple Zeta Valence* (TZV) basis [65] should be employed, where the valence shell is represented by three basis functions (eqs. 2.123-2.125), thus giving even more flexibility to the molecular orbitals.

As mentioned above SVBs provide two basis functions for the valence shell, e.g. the Co3d shell. The inner part consists of a linear combination of two CGTOs, where $d_{3d,k}$ are the 3d shell contraction coefficients, according to Eq. 2.121 [62].

$$\phi'_{SVB,3d}(x, y, z) = \sum_{k=1}^2 d'_{3d,k} g_d(x, y, z, \alpha'_{3d,k}) \quad (2.121)$$

The outer part is represented by a single primitive GTO (Eq. 2.122).

$$\phi''_{SVB,3d}(x, y, z) = g_d(x, y, z, \alpha''_{3d}) \quad (2.122)$$

The values of α and $d_{3d,k}$ are determined by those GTOs, that minimize the SCF energies of the respective atoms, and are stored in ab initio calculation packages. According to a TZV basis a 3d orbital is constructed as follows:

$$\phi'_{TZV,3d}(x, y, z) = \sum_{k=1}^4 d'_{3d,k} g_d(x, y, z, \alpha'_{3d,k}) \quad (2.123)$$

$$\phi''_{TZV,3d}(x, y, z) = g_d(x, y, z, \alpha''_{3d}) \quad (2.124)$$

$$\phi'''_{TZV,3d}(x, y, z) = g_d(x, y, z, \alpha'''_{3d}) \quad (2.125)$$

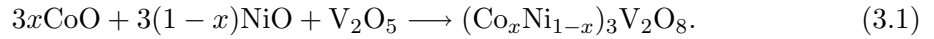
When atoms are brought close together, their charge distribution causes a polarization effect, which distorts or polarizes the shape of the atomic orbitals. The consequence is

2. *Special methodology and theory*

that even more flexibility is needed for describing the orbitals than attainable with s, p, d shapes etc. in free atoms. This is best accomplished by adding basis functions of higher angular momentum quantum number. In this way e.g. an s orbital can be polarized by mixing in p orbital symmetry. Likewise, p orbitals can be polarized by adding d orbitals and d orbitals by adding f orbitals. These additional basis functions are called polarization functions and are usually added as single, non contracted GTOs.

3. Sample preparation and characterization

$(\text{Co}_x\text{Ni}_{1-x})_3\text{V}_2\text{O}_8$ powder samples have been synthesized by stoichiometrically mixing the oxides CoO, NiO and V_2O_5 according to



The starting materials have been thoroughly ground and pressed into pellets before sintering at 1050°C for one day. After further grinding the obtained powder has again been pressed into pellets and sintered for four more days. The samples have been precharacterized by X-ray diffraction at the University of Technology Darmstadt using the powder diffractometer STOE Stadi P with $\text{Mo-K}\alpha_1$ with the confirmation of the correct phase formation. Further characterization has been done on the neutron powder diffractometers D20 and D1A of the Institut Laue-Langevin as a part of the respective experiments, which will be reported in detail in Sec. 4.

$\text{Co}_3\text{V}_2\text{O}_8$ and $(\text{Co}_{0.5}\text{Ni}_{0.5})_3\text{V}_2\text{O}_8$ single crystals have been grown from self-flux in a ZrO_2/Y crucible by the slow cooling method by Dr. Thomas Wolf, which is thankfully acknowledged. After selecting high quality single crystals by short experiments on the Laue diffractometer Orient Express, the chosen crystals have been examined on the single crystal diffractometers D9, D10 and D15 (ILL) confirming the correct phase formation. The remaining single crystals have been checked for parasitic phases by grinding and investigating them at the powder diffractometer D20 with satisfying result.

4. Results

4.1. $\text{Co}_3\text{V}_2\text{O}_8$

The magnetic phase diagram and the magnetic structures of $\text{Co}_3\text{V}_2\text{O}_8$ have been extensively investigated by several groups [6, 11–13, 16, 18], so the aim of this study is to focus the magnetic structures in more detail. Until this point only spherical magnetization density distribution on the Co^{2+} ions has been assumed in order to refine the magnetic structure models. By applying the techniques of polarized neutron diffraction and magnetic Compton scattering results shall be obtained which, due to their precision, should allow an aspheric description of the magnetic form factors of Co. In this regard *ab initio* molecular orbital wave functions have been calculated to represent the respective density distributions as accurately as possible. In order to obtain precise magnetic structure factors from observed flipping ratios, the nuclear structure factors have to be determined accurately, especially with regard to extinction, which plays a dominant role in this study.

4.1.1. Nuclear structure within the paramagnetic phase

The nuclear structure of a chosen $\text{Co}_3\text{V}_2\text{O}_8$ single crystal of approximately 50 mm^3 has been investigated at the hot neutron four-circle diffractometer D9 (ILL). The diffractometer is used for precise and accurate measurements of Bragg intensities up to very high momentum transfer. Due to the availability of short wavelengths, the instrument is very well suited for high resolution structure determination because a large part of reciprocal space can be explored. The wavelength can continuously be chosen between 0.25 and 0.85 Å by selecting the take-off angle of a Cu(200) monochromator in transmission geometry. $\lambda/2$ contributions are suppressed by the use of resonance filters. A $64 \times 64 \text{ mm}^2$ two-dimensional detector is employed, which can be used to study satellites and twinning.

Aim of this experiment has been to deduce precise nuclear structure factors, which should then be used in combination with the measured flipping ratios from the polarized neutron experiments (Sec. 4.1.4) to determine the magnetic structure factors and therewith the magnetization density. Regarding the necessity of correcting extinction effects the measurement on D9 consisted in determining the F_N of a set of more than 500 independent reflections up to $\sin \theta / \lambda = 0.92$ with two different wavelengths ($\lambda_1 = 0.835 \text{ Å}$, $\lambda_2 = 0.512$

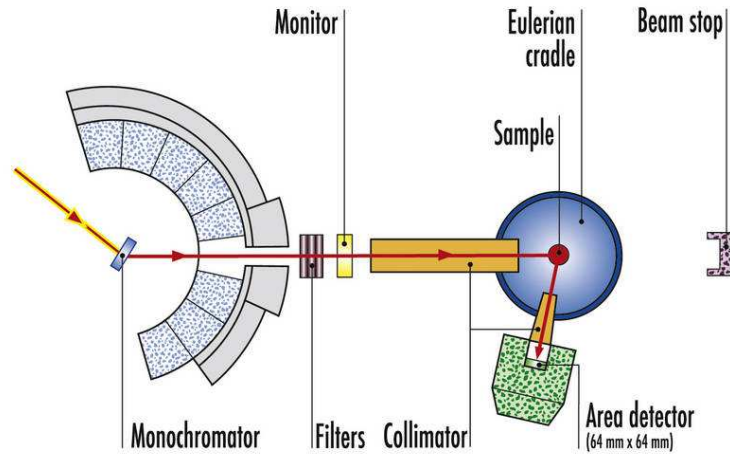


Figure 4.1.: Instrument layout of the hot neutron four-circle diffractometer D9.

Å). Only by measuring the same set of reflections with different wavelengths one can adequately reveal the wavelength dependent extinction effects. The data collection has been performed in the paramagnetic phase at $T = 13.5$ K, which is just above the Néel temperature of 11.2 K. In order to be able to apply precise absorption and extinction corrections the crystal shape has been modeled (Fig. 4.2) with 15 delimiting faces for the calculation of the beam path lengths \bar{t} . The observed integrated intensities have been corrected for absorption by applying the transmission factor integral $\exp[\mu(\bar{t}_{in} + \bar{t}_{out})]$ and analyzed by simultaneously fitting a structure model to both datasets with λ_1 and λ_2 using the programs CCSL [49] and FullProf [50]. Due to the application of different extinction models, all independent reflections were used for the CCSL refinement (beampath dependent extinction model), while for the use of FullProf the symmetry-equivalent reflections have been merged (empirical extinction model).

The orthorhombic space group $Cmca$ could be confirmed and the refinement of the orientation matrix yielded the cell constants $a = 6.015(3)$ Å, $b = 11.480(5)$ Å and $c = 8.289(4)$ Å after the sample has been aligned by centering 40 reflections. The subsequent structure refinement process included the atomic positions and isotropic temperature factors of Co and O plus additional extinction parameters. The atomic position and temperature factor of V have been fixed in all refinements, because of its low coherent neutron scattering cross section. However, every attempt of refining the extinction parameters with the CCSL program by applying the derivative integral $(\bar{t}_{in} + \bar{t}_{out}) \exp[\mu(\bar{t}_{in} + \bar{t}_{out})]$ according to the Becker and Coppens model [51] resulted in a divergence of the refinement process, which is presumably due to severe extinction effects. Due to this reason, the domain radius,

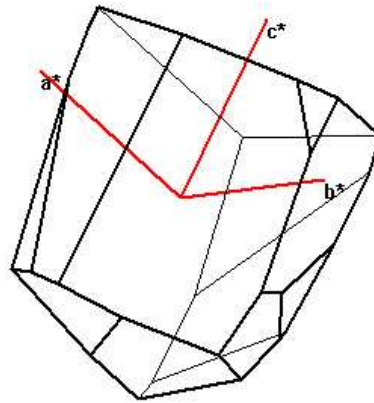


Figure 4.2.: Shape model of the investigated single crystal for the calculation of the respective beam path lengths.

which is the diverging parameter, was set to 9999 nm, the largest value readable by the CCSL. The agreement between the calculated and the observed nuclear structure factor is still quite good, which is expressed by $R=6.1$. The refined parameters can be seen in the upper part of Tab. 4.1.

In contrast, a refinement using the more stable empirical model implemented in FullProf succeeded. An anisotropic Shelx-like model was employed, where only the diagonal elements of the orientation tensor have been used and refined. The large extinction effects are manifest for the (240) reflection with $y = 0.19(3)$. The calculated nuclear structure factors show similarly good agreement with the observed ones ($R=5.3$ and $R=5.5$ for the λ_1 and λ_2 dataset, respectively), which can be seen in Fig. 4.3. The resulting structural parameters are given in the lower part of Tab. 4.1. Within the error bars the refined structure models are the same for both refinement programs with exception of the temperature factors and the O1 z -value, which is a consequence of the different extinction models.

Table 4.1.: Structural parameters of the investigated $\text{Co}_3\text{V}_2\text{O}_8$ single crystal sample resulting from a refinement using the CCSL (upper part) and FullProf (lower part).

Atom	x	y	z	$B(\text{\AA}^2)$
Co1	0	0	0	0.12(6)
Co2	$\frac{1}{4}$	0.1332(4)	$\frac{1}{4}$	0.03(4)
V	0	0.3773	0.1204	0.30
O1	0	0.2498(2)	0.2281(2)	0.22(2)
O2	0	0.0011(2)	0.2444(2)	0.24(2)
O3	0.2707(1)	0.1182(1)	0.9984(1)	0.19(2)

Extinction parameters

Domain radius(nm): 9999 Mosaicity spread(rad): 0.432(6)

Co1	0	0	0	0.27(10)
Co2	$\frac{1}{4}$	0.1328(7)	$\frac{1}{4}$	0.20(7)
V	0	0.3773	0.1204	0.30
O1	0	0.2489(3)	0.2700(4)	0.38(4)
O2	0	0.0008(4)	0.2448(4)	0.33(4)
O3	0.2702(3)	0.1185(3)	0.9990(2)	0.33(4)

Extinction parameters

$x_{11}=1.0(1)$ $x_{22}=0.36(5)$ $x_{33}=0.6(1)$

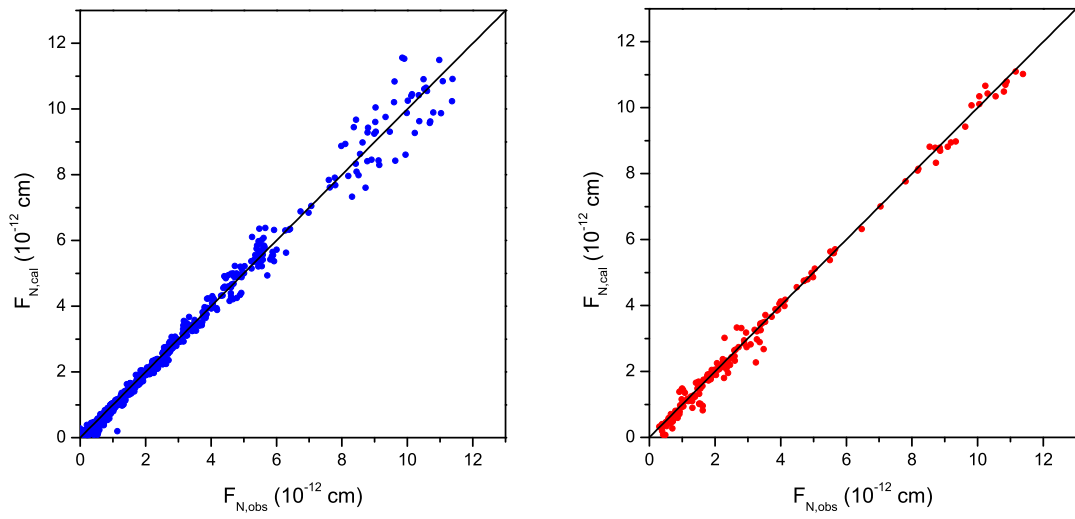


Figure 4.3.: Illustration of the fit results in a F_{obs} vs. F_{cal} plot using the CCSL (left) and FullProf (right).

4.1.2. Nuclear structure in the ferromagnetic phase

As the flipping ratio measurement has been carried out within the ferromagnetic phase it is an important detail to verify, if the system does not undergo any significant changes concerning the nuclear structure due to phase transitions or magnetostriction. Using insufficiently precise nuclear structure factors will affect the observed magnetic structure factors in the flipping ratio measurement. This is why an additional nuclear structure investigation has been undertaken at the single crystal thermal neutron diffractometer D15 (ILL). The instrument has been operated in normal-beam mode as a vertical cryomagnet has been used in order to apply a magnetic field of $H=2$ T along the crystallographic a direction. Three different wavelengths are available, from which $\lambda=0.85\text{\AA}$ [Cu(331) reflection in transmission mode] had to be chosen despite the loss of flux in order to guarantee identical absorption and extinction effects as with the polarized neutron experiment, which has been performed with $\lambda=0.84\text{\AA}$. The temperature has been set to 3.5 K

A preliminary part of the experiment has been performed at $T=13.5$ K, the same temperature as the nuclear structure investigation within the paramagnetic phase. A number of 40 reflections has been centered in order to orient the single crystal inside the cryomagnet. From the obtained angles a first orientation matrix has been deduced by refining the wavelength, the γ and the ν offset, but leaving the cell parameters constant as they have been precisely determined on D9. The same reflections have been used in order to orient the sample at the experimental conditions of $T=3.5$ K and $H=2$ T. This time the previously refined values for the wavelength, the γ and the ν offset ($\lambda=0.85368\text{\AA}$, $\gamma_{off}=-0.09^\circ$, $\nu_{off}=0.015^\circ$) have been set as constant, while the cell parameters have been refined. The obtained values of $a=6.006(6)\text{\AA}$, $b=11.451(7)\text{\AA}$ and $c=8.278(6)\text{\AA}$ indicate that no significant change of the cell dimensions has taken place.

The actual experiment consisted in measuring the integrated intensities of those reflections, for which flipping ratios have been measured. After absorption and extinction corrections have been applied the measured values correspond to

$$I \sim F_N^2 + Q_M^2 = F_N^2 + q^2 F_M^2, \quad (4.1)$$

where the proportionality factor is the scale factor. Introducing γ Eq. 4.1 can be rewritten as

$$I \sim F_N^2(1 + q^2\gamma^2), \quad (4.2)$$

i.e. the magnetic contribution to the integrated intensities can be canceled out by using the previously measured flipping ratios. That way the nuclear structure can be analyzed even while measuring within the ferromagnetic phase. The nuclear structure refinement process has been performed using the same parameters as described in the previous section and confirmed the nuclear structure concerning the atomic parameters listed in Tab. 4.1. Slight deviations of the temperature factors and extinction parameters have been observed, but the results from the previous section are regarded as much more reliable: firstly, due to the fact that extinction effects are better handled because of having used two different wavelengths and secondly, because the intensities of certain reflections can be attenuated by the pillars of the cryomagnet. The conclusion of this experiment is that the derivation of the F_M from observed flipping ratios by using the observed F_N at $T = 13.5$ K is justified.

All low-angle nuclear reflections suffer considerably from extinction, therefore, special attention has been paid to the extinction of magnetic scattering. As the flipping ratio treatment uses the same extinction parameters for both nuclear and magnetic scattering, it is important to verify, if the extinction effects are indeed comparable. Therefore, three strong magnetic reflections have been measured as a function of applied magnetic field after the sample has been cooled in zero-field to 3.5 K. Fig. 4.4 shows the integrated intensities of three reflections after the nuclear contribution has been subtracted. The field dependence of the magnetic contribution reveals a surprising and interesting tendency: Instead of increasing with increasing applied field, as one would expect if the cross-tie site gets saturated, the intensity of magnetic scattering drops significantly. This observation can be explained with field dependent increase of primary extinction. At $H=0$ T the sample exhibits a multidomain state with presumably negligible extinction effects. By increasing the field the magnetic domains grow until they reach approximately the size of the structural domains. On reaching saturation at $H \approx 0.25$ T the primary extinction effects for magnetic scattering should be comparable to those of nuclear scattering. The mosaicity which governs secondary extinction should a priori not be affected.

In order to verify these assumptions the extinction correction factor y has been calculated for three magnetic reflections according to the anisotropic FullProf model (see Sec.2.4.2). The calculated values have been compared with the observed ones, which can easily be deduced from the intensity ratios at $H=0$ T and $H=0.25$ T. The results are listed in Tab. 4.2. It can be seen that the calculated extinction factors are to a greater or lesser extent comparable with the observed ones. Nevertheless, the extinction of magnetic scattering seems to be underestimated.

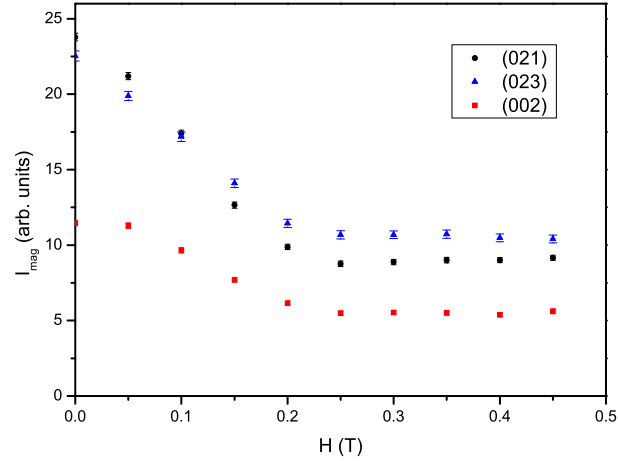


Figure 4.4.: Intensity of three different magnetic reflections in dependence of an applied magnetic field revealing primary extinction effects.

Table 4.2.: Observed and calculated extinction correction parameters for three low-angle magnetic reflections.

(hkl)	$\sin \theta / \lambda$ (\AA^{-1})	$F_{M,obs}$ (10^{-12} cm)	y_{obs}	y_{cal}
(021)	0.10595	4.87(1)	0.39(7)	0.46(3)
(002)	0.12064	3.39(1)	0.47(6)	0.64(3)
(023)	0.20083	4.72(1)	0.47(6)	0.60(3)

4.1.3. Ab initio calculations using the GAMESS code

The General Atomic and Molecular Electronic Structure System (GAMESS) [66, 67] is a general ab initio quantum chemistry package, which can compute self-consistent field (SCF) molecular wave functions using different Hartree-Fock models. The motivation for calculating such a wave function in connection with the aims of this thesis work is that its square represents the electron density distribution:

$$|\phi(\mathbf{r})|^2 = \rho(\mathbf{r}) \quad (4.3)$$

or the magnetization density if the difference between the majority and minority states is concerned:

$$|\phi_{\uparrow}(\mathbf{r})|^2 - |\phi_{\downarrow}(\mathbf{r})|^2 = \rho_{mag}(\mathbf{r}) \quad (4.4)$$

In this way experimental spin and magnetization density data can be compared with theoretical predictions. The following results have been obtained using the version PC GAMESS [68]. The two different clusters Co_cO_6 and Co_sO_6 (Fig. 4.5) were modelled separately. The calculations were performed within the framework of the Kohn-Sham formulation of the density functional. The functional B3LYP was employed to approximate the exchange-correlation interaction. The B3LYP is a hybrid model, well adapted to study transition metal compounds and magnetic interactions, in which a predefined amount of the exact Hartree-Fock exchange is added to the well known pure density functionals [69–72]. For the atoms in the clusters Ahlrich’s pVDZ AO basis set [73] $\text{Co}(14s,8p,5d,1p)/[5s,2p,2d,1p], \text{O}(7s,4p,1d)/[3s,2p,1d]$ has been employed. The notations (klm) and [klm] indicate the number of Gaussian type orbitals and contracted Gaussian type orbitals, respectively. The orbital exponents and contraction coefficients for the Co and O orbitals, which minimize the SCF energies are listed in Appendix B.1.

In order to mimic the Madelung potential, the two quantum mechanical clusters were surrounded by point charges (PC) according to the Effective Fragment Potential (EFP) method [74]. The EFP method replaces the chemically inert part of the system by EFPs, while performing a regular ab initio calculation on the chemically active part. The inert parts interact with the active part through non-bonded interactions and of course affect the *ab initio* wave functions. As previously reported for other systems [75–78], the choice of the embedding method was shown to be crucial for the physical meaning of the *ab initio* calculations. For a point charge sphere of $r = 7.5 \text{ \AA}$ around the CoO_6 cluster the calculation yielded reasonable spin density distributions on the respective ions, although spheres

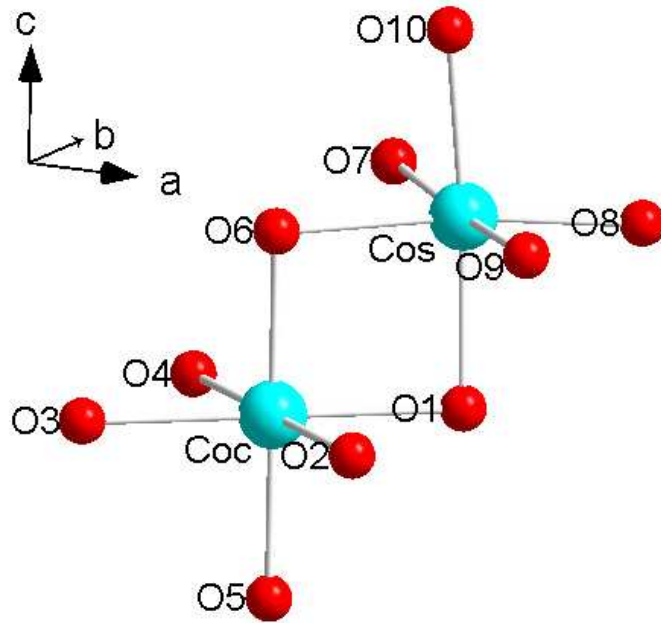


Figure 4.5.: Visualization of the two different clusters Co_cO_6 and Co_sO_6 . Co_c and Co_s are located at positions $(0,0,0)$ and $(\frac{1}{4}, 0.1332, \frac{1}{4})$, respectively.

are not recommendable for building up Madelung potentials. Increasing the number of point charges to a sphere of $r = 10 \text{ \AA}$ or to $2 \times 2 \times 2$, respectively $3 \times 3 \times 3$ unit cells ends up with unreasonably high spin density on one of the oxygen ions or even non-converging calculations. The reason for such artifacts is an improper boundary between the quantum mechanical cluster and the point charges. As a result, the electron density leaks out of the cluster due to the attraction by the positive point charges. To avoid this a boundary region has been introduced, which is formed by effective core potentials (ECP) placed in the nearest cationic positions around the cluster. The objective of the ECP method is to construct potentials which are only dependent on the valence electrons, but take into account the influence of the inert, core electrons. By replacing the core electrons with an effective potential, the need for the core basis functions is eliminated, which saves computing time. Additionally, the ECP represent relativistic effects, which are largely confined to the core. Thus, the first coordination shell of Co^{2+} and V^{5+} ions has been described by ECPs according to the SBKJC ECP basis set [79]. As native ECPs for Co and V do not treat the 3s and 3p electrons as core electrons, those ECPs would in fact be too compact due to the higher number of valence electrons. In order to overcome this problem the ECPs for Mg and Al have been used due to the fact that their ionic radii are closer to those of Co and V, respectively. Except for the 3d shells, the remaining electrons are replaced by

an effective potential. Thus, 1565 PC (3x3x3 unit cells with the respective Co ion in the center) have been built to mimic the Madelung potential on the cluster. The coefficients c_j relevant to the Co3d MO (see Appendix B.2) were extracted from the simulations and used together with the chosen basis functions to build up the MO as described in Sec. 2.5.

In order to visualize the obtained MOs, the square of the wave function, corresponding to the density, is integrated along an axis of choice and plotted as a two-dimensional density plot. The projected MOs of the Co_cO_6 and Co_sO_6 clusters are shown in Fig. 4.6 and Fig. 4.7, respectively. It can clearly be seen especially for the e_g orbitals (last two rows) that hybridization effects between the Co3d and O2p orbitals cannot be neglected. Furthermore, the visualization clarifies that every single Co3d orbitals does not consist of one pure atomic orbital. This becomes evident for the $\text{Co}_c d_{xy}$ orbital which has a strong d_{yz} mixing and vice versa the $\text{Co}_c d_{yz}$ orbital which has a strong d_{xy} mixing (see AO coefficients in Appendix B.2). The fact that the Co_c and Co_s orbitals are slightly rotated for the projections along the x and y axis, respectively, results from the anisotropic kagome staircase structure and its special point charge distribution around the cluster atoms in combination with the symmetrical degree of freedom arising from the point symmetry of the respective clusters (2/m.. for Co_cO_6 , .2. for Co_sO_6 [39]).

The results of the *ab initio* calculations concerning the special shape of each MO and the obvious hybridization effects lets assume their importance for the treatment of the spin and magnetization densities. The partially strong deviation from the Co3d AOs could make a crucial difference in the refinement of the magnetic structure.

4. Results

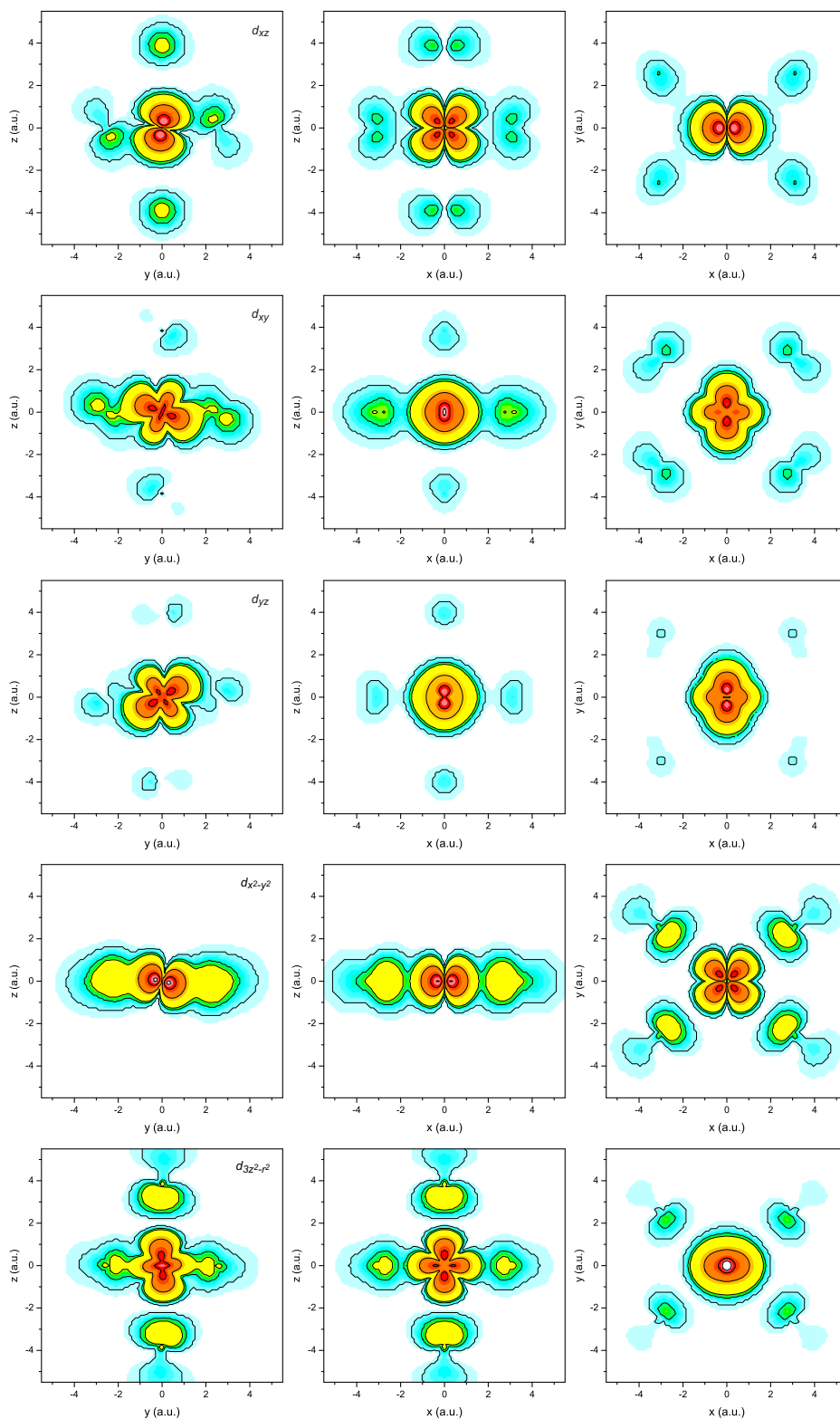


Figure 4.6.: *Ab initio* molecular orbitals corresponding to the Co3d orbitals of the Co_cO_6 cluster as projections along the principal crystallographic axes. Contour lines are drawn at 0.001, 0.003, 0.005, 0.05, 0.3 and 0.6 (arb. units).

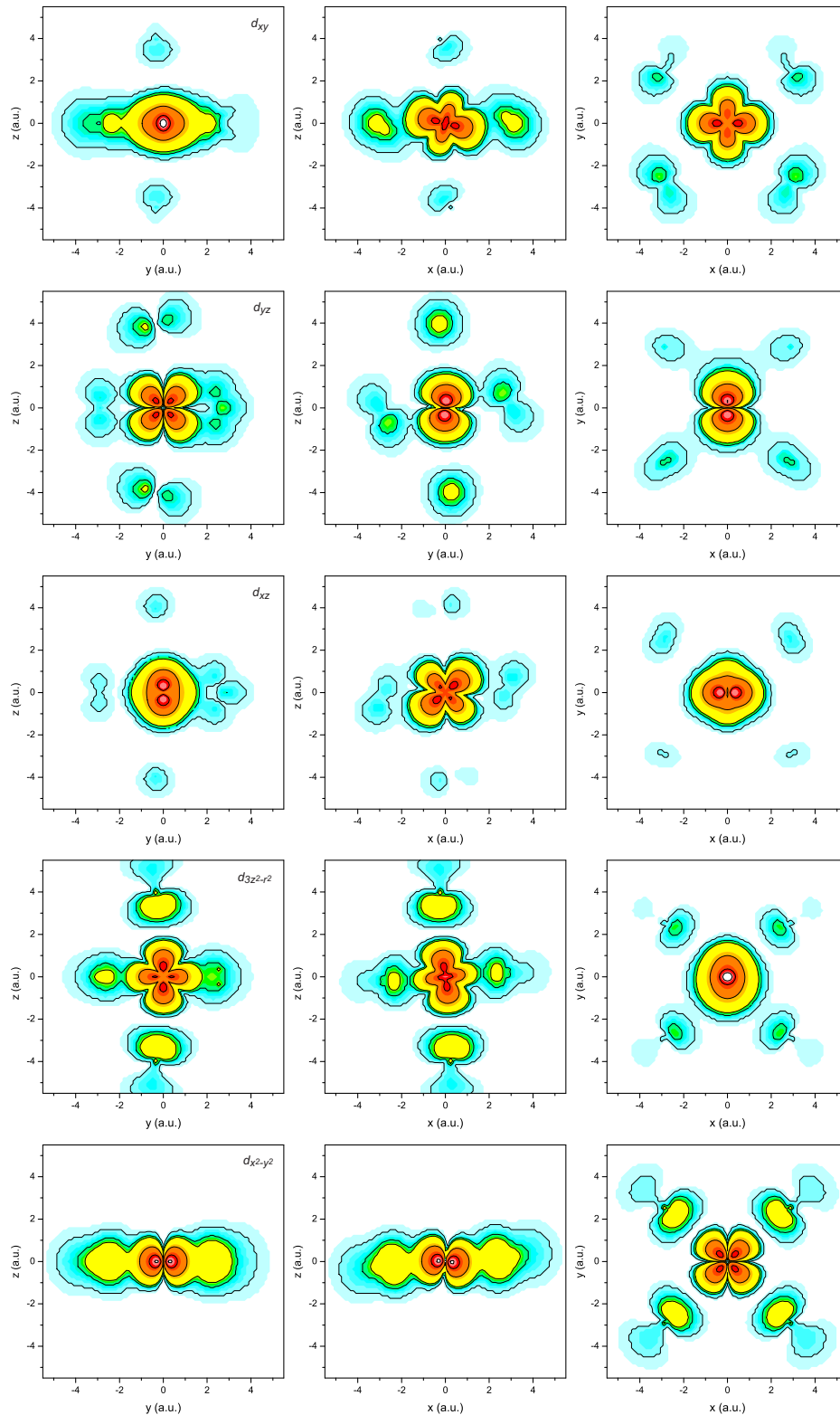


Figure 4.7.: *Ab initio* molecular orbitals corresponding to the $\text{Co}3d$ orbitals of the Co_5O_6 cluster as projections along the principal crystallographic axes. Contour lines are drawn at 0.001, 0.003, 0.005, 0.05, 0.3 and 0.6 (arb. units).

4.1.4. Magnetization density in real space

The magnetization density has been investigated at the spin polarized two-axes diffractometer 5C1, which is situated at the hot source of the Orphée reactor at the Laboratoire Léon Brillouin (Saclay). Using an incident polarized neutron beam the instrument is devoted to the determination of magnetic structure factors for magnetic form factor and magnetization density studies on single crystals. Fig. 4.8 shows the instrument layout. Neutrons emerging from the source are monochromated and polarized by the (111) reflection of a magnetized Heusler crystal Cu_2MnAl . The used wavelength is 0.84 \AA , which corresponds to the maximum flux of the hot source and is ideal for studying large domains of reciprocal space. The polarization factor of the beam is $p = -0.88$, which means that 88% of the neutrons in the incident beam are in a spin-down polarization state. The polarization direction of the incident neutron beam is defined by magnetic guide fields and can be inverted with the help of a cryogenic flipping device. The sample is mounted inside a cryomagnet, which offers a minimum temperature of 1.5 K and a maximum magnetic field of 7.5 T. The signal is detected by a lifting arm single detector (^3He counter), which covers an angular range from 0° to 123° in the horizontal and from -5° to 23° in the vertical plane. The procedure of measuring a flipping ratio of a certain (hkl) reflection consists in determining the ratio between the respective scattered intensities I^+ and I^- exactly on the peak maximum as well as off the peak on either side in order to determine the background. This procedure is called the bpb-method (background peak background). Over 500 independent reflections have been measured in this way.

As the crystal structure is centrosymmetric the experimental magnetization density can directly be reconstructed by a Fourier synthesis (Eq. 4.5) where the Fourier coefficients are the magnetic structure factors. These have been derived by solving Eq. 2.113 with respect to F_M . The correct solutions of this second-order equation have been derived iteratively with the calculated F_M as starting values using the Mathematica program [80].

$$\rho(\mathbf{r}) = \frac{1}{V} \sum_{\mathbf{q}} F(\mathbf{q}) \exp[-2\pi i(\mathbf{q}\mathbf{r})] \quad (4.5)$$

Fig. 4.9 shows the projection of the magnetization density onto the b - c plane. Like it has been assumed in Sec. 4.1.2, the Co_c does not get saturated, but significant magnetization density is present on V and O sites. While the density is quite localized for the V, O1 and O2 sites, rather diffuse density can be observed around the O3 site. The split density peaks of O1 result from the fact, that actually two O1 ions are visible in the projection. Similarly, the density around the Co_s ions seems to be much higher compared to the Co_c ions, which is due to the fact, that two Co_s ions are contained in the projection, while only

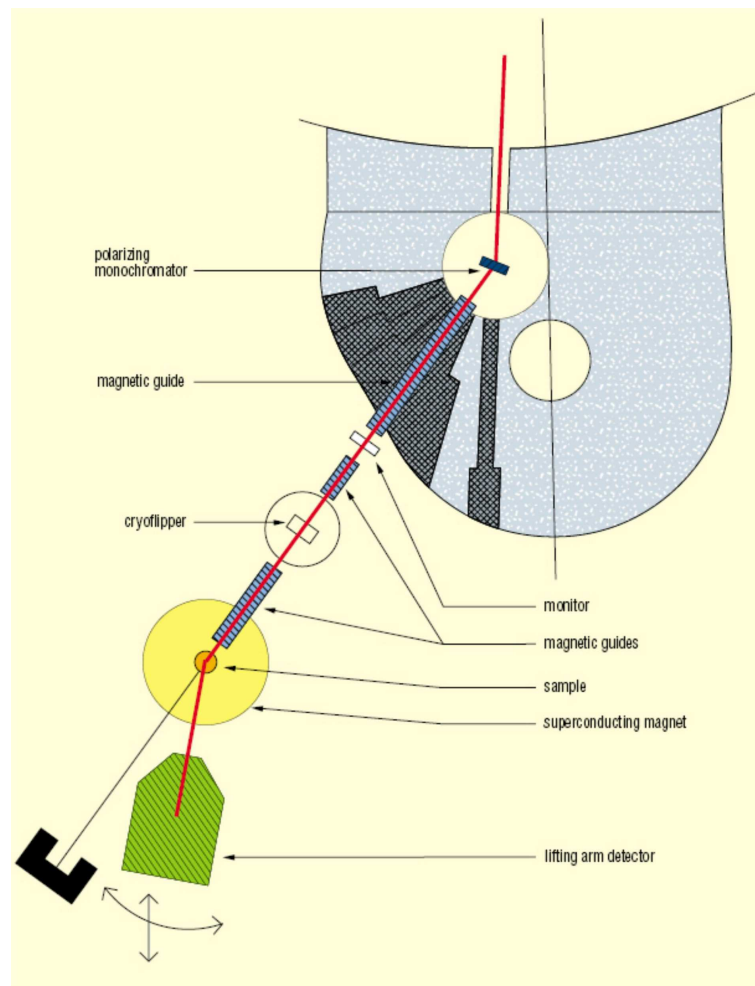


Figure 4.8.: Instrument layout of the spin polarized hot neutron two-axes diffractometer 5C1.

4. Results

one Co_c ion is projected. Besides the superexchange pathways $\text{Co}_s\text{-O2-Co}_c$ and $\text{Co}_s\text{-O3-Co}_c$ an interlayer exchange becomes evident with the non-zero magnetization density on V and O1. Further *ab initio* solid state computations are currently done to simulate the spin density map of $\text{Co}_3\text{V}_2\text{O}_8$ and to elucidate the composite mechanisms of the induced magnetic moments on the different O and V sites. This will be the subject of a forthcoming publication [81].

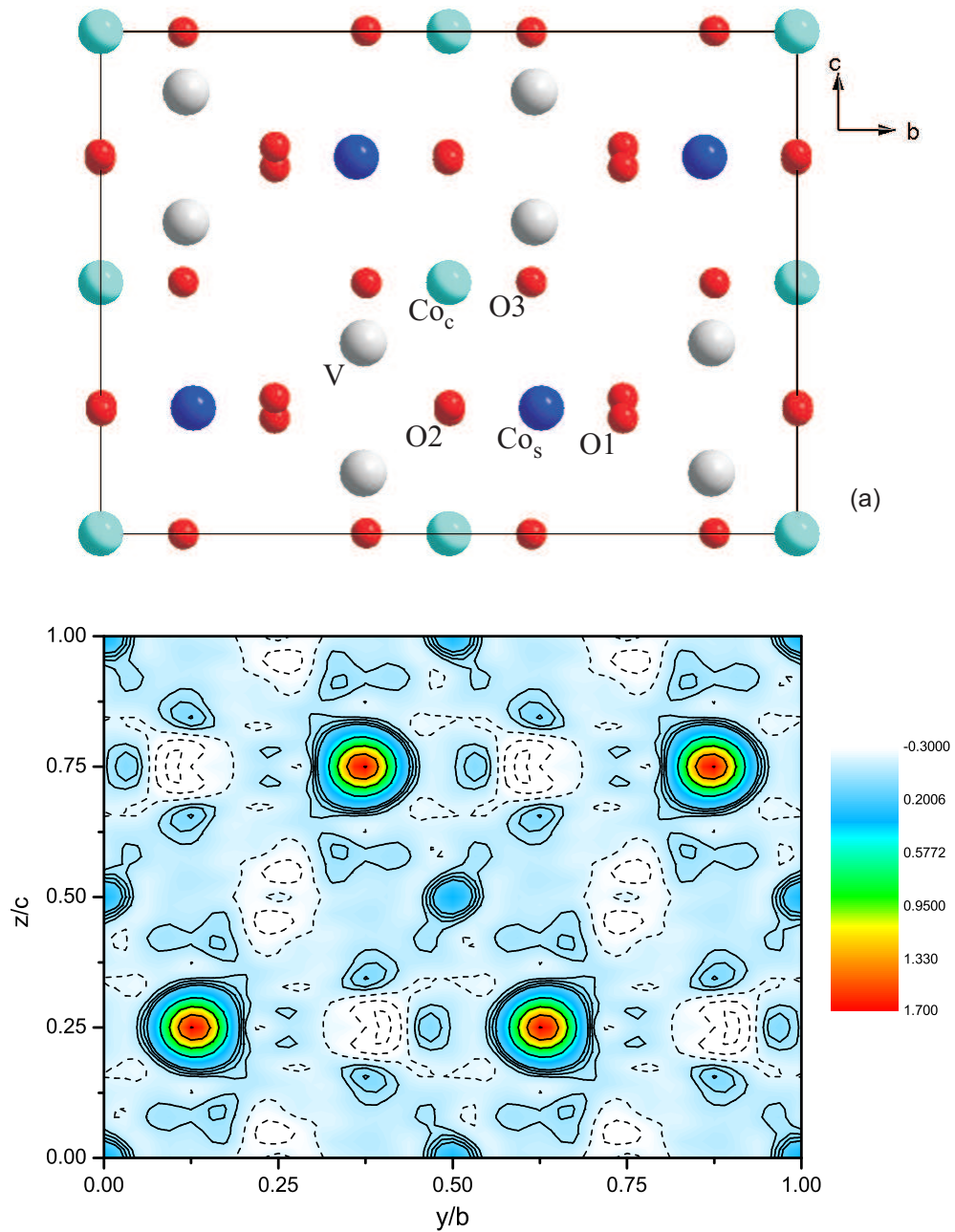


Figure 4.9.: (a) Crystal structure viewed along the a axis. (b) Experimental magnetization density as a projection onto the b - c plane. Contour lines defining positive values are drawn as solid lines in $0.05 \mu_B/\text{\AA}^2$ intervals between $0 \mu_B/\text{\AA}^2$ and $0.15 \mu_B/\text{\AA}^2$ and in $0.4 \mu_B/\text{\AA}^2$ intervals above. Negative isodensities are represented by broken lines in $0.1 \mu_B/\text{\AA}^2$ steps.

4.1.5. Spin density in momentum space

The investigation of the spin density in momentum space of $\text{Co}_3\text{V}_2\text{O}_8$ has been carried out at the High Energy Inelastic Scattering beamline BL08W at the SPring-8 (Super Photon Ring 8 GeV) synchrotron in Hyogo, Japan. This beamline is designed for Compton scattering spectroscopy as it offers elliptically polarized X-rays emitted from an Elliptic Multipole Wiggler. The incident photon beam with an energy range of 170-300 keV is monochromated and focused by an asymmetric Johann type monochromator using the Si(620) reflection. The sample magnetization is achieved with a superconducting magnet with a maximum field of 3 T and a minimum polarity-switching time of 5 seconds. The backscattered photon energy is analyzed by a 10-segmented Ge solid state detector positioned at a scattering angle of 178.4° . The experiment has been carried out with an incident photon energy of 176.3 keV, which gives a good compromise between the beam intensity and the scattering cross section.

The initial interest of applying this method to $\text{Co}_3\text{V}_2\text{O}_8$ has been to map the spin density in momentum space as a projection onto the b^*-c^* plane of the ferromagnetic phase in order to gather information about the 3d electron spin states and to correlate the results with those obtained from the polarized neutron diffraction experiment, but the experimental conditions and especially the large magnetic anisotropy of the system did not allow that. The minimal achievable sample temperature is approximately 5.6 K, i.e. close below the magnetic transition into the antiferromagnetic phase. It can be seen in the magnetic phase diagrams [13, 16] that at this temperature already weak magnetic fields applied along the b or c axis induce a magnetic phase transition into the antiferromagnetic phase, while $H||a$ stabilizes the ferromagnetic one. The necessity of applying a magnetic field of considerable strength and therewith magnetizing the sample along the incident beam in order to increase the magnetic contribution to the scattering cross-section (see 2.14) beside the requirement of turning the sample about a vertical axis to be able to reconstruct the two-dimensional momentum density, led to a change of strategy. To make sure not to induce magnetic phase transitions by rotating the sample the measurements have been carried out within the antiferromagnetic phase at $T=7.5$ K and applying a magnetic field of $H=2$ T with the induced ferromagnetic component lying in the b - c plane. In addition to the trivial directions [010] and [001] four further directional magnetic Compton profiles have been investigated in the b^*-c^* plane. An additional profile has been measured along the [100] direction with a decreased applied magnetic field of 0.25 T.

The Compton profiles of the respective sample magnetization states have been recorded for 60 seconds, repeating the cycle [+ - - + - + + -] multiple times. Due to the fact that

the more intense charge Compton profiles still exhibit relatively large values at the outermost measured positions of $p_z = \pm 10$ and in order to integrate the area correctly with respect to the magnetic effect, the profiles have been extrapolated using tabulated data for the elements resulting from Hartree-Fock calculations [82]. The MCPs were extracted by taking the difference of the scattered intensities I^+ and I^- of the respective charge Compton profiles. Before summing up the magnetic intensity of each detector cell, the data have been corrected for the detector cell efficiency, sample absorption and scattering cross-section according to [83]. Furthermore, the energy scale of each detector cell has been calibrated by measuring a radioactive sample $\text{Ba}_{133}\text{Co}_{57}$ with well known emission energies. The area under each profile has been normalized to the number of magnetic electrons per formula unit. The experimental MCPs were folded at $p_z = 0$ to increase statistical accuracy by taking the average of each branch.

The seven measured directional MCPs are depicted in Fig. 4.10, where the abscissa p_z is represented in atomic units (a.u.) and is taken to be parallel to the scattering vector, which corresponds to the incident beam direction because of the backscattering geometry. With the use of iron standards the induced ferromagnetic component can be deduced from

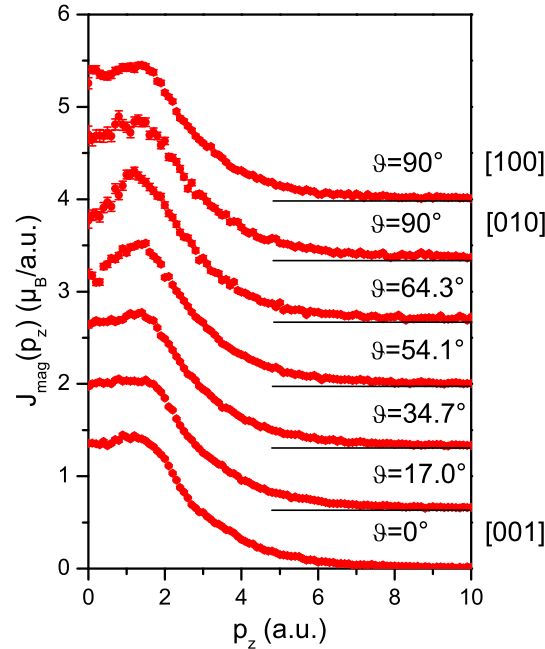


Figure 4.10.: Directional magnetic Compton profiles measured along seven different crystallographic directions. ϑ defines the angle between the b^* axis and the respective MCP.

4. Results

the magnetic effect. The magnetic effects of the respective directional MCPs are listed in Tab. 4.3 with their corresponding ferromagnetic components induced parallel to the scattering vector.

Table 4.3.: Magnetic effects of the respective directional MCPs with a magnetic field H applied along the scattering vector. ϑ denotes the angle between a MCP and the [001] direction.

MCP	ϑ ($^\circ$)	$H(T)$	M_0 (%)	S (μ_B)
[001]	0	2	0.541	0.616
[023]	17	2	0.488	0.556
[012]	34.7	2	0.415	0.472
[011]	54.1	2	0.274	0.312
[032]	64.3	2	0.229	0.261
[010]	90	2	0.095	0.108
[100]	90	0.25	0.251	0.287

Using all profiles except MCP₁₀₀ the projected spin density in the p_y - p_z plane has been reconstructed by the direct Fourier-transform method. The calculation has been performed on a grid with a distance of 0.1 a.u. between each point. The result is shown as a two-dimensional contour plot in Fig. 4.11. Low spin density can be recognized inside the first Brillouin zone (BZ), which extends beyond its border along the $\langle 010 \rangle$ and $\langle 001 \rangle$ directions. In the vicinity of the first BZ border the density increases more rapidly with increasing momentum along $\langle 021 \rangle$. Peaks are present at $(p_x, p_y) = (0.35, 1.85)$ and $(1.4, 0.55)$.

In order to analyze the observed MCPs theoretical ones have to be prepared. Therefore, the *ab initio* wave functions of the CoO₆ clusters (Sec. 4.1.3) have to be transformed into momentum space by an inverse Fourier transformation according to

$$\chi(\mathbf{p}) = (2\pi)^{-\frac{3}{2}} \int_{-\infty}^{\infty} \psi(\mathbf{r}) \exp(-i\mathbf{p}\mathbf{r}) d\mathbf{r}, \quad (4.6)$$

where \mathbf{p} and \mathbf{r} are given in atomic units. In contrast to the real space density, where the atomic wave functions must contain a translational vector in order to represent the position of each atom, the momentum space density possesses the general property of being single-centered, i.e. each momentum space wave function has zero as its origin. If a many-electron system can be understood as composed of independent particles described

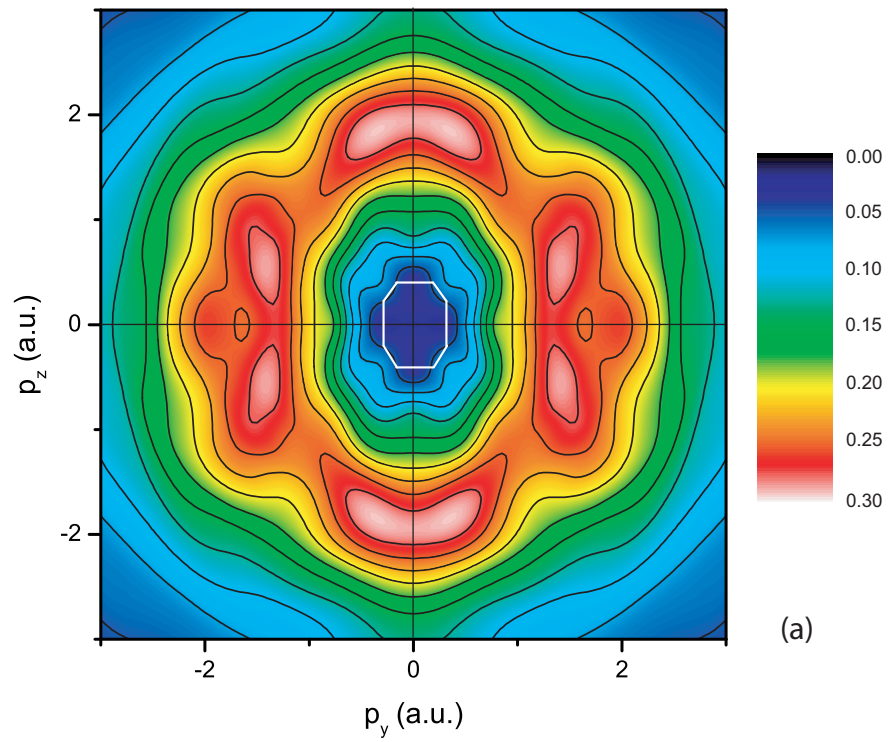


Figure 4.11.: Experimental momentum spin density as a projection onto the p_y - p_z .

4. Results

by single-particle wave functions, then, within the limits of the impulse approximation, each scattering process will only involve one electron of the system. Thus, a theoretical MCP of a respective crystallographic direction can be obtained by simply summing over the square of every wave function representing an unpaired electron. The sum of squares is then projected onto the scattering vector, i.e. integrated along two axes, which are perpendicular to it. In order to do so for crystallographic directions in the p_y - p_z plane, which are different than the principal ones, a coordinate transformation has been carried out, which rotates the momentum space wave functions around the p_x axis by the angle ϑ so that the scattering vector comes to lie on the former p_z axis ([001] direction). The expression for a theoretical MCP is

$$J_{th}(p'_z) = \int_{-\infty}^{\infty} \int_{-\infty}^{\infty} \sum_k \beta_k \chi_k^2(p'_x, p'_y, p'_z) dp'_x dp'_y, \quad (4.7)$$

where β_i are the refinable parameters, which express the contribution of each orbital to the MCP. For the integration the symmetry relations between the different cluster density distributions in the unit cell have to be taken into account, which yield two and four symmetrically inequivalent Co_cO_6 and Co_sO_6 clusters, respectively (Tab. 4.4). The point

Table 4.4.: Symmetry relations between the two and four inequivalent Co_cO_6 and Co_sO_6 , respectively.

cluster	Co position	symmetry relation to c_1/s_1
c_1	(0, 0, 0)	xyz
c_2	$(0, \frac{1}{2}, \frac{1}{2})$	$xy\bar{z}$
s_1	$(\frac{1}{4}, y, \frac{1}{4})$	xyz
s_2	$(\frac{3}{4}, y, \frac{1}{4})$	$\bar{x}yz$
s_3	$(\frac{3}{4}, \bar{y}, \frac{3}{4})$	$\bar{x}\bar{y}\bar{z}$
s_4	$(\frac{1}{4}, \bar{y}, \frac{3}{4})$	$x\bar{y}\bar{z}$

symmetries of the Co_cO_6 and Co_sO_6 clusters are $2/m..$ and $.2$. [39], which correspond to $2/m..$ and $.2/m$. in momentum space. Due to the special symmetry of the Co_sO_6 density, the projections of the different clusters in momentum space are invariant for the principal axes and those in the p_y - p_z plane. In the case of the Co_cO_6 clusters, the projections onto non-principal axes in the p_y - p_z yield different profiles, which need to be averaged. Due to the complexity of the expressions the projections of the respective orbitals have been carried out numerically by calculating discrete points according to the measured data. Then a linear combination of four Gaussians has been fitted to the calculated points showing

excellent agreement. These fit results were used in the subsequent treatment.

Like previously reported [36] the fact that the projection of each orbital has a characteristic shape makes it possible to analyze its contribution to the observed MCP. In this way the occupation of orbitals under consideration can be determined. This is done by fitting the weighted calculated MCPs simultaneously to all the observed ones. Before doing so, the theoretical MCPs have to be convoluted with a Gaussian function having a full width at half maximum (FWHM) of the instrumental resolution of BL08W, which has been deduced as follows. From the calibrating sample $Ba_{133}Co_{57}$ the FWHM of a Co emission line at $E = 122.0614$ keV has been determined to 693.71 eV, which corresponds to $\Delta E = FWHM_E/2\sqrt{2\ln(2)} = 1.7567$ keV. The conversion from energy values into momenta given in atomic units is

$$p_z = \frac{E_C - E_1 + (E_C E_1 / mc^2)(1 - \cos \phi)}{\sqrt{E_1^2 + E_C^2 - 2E_1 E_C \cos \phi}} \cdot 137.036 \text{ a.u.}, \quad (4.8)$$

where E_1 is the incident photon energy, E_C the Compton peak energy (see Eq. 2.5) and ϕ the scattering angle. The error propagation is calculated by

$$\Delta p_z = \left| \frac{dp_z}{dE_2} \right| \Delta E_2. \quad (4.9)$$

The result $FWHM_{p_z} = 0.573$ a.u. yields the gaussian resolution function

$$\delta(p_z) = \frac{2\sqrt{2\ln(2)}}{\sqrt{2\pi}FWHM_{p_z}} \exp \left[-\frac{1}{2} \left(\frac{2\sqrt{2\ln(2)}}{FWHM_{p_z}} p_z \right)^2 \right]. \quad (4.10)$$

Hence, the calculated MCPs $J(p_z)$ for the instrument BL08W are

$$J_{cal}(p_z) = (J_t h * \delta)(p_z) = \int_{-\infty}^{\infty} J_t h(\tau) \delta(p_z - \tau) d\tau. \quad (4.11)$$

The refinement of the contribution of each orbital has been carried out simultaneously with the flipping ratio refinement and will be explained in detail in the next section.

4.1.6. Correlated refinement in both spaces

The idea behind correlating the density distributions in real and momentum space is that the contribution of each spin polarized orbital to the observed density must be the same in both spaces. Like for the MCPs the contributions β_k of the real space MOs can be used to deduce the magnetic form factors $f_X(\mathbf{q})$ of the respective elements X by calculating the Fourier transform of the atomic spin density:

$$f_X(\mathbf{q}) = \int_{-\infty}^{\infty} \int_{-\infty}^{\infty} \int_{-\infty}^{\infty} \sum_k \beta_k \psi_{k,X}^2(\mathbf{r}) \exp(2\pi i \mathbf{q} \mathbf{r}) d\mathbf{r}, \quad (4.12)$$

where $\psi_{k,X}$ defines the real space MO k only including the atomic orbitals $\phi_{i,X}$ of element $X=\text{Co}, \text{O}$. For the V ions the analytic approximation of the V^{4+} form factor [84] has been used. With this procedure the observed flipping ratios can be refined based on an a simple aspheric magnetic form factor model deduced from *ab initio* wave functions.

The refinement has been made for the results of calculations using different basis sets, which were 6-31G [85, 86], 6-31G* [85, 86], Ahlrich's VDZ [73], Ahlrich's pVDZ [73], Ahlrich's VTZ [73] and Ahlrich's TZV [65]. Each basis set has been used with either SBKJC [79, 87] or Stuttgart RLC 1997 [88, 89] ECPs. The best results have been obtained with Alrich's pVDZ basis set, where the choice of the ECP did not affect the results. Refining the contribution parameters for each MCP individually yields excellent agreement with the observed profiles. But since the refinement process exhibits numerous local minima with significantly varying results, it has been considered more reasonable to include all MCPs in the refinement despite the magnetic anisotropy. The respective contribution parameters β_k have been refined simultaneously in both spaces together with the magnetic moments of Co, V and O by minimizing the function

$$\chi^2 = \frac{1}{2} \sum_i \frac{(R_{i,obs} - R_{i,cal})^2}{\sigma_{i,obs}^2} + \frac{1}{2} \sum_n \sum_j \frac{J_{n,obs}(p_{z,j}) - J_{n,cal}(p_{z,j})^2}{\sigma_{j,obs}^2} \quad (4.13)$$

with i and j defining discrete data points of the PND and MCS experiment, respectively, and n referring to the respective MCPs. The refinement yields fairly good agreement expressed by $R_{MCS}=5.7$ and $R_{PND}=9.6$ for the respective experiments. The refined total magnetic moments are

$$\begin{aligned}\mu(\text{Co}_c) &= 1.54(4) \mu_B \\ \mu(\text{Co}_s) &= 2.87(3) \mu_B \\ \mu(\text{V}) &= 0.41(4) \mu_B \\ \mu(\text{O1}) &= 0.05(5) \mu_B \\ \mu(\text{O2}) &= 0.46(5) \mu_B \\ \mu(\text{O3}) &= 0.36(5) \mu_B.\end{aligned}$$

Summing the magnetic moments of all ions in the unit cell weighted by their site multiplicity and dividing by the number of Co ions yields an averaged magnetization of $3.38 \mu_B/\text{Co}^{2+}$. This value shows excellent agreement with the macroscopic magnetization for $H = 2$ T along the a axis reported in [16]. The resulting orbital contribution parameters are listed in Tab. 4.5. The refined parameters were used to calculate the MCPs, which are shown as black solid lines in Fig. 4.12. From the calculated MCPs the momentum space spin density has been reconstructed and is shown together with the observed density in Fig. 4.13. The calculated magnetization density map is derived from a Fourier synthesis using the calculated magnetic structure factors. Fig. 4.14 shows the projection of the observed and calculated magnetization density onto the b - c plane together with the crystal structure.

The main features of the respective density maps coincide well, although some differences are evident: the dip in the momentum space density around $p_z=0$ is not pronounced well in the calculated map with a shape, which is rotated by 90° with respect to the observed map. This possibly results from strong hybridization effects between the Co3d and O2p orbitals. The real space spin density of the O1 and O3 sites is slightly underestimated. Furthermore, density peaks exist, which do not coincide with atomic positions. However, this fact can be attributed to truncation effects in the Fourier series.

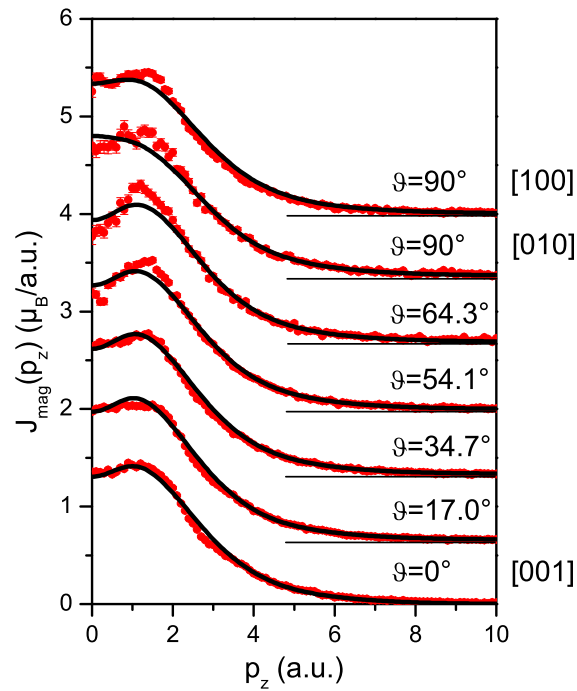


Figure 4.12.: Observed ([red] dots) and calculated ([black] solid lines) normalized directional MCPs (shifted vertically in order to improve clarity, horizontal lines serve as a guide for the eye). The abscissa p_z is taken to be parallel to the respective scattering vector. ϑ denotes the angle between a respective MCP and the [001] direction.

Table 4.5.: Refined orbital occupation parameters of the Co_cO_6 and Co_sO_6 clusters.

orbital	Co_c	Co_s
d_{xy}	0.27(2)	0.12(2)
d_{xz}	0.27(2)	0.12(2)
d_{yz}	0.16(2)	0.26(2)
$d_{x^2-y^2}$	0.17(2)	0.30(2)
$d_{3z^2-r^2}$	0.13(2)	0.20(2)

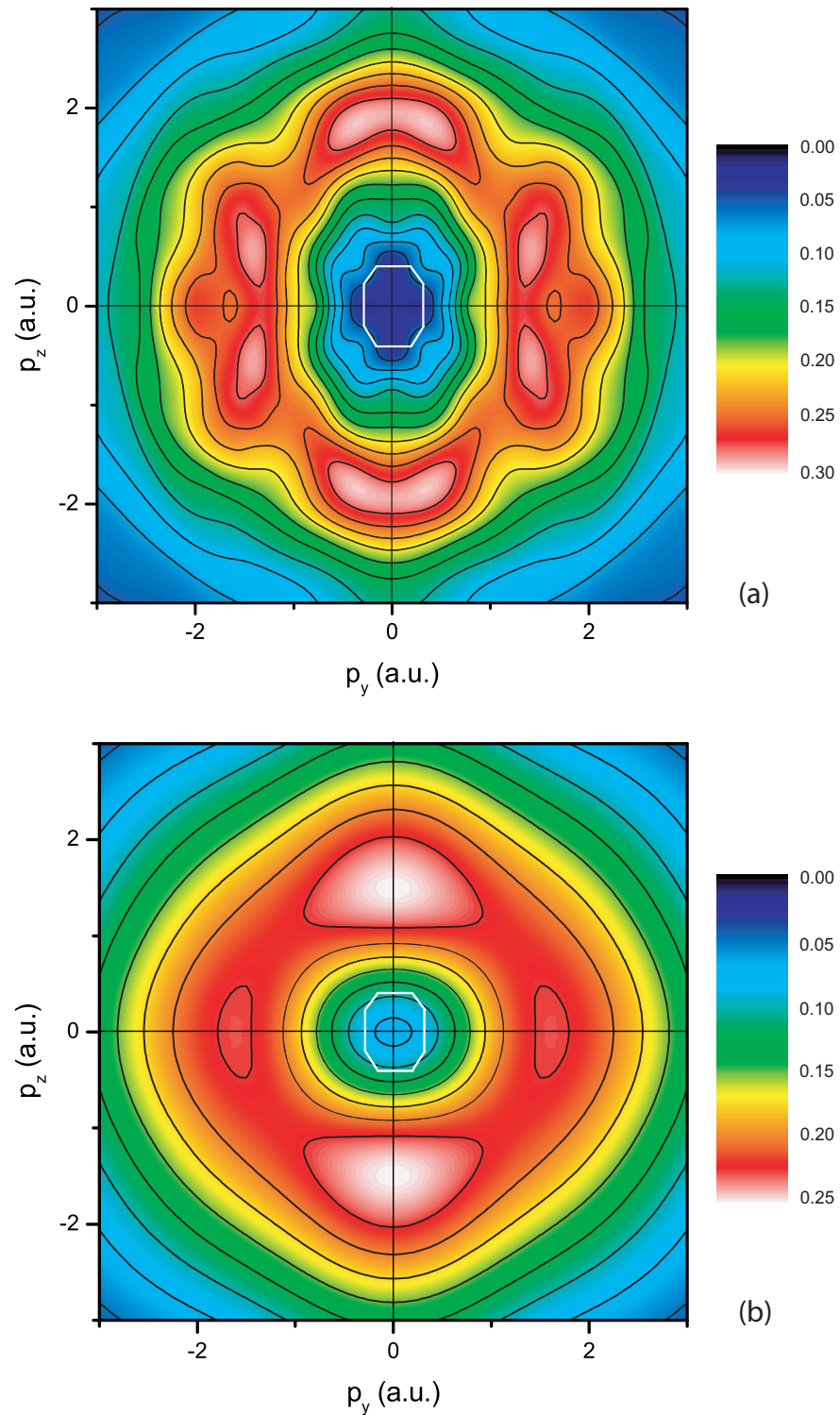


Figure 4.13.: Reconstructed experimental (a) and calculated (b) spin momentum density in the p_y - p_z plane. Contours are drawn in $0.025 \mu_B/(\text{a.u.})^3$ intervals. White solid lines depict the boundary of the first Brillouin zone.

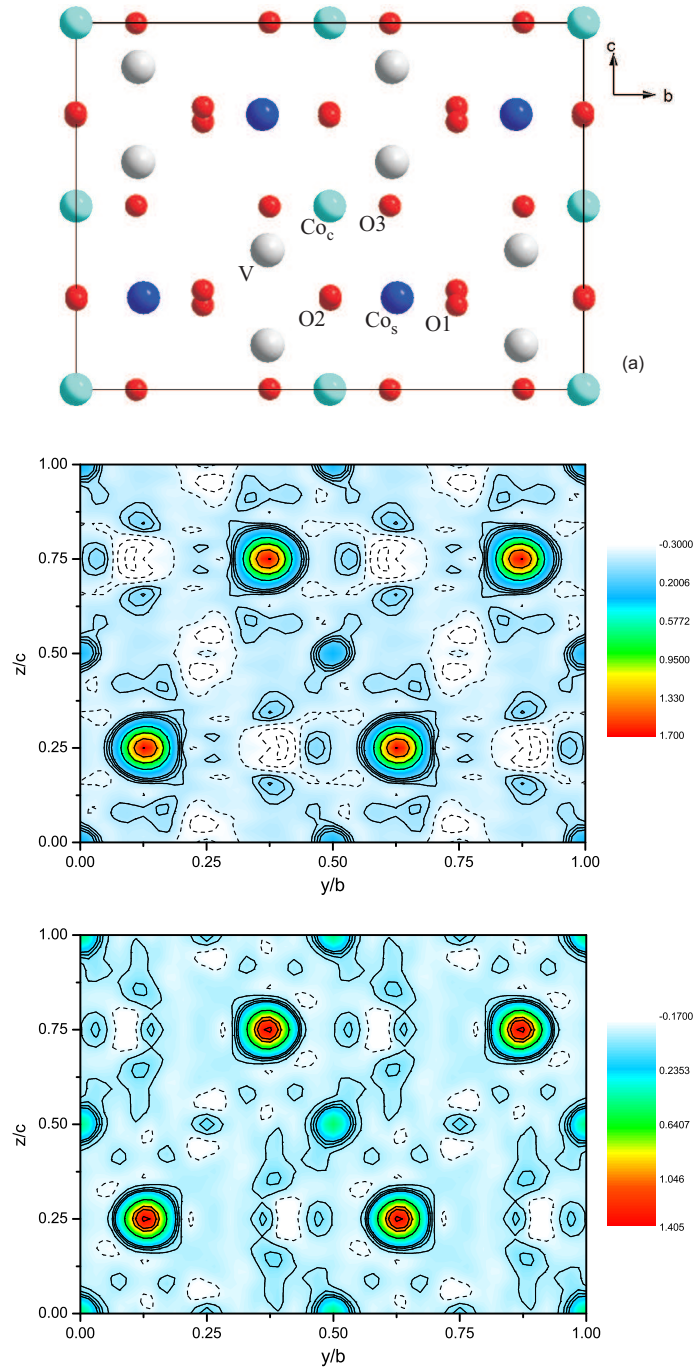


Figure 4.14.: (a) Crystal structure viewed along the a axis. (b) Experimental and (c) calculated magnetization density as a projection onto the b - c plane. Contour lines defining positive values are drawn as solid lines in $0.05 \mu_B/\text{\AA}^2$ intervals between $0 \mu_B/\text{\AA}^2$ and $0.15 \mu_B/\text{\AA}^2$ and in $0.4 \mu_B/\text{\AA}^2$ intervals above. Negative isodensities are represented by broken lines in $0.1 \mu_B/\text{\AA}^2$ steps.

4.2. $(\text{Co}_x\text{Ni}_{1-x})_3\text{V}_2\text{O}_8$

Numerous publications using various methods exist concerning the CVO and NVO compounds, but except one report about the cationic occupation factors, no study of the mixed system CNVO exists in the literature. Hence, a systematic investigation has been carried out with magnetization, heat capacity, neutron powder and neutron single-crystal diffraction experiments. Interesting aspects could be revealed concerning the magnetic phase diagram and the magnetic structure.

4.2.1. The dependence of k on the composition parameter x

The propagation vectors of the CNVO mixed system have been investigated using three powder samples with different composition parameters x at the high-resolution two-axis neutron powder diffractometer D1A (ILL). This instrument (Fig. 4.15) is able to provide high resolution at long wavelengths due to its large take-off angle, with shorter wavelength contamination eliminated by the guide tube, which makes it particularly suited to magnetic structure studies. A wide range of wavelengths from 1.39 Å to 2.99 Å is available by a simple rotation of the anisotropically squashed focussing germanium monochromator. For this experiment the optimum wavelength of 1.911 Å has been chosen, which emerges from the Ge(115) reflection. The nuclear structures have been investigated in the param-

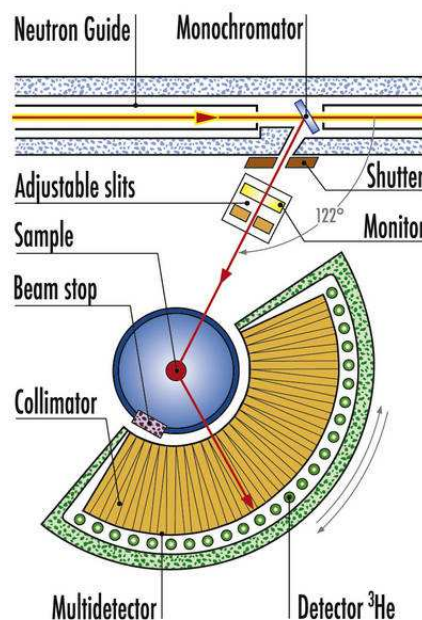


Figure 4.15.: Instrument layout of the high-resolution two-axis diffractometer D1A.

agnetic phase at 20 K, while the magnetic structures have been studied at $T=2$ K with zero magnetic field. The structural investigation confirmed the correct phase formation of the powder samples and showed close agreement to previously reported data [2, 8, 12, 90]. The cell constants of the mixed compounds behave according to Vegard's law. Like previously reported [90] the Co ions were found to preferably occupy the more symmetric 4a sites, resulting in cation distribution factors of $K_D=0.73$, 0.81 and 0.76 for $x=0.27$, 0.52 and 0.76, respectively. Table 4.6 lists the structural parameters as well as the refined composition parameter x . Fig. 4.16 shows the magnetization data of the three CNVO powder samples zooming the low temperature region. For $x=0.27$ and $x=0.52$ a slight drop of the

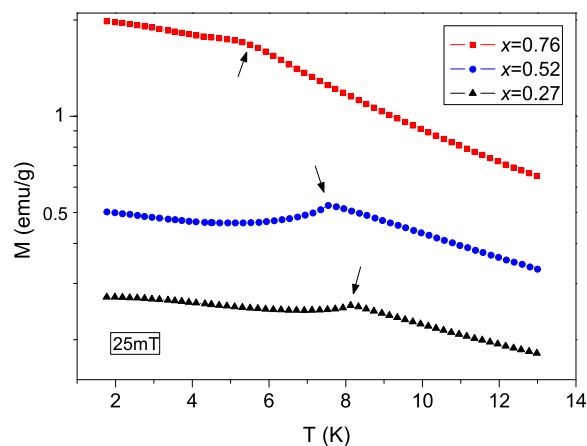


Figure 4.16.: Magnetization in dependence on the temperature of $(\text{Co}_x\text{Ni}_{1-x})_3\text{V}_2\text{O}_8$ for $x = 0.27$, 0.52 and 0.76 (logarithmic scale). Arrows mark the transition points.

magnetization can be observed at $T=8.1$ K and $T=7.5$ K, respectively, whereas the curve for $x=0.76$ only exhibits a change of slope at $T=5.5$ K. From the characteristics of the curves an antiferromagnetic ordering could be deduced and then confirmed by neutron powder diffraction experiments.

Due to the existence of multiple magnetic phases with temperature dependent propagation vectors for NVO and CVO [6, 15, 19], patterns were collected at different temperatures below the respective transition points. In contrast to its parent compounds CNVO does not exhibit temperature dependent shifts of the magnetic reflections which is illustrated in Fig. 4.17 for $x=0.27$. One can only notice an increase of intensity of the magnetic reflections with decreasing temperature which is an ordinary effect due to reduced thermal displacement. The magnetic reflections could be indexed by introducing a propagation vector $\mathbf{k} = (\delta, 0, 0)$ with δ being dependent on the composition parameter x . The shift of

Table 4.6.: Structural parameters of the investigated $(\text{Co}_x\text{Ni}_{1-x})_3\text{V}_2\text{O}_8$ powder samples.

Composition x	Cell	Position/Ion	M(1)	M(2)	V	O(1)	O(2)	O(3)
0.27	a=5.9540(3)	x	0	0.25	0	0	0	0.2674(9)
	b=11.4094(7)	y	0	0.1306(7)	0.3762	0.250(1)	0.002(1)	0.1197(6)
	c=8.2530(6)	z	0	0.25	0.1196	0.268(1)	0.244(1)	0.9998(6)
0.52	a=5.9811(3)	x	0	0.25	0	0	0	0.2683(7)
	b=11.4359(5)	y	0	0.1307(8)	0.3762	0.2509(9)	0.0030(9)	0.1197(5)
	c=8.2704(5)	z	0	0.25	0.1196	0.2687(9)	0.2443(9)	0.9989(9)
0.76	a=6.0069(3)	x	0	0.25	0	0	0	0.2683(7)
	b=11.4648(6)	y	0	0.132(1)	0.3762	0.250(1)	0.002(1)	0.1200(5)
	c=8.2876(5)	z	0	0.25	0.1196	0.2679(9)	0.2434(9)	0.9988(9)

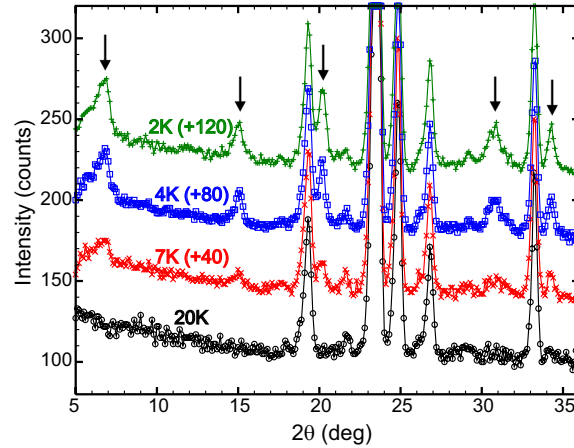


Figure 4.17.: Powder diffraction patterns of $(\text{Co}_{0.27}\text{Ni}_{0.73})_3\text{V}_2\text{O}_8$ at different temperatures. Arrows mark the magnetic reflections. The numbers in brackets indicate the vertical shift to improve clarity.

the magnetic reflections is clarified in Fig. 4.18. The values of δ are 0.372(5), 0.491(4) and 0.52(3) for $x=0.27$, 0.52 and 0.76, respectively. It has to be mentioned that the increase of background at low angles for $x=0.76$ has also been observed for CVO at all investigated temperatures below 14K. The observed patterns could be reproduced well (Fig. 4.19) based on a magnetic structure model similar to NVO with the antiferromagnetic vector along the a axis and weak ferromagnetism along c .

In contrast to NVO and CVO the mixed compounds CNVO only exhibit a single ordered magnetic structure. Within the limits of the experimental precision the modulation of the magnetic moments and the magnetic structure are similar to NVO, i.e. the magnetic moments propagate according to $\mathbf{k} = (\delta, 0, 0)$ with an antiferromagnetic vector along a and weak ferromagnetism along c , whereas CVO exhibits ferromagnetic coupling along a and a wave vector with a non-zero component along the b^* -direction. For the three investigated samples $x=0.27$, 0.52 and 0.76 the incommensurability δ has been found to be dependent on the composition parameter x (δ increases with increasing x). The compound with $x=0.76$ seems to be close to a critical amount of Co, which disturbs the antiferromagnetic structure of NVO. A higher degree of frustration can be deduced due to the small and broad magnetic reflections (Fig. 4.18), which is well correlated with the less pronounced transition point in the magnetization curve (Fig. 4.16). Since the ground state of CVO is ferromagnetic, a quantum critical point is expected where the two types of magnetic interactions lead to a fully frustrated system for a certain composition with

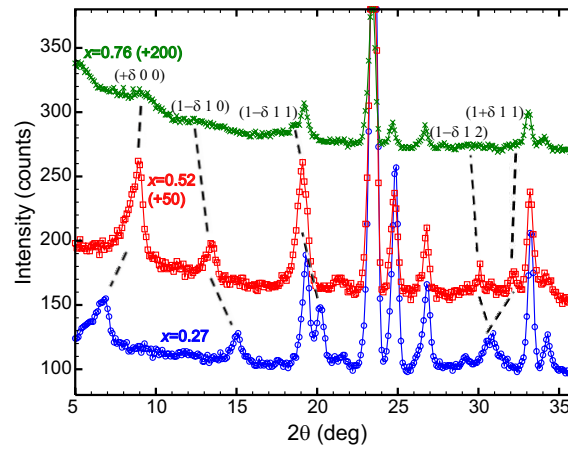


Figure 4.18.: Powder diffraction patterns of $x=0.27$, 0.52 and 0.76 at 2K. The dashed lines indicate the shift of the magnetic reflections. Again the patterns are vertically shifted for clarity.

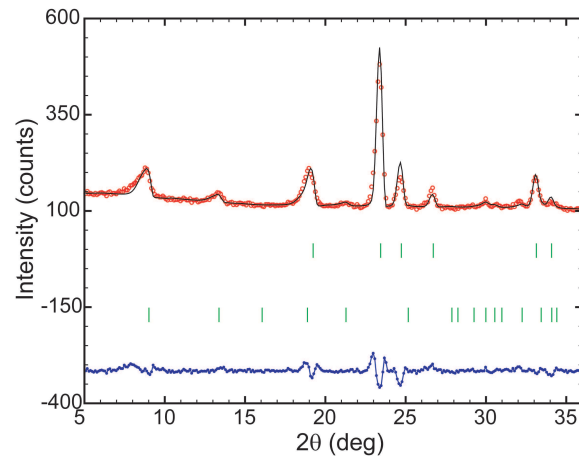


Figure 4.19.: Observed pattern (red dots), calculated pattern (black line) and difference plot (blue line) of $(\text{Co}_{0.52}\text{Ni}_{0.48})_3\text{V}_2\text{O}_8$ at 2K and zero field.

4. Results

$x > 0.76$, which is subject of the forthcoming section. More compositions with shorter steps in x have been investigated in order to specify the $\mathbf{k}(T)$ dependence and to spot the critical value of x where the magnetic structure switches from the NVO to the CVO type. Additional neutron diffraction experiments on a $(\text{Co}_{0.5}\text{Ni}_{0.5})_3\text{V}_2\text{O}_8$ single crystal have been carried out in order to extract precise information about the magnetic structure, which is shown in Section 4.3.

4.2.2. Magnetic composition-temperature phase diagram

Powder samples with short steps in the compositional parameter x , prepared like described in Section 4.2.1, were investigated at a high-resolution (D1A) and a high-intensity neutron powder diffractometer (D20) at the Institut Laue-Langevin using wavelengths of 2.99 Å supplied by the (113) reflection of a Ge monochromator and 2.41 Å from the (002) reflection of a pyrolytic graphite HOPG monochromator. Each sample was measured in the paramagnetic regime at 20 K in order to extract the nuclear structure and especially the compositional parameter x . The investigation of the magnetic properties was performed at 1.5 K. Measurements on all powder samples were made using D1A except for the samples with $x = 0, 0.35$ and 0.71 , for which D20 was used, and those with $x = 0.87, 0.92$ and 0.98 , for which both instruments were used. Due to the extremely high neutron flux at D20 and the large position-sensitive microstrip detector (see instrument layout in Fig. 4.20), diffraction patterns can be recorded as a matter of seconds, which gave rise to the possibility of the investigation as a function of temperature.

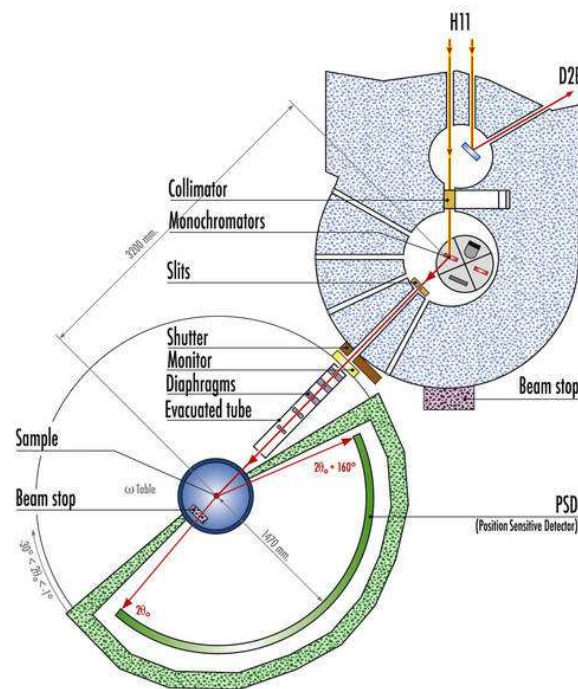


Figure 4.20.: Instrument layout of the high-intensity two-axis diffractometer D20.

Single crystals with concentrations $x = 0, 0.5, 0.65, 0.86$ and 1.0 were grown from self flux. The compositions of the mixed crystals were estimated using lattice parameters deter-

4. Results

mined using X-ray powder diffraction and Vegard's law. The specific heat was measured using a PPMS from Quantum Design. The data around the phase transitions were obtained by analyzing individual relaxation curves after a large (2-3 K) temperature pulse via a method similar to the one presented in [91].

Neutron diffraction experiments on the respective powder samples within the paramagnetic phases (PM) at 20 K revealed the correct phase formation of the orthorhombic structures (space group Cmca). The refinement process included the cell parameters, the atomic positions of M and O, an overall isotropic temperature factor and the Co:Ni ratio. The atomic position of V has been fixed in all refinements because of its low coherent neutron scattering cross section. The resolution parameters u , v and w as well as the ratios source width/detector distance and detector width/detector distance, which describe the asymmetry of the reflection profiles, have been set according to the instrumental resolution function. The recorded diffraction patterns of the paramagnetic phases (20 K) were subtracted from the respective magnetically ordered ones (1.5 K) in order to emphasize the magnetic scattering, which is depicted in Fig. 4.21.

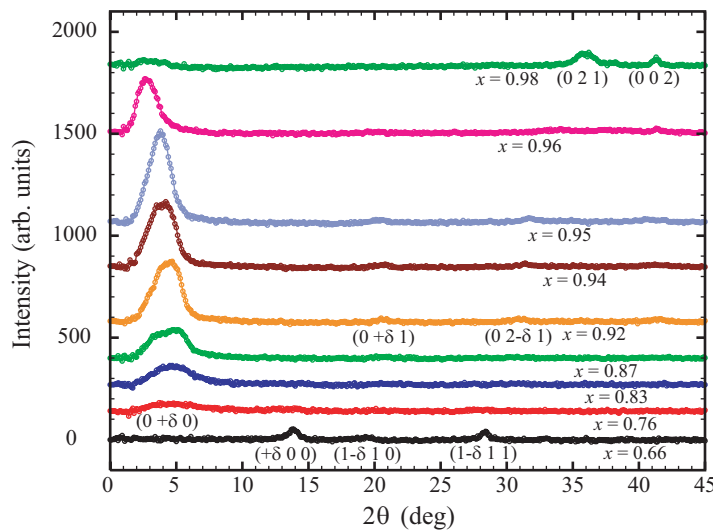


Figure 4.21.: Magnetic scattering of $(\text{Co}_x\text{Ni}_{1-x})_3\text{V}_2\text{O}_8$ powder samples with different values of x at 1.5 K and zero field obtained by measurements on D1A. The patterns are shifted vertically for clarity.

It was found that substituting 2% of Co with Ni results in a critical composition where both ferromagnetic ($2\theta = 36^\circ$ and 41°) and antiferromagnetic ($2\theta \approx 3^\circ$) reflections of the

CVO magnetic structure type can be observed. However, the antiferromagnetic $(0 + \delta 0)$ reflection is very low in intensity but significant if compared to the diffraction pattern of the $x = 0.66$ sample.

In order to be precise on the critical values especially with respect to the uniformity of the powder samples investigated the reflection profile has been examined in detail: the ratio between Co and Ni on the magnetic sites determines the cell constants according to Vegard's law; therefore the peak positions are dependent on the composition. Assuming a distribution of compositions within one powder sample, one would expect enlarged reflection profiles due to the different contributions. In the case of an uneven distribution, an asymmetry of the reflection profile may be observed. To clarify this point the profile of the nuclear (042) reflection, which is strong, isolated from others and close to the minimum of the resolution curve of the instrument, has been focussed on (Fig. 4.22). The raw data points (triangles stand for $x = 0.96$, circles represent $x = 0.98$) have been fitted with Pseudo-Voigt functions, whose FWHM are defined only by the fixed instrumental resolution and asymmetry parameters (where the latter do not affect the peak profile at such high angles anyway). The calculated points (not shown, but connected with straight lines) show excellent agreement with the observed data. From the difference plots (dashed lines with respective symbols) a minimal asymmetry might be observed. Therefore, the raw data have been fitted with an asymmetric double sigmoidal function, which is characterized by w_1 giving the main FWHM of the curve and additional parameters w_2 and w_3 describing the asymmetry of either side of the peak. The refined values are $w_2 = 0.092(8)$ and $w_3 = 0.094(7)$ for the $x = 0.96$ sample and $w_2 = 0.096(2)$ and $w_3 = 0.092(6)$ for $x = 0.98$ showing that no significant asymmetry exists. The fact that the reflection profile is neither enlarged nor asymmetric leads to the conclusion that the powder samples investigated are uniform within the limits of precision of the diffractometer. From the standard deviations of the refined occupation parameters a standard deviation of the composition of less than 0.01 can be deduced for each sample.

Below $x = 0.98$ the ferromagnetic phase is completely suppressed for $T \geq 1.5$ K with the antiferromagnetic structure being modulated by \mathbf{k}_1 with $\delta = f(T, x)$. But it is only for x between 0.92 and 0.95 that additional magnetic reflections $[(0 + \delta 1)$ and $(0 2 - \delta 1)]$ can be observed and indexed. Below $x = 0.92$ these reflections disappear; furthermore, the fundamental reflection becomes weaker and much broader than the predicted peak width, but even the better defined magnetic reflections are considerably broader than the instrumental resolution giving rise to the assumption that only antiferromagnetic short-range order is present. This case is the same for $x > 0.95$ with the difference that no information about the peak width can be deduced, because the $(000)^+$ reflection profile is

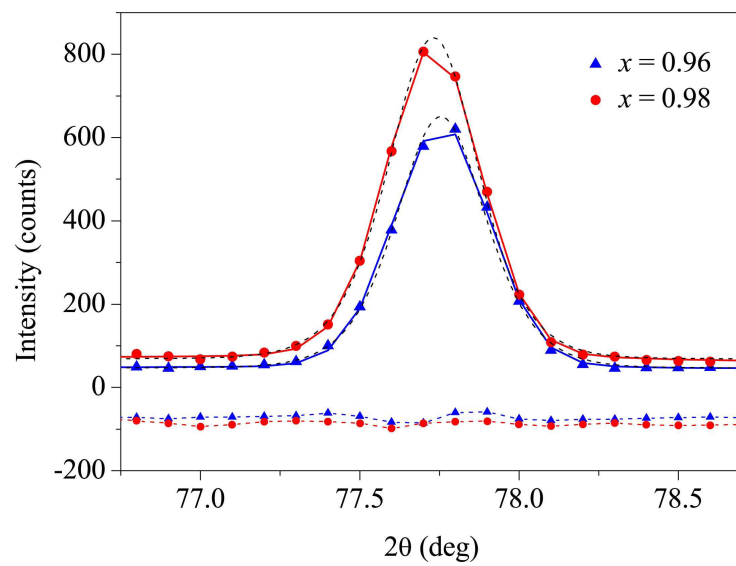


Figure 4.22.: Nuclear (042) reflection for $x = 0.96$ (triangles) and $x = 0.98$ (circles) at 20 K. The straight lines connect the calculated points (not depicted) obtained by a fit with Pseudo-Voigt functions (dashed lines with respective symbols represent the difference curves). The dashed lines without symbols are the result of the asymmetric double sigmoid fit.

influenced by the high background due to its very small diffraction angle. In contradiction to the results of Section 4.2.1 it can be seen, due to there being more samples on the Co rich side, that for $x = 0.76$, which is exactly the same powder sample, the $(000)^+$ reflection of the CVO type still can be observed in a broad and weak form (Fig. 4.21). Hence, as for $x = 0.71$ the magnetic reflections can be indexed by a propagation vector $\mathbf{k}_2 = [0.522(7), 0, 0]$ (Fig. 4.23), the critical composition, where the magnetic structure switches from the CVO to the NVO type, has to be in the region $0.71 < x < 0.76$. It can be seen from the refinement, that the width of the magnetic reflections is consistent with the instrumental resolution revealing long-range ordered antiferromagnetism for $x < 0.71$.

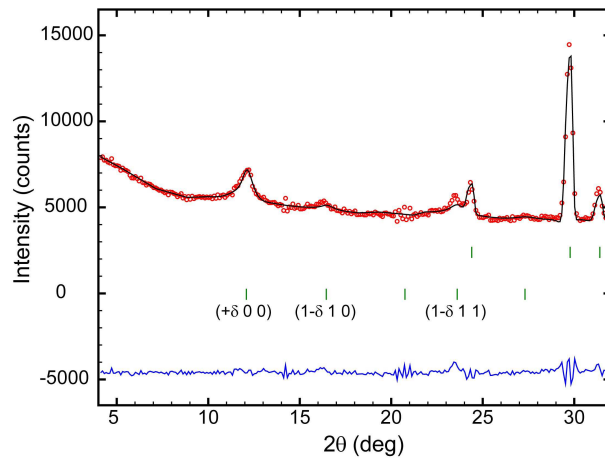


Figure 4.23.: Observed pattern (red dots), calculated pattern (black line) and difference plot (blue line) of $(\text{Co}_{0.71}\text{Ni}_{0.29})_3\text{V}_2\text{O}_8$ at 1.5 K and zero field revealing the NVO modulation type with $\mathbf{k}_2 = [0.522(7), 0, 0]$

By indexing the magnetic reflections of the respective neutron diffraction patterns the composition dependence of the incommensurabilities δ could be deduced (upper panel of Fig. 4.24), but it has to be mentioned that a precise determination of the propagation vector of the samples with $x > 0.95$ turned out to be difficult owing to background problems as mentioned above. As previously observed for $x = 0.27$ and 0.52 (Sec. 4.2.1) the positions of the magnetic reflections only change with composition and not with temperature, whereas the NVO magnetic structure exhibits a temperature dependent propagation vector [15]. Due to measurements on D20 it could be revealed that a substitution of 3.5% Ni with Co suppresses the aforementioned temperature dependence, which is shown in Fig. 4.25. Similarly, it could be observed due to thermodiffractograms with temperature steps of 0.1 K, that the previously reported temperature dependence of the propagation

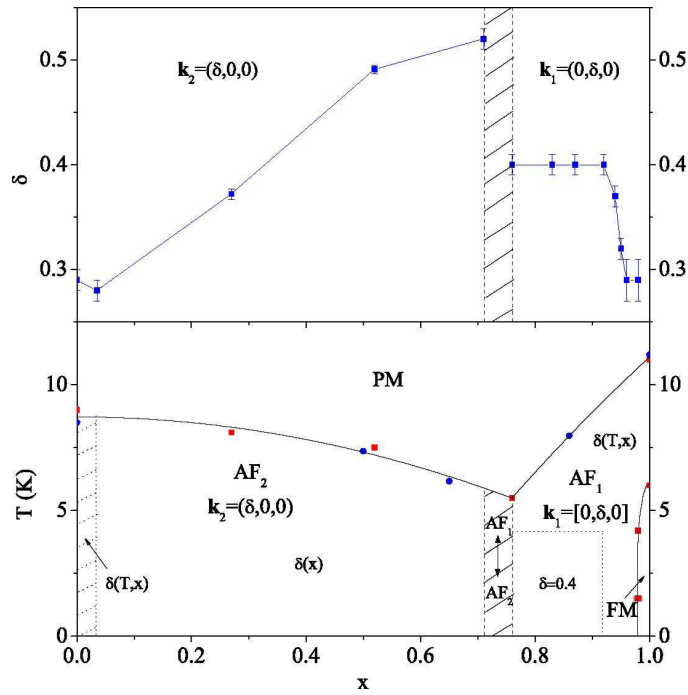


Figure 4.24.: Upper panel: Incommensurabilities δ as a function of the compositional parameter x . Lower panel: Magnetic (x, T) phase diagram of $(\text{Co}_x\text{Ni}_{1-x})_3\text{V}_2\text{O}_8$ obtained by neutron powder diffraction (red squares) and single crystal heat capacity (blue dots) experiments.

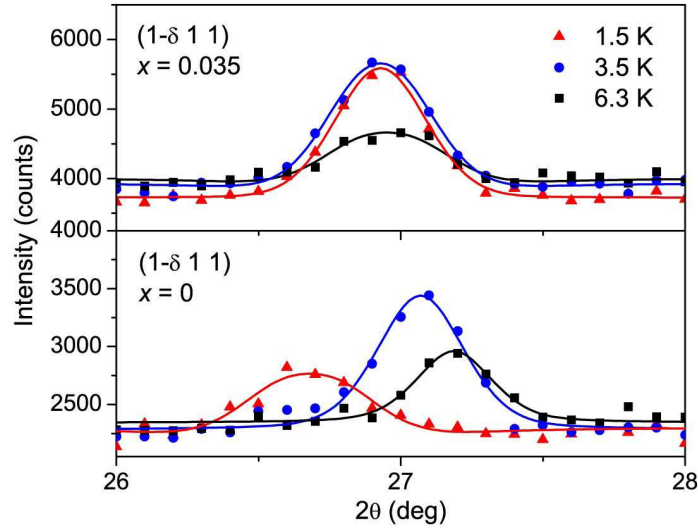


Figure 4.25.: Magnetic $(1-\delta \ 1 \ 1)$ reflection for $x = 0$ (lower panel) and $x = 0.035$ (upper panel). The data points have been fitted with Pseudo-Voigt functions. The temperature dependent shift of the magnetic reflection can clearly be seen for $x = 0$, where it does not exist for $x = 0.035$.

vector of the CVO magnetic structure [6] becomes weak on reaching a composition of $x = 0.87$ [Fig. 4.26(a)]. Only a slight shift of the fundamental $(000)^+$ reflection can be observed above approximately 4 K (exact determination results difficult due to the rather weak reflection compared to the background). The temperature dependent shift of the magnetic reflections can be clearly seen in Figs. 4.26(b) and (c). For the $x = 0.92$ sample in Fig. 4.26(b) the magnetic reflections appear at 8.6(1) K and can be indexed by a propagation vector $\mathbf{k}_1 = (0, 0.5, 0)$. Between 8.6(1) K and 4.2(1) K the positions of the magnetic reflections vary with temperature until they lock in at 4.2(1) K with $\mathbf{k}_1 = (0, 0.4, 0)$. In the case of $x = 0.98$ depicted in Fig. 4.26(c) one can observe a temperature dependent shift of the magnetic reflections throughout the antiferromagnetic phase without any lock-ins. The magnetic phase transition into the ferromagnetic phase takes place at 4.2(1) K.

Heat capacity measurements were performed on the pure Ni and Co compounds and on three intermediate ones ($x = 0.5, 0.65$ and 0.86). Fig. 4.27 shows the specific heat in a C_p/T versus T plot. The data for NVO and CVO exhibit the same sequence of transitions and are qualitatively similar to the data reported previously [6, 12, 15]. C_p/T is, however, up to a factor of 10 larger at the first-order incommensurate to commensurate magnetic transitions at about 3.8 K (NVO) and 6 K (CVO) than the data in [6], [12] and [15], which were also all acquired using a PPMS. This large difference is due to the inadequacy

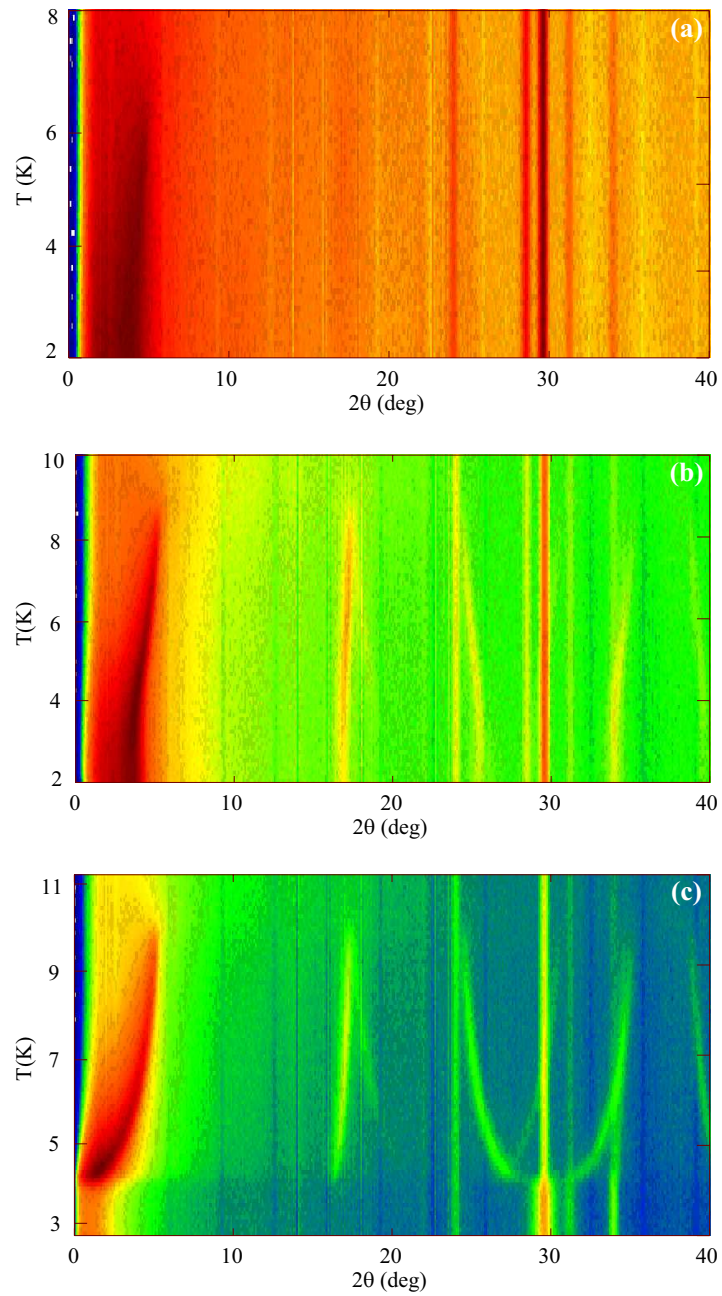


Figure 4.26.: Thermodiffractogramms of powder samples with (a) $x = 0.87$, (b) $x = 0.92$ and (c) $x = 0.98$. The patterns were recorded in 0.1 K steps.

of the standard PPMS software in dealing with sharp first-order phase transitions. For CVO especially, a large part of the magnetic entropy is gained at this first-order transition, which is missed by using the standard PPMS specific heat data acquisition. For the mixed crystals ($x = 0.5, 0.65$ and 0.86) only a single sharp feature indicating a phase transition is observed down to the lowest measured temperature of 2 K in agreement with the neutron powder diffraction experiments. These transition temperatures are plotted in the lower panel of Fig. 4.24 together with those determined by the magnetic neutron scattering data. Good agreement is found between the two sets of transition temperatures, confirming the Vegard's law approximation of the single crystal Co contents.

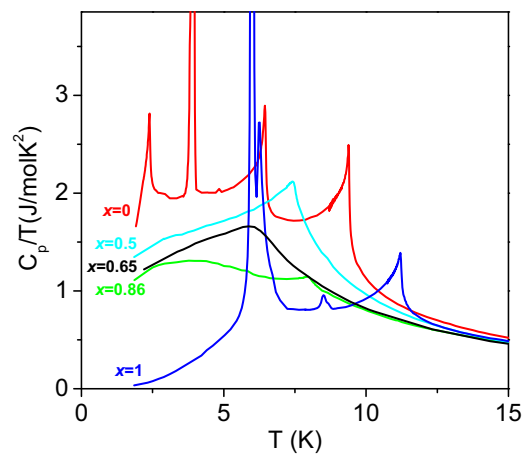


Figure 4.27.: Heat capacity curves as a function of temperature revealing a single phase transition for the mixed crystals.

4.3. $(\text{Co}_{0.5}\text{Ni}_{0.5})_3\text{V}_2\text{O}_8$

The nuclear and magnetic structure investigation of a $(\text{Co}_{0.5}\text{Ni}_{0.5})_3\text{V}_2\text{O}_8$ single crystal has been performed at the four-circle diffractometer D10 (ILL). The diffractometer, which has been used in the standard four-circle configuration (without the energy analyzer option), is suited for conventional crystallographic studies of nuclear and magnetic structures due to its good momentum resolution with relatively high flux and its low intrinsic background. It is equipped with an $80 \times 80 \text{ mm}^2$ two-dimensional microstrip detector for three-dimensional resolution in reciprocal space. In the diffraction configuration the detector may be inclined up to 30° to the equatorial plane to increase the out-of-plane access. A schematic diagram of the instrument is shown in Fig. 4.28.

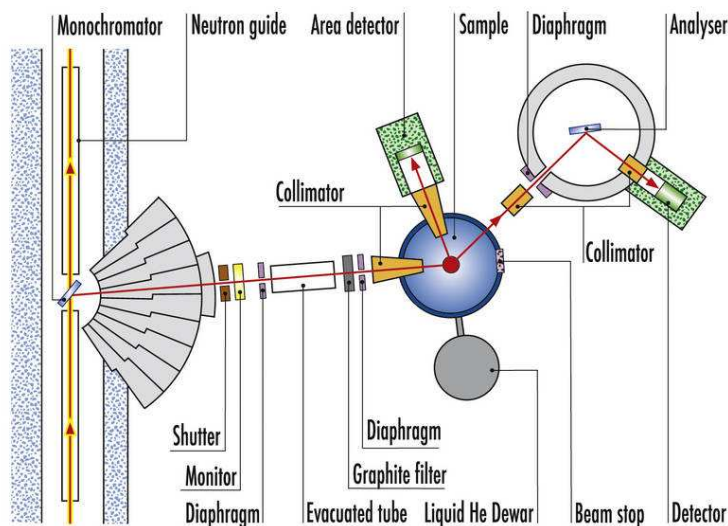


Figure 4.28.: Instrument layout of the four-circle diffractometer D10.

As no magnetic contribution from a zero wave vector could be observed on the nuclear reflections, both the nuclear and the magnetic structure were investigated at $T = 1.5 \text{ K}$ using a wavelength of 2.359 \AA from a pyrolytic graphite monochromator. An additional data set of the nuclear reflections was collected with $\lambda = 1.255 \text{ \AA}$ supplied by the (200) reflection of a Cu monochromator in order to be able to apply extinction and absorption corrections. By using a four-circle cryostat a large part of reciprocal space could be investigated offering the possibility of measuring a large number of reflections. Besides the structure investigations various scans in reciprocal space directions and in temperature have been carried out in order to extract information about the a^* , b^* and c^* components

of the propagation vector and the magnetic phase transition temperature. Magnetization curves were recorded on a Quantum Design SQUID magnetometer (Darmstadt University of Technology) as a function of temperature, in 0.05 K steps, in a magnetic field of 50 Oe applied along the principal crystallographic axes. The specific heat was measured at Forschungszentrum Karlsruhe in zero field with a standard PPMS calorimeter from Quantum Design. The data close to the transition were obtained by using a procedure similar to that presented in [91], which allows for a high temperature-resolution.

4.3.1. Nuclear structure

The nuclear structure investigation confirmed the correct phase formation of the orthorhombic structure (space group Cmca). The cell constants were found to be $a = 5.981(2)$ Å, $b = 11.436(5)$ Å and $c = 8.261(6)$ Å showing close agreement with the previously investigated powder sample with a similar composition (Sec. 4.2.1, Tab. 4.6). The integrated intensities were corrected for absorption and extinction applying the transmission factor integral $\exp[-\mu(\bar{t}_{in} + \bar{t}_{out})]$ and the derivative integral $(\bar{t}_{in} + \bar{t}_{out}) \exp[-\mu(\bar{t}_{in} + \bar{t}_{out})]$ according to the Becker and Coppens Lorentzian model [51] [μ is the linear absorption coefficient, which is 0.448 cm^{-1} for $(\text{Co}_{0.5}\text{Ni}_{0.5})_3\text{V}_2\text{O}_8$]. The structure models were refined using programs of the CCSL [49] and confirmed by FullProf [50]. The nuclear structure refinement included the respective atomic positions and isotropic temperature factors of M and O plus the cation distribution of Co and Ni on both M sites and the extinction parameters. Because of its low coherent neutron scattering cross section, the atomic position and the temperature factor of V have been fixed in all refinements. The refined values ($R_1 = 6.5$) are listed in Table 4.7. The goodness of the fit is illustrated by a F_{obs} vs. F_{cal} plot in Fig. 4.29. The analysis of the cation occupancy yields a true Co:Ni ratio of 53:47 with the Co^{2+} ions having a higher affinity for the more symmetric (4a) site as it has been observed on powder samples in Sec. 4.2.1.

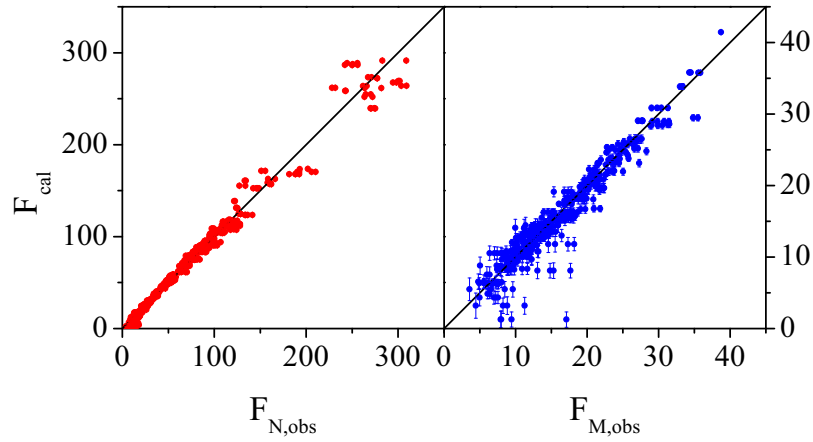


Figure 4.29.: Illustration of the fit results. The left and right panels show the nuclear and magnetic data, respectively.

Table 4.7.: Structural parameters of the investigated $(\text{Co}_{0.5}\text{Ni}_{0.5})_3\text{V}_2\text{O}_8$ single crystal sample.

Atom	x	y	z	$B(\text{\AA}^2)$	occupancy
Co1	0	0	0	0.11(5)	0.612(9)
Co2	0.25	0.1304(2)	0.25	0.12(5)	0.492(9)
Ni1	0	0	0	0.11(5)	0.388(9)
Ni2	0.25	0.1304(2)	0.25	0.12(5)	0.508(9)
V	0	0.3762	0.1196	0.24	1
O1	0	0.2489(3)	0.2306(5)	0.25(5)	1
O2	0	0.0012(3)	0.2451(5)	0.25(5)	1
O3	0.2673(3)	0.1193(2)	0.9988(5)	0.29(5)	1

Extinction parameters

Domain radius(nm): 1.4(1) Mosaicity spread(rad): 0.037(3)

4.3.2. Magnetic phase transition temperature

The investigation of the magnetic properties was first dedicated to examine the transition temperature and the propagation vector. Therefore the $(000)^+$ and $(111)^-$ reflections were measured as a function of temperature to determine the transition temperature into the antiferromagnetic phase. It can be seen in the upper right inset of Fig. 4.30 that the magnetic reflections appear at approximately 6.8(2) K. Magnetization measurements with an applied magnetic field of 50 Oe parallel to the respective crystallographic axes exhibit anomalies of the magnetization curves at 7.6(1) K (lower panel of Fig. 4.30), which agrees well with the transition temperature of the powder sample investigated on the same instrument. The specific heat is shown in the upper panel of Fig. 4.30 in a C_p/T versus T representation. The magnetic transition manifests itself as a sharp maximum in C_p/T at $T_N = 7.4(1)$ K, which is declared as the temperature of magnetic ordering as the heat capacity is considered to be the most precise of the data presented here for localizing the magnetic phase transition. The slightly different results in the magnetization and diffraction experiments are considered to be a result of the chosen criterion of determining the transition temperature.

A magnetic signal extends in the specific heat data up to about 25 K, i.e. more than 3 times T_N . This could be the signature of magnetic fluctuations, whose nature is unknown. Similar short-range ordering effects up to about $3 \times T_N$ are also observed in $\text{Cu}_3\text{V}_2\text{O}_8$ [9] and may share a similar origin. Below T_N , C_p/T remains unusually high down to the lowest measured temperature of 1.8 K, probably because of magnetic fluctuations, consequence of the frustration. Such a behaviour is sometimes observed in heavy-fermion systems, where strong fluctuations, due to Kondo and RKKY interactions, are present in the magnetically ordered phase [92]. At about 2.4 K a "bump" can be observed in the C_p/T data, whose origin is not yet understood.

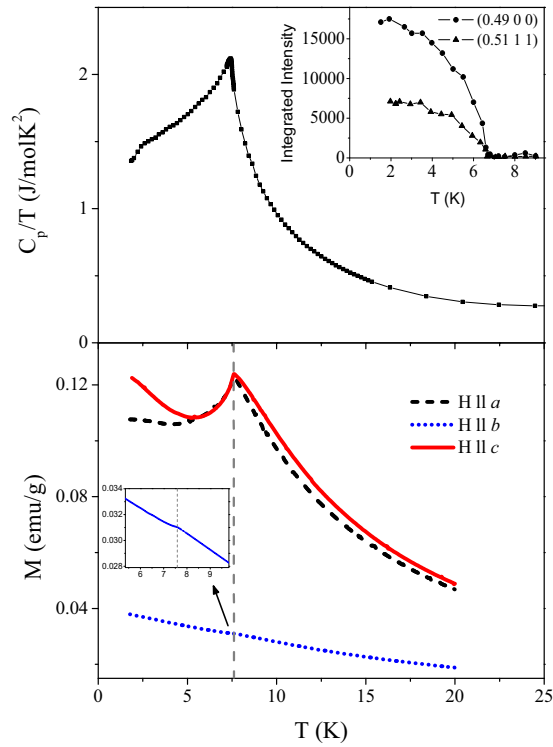


Figure 4.30.: Upper panel: Heat capacity curve as a function of temperature. The inset in the upper right corner displays the temperature dependence of the integrated intensities of two chosen magnetic reflections (data points in the upper panel and inset are connected by straight lines). Lower panel: Magnetization curves of a $(\text{Co}_{0.5}\text{Ni}_{0.5})_3\text{V}_2\text{O}_8$ single crystal with $H = 50$ Oe applied parallel to the crystal axes, respectively. The inset indicated by an arrow shows a magnification to focus the transition point of the curve with $H \parallel b$.

4.3.3. Propagation vector

In order to verify the propagation vector the $(000)^+$ reflection was scanned along the three principal directions of reciprocal space. The a^* , b^* and c^* components of the wave vector were deduced by determining the centers of Pseudo-Voigt functions, which were fitted to the observed reflection profiles (Fig. 4.31). The resulting values confirm the propagation vector $\mathbf{k} = (0.49, 0, 0)$, where it has to be stressed that an incommensurability is present. This has been checked by verifying the position of the (400) reflection, which was found to be precisely centered at $h = 4.00$.

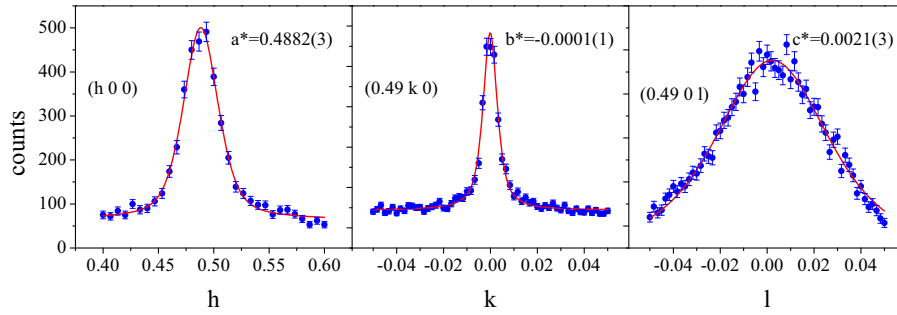


Figure 4.31.: q-scans through the $(000)^+$ reflection along the a^* , b^* and c^* direction. The centers of the Pseudo-Voigt fits are displayed in the upper right corners of the respective plots confirming the propagation vector $\mathbf{k}=(0.49, 0, 0)$.

4.3.4. Magnetic structure

For the determination of the magnetic structure more than 400 independent magnetic reflections have been measured. Magnetic structure models were obtained by the help of representation analysis. The eight symmetry operators for the $(000)^+$ set of space group $Cmca$ form the group G . As mentioned in Sec. 2.3.8.2 only four symmetry elements of group G leave the propagation vector $\mathbf{k} = (0.49, 0, 0)$ invariant, forming the little group $G_{\mathbf{k}} = \{1, 2_x, b_{xy}, c_{xz}\}$. All the elements of $G_{\mathbf{k}}$ permute, which leads to four one-dimensional irreducible representations labelled Γ^1 to Γ^4 . The decompositions of the induced representations for the respective sites are $\Gamma(4a) = \Gamma^1 + \Gamma^2 + 2\Gamma^3 + 2\Gamma^4$ and $\Gamma(8e) = 3\Gamma^1 + 3\Gamma^2 + 3\Gamma^3 + 3\Gamma^4$ (see Sec. 2.3.8.4). The observed integrated intensities are distinctly best described ($R_1=8.2$, see Fig. 4.29) by the magnetic mode $C_1(S_{1ay} - S_{1by}) + C_2(S_{1az} + S_{1bz}) + C_3(S_{2ax} + S_{2bx} - S_{2cx} - S_{2dx}) + C_4(S_{2ay} - S_{2by} - S_{2cy} + S_{2dy}) + C_5(S_{2az} + S_{2bz} + S_{2cz} + S_{2dz})$ corresponding to Γ^4 (see Sec. 2.3.8.5, Tab. 2.11), where $S_{i,n}$ represents a magnetic moment of atom n on site i (see Table 4.8 for the definition of

the respective atoms). The propagation of the magnetic mode is amplitude modulated by

Table 4.8.: Fractional coordinates of the M^{2+} ions related to the spin properties $S_{i,n}$ and the corresponding Fourier coefficients.

Site i	Atom n	x,y,z-Coordinates	Fourier coefficients
1(4a)	a	(0,0,0)	(0, v_1 , w_1)
	b	(0, $\frac{1}{2}$, $\frac{1}{2}$)	(0,- v_1 , w_1)
	a	($\frac{1}{4}$, y , $\frac{1}{4}$)	(u_2 , v_2 , w_2)
2(8e)	b	($\frac{1}{4}$, $\bar{y} + \frac{1}{2}$, $\frac{3}{4}$)	(u_2 , - v_2 , w_2)
	c	($\frac{1}{4}$, $y + \frac{1}{2}$, $\frac{1}{4}$)	(- u_2 , - v_2 , w_2)
	d	($\frac{1}{4}$, \bar{y} , $\frac{3}{4}$)	(- u_2 , v_2 , w_2)

the wave vector $\mathbf{k} = (0.49, 0, 0)$. The parameters C_1 to C_5 have been set as variables in the refinement process, where an averaged magnetic form factor consisting of the weighted analytical approximations of the Ni^{2+} and Co^{2+} form factors [84] has been used. In a first step, the refinement parameters C_1 and C_4 were found to be very small with relatively large standard deviations indicating that the magnetic moments on both crystallographic sites probably do not exhibit a b component. For further refinement steps these variables were set to zero. However, an upper bound of $0.11(3) \mu_B$ and $0.15(6) \mu_B$ can be given for the (4a) cross tie and (8e) spine moments, respectively [$C_2=1.59(2) \mu_B$, $C_3=1.44(2) \mu_B$, $C_5=0.65(1) \mu_B$]. Finally, the resulting amplitudes of the modulating waves have been refined to $1.59(1) \mu_B$ along the c axis for the cross tie spins and $1.60(1) \mu_B$ within the a - c plane for the spine spins at 1.5 K. The angle θ between the spine magnetic moments and the c axis has been refined to $65.1(3)^\circ$. A phase shift between the modulating waves of the two magnetic sites results in a considerably worse fit and is therefore not justified. The magnetic structure is depicted in Fig. 4.32.

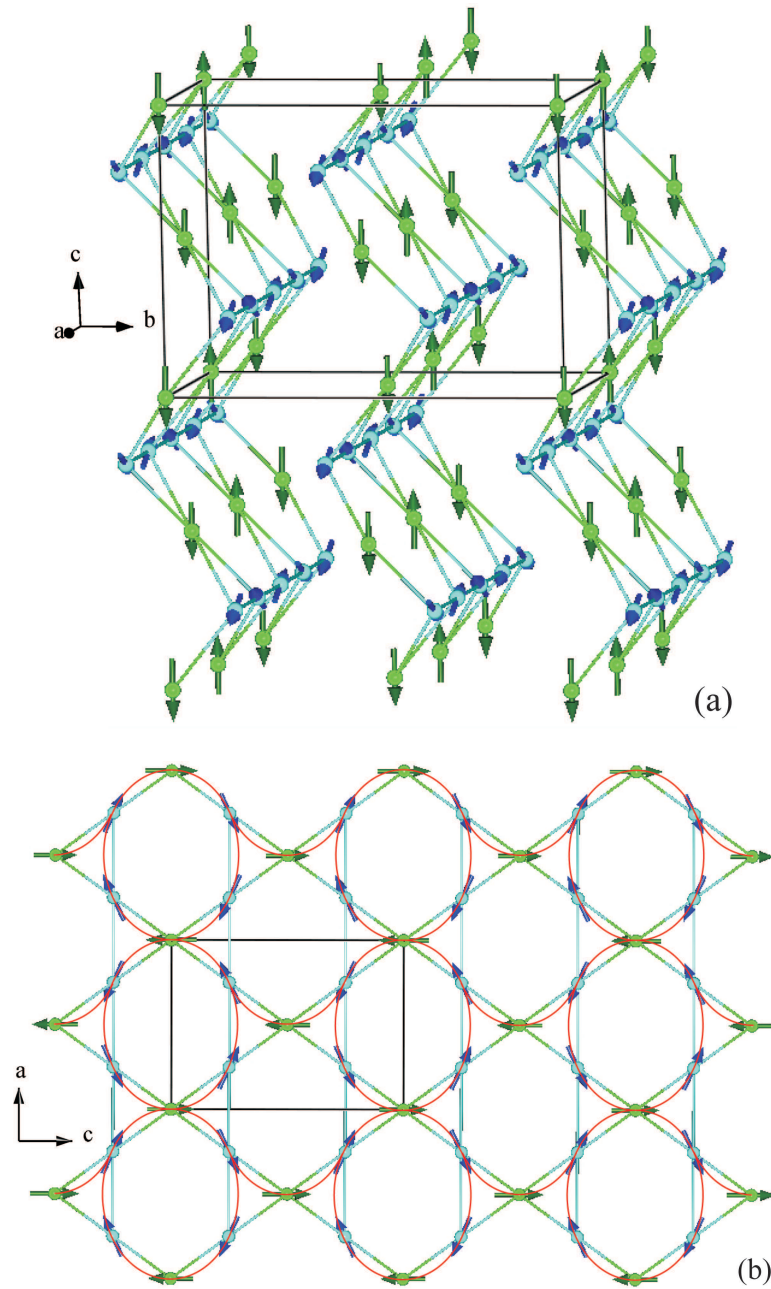


Figure 4.32.: Antiferromagnetic structure model with $\mathbf{k} = (0.49, 0, 0)$. (a) shows the perspective view on three neighbouring staircases. (b) shows a single staircase viewed along the b axis revealing the loops and waves (sketched in red) consisting of ferromagnetically coupled nearest neighbours.

5. Summary

A thorough and systematic study of the magnetic properties of the 3d transition metal orthooxovanadates $(\text{Co}_x\text{Ni}_{1-x})_3\text{V}_2\text{O}_8$ combining a variety of methods such as neutron powder and single crystal diffraction, polarized neutron diffraction, magnetization and heat capacity measurements, magnetic Compton scattering and *ab initio* calculations has been presented. On the one hand investigations on the mixed system have been carried out, which led to entirely new insights into the magnetic temperature-composition phase diagram and the magnetic structure. On the other hand detailed and precise analysis of the extensively studied compound $\text{Co}_3\text{V}_2\text{O}_8$ yielded highly interesting and valuable features, which have not been realized before.

The first part of the investigation of the mixed system $(\text{Co}_x\text{Ni}_{1-x})_3\text{V}_2\text{O}_8$ has been carried out using neutron powder diffraction on three samples with $x=0.27$, 0.52 and 0.76 . In contrast to the end members only one temperature dependent magnetic phase transition into an antiferromagnetic ground state could be observed. The measured magnetic reflections could be indexed by introducing a propagation vector $\mathbf{k} = (\delta, 0, 0)$ and it has been revealed that the incommensurability δ is dependent on the compositional parameter x , where δ increases with increasing amount of Co.

The magnetic phase transitions of the $(\text{Co}_x\text{Ni}_{1-x})_3\text{V}_2\text{O}_8$ system have been examined as a function of temperature and composition by neutron powder diffraction and single crystal heat capacity experiments. The obtained transition points of both methods match up well and are plotted together in the magnetic (x, T) phase diagram (lower panel of Fig. 4.24). One can observe a decrease of T_N with increasing amount of M^{2+} substitution starting from either end of the phase diagram, until the lowest observed Néel temperature of 5.5 K is reached with $x = 0.76$. This composition still exhibits a CVO type modulation, while $x = 0.71$ is modulated by \mathbf{k}_2 , what indicates a change of the magnetic structure for $0.71 < x < 0.76$ into the antiferromagnetic long-range ordered NVO type. Furthermore, it has been deduced that small degrees of magnetic ion substitution disturb the magnetic structures of the parent compounds. Substituting 2% of Co with Ni leads to a suppression of the ferromagnetic CVO ground state in favour of the antiferromagnetic short-range ordered CVO phase with $\mathbf{k}_1 = [0, \delta(T, x), 0]$. On the other hand, 3.5% Co on

5. Summary

the magnetic sites of NVO remove the temperature dependence of its propagation vector $\mathbf{k}_2 = [\delta(T, x), 0, 0]$. A further interesting result is the existence of a phase within AF_1 with δ having a constant value of 0.4, which is the case for $T < 4.2K$ and $0.76 < x < 0.92$. These findings allowed to draw a preliminary phase boundary inside the AF_1 phase (dotted lines in Fig. 4.24).

In the proposed magnetic structure of $(Co_{0.5}Ni_{0.5})_3V_2O_8$, which results from the same irreducible representation as the high temperature incommensurate phase of NVO and is modulated by the same type of propagation vector, the two sublattices of M^{2+} ions exhibit differently oriented magnetic moments in the a - c plane, where the cross-tie moments are collinear along the c axis, but the spine moments span a $65.1(3)^\circ$ angle with the c axis. As previously reported [15], the symmetry of the crystal structure admits a Dzyaloshinskii-Moriya interaction [93, 94] among the nearest neighbour spine spins, which justifies the observed canting between the aforementioned spins in $(Co_{0.5}Ni_{0.5})_3V_2O_8$. Fig. 4.32 displays the magnetic structure after a global phase shift of $\frac{\pi}{4}$ has been applied in order to show a picture, in which the amplitude of all magnetic moments is sufficiently high so that their orientation is clearly visible. The 4a site is represented by green atoms and magnetic moments, while the 8e site is depicted in blue. Fig. 4.32(b) shows a single staircase viewed along the b axis, which emphasizes the characteristics of this magnetic structure. Given the orientation of the magnetic moments with respect to the crystal axes, there exist in principle 2^3 possibilities to place the moments on the corners of the isosceles triangles of the kagome staircase structure. The magnetic structure presented here reveals only six of these possibilities. No triangle can be found, in which all three moments point either towards or away from each other, as it would be expected for a frustrated antiferromagnetic system. Due to the propagation vector $\mathbf{k} = (0.49, 0, 0)$ the direction of every magnetic moment is flipped after a translation of the lattice vector a . The resulting picture of the average magnetic structure shows loops, within which every pair of nearest neighbour spins couples as in a canted ferromagnet. We call this arrangement a quasiferromagnetic loop, because a ferromagnetic component exists for every pair of nearest neighbours but not for the whole loop. These loops are connected along the a axis with alternating sense of rotation, while they are separated along the c axis by cross-tie moments not belonging to the loops, but forming the same kind of canted ferromagnetic coupling with their nearest neighbour of the superior part of a loop on either side. This results in a sort of wave along the c axis, which also alternates its direction when translated by a . Similarly, we call this a quasiferromagnetic wave, because the ferromagnetic components of two neighbouring spins are not parallel for all pairs of neighbours. After a translation of $\pm 12.5a$, where the amplitudes of the magnetic moments run through the full value and zero, respectively, the loops are shifted by $(\frac{1}{2}, 0, \frac{1}{2})$, i.e. they change places with the connecting segments. This

switching has a period of $25a$. As the propagation vector possesses an a^* component the neighbouring kagome staircases do not differ concerning their spin arrangement like in the antiferromagnetic structure of CVO, where the staircases alternate between ferromagnetic and antiferromagnetic ones. It can be seen in Fig. 4.32(a) that the orientation of the spine spins within the chains along the a axis is exactly the same as in each of the two neighbouring chains of the next staircase. A mean-field approach to the first ordered state based on classical spins [95] was attempted in order to confirm the magnetic structure theoretically. The attempt failed because of the inability of adequately describing each magnetic moment's vicinity, which varies locally as a consequence of the statistical occupation of the magnetic sites by Co and Ni.

Like it has already been observed on the powder samples, only one magnetic phase transition exists down to 1.8 K, which the heat capacity measurements confirm. However, as an incommensurate magnetic structure is not likely to be a ground state, a commensurate lock-in is expected at very low temperatures.

The striking result of this experiment is the considerable deviation of the $(\text{Co}_{0.5}\text{Ni}_{0.5})_3\text{V}_2\text{O}_8$ magnetic structure from those of its parent compounds CVO and NVO, which exhibit a variety of magnetic structures with magnetic moments oriented along the a axis [6] or predominantly in the a - b plane with small components along c [19], respectively. Comparing the ground states of the parent compounds, which are a ferromagnet for CVO and a canted antiferromagnet for NVO, with the magnetic structure presented here, one can deduce a higher degree of competition between nearest neighbour interactions for $(\text{Co}_{0.5}\text{Ni}_{0.5})_3\text{V}_2\text{O}_8$. A simple global picture based on exchange interactions cannot be set as a consequence of the chemical disorder. However, the Ising-like behaviour of Co^{2+} in combination with its higher affinity for the 4a site could explain the collinear alignment of the cross-tie spins. The result of this work should be followed by a theoretical approach as it shows once again that the competition of the exchange interactions along various coupling pathways in this particular crystallographic system results in a variety of different interesting magnetic structures.

The probably most stunning results were obtained from the real space magnetization and momentum space spin density distributions. Detailed and precise analysis of these quantities were required in order to determine the exact contribution of the atomic species involved in the studied system. Quantum chemical modeling was needed to gain insights, at a molecular level, into the electronic structure of the two cobalt-oxide octahedra. In this context, *ab initio* cluster calculations were done for the Co_cO_6 and Co_sO_6 octahedra yielding precise molecular orbitals and wave functions. The latter were used to analyze the experimentally observed density distributions. The refinement of the contribution of each molecular orbital wave function, at a quantum chemical level, to the real and mo-

momentum space densities simultaneously has shown to be a powerful procedure allowing to get interesting and valuable features of the magnetic form factors. The importance of system-specific molecular orbital wave functions becomes obvious with the fact that the R value for the flipping ratio refinement could be improved from 13.8, which results from an individual refinement with tabulated spherical form factors, to 9.6 with the use of the *ab initio* results even for the correlated refinement. In order to be able to obtain such valuable results it was crucial to perform accurate extinction corrections as the very phenomena turned out to be of great magnitude. With this extensive treatment a crucial observation could be made concerning the Co_c ion. The previous assumption, that the ferromagnetic structure at zero magnetic field is not fully ordered because of the Co_c only exhibiting $1.54 \mu_B$, could be disproved. Previous macroscopic magnetization measurements [16] indeed showed a saturated moment of approximately $3.4 \mu_B$ per Co site at $H=2$ T along a , but the results presented here reveal that the field dependent increase of magnetization stems from the V, O2 and O3 sites. Hereby, the V and O2 site show quite localized magnetization density, while the O3 density seems to be smeared out due to truncation effects in the Fourier series. The spin polarized density on O2 and O3, which are those oxygen ions in the Co_cO_6 clusters, may be a strong indication for a partially covalent character of the Co_c ions and the reason for their relatively low magnetic moment compared to Co_s . Referring to an ionic spin- $\frac{3}{2}$ Co^{2+} the value of the Co_c magnetic moment would imply, that almost 50% of the spin density is transferred to the surrounding ligands. As pointed out in [96] the underlying physical process involved in the spin transfer is rather a paired O2p electron going to a half occupied Co3d orbital and not vice versa, thus reducing the cation and increasing the ligand moment. Large covalency, although to a lesser extent (28%), has also been observed in Fe_3O_4 [97].

The magnetization density distribution clearly exhibits the superexchange pathways between the two different Co sites, but it indicates also the interlayer coupling, which is mediated by the V-O1 bridge. Combining the methods of polarized neutron diffraction and magnetic Compton scattering allowed to refine the occupations of the Co3d orbitals in a stable way. Like it has been previously reported but with inverse results [7] the two crystallographically different Co ions exhibit different spin polarized orbital occupations. While the unpaired electrons are equally distributed between the t_{2g} and e_g levels for the Co_s ion, the magnetic signal stems by as much as 70% from the t_{2g} orbitals for the Co_c ion. Concerning the e_g orbitals of both ions the basal plane orbital $d_{x^2-y^2}$ is more populated than the apical $d_{3z^2-r^2}$ orbital. This possibly indicates a higher exchange interaction between the Co_s ions via an intermediate O2 ion. In the case of the Co_c ions it could be a hint that the magnetic exchange with the spine Co ions takes place preferentially via an O3 ion. In other words, the O2 sites mediate the superexchange between spine and cross-tie ions, while the O3 sites mediate the superexchange between the spine ions. The

O1 sites which are situated at the outermost positions of the staircases reveal only weak magnetic moments, but therefore they could play a role in the interlayer coupling with the V ions. Fig. 5.1 shows a part of kagome staircase, in which the different oxygen types are distinguishable. The pathways which are believed to play a more pronounced role for the exchange interaction are represented by thick bonds.

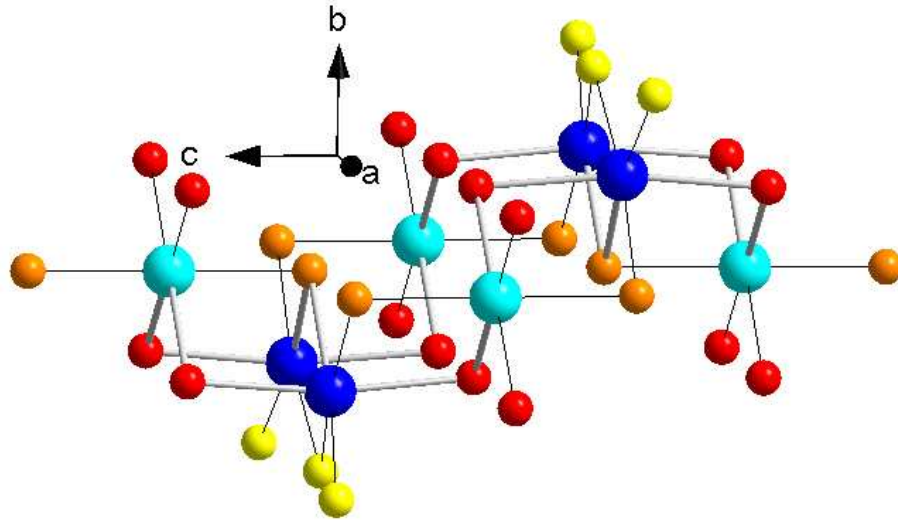


Figure 5.1.: Part of a kagome staircase showing the cross-tie (light blue) and spine Co ions (dark blue) with the respective superexchange pathways via O1 (yellow), O2 (orange) and O3 ions (red). Pathways corresponding to more populated orbitals are sketched as thick bonds.

Appendix

A. Group theory

A.1. Derivations

A.1.1. The orthogonality theorem

From the arbitrary matrix \mathbf{B} of d_U rows and d_V columns and two inequivalent representations Γ^U and Γ^V of dimensions d_U and d_V , respectively, one can construct a matrix \mathbf{A} by means of

$$\mathbf{A} = \sum_{g \in G} \Gamma^U(g) \mathbf{B} \Gamma^V(g^{-1}). \quad (\text{A.1})$$

Multiplying Eq. A.1 with a V -dimensional representation of an arbitrary group element g' on the right side yields

$$\mathbf{A} \Gamma^V(g') = \sum_{g \in G} \Gamma^U(g) \mathbf{B} \Gamma^V(g^{-1}g'). \quad (\text{A.2})$$

As $g^{-1}g'$ must be equal to some element $g_k \in G$ according to the first group axiom so that $g' = gg_k$, every element g' appears in the set gg_k . It does not appear twice in gg_k , since it should appear in the forms gg_k and gg_l , which would give $g_k = g_l$ by premultiplying by g^{-1} contrary to the assumption that the group elements are distinct. This so called *rearrangement theorem* allows to sum Eq. A.2 over $g'' \equiv g'^{-1}g$ instead of g :

$$\mathbf{A} \Gamma^V(g') = \sum_{g'' \in G} \Gamma^U(g'g'') \mathbf{B} \Gamma^V(g''^{-1}) = \Gamma^U(g') \mathbf{A}. \quad (\text{A.3})$$

Eq. A.3 shows that \mathbf{A} fulfills Schür's first lemma, hence if Γ^U and Γ^V are inequivalent, \mathbf{A} must be the zero matrix so that

$$\sum_l \sum_m \sum_{g \in G} \Gamma_{j,l}^U(g) B_{l,m} \Gamma_{m,n}^V(g^{-1}) = 0, \quad (\text{A.4})$$

which means that any successive row-column multiplication of $\Gamma^U(g) \mathbf{B} \Gamma^V(g^{-1})$ gives a zero element. As \mathbf{B} is a completely arbitrary matrix it can be chosen to have all elements

zero except for $B_{l,m} = 1$, which yields

$$\sum_{g \in G} \Gamma_{j,l}^U(g) \Gamma_{m,n}^V(g^{-1}) = 0 \quad (\text{A.5})$$

as only the elements in the last column of Γ^U and those in the last row of Γ^V are multiplied with $B_{l,m}$. With $\mathbf{\Gamma}^V$ being a unitary matrix one can write

$$\sum_{g \in G} \Gamma_{j,l}^U(g) (\Gamma_{n,m}^V(g))^* = 0 \quad (\text{A.6})$$

Eq. A.6 states the orthogonality theorem in case that $\mathbf{\Gamma}^U$ and $\mathbf{\Gamma}^V$ are inequivalent. In case of equivalency Eq. A.1 is combined with Schür's second lemma:

$$\mathbf{A} = \sum_{g \in G} \mathbf{\Gamma}^U(g) \mathbf{B} \mathbf{\Gamma}^U(g^{-1}) = c \mathbf{1}, \quad (\text{A.7})$$

where c is a complex scalar and $\mathbf{1}$ is the unit matrix of order d_U . With the same choice of \mathbf{B} as above one obtains

$$\sum_{g \in G} \Gamma_{j,l}^U(g) \Gamma_{m,n}^U(g^{-1}) = c \delta_{jn}, \quad (\text{A.8})$$

which obviously is only nonzero if the elements multiplied produce a diagonal element on the right side of Eq. A.7, hence if the j^{th} row of $\Gamma^U(g)$ is multiplied with the j^{th} column of $\Gamma^V(g^{-1})$. To determine the constant c one sets $j = n$ and sums over j . The left-hand side of Eq. A.8 yields

$$\sum_{j=1}^{d_U} \sum_{g \in G} \Gamma_{j,l}^U(g) \Gamma_{m,j}^U(g^{-1}) = \sum_{g \in G} [\mathbf{\Gamma}^U(g^{-1}) \mathbf{\Gamma}^U(g)]_{m,l} = \sum_{g \in G} \Gamma_{m,l}^U(g^{-1}g) = n_G \delta_{lm}, \quad (\text{A.9})$$

while for the right-hand side one obtains

$$c \sum_{j=1}^{d_U} 1 = c d_U. \quad (\text{A.10})$$

Combining the results of Eq. A.9 and Eq. A.10 gives

$$c = \frac{n_G}{d_U} \delta_{lm}. \quad (\text{A.11})$$

Substituting Eq. A.11 into Eq. A.8 and using unitarity yields the orthogonality theorem stated in Eq. 2.30.

A.1.2. Equality of characters for equivalent representations

Let \mathbf{T} and \mathbf{S} be two arbitrary square matrices of the same dimension. One can show with

$$\sum_i (\mathbf{TS})_{i,i} = \sum_i \sum_j T_{i,j} S_{j,i} = \sum_j \sum_i S_{j,i} T_{i,j} = \sum_j (\mathbf{ST})_{j,j}, \quad (\text{A.12})$$

the following important property:

$$\text{Tr}(\mathbf{TS}) = \text{Tr}(\mathbf{ST}) \quad (\text{A.13})$$

Setting $\mathbf{S} = \mathbf{QT}^{-1}$ in Eq. A.13 one obtains

$$\text{Tr}(\mathbf{TQT}^{-1}) = \text{Tr}(\mathbf{Q}), \quad (\text{A.14})$$

which shows that the trace is invariant with respect to similarity transformations. Since equivalent representations are related to each other through Eq. 2.22, their characters are equal owing to Eq. A.14.

A.1.3. Constancy of characters within classes

Any two conjugate elements a and b of a group G are related by

$$gag^{-1} = b \quad (\text{A.15})$$

with some group element $g \in G$. The corresponding relation among the representation matrices

$$\mathbf{\Gamma}(g)\mathbf{\Gamma}(a)\mathbf{\Gamma}(g)^{-1} = \mathbf{\Gamma}(b) \quad (\text{A.16})$$

together with Eq. A.14 yields

$$\chi(a) = \chi(b) \quad (\text{A.17})$$

showing that characters are constant over conjugacy classes.

A.1.4. Second orthogonality theorem for classes

For any class C_w of the group G Eq. 2.18 holds, which can be rewritten as

$$gC_w = C_wg, \quad (\text{A.18})$$

where g is an arbitrary element of G . Due to the homomorphism between the group and its representation, a similar relation to Eq. A.18 exists for the representation matrices as well. With defining

$$\mathbf{C}_w \equiv \sum_{g \in C_w} \mathbf{\Gamma}^U(g) \quad (\text{A.19})$$

one obtains

$$\mathbf{\Gamma}^U(g)\mathbf{C}_w = \mathbf{C}_w\mathbf{\Gamma}^U(g). \quad (\text{A.20})$$

Since $\mathbf{\Gamma}^U$ is irreducible, Schur's second lemma requires that $\mathbf{C}_w = \lambda\mathbf{1}$. To determine λ the trace is taken of both sides, which yields

$$n(C_w)\chi_w^U = \lambda d_U \quad (\text{A.21})$$

and therefore

$$\mathbf{C}_w = \frac{n(C_w)}{d_U} \chi_w^U \mathbf{1} \quad (\text{A.22})$$

Any product of classes consists of classes itself, which can straightforwardly be shown by

$$gC_eC_fg^{-1} = gC_eg^{-1}gC_fg^{-1} = C_eC_f. \quad (\text{A.23})$$

Hence any product of classes may be written as

$$C_eC_f = \sum_w c_{ef}^w C_w, \quad (\text{A.24})$$

which means that C_w appears c_{ef}^w times in the class product C_eC_f . One can use the homomorphism rule again to write

$$\mathbf{C}_e\mathbf{C}_f = \sum_w c_{ef}^w \mathbf{C}_w \quad (\text{A.25})$$

Substituting Eq. A.22 into Eq. A.25 gives

$$n(C_e)n(C_f)\chi_e^U\chi_f^U = d_U \sum_w c_{ef}^w n(C_w)\chi_w^U. \quad (\text{A.26})$$

With the result of Appendix A.1.5,

$$\sum_U d_U \chi_w^U = n_G \delta_{w1}, \quad (\text{A.27})$$

where C_1 denotes the class that consists of the single element E , and by summing both sides of Eq. A.26 over the irreducible representations U , one obtains

$$n(C_e)n(C_f) \sum_U \chi_e^U \chi_f^U = n_G c_{ef}^1 \quad (\text{A.28})$$

Now $C_{f'}$ shall denote the class consisting of the $n(C_{f'})$ inverse elements g^{-1} with respect to C_f , which consists of $n(C_f)$ elements g with $n(C_{f'}) = n(C_f)$. Due to the unitarity of the representation matrices one obtains

$$\chi_{f'}^U = (\chi_f^U)^* \quad (\text{A.29})$$

Considering the class product $C_e C_f$ (Eq. A.24) the class constant c_{ef}^1 is zero, if $C_e \neq C_{f'}$, because $C_e C_f$ does not contain the unit element. If $C_e = C_{f'}$, products of the form gg^{-1} appear $n(C_e)$ in the class product. Replacing f by f' in Eq. A.28 leads to the second orthogonality for characters

$$\sum_U \chi_e^U (\chi_f^U)^* = \frac{n_G}{n(C_e)} \delta_{ef} \quad (\text{A.30})$$

A.1.5. Sum of characters over representations

From Eq. 2.25 the character of the regular representation can be derived, which is

$$\chi^{reg}(g) = \sum_{i=1}^g \delta(g_i^{-1} g g_i) = \begin{cases} n_G, & \text{if } g = E \\ 0, & \text{otherwise} \end{cases} \quad (\text{A.31})$$

Since the regular representation is reducible, it can be decomposed into a direct sum of

irreducible representations, which can be written as

$$\Gamma^{reg}(g) = \bigoplus_U n_U \Gamma^U(g), \quad (\text{A.32})$$

where n_U are nonnegative integers. As the matrix of a regular representation can be block-diagonalized by means of equivalence transformation (see Eq. 2.24), its character can be expressed as

$$\chi^{reg}(g) = \sum_U n_U \chi^U(g). \quad (\text{A.33})$$

By multiplying by $(\chi^U(g))^*$ and summing over V instead of U yields

$$\sum_{g \in G} \chi^{reg}(g) (\chi^U(g))^* = \sum_V n_V \sum_{g \in G} \chi^V(g) (\chi^U(g))^*, \quad (\text{A.34})$$

which with application of the first orthogonality of characters (Eq. 2.34) simplifies to

$$\sum_V n_V n_G \delta_{UV} = n_U n_G. \quad (\text{A.35})$$

Combining Eq. A.34 and Eq. A.35 gives the coefficients n_U as

$$n_U = \frac{1}{n_G} \sum_{g \in G} \chi^{reg}(g) (\chi^U(g))^* = (\chi^U(E))^* = d_U. \quad (\text{A.36})$$

Using this result in Eq. A.33 leads to

$$\sum_U d_U \chi^U(g) = 0, \text{ for } g \neq E \quad (\text{A.37})$$

and

$$\sum_U d_U^2 = n_G, \text{ for } g = E. \quad (\text{A.38})$$

A.2. Calculations

A.2.1. Compatibility of symmetry elements with propagation vectors

To be compatible with a respective propagation vector a symmetry element has to fulfill

$$\alpha^* \mathbf{k} = \mathbf{k} + \mathbf{K}_p. \quad (\text{A.39})$$

$$\alpha^*(E) \mathbf{k}_2 = \begin{pmatrix} 1 & 0 & 0 \\ 0 & 1 & 0 \\ 0 & 0 & 1 \end{pmatrix} \begin{pmatrix} k_{a^*} \\ 0 \\ 0 \end{pmatrix} = \begin{pmatrix} k_{a^*} \\ 0 \\ 0 \end{pmatrix} \quad (\text{A.40})$$

$$\alpha^*(2_{1,z}) \mathbf{k}_2 = \begin{pmatrix} \bar{1} & 0 & 0 \\ 0 & \bar{1} & 0 \\ 0 & 0 & 1 \end{pmatrix} \begin{pmatrix} k_{a^*} \\ 0 \\ 0 \end{pmatrix} = \begin{pmatrix} -k_{a^*} \\ 0 \\ 0 \end{pmatrix} \neq \begin{pmatrix} k_{a^*} \\ 0 \\ 0 \end{pmatrix} + \mathbf{K}_p \quad (\text{A.41})$$

$$\alpha^*(2_{1,y}) \mathbf{k}_2 = \begin{pmatrix} \bar{1} & 0 & 0 \\ 0 & 1 & 0 \\ 0 & 0 & \bar{1} \end{pmatrix} \begin{pmatrix} k_{a^*} \\ 0 \\ 0 \end{pmatrix} = \begin{pmatrix} -k_{a^*} \\ 0 \\ 0 \end{pmatrix} \neq \begin{pmatrix} k_{a^*} \\ 0 \\ 0 \end{pmatrix} + \mathbf{K}_p \quad (\text{A.42})$$

$$\alpha^*(2_x) \mathbf{k}_2 = \begin{pmatrix} 1 & 0 & 0 \\ 0 & \bar{1} & 0 \\ 0 & 0 & \bar{1} \end{pmatrix} \begin{pmatrix} k_{a^*} \\ 0 \\ 0 \end{pmatrix} = \begin{pmatrix} k_{a^*} \\ 0 \\ 0 \end{pmatrix} \quad (\text{A.43})$$

$$\alpha^*(\bar{1}) \mathbf{k}_2 = \begin{pmatrix} \bar{1} & 0 & 0 \\ 0 & \bar{1} & 0 \\ 0 & 0 & \bar{1} \end{pmatrix} \begin{pmatrix} k_{a^*} \\ 0 \\ 0 \end{pmatrix} = \begin{pmatrix} -k_{a^*} \\ 0 \\ 0 \end{pmatrix} \neq \begin{pmatrix} k_{a^*} \\ 0 \\ 0 \end{pmatrix} + \mathbf{K}_p \quad (\text{A.44})$$

$$\alpha^*(b_{xy}) \mathbf{k}_2 = \begin{pmatrix} 1 & 0 & 0 \\ 0 & 1 & 0 \\ 0 & 0 & \bar{1} \end{pmatrix} \begin{pmatrix} k_{a^*} \\ 0 \\ 0 \end{pmatrix} = \begin{pmatrix} k_{a^*} \\ 0 \\ 0 \end{pmatrix} \quad (\text{A.45})$$

$$\alpha^*(c_{xz}) \mathbf{k}_2 = \begin{pmatrix} 1 & 0 & 0 \\ 0 & \bar{1} & 0 \\ 0 & 0 & 1 \end{pmatrix} \begin{pmatrix} k_{a^*} \\ 0 \\ 0 \end{pmatrix} = \begin{pmatrix} k_{a^*} \\ 0 \\ 0 \end{pmatrix} \quad (\text{A.46})$$

$$\alpha^*(m_{yz}) \mathbf{k}_2 = \begin{pmatrix} \bar{1} & 0 & 0 \\ 0 & 1 & 0 \\ 0 & 0 & 1 \end{pmatrix} \begin{pmatrix} k_{a^*} \\ 0 \\ 0 \end{pmatrix} = \begin{pmatrix} -k_{a^*} \\ 0 \\ 0 \end{pmatrix} \neq \begin{pmatrix} k_{a^*} \\ 0 \\ 0 \end{pmatrix} + \mathbf{K}_p \quad (\text{A.47})$$

Only $E, 2_x, b_{xy}$ and c_{xz} leave \mathbf{k}_2 invariant modulo \mathbf{K}_p . Note that $k_{a^*}=0.5$ makes no

difference for the incompatible elements as (010) is no reciprocal lattice vector because of the C-centering.

$$\alpha^*(E)\mathbf{k}_3 = \begin{pmatrix} 1 & 0 & 0 \\ 0 & 1 & 0 \\ 0 & 0 & 1 \end{pmatrix} \begin{pmatrix} 0 \\ k_{b^*} \\ 0 \end{pmatrix} = \begin{pmatrix} 0 \\ k_{b^*} \\ 0 \end{pmatrix} \quad (\text{A.48})$$

$$\alpha^*(2_{1,z})\mathbf{k}_3 = \begin{pmatrix} \bar{1} & 0 & 0 \\ 0 & \bar{1} & 0 \\ 0 & 0 & 1 \end{pmatrix} \begin{pmatrix} 0 \\ k_{b^*} \\ 0 \end{pmatrix} = \begin{pmatrix} 0 \\ -k_{b^*} \\ 0 \end{pmatrix} \neq \begin{pmatrix} 0 \\ k_{b^*} \\ 0 \end{pmatrix} + \mathbf{K}_p \quad (\text{A.49})$$

$$\alpha^*(2_{1,y})\mathbf{k}_3 = \begin{pmatrix} \bar{1} & 0 & 0 \\ 0 & 1 & 0 \\ 0 & 0 & \bar{1} \end{pmatrix} \begin{pmatrix} 0 \\ k_{b^*} \\ 0 \end{pmatrix} = \begin{pmatrix} 0 \\ k_{b^*} \\ 0 \end{pmatrix} \quad (\text{A.50})$$

$$\alpha^*(2_x)\mathbf{k}_3 = \begin{pmatrix} 1 & 0 & 0 \\ 0 & \bar{1} & 0 \\ 0 & 0 & \bar{1} \end{pmatrix} \begin{pmatrix} 0 \\ k_{b^*} \\ 0 \end{pmatrix} = \begin{pmatrix} 0 \\ -k_{b^*} \\ 0 \end{pmatrix} \neq \begin{pmatrix} 0 \\ k_{b^*} \\ 0 \end{pmatrix} + \mathbf{K}_p \quad (\text{A.51})$$

$$\alpha^*(\bar{1})\mathbf{k}_3 = \begin{pmatrix} \bar{1} & 0 & 0 \\ 0 & \bar{1} & 0 \\ 0 & 0 & \bar{1} \end{pmatrix} \begin{pmatrix} 0 \\ k_{b^*} \\ 0 \end{pmatrix} = \begin{pmatrix} 0 \\ -k_{b^*} \\ 0 \end{pmatrix} \neq \begin{pmatrix} 0 \\ k_{b^*} \\ 0 \end{pmatrix} + \mathbf{K}_p \quad (\text{A.52})$$

$$\alpha^*(b_{xy})\mathbf{k}_3 = \begin{pmatrix} 1 & 0 & 0 \\ 0 & 1 & 0 \\ 0 & 0 & \bar{1} \end{pmatrix} \begin{pmatrix} 0 \\ k_{b^*} \\ 0 \end{pmatrix} = \begin{pmatrix} 0 \\ k_{b^*} \\ 0 \end{pmatrix} \quad (\text{A.53})$$

$$\alpha^*(c_{xz})\mathbf{k}_3 = \begin{pmatrix} 1 & 0 & 0 \\ 0 & \bar{1} & 0 \\ 0 & 0 & 1 \end{pmatrix} \begin{pmatrix} 0 \\ k_{b^*} \\ 0 \end{pmatrix} = \begin{pmatrix} 0 \\ -k_{b^*} \\ 0 \end{pmatrix} \neq \begin{pmatrix} 0 \\ k_{b^*} \\ 0 \end{pmatrix} + \mathbf{K}_p \quad (\text{A.54})$$

$$\alpha^*(m_{yz})\mathbf{k}_3 = \begin{pmatrix} \bar{1} & 0 & 0 \\ 0 & 1 & 0 \\ 0 & 0 & 1 \end{pmatrix} \begin{pmatrix} 0 \\ k_{b^*} \\ 0 \end{pmatrix} = \begin{pmatrix} 0 \\ k_{b^*} \\ 0 \end{pmatrix} \quad (\text{A.55})$$

As one can see $G_{\mathbf{k}_3}$ consists of $E, 2_{1,y}, b_{xy}$ and m_{yz} .

A.2.2. Reduction of the permutation representation

The multiplicity coefficients $n_{\mathbf{k},U}$ are obtained by

$$n_{\mathbf{k},U} = \frac{1}{n_{G_{\mathbf{k}}}} \sum_{g \in G_{\mathbf{k}}} \chi_j^{\mathbf{k},perm}(g) \left(\chi^{\mathbf{k},U}(g) \right)^* \quad (\text{A.56})$$

1. $\mathbf{k}_1 = 0$

• M1 site 4a

$$n_{\mathbf{k}_1,1} = \frac{1}{8} (2 \cdot 1 + 2 \cdot 1 + 2 \cdot 1 + 2 \cdot 1) = 1 \quad (\text{A.57})$$

$$n_{\mathbf{k}_1,2} = \frac{1}{8} [2 \cdot 1 + 2 \cdot 1 + 2 \cdot (-1) + 2 \cdot (-1)] = 0 \quad (\text{A.58})$$

$$n_{\mathbf{k}_1,3} = \frac{1}{8} [2 \cdot 1 + 2 \cdot (-1) + 2 \cdot 1 + 2 \cdot (-1)] = 0 \quad (\text{A.59})$$

$$n_{\mathbf{k}_1,4} = \frac{1}{8} [2 \cdot 1 + 2 \cdot (-1) + 2 \cdot (-1) + 2 \cdot 1] = 0 \quad (\text{A.60})$$

$$n_{\mathbf{k}_1,5} = \frac{1}{8} [2 \cdot 1 + 2 \cdot (-1) + 2 \cdot 1 + 2 \cdot (-1)] = 0 \quad (\text{A.61})$$

$$n_{\mathbf{k}_1,6} = \frac{1}{8} [2 \cdot 1 + 2 \cdot (-1) + 2 \cdot (-1) + 2 \cdot 1] = 0 \quad (\text{A.62})$$

$$n_{\mathbf{k}_1,7} = \frac{1}{8} (2 \cdot 1 + 2 \cdot 1 + 2 \cdot 1 + 2 \cdot 1) = 1 \quad (\text{A.63})$$

$$n_{\mathbf{k}_1,8} = \frac{1}{8} [2 \cdot 1 + 2 \cdot 1 + 2 \cdot (-1) + 2 \cdot (-1)] = 0 \quad (\text{A.64})$$

Hence, the decomposition

$$\Gamma_{4a}^{\mathbf{k}_1, perm} = \Gamma^{\mathbf{k}_1,1} \oplus \Gamma^{\mathbf{k}_1,7}, \quad (\text{A.65})$$

• M2 site 8e

$$n_{\mathbf{k}_1,1} = \frac{1}{8} (4 \cdot 1 + 4 \cdot 1) = 1 \quad (\text{A.66})$$

$$n_{\mathbf{k}_1,2} = \frac{1}{8} (4 \cdot 1 + 4 \cdot 1) = 1 \quad (\text{A.67})$$

$$n_{\mathbf{k}_1,3} = \frac{1}{8} [4 \cdot 1 + 4 \cdot (-1)] = 0 \quad (\text{A.68})$$

$$n_{\mathbf{k}_1,4} = \frac{1}{8} [4 \cdot 1 + 4 \cdot (-1)] = 0 \quad (\text{A.69})$$

$$n_{\mathbf{k}_1,5} = \frac{1}{8} (4 \cdot 1 + 4 \cdot 1) = 1 \quad (\text{A.70})$$

$$n_{\mathbf{k}_1,6} = \frac{1}{8} (4 \cdot 1 + 4 \cdot 1) = 1 \quad (\text{A.71})$$

$$n_{\mathbf{k}_1,7} = \frac{1}{8} [4 \cdot 1 + 4 \cdot (-1)] = 0 \quad (\text{A.72})$$

$$n_{\mathbf{k}_1,8} = \frac{1}{8} [4 \cdot 1 + 4 \cdot (-1)] = 0 \quad (\text{A.73})$$

This results in

$$\Gamma_{8e}^{\mathbf{k}_1,perm} = \Gamma^{\mathbf{k}_1,1} \oplus \Gamma^{\mathbf{k}_1,2} \oplus \Gamma^{\mathbf{k}_1,5} \oplus \Gamma^{\mathbf{k}_1,6}. \quad (\text{A.74})$$

2. $\mathbf{k}_2 = (\mathbf{k}_{a^*}, 0, 0)$

- M1 site 4a

$$n_{\mathbf{k}_2,1} = \frac{1}{4} (2 \cdot 1 + 2 \cdot 1) = 1 \quad (\text{A.75})$$

$$n_{\mathbf{k}_2,2} = \frac{1}{4} (2 \cdot 1 + 2 \cdot 1) = 1 \quad (\text{A.76})$$

$$n_{\mathbf{k}_2,3} = \frac{1}{4} [2 \cdot 1 + 2 \cdot (-1)] = 0 \quad (\text{A.77})$$

$$n_{\mathbf{k}_2,4} = \frac{1}{4} [2 \cdot 1 + 2 \cdot (-1)] = 0 \quad (\text{A.78})$$

$$\Gamma_{4a}^{\mathbf{k}_2,perm} = \Gamma^{\mathbf{k}_2,1} \oplus \Gamma^{\mathbf{k}_2,2} \quad (\text{A.79})$$

- M2 site 8e

$$n_{\mathbf{k}_2,1} = \frac{1}{4} (4 \cdot 1) = 1 \quad (\text{A.80})$$

$$n_{\mathbf{k}_2,2} = \frac{1}{4} (4 \cdot 1) = 1 \quad (\text{A.81})$$

$$n_{\mathbf{k}_2,3} = \frac{1}{4} (4 \cdot 1) = 1 \quad (\text{A.82})$$

$$n_{\mathbf{k}_2,4} = \frac{1}{4} (4 \cdot 1) = 1 \quad (\text{A.83})$$

$$\Gamma_{8e}^{\mathbf{k}_2,perm} = \Gamma^{\mathbf{k}_2,1} \oplus \Gamma^{\mathbf{k}_2,2} \oplus \Gamma^{\mathbf{k}_2,3} \oplus \Gamma^{\mathbf{k}_2,4} \quad (\text{A.84})$$

3. $\mathbf{k}_3 = (0, k_{b^*}, 0)$

- M1 site 4a

$$n_{\mathbf{k}_3,1} = \frac{1}{4} [2 \cdot 1 + 2 \cdot (-1)] = 0 \quad (\text{A.85})$$

$$n_{\mathbf{k}_3,2} = \frac{1}{4} (2 \cdot 1 + 2 \cdot 1) = 1 \quad (\text{A.86})$$

$$n_{\mathbf{k}_3,3} = \frac{1}{4} (2 \cdot 1 + 2 \cdot 1) = 1 \quad (\text{A.87})$$

$$n_{\mathbf{k}_3,4} = \frac{1}{4} [2 \cdot 1 + 2 \cdot (-1)] = 0 \quad (\text{A.88})$$

$$\Gamma_{4a}^{\mathbf{k}_3,perm} = \Gamma^{\mathbf{k}_3,2} \oplus \Gamma^{\mathbf{k}_3,3} \quad (\text{A.89})$$

- M2 site 8e (valid for o_1 and o_2)

$$n_{\mathbf{k}_3,1} = \frac{1}{4} [2 \cdot 1 + 2 \exp(\pi i k_{b^*}) \cdot (\exp(\pi i k_{b^*}))^*] = 1 \quad (\text{A.90})$$

$$n_{\mathbf{k}_3,2} = \frac{1}{4} [2 \cdot 1 + 2 \exp(\pi i k_{b^*}) \cdot (\exp(\pi i k_{b^*}))^*] = 1 \quad (\text{A.91})$$

$$n_{\mathbf{k}_3,3} = \frac{1}{4} [2 \cdot 1 + 2 \exp(\pi i k_{b^*}) \cdot (-\exp(\pi i k_{b^*}))^*] = 0 \quad (\text{A.92})$$

$$n_{\mathbf{k}_3,4} = \frac{1}{4} [2 \cdot 1 + 2 \exp(\pi i k_{b^*}) \cdot (-\exp(\pi i k_{b^*}))^*] = 0 \quad (\text{A.93})$$

$$\Gamma_{8e}^{\mathbf{k}_3,perm} = \Gamma^{\mathbf{k}_3,1} \oplus \Gamma^{\mathbf{k}_3,2} \quad (\text{A.94})$$

A.2.3. Reduction of the axial vector representation

The multiplicity coefficients $n_{\mathbf{k},U}$ are obtained by

$$n_{\mathbf{k},U} = \frac{1}{n_{G_{\mathbf{k}}}} \sum_{g \in G_{\mathbf{k}}} \chi^{\mathbf{k},vect}(g) \left(\chi^{\mathbf{k},U}(g) \right)^* \quad (\text{A.95})$$

1. $\mathbf{k}_1 = 0$

$$\begin{aligned} n_{\mathbf{k}_1,1} &= \frac{1}{8} [3 \cdot 1 + (-1) \cdot 1 + (-1) \cdot 1 + (-1) \cdot 1 \\ &\quad + 3 \cdot 1 + (-1) \cdot 1 + (-1) \cdot 1 + (-1) \cdot 1] = 0 \end{aligned} \quad (\text{A.96})$$

$$\begin{aligned} n_{\mathbf{k}_1,2} &= \frac{1}{8} [3 \cdot 1 + (-1) \cdot 1 + (-1) \cdot 1 + (-1) \cdot 1 + 3 \cdot (-1) \\ &\quad + (-1) \cdot (-1) + (-1) \cdot (-1) + (-1) \cdot (-1)] = 0 \end{aligned} \quad (\text{A.97})$$

$$\begin{aligned} n_{\mathbf{k}_1,3} &= \frac{1}{8} [3 \cdot 1 + (-1) \cdot 1 + (-1) \cdot (-1) + (-1) \cdot (-1) \\ &\quad + 3 \cdot 1 + (-1) \cdot 1 + (-1) \cdot (-1) + (-1) \cdot (-1)] = 1 \end{aligned} \quad (\text{A.98})$$

$$\begin{aligned} n_{\mathbf{k}_1,4} &= \frac{1}{8} [3 \cdot 1 + (-1) \cdot 1 + (-1) \cdot (-1) + (-1) \cdot (-1) \\ &\quad + 3 \cdot (-1) + (-1) \cdot (-1) + (-1) \cdot 1 + (-1) \cdot 1] = 0 \end{aligned} \quad (\text{A.99})$$

$$\begin{aligned} n_{\mathbf{k}_1,5} &= \frac{1}{8} [3 \cdot 1 + (-1) \cdot (-1) + (-1) \cdot 1 + (-1) \cdot (-1) \\ &\quad + 3 \cdot 1 + (-1) \cdot (-1) + (-1) \cdot 1 + (-1) \cdot (-1)] = 1 \end{aligned} \quad (\text{A.100})$$

$$\begin{aligned} n_{\mathbf{k}_1,6} &= \frac{1}{8} [3 \cdot 1 + (-1) \cdot (-1) + (-1) \cdot 1 + (-1) \cdot (-1) \\ &\quad + 3 \cdot (-1) + (-1) \cdot 1 + (-1) \cdot (-1) + (-1) \cdot 1] = 0 \end{aligned} \quad (\text{A.101})$$

$$\begin{aligned} n_{\mathbf{k}_1,7} &= \frac{1}{8} [3 \cdot 1 + (-1) \cdot (-1) + (-1) \cdot (-1) + (-1) \cdot 1 \\ &\quad + 3 \cdot 1 + (-1) \cdot (-1) + (-1) \cdot (-1) + (-1) \cdot 1] = 1 \end{aligned} \quad (\text{A.102})$$

$$\begin{aligned} n_{\mathbf{k}_1,8} &= \frac{1}{8} [3 \cdot 1 + (-1) \cdot (-1) + (-1) \cdot (-1) + (-1) \cdot 1 \\ &\quad + 3 \cdot (-1) + (-1) \cdot 1 + (-1) \cdot 1 + (-1) \cdot (-1)] = 0 \end{aligned} \quad (\text{A.103})$$

The 3-dimensional axial vector representation decomposes as

$$\Gamma^{\mathbf{k}_1, vect} = \Gamma^{\mathbf{k}_1, 3} \oplus \Gamma^{\mathbf{k}_1, 5} \oplus \Gamma^{\mathbf{k}_1, 7} \quad (\text{A.104})$$

2. $\mathbf{k}_2 = (k_{a^*}, 0, 0)$

$$n_{\mathbf{k}_2, 1} = \frac{1}{4} [3 \cdot 1 + (-1) \cdot 1 + (-1) \cdot 1 + (-1) \cdot 1] = 0 \quad (\text{A.105})$$

$$n_{\mathbf{k}_2, 2} = \frac{1}{4} [3 \cdot 1 + (-1) \cdot 1 + (-1) \cdot (-1) + (-1) \cdot (-1)] = 1 \quad (\text{A.106})$$

$$n_{\mathbf{k}_2, 3} = \frac{1}{4} [3 \cdot 1 + (-1) \cdot (-1) + (-1) \cdot 1 + (-1) \cdot (-1)] = 1 \quad (\text{A.107})$$

$$n_{\mathbf{k}_2, 4} = \frac{1}{4} [3 \cdot 1 + (-1) \cdot (-1) + (-1) \cdot (-1) + (-1) \cdot 1] = 1 \quad (\text{A.108})$$

$$\Gamma^{\mathbf{k}_2, vect} = \Gamma^{\mathbf{k}_2, 2} \oplus \Gamma^{\mathbf{k}_2, 3} \oplus \Gamma^{\mathbf{k}_2, 4} \quad (\text{A.109})$$

3. $\mathbf{k}_3 = (0, k_{b^*}, 0)$

$$\begin{aligned} n_{\mathbf{k}_3, 1} &= \frac{1}{4} [3 \cdot 1 + (-\exp(\pi i k_{b^*})) \cdot \exp((\pi i k_{b^*}))^* \\ &\quad + (-\exp(\pi i k_{b^*})) \cdot (-\exp(\pi i k_{b^*}))^* + (-1) \cdot (-1)] = 1 \end{aligned} \quad (\text{A.110})$$

$$\begin{aligned} n_{\mathbf{k}_3, 2} &= \frac{1}{4} [3 \cdot 1 + (-\exp(\pi i k_{b^*})) \cdot (\exp(\pi i k_{b^*}))^* \\ &\quad + (-\exp(\pi i k_{b^*})) \cdot (\exp(\pi i k_{b^*}))^* + (-1) \cdot 1] = 0 \end{aligned} \quad (\text{A.111})$$

$$\begin{aligned} n_{\mathbf{k}_3, 3} &= \frac{1}{4} [3 \cdot 1 + (-\exp(\pi i k_{b^*})) \cdot (-\exp(\pi i k_{b^*}))^* \\ &\quad + (-\exp(\pi i k_{b^*})) \cdot (-\exp(\pi i k_{b^*}))^* + (-1) \cdot 1] = 1 \end{aligned} \quad (\text{A.112})$$

$$\begin{aligned} n_{\mathbf{k}_3, 4} &= \frac{1}{4} [3 \cdot 1 + (-\exp(\pi i k_{b^*})) \cdot (-\exp(\pi i k_{b^*}))^* \\ &\quad + (-\exp(\pi i k_{b^*})) \cdot (\exp(\pi i k_{b^*}))^* + (-1) \cdot (-1)] = 1 \end{aligned} \quad (\text{A.113})$$

$$\mathbf{\Gamma}^{\mathbf{k}_3, vect} = \mathbf{\Gamma}^{\mathbf{k}_3, 1} \oplus \mathbf{\Gamma}^{\mathbf{k}_3, 3} \oplus \mathbf{\Gamma}^{\mathbf{k}_3, 4} \quad (\text{A.114})$$

A.2.4. Reduction of some direct products

The direct product $\mathbf{\Gamma}^{\mathbf{k}, U} \otimes \mathbf{\Gamma}^{\mathbf{k}, V}$ of two irreducible matrix representations is generally reducible and expands as

$$\mathbf{\Gamma}^{\mathbf{k}, U} \otimes \mathbf{\Gamma}^{\mathbf{k}, V} = \bigoplus_W n_{\mathbf{k}, W}^{UV} \mathbf{\Gamma}^{\mathbf{k}, W}, \quad (\text{A.115})$$

where the $n_{\mathbf{k}, W}^{UV}$ are the Clebsh-Gordan coefficients, which can be expressed by

$$n_{\mathbf{k}, W}^{UV} = \frac{1}{n_{G_{\mathbf{k}}}} \sum_{g \in G_{\mathbf{k}}} \chi^{\mathbf{k}, U}(g) \chi^{\mathbf{k}, V}(g) \left(\chi^{\mathbf{k}, W}(g) \right)^* \quad (\text{A.116})$$

as the character of a direct product representation is simply the product of the respective characters. Now the following direct products can be decomposed into irreducible representations:

1. $\mathbf{k}_1 = 0$

• $\mathbf{\Gamma}^{\mathbf{k}_1, 3} \otimes \mathbf{\Gamma}^{\mathbf{k}_1, 1}$

$$\begin{aligned} n_{\mathbf{k}_1, 1}^{3, 1} &= \frac{1}{8} [1 \cdot 1 \cdot 1 + 1 \cdot 1 \cdot 1 + (-1) \cdot 1 \cdot 1 + (-1) \cdot 1 \cdot 1 \\ &\quad + 1 \cdot 1 \cdot 1 + 1 \cdot 1 \cdot 1 + (-1) \cdot 1 \cdot 1 + (-1) \cdot 1 \cdot 1] = 0 \end{aligned} \quad (\text{A.117})$$

$$\begin{aligned} n_{\mathbf{k}_1, 2}^{3, 1} &= \frac{1}{8} [1 \cdot 1 \cdot 1 + 1 \cdot 1 \cdot 1 + (-1) \cdot 1 \cdot 1 + (-1) \cdot 1 \cdot 1 + 1 \cdot 1 \cdot (-1) \\ &\quad + 1 \cdot 1 \cdot (-1) + (-1) \cdot 1 \cdot (-1) + (-1) \cdot 1 \cdot (-1)] = 0 \end{aligned} \quad (\text{A.118})$$

$$\begin{aligned} n_{\mathbf{k}_1, 3}^{3, 1} &= \frac{1}{8} [1 \cdot 1 \cdot 1 + 1 \cdot 1 \cdot 1 + (-1) \cdot 1 \cdot (-1) + (-1) \cdot 1 \cdot (-1) + 1 \cdot 1 \cdot 1 \\ &\quad + 1 \cdot 1 \cdot 1 + (-1) \cdot 1 \cdot (-1) + (-1) \cdot 1 \cdot (-1)] = 1 \end{aligned} \quad (\text{A.119})$$

$$\begin{aligned} n_{\mathbf{k}_1, 4}^{3, 1} &= \frac{1}{8} [1 \cdot 1 \cdot 1 + 1 \cdot 1 \cdot 1 + (-1) \cdot 1 \cdot (-1) + (-1) \cdot 1 \cdot (-1) + 1 \cdot 1 \cdot (-1) \\ &\quad + 1 \cdot 1 \cdot (-1) + (-1) \cdot 1 \cdot 1 + (-1) \cdot 1 \cdot 1] = 0 \end{aligned} \quad (\text{A.120})$$

$$n_{\mathbf{k}_1,5}^{3,1} = \frac{1}{8}[1 \cdot 1 \cdot 1 + 1 \cdot 1 \cdot (-1) + (-1) \cdot 1 \cdot 1 + (-1) \cdot 1 \cdot (-1) + 1 \cdot 1 \cdot 1 + 1 \cdot 1 \cdot (-1) + (-1) \cdot 1 \cdot 1 + (-1) \cdot 1 \cdot (-1)] = 0 \quad (\text{A.121})$$

$$n_{\mathbf{k}_1,6}^{3,1} = \frac{1}{8}[1 \cdot 1 \cdot 1 + 1 \cdot 1 \cdot (-1) + (-1) \cdot 1 \cdot 1 + (-1) \cdot 1 \cdot (-1) + 1 \cdot 1 \cdot (-1) + 1 \cdot 1 \cdot 1 + (-1) \cdot 1 \cdot (-1) + (-1) \cdot 1 \cdot 1] = 0 \quad (\text{A.122})$$

$$n_{\mathbf{k}_1,7}^{3,1} = \frac{1}{8}[1 \cdot 1 \cdot 1 + 1 \cdot 1 \cdot (-1) + (-1) \cdot 1 \cdot (-1) + (-1) \cdot 1 \cdot 1 + 1 \cdot 1 \cdot 1 + 1 \cdot 1 \cdot (-1) + (-1) \cdot 1 \cdot (-1) + (-1) \cdot 1 \cdot 1] = 0 \quad (\text{A.123})$$

$$n_{\mathbf{k}_1,8}^{3,1} = \frac{1}{8}[1 \cdot 1 \cdot 1 + 1 \cdot 1 \cdot (-1) + (-1) \cdot 1 \cdot (-1) + (-1) \cdot 1 \cdot 1 + 1 \cdot 1 \cdot (-1) + 1 \cdot 1 \cdot 1 + (-1) \cdot 1 \cdot 1 + (-1) \cdot 1 \cdot (-1)] = 0 \quad (\text{A.124})$$

The decomposition is

$$\Gamma^{\mathbf{k}_1,3} \otimes \Gamma^{\mathbf{k}_1,1} = \Gamma^{\mathbf{k}_1,3} \quad (\text{A.125})$$

• $\Gamma^{\mathbf{k}_1,5} \otimes \Gamma^{\mathbf{k}_1,1}$

$$n_{\mathbf{k}_1,1}^{5,1} = \frac{1}{8}[1 \cdot 1 \cdot 1 + (-1) \cdot 1 \cdot 1 + 1 \cdot 1 \cdot 1 + (-1) \cdot 1 \cdot 1 + 1 \cdot 1 \cdot 1 + (-1) \cdot 1 \cdot 1 + 1 \cdot 1 \cdot 1 + (-1) \cdot 1 \cdot 1] = 0 \quad (\text{A.126})$$

$$n_{\mathbf{k}_1,2}^{5,1} = \frac{1}{8}[1 \cdot 1 \cdot 1 + (-1) \cdot 1 \cdot 1 + 1 \cdot 1 \cdot 1 + (-1) \cdot 1 \cdot 1 + 1 \cdot 1 \cdot (-1) + (-1) \cdot 1 \cdot (-1) + 1 \cdot 1 \cdot (-1) + (-1) \cdot 1 \cdot (-1)] = 0 \quad (\text{A.127})$$

$$n_{\mathbf{k}_1,3}^{5,1} = \frac{1}{8}[1 \cdot 1 \cdot 1 + (-1) \cdot 1 \cdot 1 + 1 \cdot 1 \cdot (-1) + (-1) \cdot 1 \cdot (-1) + 1 \cdot 1 \cdot 1 + (-1) \cdot 1 \cdot 1 + 1 \cdot 1 \cdot (-1) + (-1) \cdot 1 \cdot (-1)] = 0 \quad (\text{A.128})$$

$$n_{\mathbf{k}_1,4}^{5,1} = \frac{1}{8}[1 \cdot 1 \cdot 1 + (-1) \cdot 1 \cdot 1 + 1 \cdot 1 \cdot (-1) + (-1) \cdot 1 \cdot (-1) + 1 \cdot 1 \cdot (-1) + (-1) \cdot 1 \cdot (-1) + 1 \cdot 1 \cdot 1 + (-1) \cdot 1 \cdot 1] = 0 \quad (\text{A.129})$$

$$n_{\mathbf{k}_1,5}^{5,1} = \frac{1}{8}[1 \cdot 1 \cdot 1 + (-1) \cdot 1 \cdot (-1) + 1 \cdot 1 \cdot 1 + (-1) \cdot 1 \cdot (-1) + 1 \cdot 1 \cdot 1 + (-1) \cdot 1 \cdot (-1) + 1 \cdot 1 \cdot 1 + (-1) \cdot 1 \cdot (-1)] = 1 \quad (\text{A.130})$$

$$n_{\mathbf{k}_1,6}^{5,1} = \frac{1}{8}[1 \cdot 1 \cdot 1 + (-1) \cdot 1 \cdot (-1) + 1 \cdot 1 \cdot 1 + (-1) \cdot 1 \cdot (-1) + 1 \cdot 1 \cdot (-1) + (-1) \cdot 1 \cdot 1 + 1 \cdot 1 \cdot (-1) + (-1) \cdot 1 \cdot 1] = 0 \quad (\text{A.131})$$

$$n_{\mathbf{k}_1,7}^{5,1} = \frac{1}{8}[1 \cdot 1 \cdot 1 + (-1) \cdot 1 \cdot (-1) + 1 \cdot 1 \cdot (-1) + (-1) \cdot 1 \cdot 1 + 1 \cdot 1 \cdot 1 + (-1) \cdot 1 \cdot (-1) + 1 \cdot 1 \cdot (-1) + (-1) \cdot 1 \cdot 1] = 0 \quad (\text{A.132})$$

$$n_{\mathbf{k}_1,8}^{5,1} = \frac{1}{8}[1 \cdot 1 \cdot 1 + (-1) \cdot 1 \cdot (-1) + 1 \cdot 1 \cdot (-1) + (-1) \cdot 1 \cdot 1 + 1 \cdot 1 \cdot (-1) + (-1) \cdot 1 \cdot 1 + 1 \cdot 1 \cdot 1 + (-1) \cdot 1 \cdot (-1)] = 0 \quad (\text{A.133})$$

The decomposition is

$$\mathbf{\Gamma}^{\mathbf{k}_1,5} \otimes \mathbf{\Gamma}^{\mathbf{k}_1,1} = \mathbf{\Gamma}^{\mathbf{k}_1,5} \quad (\text{A.134})$$

• $\mathbf{\Gamma}^{\mathbf{k}_1,7} \otimes \mathbf{\Gamma}^{\mathbf{k}_1,1}$

$$n_{\mathbf{k}_1,1}^{7,1} = \frac{1}{8}[1 \cdot 1 \cdot 1 + (-1) \cdot 1 \cdot 1 + (-1) \cdot 1 \cdot 1 + 1 \cdot 1 \cdot 1 + 1 \cdot 1 \cdot 1 + (-1) \cdot 1 \cdot 1 + (-1) \cdot 1 \cdot 1 + 1 \cdot 1 \cdot 1] = 0 \quad (\text{A.135})$$

$$n_{\mathbf{k}_1,2}^{7,1} = \frac{1}{8}[1 \cdot 1 \cdot 1 + (-1) \cdot 1 \cdot 1 + (-1) \cdot 1 \cdot 1 + 1 \cdot 1 \cdot 1 + 1 \cdot 1 \cdot (-1) + (-1) \cdot 1 \cdot (-1) + (-1) \cdot 1 \cdot (-1) + 1 \cdot 1 \cdot (-1)] = 0 \quad (\text{A.136})$$

$$n_{\mathbf{k}_1,3}^{7,1} = \frac{1}{8}[1 \cdot 1 \cdot 1 + (-1) \cdot 1 \cdot 1 + (-1) \cdot 1 \cdot (-1) + 1 \cdot 1 \cdot (-1) + 1 \cdot 1 \cdot 1 + (-1) \cdot 1 \cdot 1 + (-1) \cdot 1 \cdot (-1) + 1 \cdot 1 \cdot (-1)] = 0 \quad (\text{A.137})$$

$$n_{\mathbf{k}_1,4}^{7,1} = \frac{1}{8}[1 \cdot 1 \cdot 1 + (-1) \cdot 1 \cdot 1 + (-1) \cdot 1 \cdot (-1) + 1 \cdot 1 \cdot (-1) + 1 \cdot 1 \cdot (-1) + (-1) \cdot 1 \cdot (-1) + (-1) \cdot 1 \cdot 1 + 1 \cdot 1 \cdot 1] = 0 \quad (\text{A.138})$$

$$n_{\mathbf{k}_1,5}^{7,1} = \frac{1}{8}[1 \cdot 1 \cdot 1 + (-1) \cdot 1 \cdot (-1) + (-1) \cdot 1 \cdot 1 + 1 \cdot 1 \cdot (-1) + 1 \cdot 1 \cdot 1 + (-1) \cdot 1 \cdot (-1) + (-1) \cdot 1 \cdot 1 + 1 \cdot 1 \cdot (-1)] = 0 \quad (\text{A.139})$$

$$n_{\mathbf{k}_1,6}^{7,1} = \frac{1}{8}[1 \cdot 1 \cdot 1 + (-1) \cdot 1 \cdot (-1) + (-1) \cdot 1 \cdot 1 + 1 \cdot 1 \cdot (-1) + 1 \cdot 1 \cdot (-1) + (-1) \cdot 1 \cdot 1 + (-1) \cdot 1 \cdot (-1) + 1 \cdot 1 \cdot 1] = 0 \quad (\text{A.140})$$

$$n_{\mathbf{k}_1,7}^{7,1} = \frac{1}{8}[1 \cdot 1 \cdot 1 + (-1) \cdot 1 \cdot (-1) + (-1) \cdot 1 \cdot (-1) + 1 \cdot 1 \cdot 1 + 1 \cdot 1 \cdot 1 + (-1) \cdot 1 \cdot (-1) + (-1) \cdot 1 \cdot (-1) + 1 \cdot 1 \cdot 1] = 1 \quad (\text{A.141})$$

$$n_{\mathbf{k}_1,8}^{7,1} = \frac{1}{8}[1 \cdot 1 \cdot 1 + (-1) \cdot 1 \cdot (-1) + (-1) \cdot 1 \cdot (-1) + 1 \cdot 1 \cdot 1 + 1 \cdot 1 \cdot (-1) + (-1) \cdot 1 \cdot 1 + (-1) \cdot 1 \cdot 1 + 1 \cdot 1 \cdot (-1)] = 0 \quad (\text{A.142})$$

The decomposition is

$$\Gamma^{\mathbf{k}_1,7} \otimes \Gamma^{\mathbf{k}_1,1} = \Gamma^{\mathbf{k}_1,7} \quad (\text{A.143})$$

• $\Gamma^{\mathbf{k}_1,3} \otimes \Gamma^{\mathbf{k}_1,7}$

$$n_{\mathbf{k}_1,1}^{3,7} = \frac{1}{8}[1 \cdot 1 \cdot 1 + 1 \cdot (-1) \cdot 1 + (-1) \cdot (-1) \cdot 1 + (-1) \cdot 1 \cdot 1 + 1 \cdot 1 \cdot 1 + 1 \cdot (-1) \cdot 1 + (-1) \cdot (-1) \cdot 1 + (-1) \cdot 1 \cdot 1] = 0 \quad (\text{A.144})$$

$$n_{\mathbf{k}_1,2}^{3,7} = \frac{1}{8}[1 \cdot 1 \cdot 1 + 1 \cdot (-1) \cdot 1 + (-1) \cdot (-1) \cdot 1 + (-1) \cdot 1 \cdot 1 + 1 \cdot 1 \cdot (-1) + 1 \cdot (-1) \cdot (-1) + (-1) \cdot (-1) \cdot (-1) + (-1) \cdot 1 \cdot (-1)] = 0 \quad (\text{A.145})$$

$$n_{\mathbf{k}_1,3}^{3,7} = \frac{1}{8}[1 \cdot 1 \cdot 1 + 1 \cdot (-1) \cdot 1 + (-1) \cdot (-1) \cdot (-1) + (-1) \cdot 1 \cdot (-1) + 1 \cdot 1 \cdot 1 + 1 \cdot (-1) \cdot 1 + (-1) \cdot (-1) \cdot (-1) + (-1) \cdot 1 \cdot (-1)] = 0 \quad (\text{A.146})$$

$$n_{\mathbf{k}_1,4}^{3,7} = \frac{1}{8}[1 \cdot 1 \cdot 1 + 1 \cdot (-1) \cdot 1 + (-1) \cdot (-1) \cdot (-1) + (-1) \cdot 1 \cdot (-1) + 1 \cdot 1 \cdot (-1) + 1 \cdot (-1) \cdot (-1) + (-1) \cdot (-1) \cdot 1 + (-1) \cdot 1 \cdot 1] = 0 \quad (\text{A.147})$$

$$n_{\mathbf{k}_1,5}^{3,7} = \frac{1}{8}[1 \cdot 1 \cdot 1 + 1 \cdot (-1) \cdot (-1) + (-1) \cdot (-1) \cdot 1 + (-1) \cdot 1 \cdot (-1) + 1 \cdot 1 \cdot 1 + 1 \cdot (-1) \cdot (-1) + (-1) \cdot (-1) \cdot 1 + (-1) \cdot 1 \cdot (-1)] = 1 \quad (\text{A.148})$$

$$n_{\mathbf{k}_1,6}^{3,7} = \frac{1}{8}[1 \cdot 1 \cdot 1 + 1 \cdot (-1) \cdot (-1) + (-1) \cdot (-1) \cdot 1 + (-1) \cdot 1 \cdot (-1) + 1 \cdot 1 \cdot (-1) + 1 \cdot (-1) \cdot 1 + (-1) \cdot (-1) \cdot (-1) + (-1) \cdot 1 \cdot 1] = 0 \quad (\text{A.149})$$

$$n_{\mathbf{k}_1,7}^{3,7} = \frac{1}{8}[1 \cdot 1 \cdot 1 + 1 \cdot (-1) \cdot (-1) + (-1) \cdot (-1) \cdot (-1) + (-1) \cdot 1 \cdot 1 + 1 \cdot 1 \cdot 1 + 1 \cdot (-1) \cdot (-1) + (-1) \cdot (-1) \cdot (-1) + (-1) \cdot 1 \cdot 1] = 0 \quad (\text{A.150})$$

$$n_{\mathbf{k}_1,8}^{3,7} = \frac{1}{8}[1 \cdot 1 \cdot 1 + 1 \cdot (-1) \cdot (-1) + (-1) \cdot (-1) \cdot (-1) + (-1) \cdot 1 \cdot 1 + 1 \cdot 1 \cdot (-1) + 1 \cdot (-1) \cdot 1 + (-1) \cdot (-1) \cdot 1 + (-1) \cdot 1 \cdot (-1)] = 0 \quad (\text{A.151})$$

The decomposition is

$$\mathbf{\Gamma}^{\mathbf{k}_1,3} \otimes \mathbf{\Gamma}^{\mathbf{k}_1,7} = \mathbf{\Gamma}^{\mathbf{k}_1,5} \quad (\text{A.152})$$

• $\mathbf{\Gamma}^{\mathbf{k}_1,5} \otimes \mathbf{\Gamma}^{\mathbf{k}_1,7}$

$$n_{\mathbf{k}_1,1}^{5,7} = \frac{1}{8}[1 \cdot 1 \cdot 1 + (-1) \cdot (-1) \cdot 1 + 1 \cdot (-1) \cdot 1 + (-1) \cdot 1 \cdot 1 + 1 \cdot 1 \cdot 1 + (-1) \cdot (-1) \cdot 1 + 1 \cdot (-1) \cdot 1 + (-1) \cdot 1 \cdot 1] = 0 \quad (\text{A.153})$$

$$n_{\mathbf{k}_1,2}^{5,7} = \frac{1}{8}[1 \cdot 1 \cdot 1 + (-1) \cdot (-1) \cdot 1 + 1 \cdot (-1) \cdot 1 + (-1) \cdot 1 \cdot 1 + 1 \cdot 1 \cdot (-1) + (-1) \cdot (-1) \cdot (-1) + 1 \cdot (-1) \cdot (-1) + (-1) \cdot 1 \cdot (-1)] = 0 \quad (\text{A.154})$$

$$n_{\mathbf{k}_1,3}^{5,7} = \frac{1}{8}[1 \cdot 1 \cdot 1 + (-1) \cdot (-1) \cdot 1 + 1 \cdot (-1) \cdot (-1) + (-1) \cdot 1 \cdot (-1) + 1 \cdot 1 \cdot 1 + (-1) \cdot (-1) \cdot 1 + 1 \cdot (-1) \cdot (-1) + (-1) \cdot 1 \cdot (-1)] = 1 \quad (\text{A.155})$$

$$n_{\mathbf{k}_1,4}^{5,7} = \frac{1}{8}[1 \cdot 1 \cdot 1 + (-1) \cdot (-1) \cdot 1 + 1 \cdot (-1) \cdot (-1) + (-1) \cdot 1 \cdot (-1) + 1 \cdot 1 \cdot (-1) + (-1) \cdot (-1) \cdot (-1) + 1 \cdot (-1) \cdot 1 + (-1) \cdot 1 \cdot 1] = 0 \quad (\text{A.156})$$

$$n_{\mathbf{k}_1,5}^{5,7} = \frac{1}{8}[1 \cdot 1 \cdot 1 + (-1) \cdot (-1) \cdot (-1) + 1 \cdot (-1) \cdot 1 + (-1) \cdot 1 \cdot (-1) + 1 \cdot 1 \cdot 1 + (-1) \cdot (-1) \cdot (-1) + 1 \cdot (-1) \cdot 1 + (-1) \cdot 1 \cdot (-1)] = 0 \quad (\text{A.157})$$

$$n_{\mathbf{k}_1,6}^{5,7} = \frac{1}{8}[1 \cdot 1 \cdot 1 + (-1) \cdot (-1) \cdot (-1) + 1 \cdot (-1) \cdot 1 + (-1) \cdot 1 \cdot (-1) + 1 \cdot 1 \cdot (-1) + (-1) \cdot (-1) \cdot 1 + 1 \cdot (-1) \cdot (-1) + (-1) \cdot 1 \cdot 1] = 0 \quad (\text{A.158})$$

$$n_{\mathbf{k}_1,7}^{5,7} = \frac{1}{8}[1 \cdot 1 \cdot 1 + (-1) \cdot (-1) \cdot (-1) + 1 \cdot (-1) \cdot (-1) + (-1) \cdot 1 \cdot 1 + 1 \cdot 1 \cdot 1 + (-1) \cdot (-1) \cdot (-1) + 1 \cdot (-1) \cdot (-1) + (-1) \cdot 1 \cdot 1] = 0 \quad (\text{A.159})$$

$$n_{\mathbf{k}_1,8}^{5,7} = \frac{1}{8}[1 \cdot 1 \cdot 1 + (-1) \cdot (-1) \cdot (-1) + 1 \cdot (-1) \cdot (-1) + (-1) \cdot 1 \cdot 1 + 1 \cdot 1 \cdot (-1) + (-1) \cdot (-1) \cdot 1 + 1 \cdot (-1) \cdot 1 + (-1) \cdot 1 \cdot (-1)] = 0 \quad (\text{A.160})$$

The decomposition is

$$\mathbf{\Gamma}^{\mathbf{k}_1,5} \otimes \mathbf{\Gamma}^{\mathbf{k}_1,7} = \mathbf{\Gamma}^{\mathbf{k}_1,3} \quad (\text{A.161})$$

• $\mathbf{\Gamma}^{\mathbf{k}_1,7} \otimes \mathbf{\Gamma}^{\mathbf{k}_1,7}$

$$\begin{aligned} n_{\mathbf{k}_1,1}^{7,7} &= \frac{1}{8}[1 \cdot 1 \cdot 1 + (-1) \cdot (-1) \cdot 1 + (-1) \cdot (-1) \cdot 1 + 1 \cdot 1 \cdot 1 + 1 \cdot 1 \cdot 1 \\ &\quad + (-1) \cdot (-1) \cdot 1 + (-1) \cdot (-1) \cdot 1 + 1 \cdot 1 \cdot 1] = 1 \end{aligned} \quad (\text{A.162})$$

$$\begin{aligned} n_{\mathbf{k}_1,2}^{7,7} &= \frac{1}{8}[1 \cdot 1 \cdot 1 + (-1) \cdot (-1) \cdot 1 + (-1) \cdot (-1) \cdot 1 + 1 \cdot 1 \cdot 1 + 1 \cdot 1 \cdot (-1) \\ &\quad + (-1) \cdot (-1) \cdot (-1) + (-1) \cdot (-1) \cdot (-1) + 1 \cdot 1 \cdot (-1)] = 0 \end{aligned} \quad (\text{A.163})$$

$$\begin{aligned} n_{\mathbf{k}_1,3}^{7,7} &= \frac{1}{8}[1 \cdot 1 \cdot 1 + (-1) \cdot (-1) \cdot 1 + (-1) \cdot (-1) \cdot (-1) + 1 \cdot 1 \cdot (-1) + 1 \cdot 1 \cdot 1 \\ &\quad + (-1) \cdot (-1) \cdot 1 + (-1) \cdot (-1) \cdot (-1) + 1 \cdot 1 \cdot (-1)] = 0 \end{aligned} \quad (\text{A.164})$$

$$\begin{aligned} n_{\mathbf{k}_1,4}^{7,7} &= \frac{1}{8}[1 \cdot 1 \cdot 1 + (-1) \cdot (-1) \cdot 1 + (-1) \cdot (-1) \cdot (-1) + 1 \cdot 1 \cdot (-1) + 1 \cdot 1 \cdot (-1) \\ &\quad + (-1) \cdot (-1) \cdot (-1) + (-1) \cdot (-1) \cdot 1 + 1 \cdot 1 \cdot 1] = 0 \end{aligned} \quad (\text{A.165})$$

$$\begin{aligned} n_{\mathbf{k}_1,5}^{7,7} &= \frac{1}{8}[1 \cdot 1 \cdot 1 + (-1) \cdot (-1) \cdot (-1) + (-1) \cdot (-1) \cdot 1 + 1 \cdot 1 \cdot (-1) + 1 \cdot 1 \cdot 1 \\ &\quad + (-1) \cdot (-1) \cdot (-1) + (-1) \cdot (-1) \cdot 1 + 1 \cdot 1 \cdot (-1)] = 0 \end{aligned} \quad (\text{A.166})$$

$$\begin{aligned} n_{\mathbf{k}_1,6}^{7,7} &= \frac{1}{8}[1 \cdot 1 \cdot 1 + (-1) \cdot (-1) \cdot (-1) + (-1) \cdot (-1) \cdot 1 + 1 \cdot 1 \cdot (-1) + 1 \cdot 1 \cdot (-1) \\ &\quad + (-1) \cdot (-1) \cdot 1 + (-1) \cdot (-1) \cdot (-1) + 1 \cdot 1 \cdot 1] = 0 \end{aligned} \quad (\text{A.167})$$

$$\begin{aligned} n_{\mathbf{k}_1,7}^{7,7} &= \frac{1}{8}[1 \cdot 1 \cdot 1 + (-1) \cdot (-1) \cdot (-1) + (-1) \cdot (-1) \cdot (-1) + 1 \cdot 1 \cdot 1 + 1 \cdot 1 \cdot 1 \\ &\quad + (-1) \cdot (-1) \cdot (-1) + (-1) \cdot (-1) \cdot (-1) + 1 \cdot 1 \cdot 1] = 0 \end{aligned} \quad (\text{A.168})$$

$$\begin{aligned} n_{\mathbf{k}_1,8}^{7,7} &= \frac{1}{8}[1 \cdot 1 \cdot 1 + (-1) \cdot (-1) \cdot (-1) + 1 \cdot (-1) \cdot (-1) + (-1) \cdot 1 \cdot 1 + 1 \cdot 1 \cdot (-1) \\ &\quad + (-1) \cdot (-1) \cdot 1 + 1 \cdot (-1) \cdot 1 + (-1) \cdot 1 \cdot (-1)] = 0 \end{aligned} \quad (\text{A.169})$$

The decomposition is

$$\mathbf{\Gamma}^{\mathbf{k}_1,7} \otimes \mathbf{\Gamma}^{\mathbf{k}_1,7} = \mathbf{\Gamma}^{\mathbf{k}_1,1} \quad (\text{A.170})$$

- $\Gamma^{\mathbf{k}_1,3} \otimes \Gamma^{\mathbf{k}_1,2}$

$$n_{\mathbf{k}_1,1}^{3,2} = \frac{1}{8} [1 \cdot 1 \cdot 1 + 1 \cdot 1 \cdot 1 + (-1) \cdot 1 \cdot 1 + (-1) \cdot 1 \cdot 1 + 1 \cdot (-1) \cdot 1 + 1 \cdot (-1) \cdot 1 + (-1) \cdot (-1) \cdot 1 + (-1) \cdot (-1) \cdot 1] = 0 \quad (\text{A.171})$$

$$n_{\mathbf{k}_1,2}^{3,2} = \frac{1}{8} [1 \cdot 1 \cdot 1 + 1 \cdot 1 \cdot 1 + (-1) \cdot 1 \cdot 1 + (-1) \cdot 1 \cdot 1 + 1 \cdot (-1) \cdot (-1) + 1 \cdot (-1) \cdot (-1) + (-1) \cdot (-1) \cdot (-1) + (-1) \cdot (-1) \cdot (-1)] = 0 \quad (\text{A.172})$$

$$n_{\mathbf{k}_1,3}^{3,2} = \frac{1}{8} [1 \cdot 1 \cdot 1 + 1 \cdot 1 \cdot 1 + (-1) \cdot 1 \cdot (-1) + (-1) \cdot 1 \cdot (-1) + 1 \cdot (-1) \cdot 1 + 1 \cdot (-1) \cdot 1 + (-1) \cdot (-1) \cdot (-1) + (-1) \cdot (-1) \cdot (-1)] = 0 \quad (\text{A.173})$$

$$n_{\mathbf{k}_1,4}^{3,2} = \frac{1}{8} [1 \cdot 1 \cdot 1 + 1 \cdot 1 \cdot 1 + (-1) \cdot 1 \cdot (-1) + (-1) \cdot 1 \cdot (-1) + 1 \cdot (-1) \cdot (-1) + 1 \cdot (-1) \cdot (-1) + (-1) \cdot (-1) \cdot 1 + (-1) \cdot (-1) \cdot 1] = 1 \quad (\text{A.174})$$

$$n_{\mathbf{k}_1,5}^{3,2} = \frac{1}{8} [1 \cdot 1 \cdot 1 + 1 \cdot 1 \cdot (-1) + (-1) \cdot 1 \cdot 1 + (-1) \cdot 1 \cdot (-1) + 1 \cdot (-1) \cdot 1 + 1 \cdot (-1) \cdot (-1) + (-1) \cdot (-1) \cdot 1 + (-1) \cdot (-1) \cdot (-1)] = 0 \quad (\text{A.175})$$

$$n_{\mathbf{k}_1,6}^{3,2} = \frac{1}{8} [1 \cdot 1 \cdot 1 + 1 \cdot 1 \cdot (-1) + (-1) \cdot 1 \cdot 1 + (-1) \cdot 1 \cdot (-1) + 1 \cdot (-1) \cdot (-1) + 1 \cdot (-1) \cdot (-1) + (-1) \cdot (-1) \cdot (-1) + (-1) \cdot (-1) \cdot 1] = 0 \quad (\text{A.176})$$

$$n_{\mathbf{k}_1,7}^{3,2} = \frac{1}{8} [1 \cdot 1 \cdot 1 + 1 \cdot 1 \cdot (-1) + (-1) \cdot 1 \cdot (-1) + (-1) \cdot 1 \cdot 1 + 1 \cdot (-1) \cdot 1 + 1 \cdot (-1) \cdot (-1) + (-1) \cdot (-1) \cdot (-1) + (-1) \cdot (-1) \cdot 1] = 0 \quad (\text{A.177})$$

$$n_{\mathbf{k}_1,8}^{3,2} = \frac{1}{8} [1 \cdot 1 \cdot 1 + 1 \cdot 1 \cdot (-1) + (-1) \cdot 1 \cdot (-1) + (-1) \cdot 1 \cdot 1 + 1 \cdot (-1) \cdot (-1) + 1 \cdot (-1) \cdot 1 + (-1) \cdot (-1) \cdot 1 + (-1) \cdot (-1) \cdot (-1)] = 0 \quad (\text{A.178})$$

The decomposition is

$$\Gamma^{\mathbf{k}_1,3} \otimes \Gamma^{\mathbf{k}_1,2} = \Gamma^{\mathbf{k}_1,4} \quad (\text{A.179})$$

• $\Gamma^{\mathbf{k}_1,3} \otimes \Gamma^{\mathbf{k}_1,5}$

$$n_{\mathbf{k}_1,1}^{3,5} = \frac{1}{8}[1 \cdot 1 \cdot 1 + 1 \cdot (-1) \cdot 1 + (-1) \cdot 1 \cdot 1 + (-1) \cdot (-1) \cdot 1 + 1 \cdot 1 \cdot 1 + 1 \cdot (-1) \cdot 1 + (-1) \cdot 1 \cdot 1 + (-1) \cdot (-1) \cdot 1] = 0 \quad (\text{A.180})$$

$$n_{\mathbf{k}_1,2}^{3,5} = \frac{1}{8}[1 \cdot 1 \cdot 1 + 1 \cdot (-1) \cdot 1 + (-1) \cdot 1 \cdot 1 + (-1) \cdot (-1) \cdot 1 + 1 \cdot 1 \cdot (-1) + 1 \cdot (-1) \cdot (-1) + (-1) \cdot 1 \cdot (-1) + (-1) \cdot (-1) \cdot (-1)] = 0 \quad (\text{A.181})$$

$$n_{\mathbf{k}_1,3}^{3,5} = \frac{1}{8}[1 \cdot 1 \cdot 1 + 1 \cdot (-1) \cdot 1 + (-1) \cdot 1 \cdot (-1) + (-1) \cdot (-1) \cdot (-1) + 1 \cdot 1 \cdot 1 + 1 \cdot (-1) \cdot 1 + (-1) \cdot 1 \cdot (-1) + (-1) \cdot (-1) \cdot (-1)] = 0 \quad (\text{A.182})$$

$$n_{\mathbf{k}_1,4}^{3,5} = \frac{1}{8}[1 \cdot 1 \cdot 1 + 1 \cdot (-1) \cdot 1 + (-1) \cdot 1 \cdot (-1) + (-1) \cdot (-1) \cdot (-1) + 1 \cdot 1 \cdot (-1) + 1 \cdot (-1) \cdot (-1) + (-1) \cdot 1 \cdot 1 + (-1) \cdot (-1) \cdot 1] = 0 \quad (\text{A.183})$$

$$n_{\mathbf{k}_1,5}^{3,5} = \frac{1}{8}[1 \cdot 1 \cdot 1 + 1 \cdot (-1) \cdot (-1) + (-1) \cdot 1 \cdot 1 + (-1) \cdot (-1) \cdot (-1) + 1 \cdot 1 \cdot 1 + 1 \cdot (-1) \cdot (-1) + (-1) \cdot 1 \cdot 1 + (-1) \cdot (-1) \cdot (-1)] = 0 \quad (\text{A.184})$$

$$n_{\mathbf{k}_1,6}^{3,5} = \frac{1}{8}[1 \cdot 1 \cdot 1 + 1 \cdot (-1) \cdot (-1) + (-1) \cdot 1 \cdot 1 + (-1) \cdot (-1) \cdot (-1) + 1 \cdot 1 \cdot (-1) + 1 \cdot (-1) \cdot 1 + (-1) \cdot 1 \cdot (-1) + (-1) \cdot (-1) \cdot 1] = 0 \quad (\text{A.185})$$

$$n_{\mathbf{k}_1,7}^{3,5} = \frac{1}{8}[1 \cdot 1 \cdot 1 + 1 \cdot (-1) \cdot (-1) + (-1) \cdot 1 \cdot (-1) + (-1) \cdot (-1) \cdot 1 + 1 \cdot 1 \cdot 1 + 1 \cdot (-1) \cdot (-1) + (-1) \cdot 1 \cdot (-1) + (-1) \cdot (-1) \cdot 1] = 1 \quad (\text{A.186})$$

$$n_{\mathbf{k}_1,8}^{3,5} = \frac{1}{8}[1 \cdot 1 \cdot 1 + 1 \cdot (-1) \cdot (-1) + (-1) \cdot 1 \cdot (-1) + (-1) \cdot (-1) \cdot 1 + 1 \cdot 1 \cdot (-1) + 1 \cdot (-1) \cdot 1 + (-1) \cdot 1 \cdot 1 + (-1) \cdot (-1) \cdot (-1)] = 0 \quad (\text{A.187})$$

The decomposition is

$$\Gamma^{\mathbf{k}_1,3} \otimes \Gamma^{\mathbf{k}_1,5} = \Gamma^{\mathbf{k}_1,7} \quad (\text{A.188})$$

- $\Gamma^{\mathbf{k}_1,3} \otimes \Gamma^{\mathbf{k}_1,6}$

$$n_{\mathbf{k}_1,1}^{3,6} = \frac{1}{8}[1 \cdot 1 \cdot 1 + 1 \cdot (-1) \cdot 1 + (-1) \cdot 1 \cdot 1 + (-1) \cdot (-1) \cdot 1 + 1 \cdot (-1) \cdot 1 + 1 \cdot 1 \cdot 1 + (-1) \cdot (-1) \cdot 1 + (-1) \cdot 1 \cdot 1] = 0 \quad (\text{A.189})$$

$$n_{\mathbf{k}_1,2}^{3,6} = \frac{1}{8}[1 \cdot 1 \cdot 1 + 1 \cdot (-1) \cdot 1 + (-1) \cdot 1 \cdot 1 + (-1) \cdot (-1) \cdot 1 + 1 \cdot (-1) \cdot (-1) + 1 \cdot 1 \cdot (-1) + (-1) \cdot (-1) \cdot (-1) + (-1) \cdot 1 \cdot (-1)] = 0 \quad (\text{A.190})$$

$$n_{\mathbf{k}_1,3}^{3,6} = \frac{1}{8}[1 \cdot 1 \cdot 1 + 1 \cdot (-1) \cdot 1 + (-1) \cdot 1 \cdot (-1) + (-1) \cdot (-1) \cdot (-1) + 1 \cdot (-1) \cdot 1 + 1 \cdot 1 \cdot 1 + (-1) \cdot (-1) \cdot (-1) + (-1) \cdot 1 \cdot (-1)] = 0 \quad (\text{A.191})$$

$$n_{\mathbf{k}_1,4}^{3,6} = \frac{1}{8}[1 \cdot 1 \cdot 1 + 1 \cdot (-1) \cdot 1 + (-1) \cdot 1 \cdot (-1) + (-1) \cdot (-1) \cdot (-1) + 1 \cdot (-1) \cdot (-1) + 1 \cdot 1 \cdot (-1) + (-1) \cdot (-1) \cdot 1 + (-1) \cdot 1 \cdot 1] = 0 \quad (\text{A.192})$$

$$n_{\mathbf{k}_1,5}^{3,6} = \frac{1}{8}[1 \cdot 1 \cdot 1 + 1 \cdot (-1) \cdot (-1) + (-1) \cdot 1 \cdot 1 + (-1) \cdot (-1) \cdot (-1) + 1 \cdot (-1) \cdot 1 + 1 \cdot 1 \cdot (-1) + (-1) \cdot (-1) \cdot 1 + (-1) \cdot 1 \cdot (-1)] = 0 \quad (\text{A.193})$$

$$n_{\mathbf{k}_1,6}^{3,6} = \frac{1}{8}[1 \cdot 1 \cdot 1 + 1 \cdot (-1) \cdot (-1) + (-1) \cdot 1 \cdot 1 + (-1) \cdot (-1) \cdot (-1) + 1 \cdot (-1) \cdot (-1) + 1 \cdot 1 \cdot 1 + (-1) \cdot (-1) \cdot (-1) + (-1) \cdot 1 \cdot 1] = 0 \quad (\text{A.194})$$

$$n_{\mathbf{k}_1,7}^{3,6} = \frac{1}{8}[1 \cdot 1 \cdot 1 + 1 \cdot (-1) \cdot (-1) + (-1) \cdot 1 \cdot (-1) + (-1) \cdot (-1) \cdot 1 + 1 \cdot (-1) \cdot 1 + 1 \cdot 1 \cdot (-1) + (-1) \cdot (-1) \cdot (-1) + (-1) \cdot 1 \cdot 1] = 0 \quad (\text{A.195})$$

$$n_{\mathbf{k}_1,8}^{3,6} = \frac{1}{8}[1 \cdot 1 \cdot 1 + 1 \cdot (-1) \cdot (-1) + (-1) \cdot 1 \cdot (-1) + (-1) \cdot (-1) \cdot 1 + 1 \cdot (-1) \cdot (-1) + 1 \cdot 1 \cdot 1 + (-1) \cdot (-1) \cdot 1 + (-1) \cdot 1 \cdot (-1)] = 1 \quad (\text{A.196})$$

The decomposition is

$$\Gamma^{\mathbf{k}_1,3} \otimes \Gamma^{\mathbf{k}_1,6} = \Gamma^{\mathbf{k}_1,8} \quad (\text{A.197})$$

• $\Gamma^{\mathbf{k}_1,5} \otimes \Gamma^{\mathbf{k}_1,2}$

$$n_{\mathbf{k}_1,1}^{5,2} = \frac{1}{8}[1 \cdot 1 \cdot 1 + (-1) \cdot 1 \cdot 1 + 1 \cdot 1 \cdot 1 + (-1) \cdot 1 \cdot 1 + 1 \cdot (-1) \cdot 1 + (-1) \cdot (-1) \cdot 1 + 1 \cdot (-1) \cdot 1 + (-1) \cdot (-1) \cdot 1] = 0 \quad (\text{A.198})$$

$$n_{\mathbf{k}_1,2}^{5,2} = \frac{1}{8}[1 \cdot 1 \cdot 1 + (-1) \cdot 1 \cdot 1 + 1 \cdot 1 \cdot 1 + (-1) \cdot 1 \cdot 1 + 1 \cdot (-1) \cdot (-1) + (-1) \cdot (-1) \cdot (-1) + 1 \cdot (-1) \cdot (-1) + (-1) \cdot (-1) \cdot (-1)] = 0 \quad (\text{A.199})$$

$$n_{\mathbf{k}_1,3}^{5,2} = \frac{1}{8}[1 \cdot 1 \cdot 1 + (-1) \cdot 1 \cdot 1 + 1 \cdot 1 \cdot (-1) + (-1) \cdot 1 \cdot (-1) + 1 \cdot (-1) \cdot 1 + (-1) \cdot (-1) \cdot 1 + 1 \cdot (-1) \cdot (-1) + (-1) \cdot (-1) \cdot (-1)] = 0 \quad (\text{A.200})$$

$$n_{\mathbf{k}_1,4}^{5,2} = \frac{1}{8}[1 \cdot 1 \cdot 1 + (-1) \cdot 1 \cdot 1 + 1 \cdot 1 \cdot (-1) + (-1) \cdot 1 \cdot (-1) + 1 \cdot (-1) \cdot (-1) + (-1) \cdot (-1) \cdot (-1) + 1 \cdot (-1) \cdot 1 + (-1) \cdot (-1) \cdot 1] = 0 \quad (\text{A.201})$$

$$n_{\mathbf{k}_1,5}^{5,2} = \frac{1}{8}[1 \cdot 1 \cdot 1 + (-1) \cdot 1 \cdot (-1) + 1 \cdot 1 \cdot 1 + (-1) \cdot 1 \cdot (-1) + 1 \cdot (-1) \cdot 1 + (-1) \cdot (-1) \cdot (-1) + 1 \cdot (-1) \cdot 1 + (-1) \cdot (-1) \cdot (-1)] = 0 \quad (\text{A.202})$$

$$n_{\mathbf{k}_1,6}^{5,2} = \frac{1}{8}[1 \cdot 1 \cdot 1 + (-1) \cdot 1 \cdot (-1) + 1 \cdot 1 \cdot 1 + (-1) \cdot 1 \cdot (-1) + 1 \cdot (-1) \cdot (-1) + (-1) \cdot (-1) \cdot 1 + 1 \cdot (-1) \cdot (-1) + (-1) \cdot (-1) \cdot 1] = 1 \quad (\text{A.203})$$

$$n_{\mathbf{k}_1,7}^{5,2} = \frac{1}{8}[1 \cdot 1 \cdot 1 + (-1) \cdot 1 \cdot (-1) + 1 \cdot 1 \cdot (-1) + (-1) \cdot 1 \cdot 1 + 1 \cdot (-1) \cdot 1 + (-1) \cdot (-1) \cdot (-1) + 1 \cdot (-1) \cdot (-1) + (-1) \cdot (-1) \cdot 1] = 0 \quad (\text{A.204})$$

$$n_{\mathbf{k}_1,8}^{5,2} = \frac{1}{8}[1 \cdot 1 \cdot 1 + (-1) \cdot 1 \cdot (-1) + 1 \cdot 1 \cdot (-1) + (-1) \cdot 1 \cdot 1 + 1 \cdot (-1) \cdot (-1) + (-1) \cdot (-1) \cdot 1 + 1 \cdot (-1) \cdot 1 + (-1) \cdot (-1) \cdot (-1)] = 0 \quad (\text{A.205})$$

The decomposition is

$$\Gamma^{\mathbf{k}_1,5} \otimes \Gamma^{\mathbf{k}_1,2} = \Gamma^{\mathbf{k}_1,6} \quad (\text{A.206})$$

• $\Gamma^{\mathbf{k}_1,5} \otimes \Gamma^{\mathbf{k}_1,5}$

$$n_{\mathbf{k}_1,1}^{5,5} = \frac{1}{8} [1 \cdot 1 \cdot 1 + (-1) \cdot (-1) \cdot 1 + 1 \cdot 1 \cdot 1 + (-1) \cdot (-1) \cdot 1 + 1 \cdot 1 \cdot 1 + (-1) \cdot (-1) \cdot 1 + 1 \cdot 1 \cdot 1 + (-1) \cdot (-1) \cdot 1] = 1 \quad (\text{A.207})$$

$$n_{\mathbf{k}_1,2}^{5,5} = \frac{1}{8} [1 \cdot 1 \cdot 1 + (-1) \cdot (-1) \cdot 1 + 1 \cdot 1 \cdot 1 + (-1) \cdot (-1) \cdot 1 + 1 \cdot 1 \cdot (-1) + (-1) \cdot (-1) \cdot (-1) + 1 \cdot 1 \cdot (-1) + (-1) \cdot (-1) \cdot (-1)] = 0 \quad (\text{A.208})$$

$$n_{\mathbf{k}_1,3}^{5,5} = \frac{1}{8} [1 \cdot 1 \cdot 1 + (-1) \cdot (-1) \cdot 1 + 1 \cdot 1 \cdot (-1) + (-1) \cdot (-1) \cdot (-1) + 1 \cdot 1 \cdot 1 + (-1) \cdot (-1) \cdot 1 + 1 \cdot 1 \cdot (-1) + (-1) \cdot (-1) \cdot (-1)] = 0 \quad (\text{A.209})$$

$$n_{\mathbf{k}_1,4}^{5,5} = \frac{1}{8} [1 \cdot 1 \cdot 1 + (-1) \cdot (-1) \cdot 1 + 1 \cdot 1 \cdot (-1) + (-1) \cdot (-1) \cdot (-1) + 1 \cdot 1 \cdot (-1) + (-1) \cdot (-1) \cdot (-1) + 1 \cdot 1 \cdot 1 + (-1) \cdot (-1) \cdot 1] = 0 \quad (\text{A.210})$$

$$n_{\mathbf{k}_1,5}^{5,5} = \frac{1}{8} [1 \cdot 1 \cdot 1 + (-1) \cdot (-1) \cdot (-1) + 1 \cdot 1 \cdot 1 + (-1) \cdot (-1) \cdot (-1) + 1 \cdot 1 \cdot 1 + (-1) \cdot (-1) \cdot (-1) + 1 \cdot 1 \cdot 1 + (-1) \cdot (-1) \cdot (-1)] = 0 \quad (\text{A.211})$$

$$n_{\mathbf{k}_1,6}^{5,5} = \frac{1}{8} [1 \cdot 1 \cdot 1 + (-1) \cdot (-1) \cdot (-1) + 1 \cdot 1 \cdot 1 + (-1) \cdot (-1) \cdot (-1) + 1 \cdot 1 \cdot (-1) + (-1) \cdot (-1) \cdot (-1) + 1 \cdot 1 \cdot (-1) + (-1) \cdot (-1) \cdot 1] = 0 \quad (\text{A.212})$$

$$n_{\mathbf{k}_1,7}^{5,5} = \frac{1}{8} [1 \cdot 1 \cdot 1 + (-1) \cdot (-1) \cdot (-1) + 1 \cdot 1 \cdot (-1) + (-1) \cdot (-1) \cdot 1 + 1 \cdot 1 \cdot 1 + (-1) \cdot (-1) \cdot (-1) + 1 \cdot 1 \cdot (-1) + (-1) \cdot (-1) \cdot 1] = 0 \quad (\text{A.213})$$

$$n_{\mathbf{k}_1,8}^{5,5} = \frac{1}{8} [1 \cdot 1 \cdot 1 + (-1) \cdot (-1) \cdot (-1) + 1 \cdot 1 \cdot (-1) + (-1) \cdot (-1) \cdot 1 + 1 \cdot 1 \cdot (-1) + (-1) \cdot (-1) \cdot 1 + 1 \cdot 1 \cdot 1 + (-1) \cdot (-1) \cdot (-1)] = 0 \quad (\text{A.214})$$

The decomposition is

$$\Gamma^{\mathbf{k}_1,5} \otimes \Gamma^{\mathbf{k}_1,5} = \Gamma^{\mathbf{k}_1,1} \quad (\text{A.215})$$

• $\Gamma^{\mathbf{k}_1,5} \otimes \Gamma^{\mathbf{k}_1,6}$

$$n_{\mathbf{k}_1,1}^{5,6} = \frac{1}{8}[1 \cdot 1 \cdot 1 + (-1) \cdot (-1) \cdot 1 + 1 \cdot 1 \cdot 1 + (-1) \cdot (-1) \cdot 1 + 1 \cdot (-1) \cdot 1 + (-1) \cdot 1 \cdot 1 + 1 \cdot (-1) \cdot 1 + (-1) \cdot 1 \cdot 1] = 0 \quad (\text{A.216})$$

$$n_{\mathbf{k}_1,2}^{5,6} = \frac{1}{8}[1 \cdot 1 \cdot 1 + (-1) \cdot (-1) \cdot 1 + 1 \cdot 1 \cdot 1 + (-1) \cdot (-1) \cdot 1 + 1 \cdot (-1) \cdot (-1) + (-1) \cdot 1 \cdot (-1) + 1 \cdot (-1) \cdot (-1) + (-1) \cdot 1 \cdot (-1)] = 1 \quad (\text{A.217})$$

$$n_{\mathbf{k}_1,3}^{5,6} = \frac{1}{8}[1 \cdot 1 \cdot 1 + (-1) \cdot (-1) \cdot 1 + 1 \cdot 1 \cdot (-1) + (-1) \cdot (-1) \cdot (-1) + 1 \cdot (-1) \cdot 1 + (-1) \cdot 1 \cdot 1 + 1 \cdot (-1) \cdot (-1) + (-1) \cdot 1 \cdot (-1)] = 0 \quad (\text{A.218})$$

$$n_{\mathbf{k}_1,4}^{5,6} = \frac{1}{8}[1 \cdot 1 \cdot 1 + (-1) \cdot (-1) \cdot 1 + 1 \cdot 1 \cdot (-1) + (-1) \cdot (-1) \cdot (-1) + 1 \cdot (-1) \cdot (-1) + (-1) \cdot 1 \cdot (-1) + 1 \cdot (-1) \cdot 1 + (-1) \cdot 1 \cdot 1] = 0 \quad (\text{A.219})$$

$$n_{\mathbf{k}_1,5}^{5,6} = \frac{1}{8}[1 \cdot 1 \cdot 1 + (-1) \cdot (-1) \cdot (-1) + 1 \cdot 1 \cdot 1 + (-1) \cdot (-1) \cdot (-1) + 1 \cdot (-1) \cdot 1 + (-1) \cdot 1 \cdot (-1) + 1 \cdot (-1) \cdot 1 + (-1) \cdot 1 \cdot (-1)] = 0 \quad (\text{A.220})$$

$$n_{\mathbf{k}_1,6}^{5,6} = \frac{1}{8}[1 \cdot 1 \cdot 1 + (-1) \cdot (-1) \cdot (-1) + 1 \cdot 1 \cdot 1 + (-1) \cdot (-1) \cdot (-1) + 1 \cdot (-1) \cdot (-1) + (-1) \cdot 1 \cdot 1 + 1 \cdot (-1) \cdot (-1) + (-1) \cdot 1 \cdot 1] = 0 \quad (\text{A.221})$$

$$n_{\mathbf{k}_1,7}^{5,6} = \frac{1}{8}[1 \cdot 1 \cdot 1 + (-1) \cdot (-1) \cdot (-1) + 1 \cdot 1 \cdot (-1) + (-1) \cdot (-1) \cdot 1 + 1 \cdot (-1) \cdot 1 + (-1) \cdot 1 \cdot (-1) + 1 \cdot (-1) \cdot (-1) + (-1) \cdot 1 \cdot 1] = 0 \quad (\text{A.222})$$

$$n_{\mathbf{k}_1,8}^{5,6} = \frac{1}{8}[1 \cdot 1 \cdot 1 + (-1) \cdot (-1) \cdot (-1) + 1 \cdot 1 \cdot (-1) + (-1) \cdot (-1) \cdot 1 + 1 \cdot (-1) \cdot (-1) + (-1) \cdot 1 \cdot 1 + 1 \cdot (-1) \cdot 1 + (-1) \cdot 1 \cdot (-1)] = 0 \quad (\text{A.223})$$

The decomposition is

$$\Gamma^{\mathbf{k}_1,5} \otimes \Gamma^{\mathbf{k}_1,6} = \Gamma^{\mathbf{k}_1,1} \quad (\text{A.224})$$

• $\Gamma^{\mathbf{k}_1,7} \otimes \Gamma^{\mathbf{k}_1,2}$

$$n_{\mathbf{k}_1,1}^{7,2} = \frac{1}{8}[1 \cdot 1 \cdot 1 + (-1) \cdot 1 \cdot 1 + (-1) \cdot 1 \cdot 1 + 1 \cdot 1 \cdot 1 + 1 \cdot (-1) \cdot 1 + (-1) \cdot (-1) \cdot 1 + (-1) \cdot (-1) \cdot 1 + 1 \cdot (-1) \cdot 1] = 0 \quad (\text{A.225})$$

$$n_{\mathbf{k}_1,2}^{7,2} = \frac{1}{8}[1 \cdot 1 \cdot 1 + (-1) \cdot 1 \cdot 1 + (-1) \cdot 1 \cdot 1 + 1 \cdot 1 \cdot 1 + 1 \cdot (-1) \cdot (-1) + (-1) \cdot (-1) \cdot (-1) + (-1) \cdot (-1) \cdot (-1) + 1 \cdot (-1) \cdot (-1)] = 0 \quad (\text{A.226})$$

$$n_{\mathbf{k}_1,3}^{7,2} = \frac{1}{8}[1 \cdot 1 \cdot 1 + (-1) \cdot 1 \cdot 1 + (-1) \cdot 1 \cdot (-1) + 1 \cdot 1 \cdot (-1) + 1 \cdot (-1) \cdot 1 + (-1) \cdot (-1) \cdot 1 + (-1) \cdot (-1) \cdot (-1) + 1 \cdot (-1) \cdot (-1)] = 0 \quad (\text{A.227})$$

$$n_{\mathbf{k}_1,4}^{7,2} = \frac{1}{8}[1 \cdot 1 \cdot 1 + (-1) \cdot 1 \cdot 1 + (-1) \cdot 1 \cdot (-1) + 1 \cdot 1 \cdot (-1) + 1 \cdot (-1) \cdot (-1) + (-1) \cdot (-1) \cdot (-1) + (-1) \cdot (-1) \cdot 1 + 1 \cdot (-1) \cdot 1] = 0 \quad (\text{A.228})$$

$$n_{\mathbf{k}_1,5}^{7,2} = \frac{1}{8}[1 \cdot 1 \cdot 1 + (-1) \cdot 1 \cdot (-1) + (-1) \cdot 1 \cdot 1 + 1 \cdot 1 \cdot (-1) + 1 \cdot (-1) \cdot 1 + (-1) \cdot (-1) \cdot (-1) + (-1) \cdot (-1) \cdot 1 + 1 \cdot (-1) \cdot (-1)] = 0 \quad (\text{A.229})$$

$$n_{\mathbf{k}_1,6}^{7,2} = \frac{1}{8}[1 \cdot 1 \cdot 1 + (-1) \cdot 1 \cdot (-1) + (-1) \cdot 1 \cdot 1 + 1 \cdot 1 \cdot (-1) + 1 \cdot (-1) \cdot (-1) + (-1) \cdot (-1) \cdot 1 + (-1) \cdot (-1) \cdot (-1) + 1 \cdot (-1) \cdot 1] = 0 \quad (\text{A.230})$$

$$n_{\mathbf{k}_1,7}^{7,2} = \frac{1}{8}[1 \cdot 1 \cdot 1 + (-1) \cdot 1 \cdot (-1) + (-1) \cdot 1 \cdot (-1) + 1 \cdot 1 \cdot 1 + 1 \cdot (-1) \cdot 1 + (-1) \cdot (-1) \cdot (-1) + (-1) \cdot (-1) \cdot (-1) + 1 \cdot (-1) \cdot 1] = 0 \quad (\text{A.231})$$

$$n_{\mathbf{k}_1,8}^{7,2} = \frac{1}{8}[1 \cdot 1 \cdot 1 + (-1) \cdot 1 \cdot (-1) + (-1) \cdot 1 \cdot (-1) + 1 \cdot 1 \cdot 1 + 1 \cdot (-1) \cdot (-1) + (-1) \cdot (-1) \cdot 1 + (-1) \cdot (-1) \cdot 1 + 1 \cdot (-1) \cdot (-1)] = 1 \quad (\text{A.232})$$

The decomposition is

$$\Gamma^{\mathbf{k}_1,7} \otimes \Gamma^{\mathbf{k}_1,2} = \Gamma^{\mathbf{k}_1,8} \quad (\text{A.233})$$

• $\Gamma^{\mathbf{k}_1,7} \otimes \Gamma^{\mathbf{k}_1,5}$

$$n_{\mathbf{k}_1,1}^{7,5} = \frac{1}{8}[1 \cdot 1 \cdot 1 + (-1) \cdot (-1) \cdot 1 + (-1) \cdot 1 \cdot 1 + 1 \cdot (-1) \cdot 1 + 1 \cdot 1 \cdot 1 + (-1) \cdot (-1) \cdot 1 + (-1) \cdot 1 \cdot 1 + 1 \cdot (-1) \cdot 1] = 0 \quad (\text{A.234})$$

$$n_{\mathbf{k}_1,2}^{7,5} = \frac{1}{8}[1 \cdot 1 \cdot 1 + (-1) \cdot (-1) \cdot 1 + (-1) \cdot 1 \cdot 1 + 1 \cdot (-1) \cdot 1 + 1 \cdot 1 \cdot (-1) + (-1) \cdot (-1) \cdot (-1) + (-1) \cdot 1 \cdot (-1) + 1 \cdot (-1) \cdot (-1)] = 0 \quad (\text{A.235})$$

$$n_{\mathbf{k}_1,3}^{7,5} = \frac{1}{8}[1 \cdot 1 \cdot 1 + (-1) \cdot (-1) \cdot 1 + (-1) \cdot 1 \cdot (-1) + 1 \cdot (-1) \cdot (-1) + 1 \cdot 1 \cdot 1 + (-1) \cdot (-1) \cdot 1 + (-1) \cdot 1 \cdot (-1) + 1 \cdot (-1) \cdot (-1)] = 1 \quad (\text{A.236})$$

$$n_{\mathbf{k}_1,4}^{7,5} = \frac{1}{8}[1 \cdot 1 \cdot 1 + (-1) \cdot (-1) \cdot 1 + (-1) \cdot 1 \cdot (-1) + 1 \cdot (-1) \cdot (-1) + 1 \cdot 1 \cdot (-1) + (-1) \cdot (-1) \cdot (-1) + (-1) \cdot 1 \cdot 1 + 1 \cdot (-1) \cdot 1] = 0 \quad (\text{A.237})$$

$$n_{\mathbf{k}_1,5}^{7,5} = \frac{1}{8}[1 \cdot 1 \cdot 1 + (-1) \cdot (-1) \cdot (-1) + (-1) \cdot 1 \cdot 1 + 1 \cdot (-1) \cdot (-1) + 1 \cdot 1 \cdot 1 + (-1) \cdot (-1) \cdot (-1) + (-1) \cdot 1 \cdot 1 + 1 \cdot (-1) \cdot (-1)] = 0 \quad (\text{A.238})$$

$$n_{\mathbf{k}_1,6}^{7,5} = \frac{1}{8}[1 \cdot 1 \cdot 1 + (-1) \cdot (-1) \cdot (-1) + (-1) \cdot 1 \cdot 1 + 1 \cdot (-1) \cdot (-1) + 1 \cdot 1 \cdot (-1) + (-1) \cdot (-1) \cdot 1 + (-1) \cdot 1 \cdot (-1) + 1 \cdot (-1) \cdot 1] = 0 \quad (\text{A.239})$$

$$n_{\mathbf{k}_1,7}^{7,5} = \frac{1}{8}[1 \cdot 1 \cdot 1 + (-1) \cdot (-1) \cdot (-1) + (-1) \cdot 1 \cdot (-1) + 1 \cdot (-1) \cdot 1 + 1 \cdot 1 \cdot 1 + (-1) \cdot (-1) \cdot (-1) + (-1) \cdot 1 \cdot (-1) + 1 \cdot (-1) \cdot 1] = 0 \quad (\text{A.240})$$

$$n_{\mathbf{k}_1,8}^{7,5} = \frac{1}{8}[1 \cdot 1 \cdot 1 + (-1) \cdot (-1) \cdot (-1) + (-1) \cdot 1 \cdot (-1) + 1 \cdot (-1) \cdot 1 + 1 \cdot 1 \cdot (-1) + (-1) \cdot (-1) \cdot 1 + (-1) \cdot 1 \cdot 1 + 1 \cdot (-1) \cdot (-1)] = 0 \quad (\text{A.241})$$

The decomposition is

$$\Gamma^{\mathbf{k}_1,7} \otimes \Gamma^{\mathbf{k}_1,5} = \Gamma^{\mathbf{k}_1,3} \quad (\text{A.242})$$

• $\Gamma^{\mathbf{k}_1,7} \otimes \Gamma^{\mathbf{k}_1,6}$

$$n_{\mathbf{k}_1,1}^{7,6} = \frac{1}{8}[1 \cdot 1 \cdot 1 + (-1) \cdot (-1) \cdot 1 + (-1) \cdot 1 \cdot 1 + 1 \cdot (-1) \cdot 1 + 1 \cdot (-1) \cdot 1 + (-1) \cdot 1 \cdot 1 + (-1) \cdot (-1) \cdot 1 + 1 \cdot 1 \cdot 1] = 0 \quad (\text{A.243})$$

$$n_{\mathbf{k}_1,2}^{7,6} = \frac{1}{8}[1 \cdot 1 \cdot 1 + (-1) \cdot (-1) \cdot 1 + (-1) \cdot 1 \cdot 1 + 1 \cdot (-1) \cdot 1 + 1 \cdot (-1) \cdot (-1) + (-1) \cdot 1 \cdot (-1) + (-1) \cdot (-1) \cdot (-1) + 1 \cdot 1 \cdot (-1)] = 0 \quad (\text{A.244})$$

$$n_{\mathbf{k}_1,3}^{7,6} = \frac{1}{8}[1 \cdot 1 \cdot 1 + (-1) \cdot (-1) \cdot 1 + (-1) \cdot 1 \cdot (-1) + 1 \cdot (-1) \cdot (-1) + 1 \cdot (-1) \cdot 1 + (-1) \cdot 1 \cdot 1 + (-1) \cdot (-1) \cdot (-1) + 1 \cdot 1 \cdot (-1)] = 0 \quad (\text{A.245})$$

$$n_{\mathbf{k}_1,4}^{7,6} = \frac{1}{8}[1 \cdot 1 \cdot 1 + (-1) \cdot (-1) \cdot 1 + (-1) \cdot 1 \cdot (-1) + 1 \cdot (-1) \cdot (-1) + 1 \cdot (-1) \cdot (-1) + (-1) \cdot 1 \cdot (-1) + (-1) \cdot (-1) \cdot 1 + 1 \cdot 1 \cdot 1] = 1 \quad (\text{A.246})$$

$$n_{\mathbf{k}_1,5}^{7,6} = \frac{1}{8}[1 \cdot 1 \cdot 1 + (-1) \cdot (-1) \cdot (-1) + (-1) \cdot 1 \cdot 1 + 1 \cdot (-1) \cdot (-1) + 1 \cdot 1 \cdot 1 + (-1) \cdot (-1) \cdot (-1) + (-1) \cdot 1 \cdot 1 + 1 \cdot (-1) \cdot (-1)] = 0 \quad (\text{A.247})$$

$$n_{\mathbf{k}_1,6}^{7,6} = \frac{1}{8}[1 \cdot 1 \cdot 1 + (-1) \cdot (-1) \cdot (-1) + (-1) \cdot 1 \cdot 1 + 1 \cdot (-1) \cdot (-1) + 1 \cdot (-1) \cdot (-1) + (-1) \cdot 1 \cdot 1 + (-1) \cdot (-1) \cdot (-1) + 1 \cdot 1 \cdot 1] = 0 \quad (\text{A.248})$$

$$n_{\mathbf{k}_1,7}^{7,6} = \frac{1}{8}[1 \cdot 1 \cdot 1 + (-1) \cdot (-1) \cdot (-1) + (-1) \cdot 1 \cdot (-1) + 1 \cdot (-1) \cdot 1 + 1 \cdot (-1) \cdot 1 + (-1) \cdot 1 \cdot (-1) + (-1) \cdot (-1) \cdot (-1) + 1 \cdot 1 \cdot 1] = 0 \quad (\text{A.249})$$

$$n_{\mathbf{k}_1,8}^{7,6} = \frac{1}{8}[1 \cdot 1 \cdot 1 + (-1) \cdot (-1) \cdot (-1) + (-1) \cdot 1 \cdot (-1) + 1 \cdot (-1) \cdot 1 + 1 \cdot (-1) \cdot (-1) + (-1) \cdot 1 \cdot 1 + (-1) \cdot (-1) \cdot 1 + 1 \cdot 1 \cdot (-1)] = 0 \quad (\text{A.250})$$

The decomposition is

$$\Gamma^{\mathbf{k}_1,7} \otimes \Gamma^{\mathbf{k}_1,6} = \Gamma^{\mathbf{k}_1,4} \quad (\text{A.251})$$

2. $\mathbf{k}_2 = (k_{a^*}, 0, 0)$

• $\Gamma^{\mathbf{k}_2,2} \otimes \Gamma^{\mathbf{k}_2,1}$

$$n_{\mathbf{k}_2,1}^{2,1} = \frac{1}{4}[1 \cdot 1 \cdot 1 + 1 \cdot 1 \cdot 1 + (-1) \cdot 1 \cdot 1 + (-1) \cdot 1 \cdot 1] = 0 \quad (\text{A.252})$$

$$n_{\mathbf{k}_2,2}^{2,1} = \frac{1}{4}[1 \cdot 1 \cdot 1 + 1 \cdot 1 \cdot 1 + (-1) \cdot 1 \cdot (-1) + (-1) \cdot 1 \cdot (-1)] = 1 \quad (\text{A.253})$$

$$n_{\mathbf{k}_2,3}^{2,1} = \frac{1}{4}[1 \cdot 1 \cdot 1 + 1 \cdot 1 \cdot (-1) + (-1) \cdot 1 \cdot 1 + (-1) \cdot 1 \cdot (-1)] = 0 \quad (\text{A.254})$$

$$n_{\mathbf{k}_2,4}^{2,1} = \frac{1}{4}[1 \cdot 1 \cdot 1 + 1 \cdot 1 \cdot (-1) + (-1) \cdot 1 \cdot (-1) + (-1) \cdot 1 \cdot 1] = 0 \quad (\text{A.255})$$

The decomposition is

$$\Gamma^{\mathbf{k}_2,2} \otimes \Gamma^{\mathbf{k}_2,1} = \Gamma^{\mathbf{k}_2,2} \quad (\text{A.256})$$

- $\Gamma^{\mathbf{k}_2,2} \otimes \Gamma^{\mathbf{k}_2,2}$

$$n_{\mathbf{k}_2,1}^{2,2} = \frac{1}{4}[1 \cdot 1 \cdot 1 + 1 \cdot 1 \cdot 1 + (-1) \cdot (-1) \cdot 1 + (-1) \cdot (-1) \cdot 1] = 1 \quad (\text{A.257})$$

$$n_{\mathbf{k}_2,2}^{2,2} = \frac{1}{4}[1 \cdot 1 \cdot 1 + 1 \cdot 1 \cdot 1 + (-1) \cdot (-1) \cdot (-1) + (-1) \cdot (-1) \cdot (-1)] = 0 \quad (\text{A.258})$$

$$n_{\mathbf{k}_2,3}^{2,2} = \frac{1}{4}[1 \cdot 1 \cdot 1 + 1 \cdot 1 \cdot (-1) + (-1) \cdot (-1) \cdot 1 + (-1) \cdot (-1) \cdot (-1)] = 0 \quad (\text{A.259})$$

$$n_{\mathbf{k}_2,4}^{2,2} = \frac{1}{4}[1 \cdot 1 \cdot 1 + 1 \cdot 1 \cdot (-1) + (-1) \cdot (-1) \cdot (-1) + (-1) \cdot (-1) \cdot 1] = 0 \quad (\text{A.260})$$

The decomposition is

$$\Gamma^{\mathbf{k}_2,2} \otimes \Gamma^{\mathbf{k}_2,2} = \Gamma^{\mathbf{k}_2,1} \quad (\text{A.261})$$

- $\Gamma^{\mathbf{k}_2,3} \otimes \Gamma^{\mathbf{k}_2,1}$

$$n_{\mathbf{k}_2,1}^{3,1} = \frac{1}{4}[1 \cdot 1 \cdot 1 + (-1) \cdot 1 \cdot 1 + 1 \cdot 1 \cdot 1 + (-1) \cdot 1 \cdot 1] = 0 \quad (\text{A.262})$$

$$n_{\mathbf{k}_2,2}^{3,1} = \frac{1}{4}[1 \cdot 1 \cdot 1 + (-1) \cdot 1 \cdot 1 + 1 \cdot 1 \cdot (-1) + (-1) \cdot 1 \cdot (-1)] = 0 \quad (\text{A.263})$$

$$n_{\mathbf{k}_2,3}^{3,1} = \frac{1}{4}[1 \cdot 1 \cdot 1 + (-1) \cdot 1 \cdot (-1) + 1 \cdot 1 \cdot 1 + (-1) \cdot 1 \cdot (-1)] = 1 \quad (\text{A.264})$$

$$n_{\mathbf{k}_2,4}^{3,1} = \frac{1}{4}[1 \cdot 1 \cdot 1 + (-1) \cdot 1 \cdot (-1) + 1 \cdot 1 \cdot (-1) + (-1) \cdot 1 \cdot 1] = 0 \quad (\text{A.265})$$

The decomposition is

$$\Gamma^{\mathbf{k}_2,3} \otimes \Gamma^{\mathbf{k}_2,1} = \Gamma^{\mathbf{k}_2,3} \quad (\text{A.266})$$

- $\Gamma^{\mathbf{k}_2,3} \otimes \Gamma^{\mathbf{k}_2,2}$

$$n_{\mathbf{k}_2,1}^{3,2} = \frac{1}{4}[1 \cdot 1 \cdot 1 + (-1) \cdot 1 \cdot 1 + 1 \cdot (-1) \cdot 1 + (-1) \cdot (-1) \cdot 1] = 0 \quad (\text{A.267})$$

$$n_{\mathbf{k}_2,2}^{3,2} = \frac{1}{4}[1 \cdot 1 \cdot 1 + (-1) \cdot 1 \cdot 1 + 1 \cdot (-1) \cdot (-1) + (-1) \cdot (-1) \cdot (-1)] = 0 \quad (\text{A.268})$$

$$n_{\mathbf{k}_2,3}^{3,2} = \frac{1}{4}[1 \cdot 1 \cdot 1 + (-1) \cdot 1 \cdot (-1) + 1 \cdot (-1) \cdot 1 + (-1) \cdot (-1) \cdot (-1)] = 0 \quad (\text{A.269})$$

$$n_{\mathbf{k}_2,4}^{3,2} = \frac{1}{4}[1 \cdot 1 \cdot 1 + (-1) \cdot 1 \cdot (-1) + 1 \cdot (-1) \cdot (-1) + (-1) \cdot (-1) \cdot 1] = 1 \quad (\text{A.270})$$

The decomposition is

$$\Gamma^{\mathbf{k}_2,3} \otimes \Gamma^{\mathbf{k}_2,2} = \Gamma^{\mathbf{k}_2,4} \quad (\text{A.271})$$

- $\Gamma^{\mathbf{k}_2,4} \otimes \Gamma^{\mathbf{k}_2,1}$

$$n_{\mathbf{k}_2,1}^{4,1} = \frac{1}{4}[1 \cdot 1 \cdot 1 + (-1) \cdot 1 \cdot 1 + (-1) \cdot 1 \cdot 1 + 1 \cdot 1 \cdot 1] = 0 \quad (\text{A.272})$$

$$n_{\mathbf{k}_2,2}^{4,1} = \frac{1}{4}[1 \cdot 1 \cdot 1 + (-1) \cdot 1 \cdot 1 + (-1) \cdot 1 \cdot (-1) + 1 \cdot 1 \cdot (-1)] = 0 \quad (\text{A.273})$$

$$n_{\mathbf{k}_2,3}^{4,1} = \frac{1}{4}[1 \cdot 1 \cdot 1 + (-1) \cdot 1 \cdot (-1) + (-1) \cdot 1 \cdot 1 + 1 \cdot 1 \cdot (-1)] = 0 \quad (\text{A.274})$$

$$n_{\mathbf{k}_2,4}^{4,1} = \frac{1}{4}[1 \cdot 1 \cdot 1 + (-1) \cdot 1 \cdot (-1) + (-1) \cdot 1 \cdot (-1) + 1 \cdot 1 \cdot 1] = 1 \quad (\text{A.275})$$

The decomposition is

$$\Gamma^{\mathbf{k}_2,4} \otimes \Gamma^{\mathbf{k}_2,1} = \Gamma^{\mathbf{k}_2,4} \quad (\text{A.276})$$

- $\Gamma^{\mathbf{k}_2,4} \otimes \Gamma^{\mathbf{k}_2,2}$

$$n_{\mathbf{k}_2,1}^{4,2} = \frac{1}{4}[1 \cdot 1 \cdot 1 + (-1) \cdot 1 \cdot 1 + (-1) \cdot (-1) \cdot 1 + 1 \cdot (-1) \cdot 1] = 0 \quad (\text{A.277})$$

$$n_{\mathbf{k}_2,2}^{4,2} = \frac{1}{4}[1 \cdot 1 \cdot 1 + (-1) \cdot 1 \cdot 1 + (-1) \cdot (-1) \cdot (-1) + 1 \cdot (-1) \cdot (-1)] = 0 \quad (\text{A.278})$$

$$n_{\mathbf{k}_2,3}^{4,2} = \frac{1}{4}[1 \cdot 1 \cdot 1 + (-1) \cdot 1 \cdot (-1) + (-1) \cdot (-1) \cdot 1 + 1 \cdot (-1) \cdot (-1)] = 1 \quad (\text{A.279})$$

$$n_{\mathbf{k}_2,4}^{4,2} = \frac{1}{4}[1 \cdot 1 \cdot 1 + (-1) \cdot 1 \cdot (-1) + (-1) \cdot (-1) \cdot (-1) + 1 \cdot (-1) \cdot 1] = 0 \quad (\text{A.280})$$

The decomposition is

$$\Gamma^{\mathbf{k}_2,4} \otimes \Gamma^{\mathbf{k}_2,2} = \Gamma^{\mathbf{k}_2,3} \quad (\text{A.281})$$

• $\Gamma^{\mathbf{k}_2,3} \otimes \Gamma^{\mathbf{k}_2,3}$

$$n_{\mathbf{k}_2,1}^{3,3} = \frac{1}{4}[1 \cdot 1 \cdot 1 + (-1) \cdot (-1) \cdot 1 + 1 \cdot 1 \cdot 1 + (-1) \cdot (-1) \cdot 1] = 1 \quad (\text{A.282})$$

$$n_{\mathbf{k}_2,2}^{3,3} = \frac{1}{4}[1 \cdot 1 \cdot 1 + (-1) \cdot (-1) \cdot 1 + 1 \cdot 1 \cdot (-1) + (-1) \cdot (-1) \cdot (-1)] = 0 \quad (\text{A.283})$$

$$n_{\mathbf{k}_2,3}^{3,3} = \frac{1}{4}[1 \cdot 1 \cdot 1 + (-1) \cdot (-1) \cdot (-1) + 1 \cdot 1 \cdot 1 + (-1) \cdot (-1) \cdot (-1)] = 0 \quad (\text{A.284})$$

$$n_{\mathbf{k}_2,4}^{3,3} = \frac{1}{4}[1 \cdot 1 \cdot 1 + (-1) \cdot (-1) \cdot (-1) + 1 \cdot 1 \cdot (-1) + (-1) \cdot (-1) \cdot 1] = 0 \quad (\text{A.285})$$

The decomposition is

$$\Gamma^{\mathbf{k}_2,3} \otimes \Gamma^{\mathbf{k}_2,3} = \Gamma^{\mathbf{k}_2,1} \quad (\text{A.286})$$

• $\Gamma^{\mathbf{k}_2,4} \otimes \Gamma^{\mathbf{k}_2,3}$

$$n_{\mathbf{k}_2,1}^{4,3} = \frac{1}{4}[1 \cdot 1 \cdot 1 + (-1) \cdot (-1) \cdot 1 + (-1) \cdot 1 \cdot 1 + 1 \cdot (-1) \cdot 1] = 0 \quad (\text{A.287})$$

$$n_{\mathbf{k}_2,2}^{4,3} = \frac{1}{4}[1 \cdot 1 \cdot 1 + (-1) \cdot (-1) \cdot 1 + (-1) \cdot 1 \cdot (-1) + 1 \cdot (-1) \cdot (-1)] = 1 \quad (\text{A.288})$$

$$n_{\mathbf{k}_2,3}^{4,3} = \frac{1}{4}[1 \cdot 1 \cdot 1 + (-1) \cdot (-1) \cdot (-1) + (-1) \cdot 1 \cdot 1 + 1 \cdot (-1) \cdot (-1)] = 0 \quad (\text{A.289})$$

$$n_{\mathbf{k}_2,4}^{4,3} = \frac{1}{4}[1 \cdot 1 \cdot 1 + (-1) \cdot (-1) \cdot (-1) + (-1) \cdot 1 \cdot (-1) + 1 \cdot (-1) \cdot 1] = 0 \quad (\text{A.290})$$

The decomposition is

$$\Gamma^{\mathbf{k}_2,3} = \Gamma^{\mathbf{k}_2,2} \quad (\text{A.291})$$

- $\Gamma^{\mathbf{k}_2,4} \otimes \Gamma^{\mathbf{k}_2,4}$

$$n_{\mathbf{k}_2,1}^{4,4} = \frac{1}{4}[1 \cdot 1 \cdot 1 + (-1) \cdot (-1) \cdot 1 + (-1) \cdot (-1) \cdot 1 + 1 \cdot 1 \cdot 1] = 1 \quad (\text{A.292})$$

$$n_{\mathbf{k}_2,2}^{4,4} = \frac{1}{4}[1 \cdot 1 \cdot 1 + (-1) \cdot (-1) \cdot 1 + (-1) \cdot (-1) \cdot (-1) + 1 \cdot 1 \cdot (-1)] = 0 \quad (\text{A.293})$$

$$n_{\mathbf{k}_2,3}^{4,4} = \frac{1}{4}[1 \cdot 1 \cdot 1 + (-1) \cdot (-1) \cdot (-1) + (-1) \cdot (-1) \cdot 1 + 1 \cdot 1 \cdot (-1)] = 0 \quad (\text{A.294})$$

$$n_{\mathbf{k}_2,4}^{4,4} = \frac{1}{4}[1 \cdot 1 \cdot 1 + (-1) \cdot (-1) \cdot (-1) + (-1) \cdot (-1) \cdot (-1) + 1 \cdot 1 \cdot 1] = 0 \quad (\text{A.295})$$

The decomposition is

$$\Gamma^{\mathbf{k}_2,4} \otimes \Gamma^{\mathbf{k}_2,4} = \Gamma^{\mathbf{k}_2,1} \quad (\text{A.296})$$

3. $\mathbf{k}_3 = (0, k_b^*, 0)$

The exponential term $\exp(\pi i k_b^*)$ shall be replaced by a .

- $\Gamma^{\mathbf{k}_3,1} \otimes \Gamma^{\mathbf{k}_3,1}$

$$\begin{aligned} n_{\mathbf{k}_3,1}^{1,1} &= \frac{1}{4}[1 \cdot 1 \cdot 1 + a \cdot a \cdot (a)^* \\ &\quad + (-a) \cdot (-a) \cdot (-a)^* \\ &\quad + (-1) \cdot (-1) \cdot (-1)] = 0 \end{aligned} \quad (\text{A.297})$$

$$\begin{aligned} n_{\mathbf{k}_3,2}^{1,1} &= \frac{1}{4}[1 \cdot 1 \cdot 1 + a \cdot a \cdot (a)^* \\ &\quad + (-a) \cdot (-a) \cdot (a)^* \\ &\quad + (-1) \cdot (-1) \cdot 1] = 1 \end{aligned} \quad (\text{A.298})$$

$$\begin{aligned} n_{\mathbf{k}_3,3}^{1,1} &= \frac{1}{4}[1 \cdot 1 \cdot 1 + a \cdot a \cdot (-a)^* \\ &\quad + (-a) \cdot (-a) \cdot (-a)^* \\ &\quad + (-1) \cdot (-1) \cdot 1] = 0 \end{aligned} \quad (\text{A.299})$$

$$\begin{aligned} n_{\mathbf{k}_3,4}^{1,1} &= \frac{1}{4}[1 \cdot 1 \cdot 1 + a \cdot a \cdot (-a)^* \\ &\quad + (-a) \cdot (-a) \cdot (a)^* \\ &\quad + (-1) \cdot (-1) \cdot (-1)] = 0 \end{aligned} \quad (\text{A.300})$$

The decomposition is

$$\Gamma^{\mathbf{k}_3,1} \otimes \Gamma^{\mathbf{k}_3,1} = \Gamma^{\mathbf{k}_3,2} \quad (\text{A.301})$$

- $\Gamma^{\mathbf{k}_3,3} \otimes \Gamma^{\mathbf{k}_3,1}$

$$\begin{aligned} n_{\mathbf{k}_3,1}^{3,1} &= \frac{1}{4}[1 \cdot 1 \cdot 1 + (-a) \cdot a \cdot (a)^* \\ &\quad + (-a) \cdot (-a) \cdot (-a)^* \\ &\quad + 1 \cdot (-1) \cdot (-1)] = 0 \end{aligned} \quad (\text{A.302})$$

$$\begin{aligned} n_{\mathbf{k}_3,2}^{3,1} &= \frac{1}{4}[1 \cdot 1 \cdot 1 + (-a) \cdot a \cdot (a)^* \\ &\quad + (-a) \cdot (-a) \cdot (a)^* \\ &\quad + 1 \cdot (-1) \cdot 1] = 0 \end{aligned} \quad (\text{A.303})$$

$$\begin{aligned} n_{\mathbf{k}_3,3}^{3,1} &= \frac{1}{4}[1 \cdot 1 \cdot 1 + (-a) \cdot a \cdot (-a)^* \\ &\quad + (-a) \cdot (-a) \cdot (-a)^* \\ &\quad + 1 \cdot (-1) \cdot 1] = 0 \end{aligned} \quad (\text{A.304})$$

$$\begin{aligned} n_{\mathbf{k}_3,4}^{3,1} &= \frac{1}{4}[1 \cdot 1 \cdot 1 + (-a) \cdot a \cdot (-a)^* \\ &\quad + (-a) \cdot (-a) \cdot (a)^* \\ &\quad + 1 \cdot (-1) \cdot (-1)] = 1 \end{aligned} \quad (\text{A.305})$$

The decomposition is

$$\Gamma^{\mathbf{k}_3,3} \otimes \Gamma^{\mathbf{k}_3,1} = \Gamma^{\mathbf{k}_3,4} \quad (\text{A.306})$$

- $\Gamma^{\mathbf{k}_3,4} \otimes \Gamma^{\mathbf{k}_3,1}$

$$\begin{aligned} n_{\mathbf{k}_3,1}^{4,1} &= \frac{1}{4}[1 \cdot 1 \cdot 1 + (-a) \cdot a \cdot (a)^* \\ &\quad + a \cdot (-a) \cdot (-a)^* \\ &\quad + (-1) \cdot (-1) \cdot (-1)] = 0 \end{aligned} \quad (\text{A.307})$$

$$\begin{aligned}
 n_{\mathbf{k}_3,2}^{4,1} &= \frac{1}{4}[1 \cdot 1 \cdot 1 + (-a) \cdot a \cdot (a)^* \\
 &\quad + a \cdot (-a) \cdot (a)^* \\
 &\quad + (-1) \cdot (-1) \cdot 1] = 0
 \end{aligned} \tag{A.308}$$

$$\begin{aligned}
 n_{\mathbf{k}_3,3}^{4,1} &= \frac{1}{4}[1 \cdot 1 \cdot 1 + (-a) \cdot a \cdot (-a)^* \\
 &\quad + a \cdot (-a) \cdot (-a)^* \\
 &\quad + (-1) \cdot (-1) \cdot 1] = 1
 \end{aligned} \tag{A.309}$$

$$\begin{aligned}
 n_{\mathbf{k}_3,4}^{4,1} &= \frac{1}{4}[1 \cdot 1 \cdot 1 + (-a) \cdot a \cdot (-a)^* \\
 &\quad + a \cdot (-a) \cdot (a)^* \\
 &\quad + (-1) \cdot (-1) \cdot (-1)] = 0
 \end{aligned} \tag{A.310}$$

The decomposition is

$$\Gamma^{\mathbf{k}_3,4} \otimes \Gamma^{\mathbf{k}_3,1} = \Gamma^{\mathbf{k}_3,1} \tag{A.311}$$

• $\Gamma^{\mathbf{k}_3,1} \otimes \Gamma^{\mathbf{k}_3,2}$

$$\begin{aligned}
 n_{\mathbf{k}_3,1}^{1,2} &= \frac{1}{4}[1 \cdot 1 \cdot 1 + a \cdot a \cdot (a)^* \\
 &\quad + (-a) \cdot a \cdot (-a)^* \\
 &\quad + (-1) \cdot 1 \cdot (-1)] = 1
 \end{aligned} \tag{A.312}$$

$$\begin{aligned}
 n_{\mathbf{k}_3,2}^{1,2} &= \frac{1}{4}[1 \cdot 1 \cdot 1 + a \cdot a \cdot (a)^* \\
 &\quad + (-a) \cdot a \cdot (a)^* \\
 &\quad + (-1) \cdot 1 \cdot 1] = 0
 \end{aligned} \tag{A.313}$$

$$\begin{aligned}
 n_{\mathbf{k}_3,3}^{1,2} &= \frac{1}{4}[1 \cdot 1 \cdot 1 + a \cdot a \cdot (-a)^* \\
 &\quad + (-a) \cdot a \cdot (-a)^* \\
 &\quad + (-1) \cdot 1 \cdot 1] = 0
 \end{aligned} \tag{A.314}$$

$$\begin{aligned}
 n_{\mathbf{k}_3,4}^{1,2} &= \frac{1}{4}[1 \cdot 1 \cdot 1 + a \cdot a \cdot (-a)^* \\
 &\quad + (-a) \cdot (a) \cdot (a)^* \\
 &\quad + (-1) \cdot 1 \cdot (-1)] = 0
 \end{aligned} \tag{A.315}$$

The decomposition is

$$\Gamma^{\mathbf{k}_3,1} \otimes \Gamma^{\mathbf{k}_3,2} = \Gamma^{\mathbf{k}_3,1} \quad (\text{A.316})$$

• $\Gamma^{\mathbf{k}_3,3} \otimes \Gamma^{\mathbf{k}_3,2}$

$$\begin{aligned} n_{\mathbf{k}_3,1}^{3,2} &= \frac{1}{4}[1 \cdot 1 \cdot 1 + (-a) \cdot a \cdot (a)^* \\ &\quad + (-a) \cdot a \cdot (-a)^* \\ &\quad + 1 \cdot 1 \cdot (-1)] = 0 \end{aligned} \quad (\text{A.317})$$

$$\begin{aligned} n_{\mathbf{k}_3,2}^{3,2} &= \frac{1}{4}[1 \cdot 1 \cdot 1 + (-a) \cdot a \cdot (a)^* \\ &\quad + (-a) \cdot a \cdot (a)^* \\ &\quad + 1 \cdot 1 \cdot 1] = 0 \end{aligned} \quad (\text{A.318})$$

$$\begin{aligned} n_{\mathbf{k}_3,3}^{3,2} &= \frac{1}{4}[1 \cdot 1 \cdot 1 + (-a) \cdot a \cdot (-a)^* \\ &\quad + (-a) \cdot a \cdot (-a)^* \\ &\quad + 1 \cdot 1 \cdot 1] = 1 \end{aligned} \quad (\text{A.319})$$

$$\begin{aligned} n_{\mathbf{k}_3,4}^{3,2} &= \frac{1}{4}[1 \cdot 1 \cdot 1 + (-a) \cdot a \cdot (-a)^* \\ &\quad + (-a) \cdot (a) \cdot (a)^* \\ &\quad + 1 \cdot 1 \cdot (-1)] = 0 \end{aligned} \quad (\text{A.320})$$

The decomposition is

$$\Gamma^{\mathbf{k}_3,3} \otimes \Gamma^{\mathbf{k}_3,2} = \Gamma^{\mathbf{k}_3,3} \quad (\text{A.321})$$

• $\Gamma^{\mathbf{k}_3,4} \otimes \Gamma^{\mathbf{k}_3,2}$

$$\begin{aligned} n_{\mathbf{k}_3,1}^{4,2} &= \frac{1}{4}[1 \cdot 1 \cdot 1 + (-a) \cdot a \cdot (a)^* \\ &\quad + a \cdot a \cdot (-a)^* \\ &\quad + (-1) \cdot 1 \cdot (-1)] = 0 \end{aligned} \quad (\text{A.322})$$

$$\begin{aligned}
 n_{\mathbf{k}_3,2}^{4,2} &= \frac{1}{4}[1 \cdot 1 \cdot 1 + (-a) \cdot a \cdot (a)^* \\
 &\quad + a \cdot a \cdot (a)^* \\
 &\quad + (-1) \cdot 1 \cdot 1] = 0
 \end{aligned} \tag{A.323}$$

$$\begin{aligned}
 n_{\mathbf{k}_3,3}^{4,2} &= \frac{1}{4}[1 \cdot 1 \cdot 1 + (-a) \cdot a \cdot (-a)^* \\
 &\quad + a \cdot a \cdot (-a)^* \\
 &\quad + (-1) \cdot 1 \cdot 1] = 0
 \end{aligned} \tag{A.324}$$

$$\begin{aligned}
 n_{\mathbf{k}_3,4}^{4,2} &= \frac{1}{4}[1 \cdot 1 \cdot 1 + (-a) \cdot a \cdot (-a)^* \\
 &\quad + a \cdot (a) \cdot (a)^* \\
 &\quad + (-1) \cdot 1 \cdot (-1)] = 1
 \end{aligned} \tag{A.325}$$

The decomposition is

$$\Gamma^{\mathbf{k}_3,4} \otimes \Gamma^{\mathbf{k}_3,2} = \Gamma^{\mathbf{k}_3,4} \tag{A.326}$$

• $\Gamma^{\mathbf{k}_3,3} \otimes \Gamma^{\mathbf{k}_3,3}$

$$\begin{aligned}
 n_{\mathbf{k}_3,1}^{3,3} &= \frac{1}{4}[1 \cdot 1 \cdot 1 + (-a) \cdot (-a) \cdot (a)^* \\
 &\quad + (-a) \cdot (-a) \cdot (-a)^* \\
 &\quad + 1 \cdot 1 \cdot (-1)] = 0
 \end{aligned} \tag{A.327}$$

$$\begin{aligned}
 n_{\mathbf{k}_3,2}^{3,3} &= \frac{1}{4}[1 \cdot 1 \cdot 1 + (-a) \cdot (-a) \cdot (a)^* \\
 &\quad + (-a) \cdot (-a) \cdot (a)^* \\
 &\quad + 1 \cdot 1 \cdot 1] = 1
 \end{aligned} \tag{A.328}$$

$$\begin{aligned}
 n_{\mathbf{k}_3,3}^{3,3} &= \frac{1}{4}[1 \cdot 1 \cdot 1 + (-a) \cdot (-a) \cdot (-a)^* \\
 &\quad + (-a) \cdot (-a) \cdot (-a)^* \\
 &\quad + 1 \cdot 1 \cdot 1] = 0
 \end{aligned} \tag{A.329}$$

$$\begin{aligned}
 n_{\mathbf{k}_3,4}^{3,3} &= \frac{1}{4}[1 \cdot 1 \cdot 1 + (-a)(-a) \cdot (-a)^* \\
 &\quad + (-a) \cdot (-a) \cdot (a)^* \\
 &\quad + 1 \cdot 1 \cdot (-1)] = 0
 \end{aligned} \tag{A.330}$$

The decomposition is

$$\Gamma^{\mathbf{k}_3,3} \otimes \Gamma^{\mathbf{k}_3,3} = \Gamma^{\mathbf{k}_3,2} \quad (\text{A.331})$$

• $\Gamma^{\mathbf{k}_3,4} \otimes \Gamma^{\mathbf{k}_3,3}$

$$\begin{aligned} n_{\mathbf{k}_3,1}^{4,3} &= \frac{1}{4} [1 \cdot 1 \cdot 1 + (-a) \cdot (-a) \cdot (a)^* \\ &\quad + a \cdot (-a) \cdot (-a)^* \\ &\quad + (-1) \cdot 1 \cdot (-1)] = 1 \end{aligned} \quad (\text{A.332})$$

$$\begin{aligned} n_{\mathbf{k}_3,2}^{4,3} &= \frac{1}{4} [1 \cdot 1 \cdot 1 + (-a) \cdot (-a) \cdot (a)^* \\ &\quad + a \cdot (-a) \cdot (a)^* \\ &\quad + (-1) \cdot 1 \cdot 1] = 0 \end{aligned} \quad (\text{A.333})$$

$$\begin{aligned} n_{\mathbf{k}_3,3}^{4,3} &= \frac{1}{4} [1 \cdot 1 \cdot 1 + (-a) \cdot (-a) \cdot (-a)^* \\ &\quad + a \cdot (-a) \cdot (-a)^* \\ &\quad + (-1) \cdot 1 \cdot 1] = 0 \end{aligned} \quad (\text{A.334})$$

$$\begin{aligned} n_{\mathbf{k}_3,4}^{4,3} &= \frac{1}{4} [1 \cdot 1 \cdot 1 + (-a)(- \cdot a) \cdot (-a)^* \\ &\quad + a \cdot (-a) \cdot (a)^* \\ &\quad + (-1) \cdot 1 \cdot (-1)] = 0 \end{aligned} \quad (\text{A.335})$$

The decomposition is

$$\Gamma^{\mathbf{k}_3,4} \otimes \Gamma^{\mathbf{k}_3,3} = \Gamma^{\mathbf{k}_3,1} \quad (\text{A.336})$$

A.2.5. Deduction of the basis vectors

The calculation of the basis vectors for the irreducible representations Γ^2 to Γ^8 is shown below.

1. $\mathbf{k}_1 = 0$

• $\Gamma^{\mathbf{k}_1,2}$ 4a

$$\begin{aligned} \psi_{1,1}^{\mathbf{k}_1,2} &= \frac{1}{8} \left[1 \cdot \begin{pmatrix} S_{1x} \\ S_{1y} \\ S_{1z} \end{pmatrix} + 1 \cdot \begin{pmatrix} -S_{2x} \\ -S_{2y} \\ S_{2z} \end{pmatrix} + 1 \cdot \begin{pmatrix} -S_{2x} \\ S_{2y} \\ -S_{2z} \end{pmatrix} + 1 \cdot \begin{pmatrix} S_{1x} \\ -S_{1y} \\ -S_{1z} \end{pmatrix} \right] \\ &\quad + \frac{1}{8} \left[(-1) \cdot \begin{pmatrix} S_{1x} \\ S_{1y} \\ S_{1z} \end{pmatrix} + (-1) \cdot \begin{pmatrix} -S_{2x} \\ -S_{2y} \\ S_{2z} \end{pmatrix} + (-1) \cdot \begin{pmatrix} -S_{2x} \\ S_{2y} \\ -S_{2z} \end{pmatrix} + (-1) \cdot \begin{pmatrix} S_{1x} \\ -S_{1y} \\ -S_{1z} \end{pmatrix} \right] \\ &= 0 \end{aligned} \tag{A.337}$$

As expected, because $\Gamma^{\mathbf{k}_1,2}$ is not contained in the decomposition of $\Gamma_{4a}^{\mathbf{k}_1}$.

• $\Gamma^{\mathbf{k}_1,2}$ 8e

$$\begin{aligned} \psi_{1,1}^{\mathbf{k}_1,2} &= \frac{1}{8} \left[1 \cdot \begin{pmatrix} S_{1x} \\ S_{1y} \\ S_{1z} \end{pmatrix} + 1 \cdot \begin{pmatrix} -S_{2x} \\ -S_{2y} \\ S_{2z} \end{pmatrix} + 1 \cdot \begin{pmatrix} -S_{1x} \\ S_{1y} \\ -S_{1z} \end{pmatrix} + 1 \cdot \begin{pmatrix} S_{2x} \\ -S_{2y} \\ -S_{2z} \end{pmatrix} \right] \\ &\quad + \frac{1}{8} \left[(-1) \cdot \begin{pmatrix} S_{3x} \\ S_{3y} \\ S_{3z} \end{pmatrix} + (-1) \cdot \begin{pmatrix} -S_{4x} \\ -S_{4y} \\ S_{4z} \end{pmatrix} + (-1) \cdot \begin{pmatrix} -S_{3x} \\ S_{3y} \\ -S_{3z} \end{pmatrix} + (-1) \cdot \begin{pmatrix} S_{4x} \\ -S_{4y} \\ -S_{4z} \end{pmatrix} \right] \\ &= \frac{1}{4} \left[\begin{pmatrix} 0 \\ S_{1y} \\ 0 \end{pmatrix} - \begin{pmatrix} 0 \\ S_{2y} \\ 0 \end{pmatrix} - \begin{pmatrix} 0 \\ S_{3y} \\ 0 \end{pmatrix} + \begin{pmatrix} 0 \\ S_{4y} \\ 0 \end{pmatrix} \right]. \end{aligned} \tag{A.338}$$

• $\Gamma^{\mathbf{k}_1,3}$ 4a

$$\begin{aligned} \psi_{1,1}^{\mathbf{k}_1,3} &= \frac{1}{8} \left[1 \cdot \begin{pmatrix} S_{1x} \\ S_{1y} \\ S_{1z} \end{pmatrix} + 1 \cdot \begin{pmatrix} -S_{2x} \\ -S_{2y} \\ S_{2z} \end{pmatrix} + (-1) \cdot \begin{pmatrix} -S_{2x} \\ S_{2y} \\ -S_{2z} \end{pmatrix} + (-1) \cdot \begin{pmatrix} S_{1x} \\ -S_{1y} \\ -S_{1z} \end{pmatrix} \right] \\ &\quad + \frac{1}{8} \left[1 \cdot \begin{pmatrix} S_{1x} \\ S_{1y} \\ S_{1z} \end{pmatrix} + 1 \cdot \begin{pmatrix} -S_{2x} \\ -S_{2y} \\ S_{2z} \end{pmatrix} + (-1) \cdot \begin{pmatrix} -S_{2x} \\ S_{2y} \\ -S_{2z} \end{pmatrix} + (-1) \cdot \begin{pmatrix} S_{1x} \\ -S_{1y} \\ -S_{1z} \end{pmatrix} \right] \\ &= \frac{1}{2} \left[\begin{pmatrix} 0 \\ S_{1y} \\ S_{1z} \end{pmatrix} + \begin{pmatrix} 0 \\ -S_{2y} \\ S_{2z} \end{pmatrix} \right] \end{aligned} \tag{A.339}$$

- $\Gamma^{\mathbf{k}_1,3}$ 8e

$$\begin{aligned}
\psi_{1,1}^{\mathbf{k}_1,3} &= \frac{1}{8} \left[1 \cdot \begin{pmatrix} S_{1x} \\ S_{1y} \\ S_{1z} \end{pmatrix} + 1 \cdot \begin{pmatrix} -S_{2x} \\ -S_{2y} \\ S_{2z} \end{pmatrix} + (-1) \cdot \begin{pmatrix} -S_{1x} \\ S_{1y} \\ -S_{1z} \end{pmatrix} + (-1) \cdot \begin{pmatrix} S_{2x} \\ -S_{2y} \\ -S_{2z} \end{pmatrix} \right] \\
&+ \frac{1}{8} \left[1 \cdot \begin{pmatrix} S_{3x} \\ S_{3y} \\ S_{3z} \end{pmatrix} + 1 \cdot \begin{pmatrix} -S_{4x} \\ -S_{4y} \\ S_{4z} \end{pmatrix} + (-1) \cdot \begin{pmatrix} -S_{3x} \\ S_{3y} \\ -S_{3z} \end{pmatrix} + (-1) \cdot \begin{pmatrix} S_{4x} \\ -S_{4y} \\ -S_{4z} \end{pmatrix} \right] \\
&= \frac{1}{4} \left[\begin{pmatrix} S_{1x} \\ 0 \\ S_{1z} \end{pmatrix} + \begin{pmatrix} -S_{2x} \\ 0 \\ S_{2z} \end{pmatrix} + \begin{pmatrix} S_{3x} \\ 0 \\ S_{3z} \end{pmatrix} + \begin{pmatrix} -S_{4x} \\ 0 \\ S_{4z} \end{pmatrix} \right]. \tag{A.340}
\end{aligned}$$

- $\Gamma^{\mathbf{k}_1,4}$ 4a

$$\begin{aligned}
\psi_{1,1}^{\mathbf{k}_1,4} &= \frac{1}{8} \left[1 \cdot \begin{pmatrix} S_{1x} \\ S_{1y} \\ S_{1z} \end{pmatrix} + 1 \cdot \begin{pmatrix} -S_{2x} \\ -S_{2y} \\ S_{2z} \end{pmatrix} + (-1) \cdot \begin{pmatrix} -S_{2x} \\ S_{2y} \\ -S_{2z} \end{pmatrix} + (-1) \cdot \begin{pmatrix} S_{1x} \\ -S_{1y} \\ -S_{1z} \end{pmatrix} \right] \\
&+ \frac{1}{8} \left[(-1) \cdot \begin{pmatrix} S_{1x} \\ S_{1y} \\ S_{1z} \end{pmatrix} + (-1) \cdot \begin{pmatrix} -S_{2x} \\ -S_{2y} \\ S_{2z} \end{pmatrix} + 1 \cdot \begin{pmatrix} -S_{2x} \\ S_{2y} \\ -S_{2z} \end{pmatrix} + 1 \cdot \begin{pmatrix} S_{1x} \\ -S_{1y} \\ -S_{1z} \end{pmatrix} \right] \\
&= 0 \tag{A.341}
\end{aligned}$$

As expected, because $\Gamma^{\mathbf{k}_1,4}$ is not contained in the decomposition of $\Gamma_{4a}^{\mathbf{k}_1}$.

- $\Gamma^{\mathbf{k}_1,4}$ 8e

$$\begin{aligned}
\psi_{1,1}^{\mathbf{k}_1,4} &= \frac{1}{8} \left[1 \cdot \begin{pmatrix} S_{1x} \\ S_{1y} \\ S_{1z} \end{pmatrix} + 1 \cdot \begin{pmatrix} -S_{2x} \\ -S_{2y} \\ S_{2z} \end{pmatrix} + (-1) \cdot \begin{pmatrix} -S_{1x} \\ S_{1y} \\ -S_{1z} \end{pmatrix} + (-1) \cdot \begin{pmatrix} S_{2x} \\ -S_{2y} \\ -S_{2z} \end{pmatrix} \right] \\
&+ \frac{1}{8} \left[(-1) \cdot \begin{pmatrix} S_{3x} \\ S_{3y} \\ S_{3z} \end{pmatrix} + (-1) \cdot \begin{pmatrix} -S_{4x} \\ -S_{4y} \\ S_{4z} \end{pmatrix} + 1 \cdot \begin{pmatrix} -S_{3x} \\ S_{3y} \\ -S_{3z} \end{pmatrix} + 1 \cdot \begin{pmatrix} S_{4x} \\ -S_{4y} \\ -S_{4z} \end{pmatrix} \right] \\
&= \frac{1}{4} \left[\begin{pmatrix} S_{1x} \\ 0 \\ S_{1z} \end{pmatrix} + \begin{pmatrix} -S_{2x} \\ 0 \\ S_{2z} \end{pmatrix} + \begin{pmatrix} -S_{3x} \\ 0 \\ -S_{3z} \end{pmatrix} + \begin{pmatrix} S_{4x} \\ 0 \\ -S_{4z} \end{pmatrix} \right]. \tag{A.342}
\end{aligned}$$

- $\Gamma^{\mathbf{k}_1,5}$ 4a

$$\begin{aligned}
 \psi_{1,1}^{\mathbf{k}_1,5} &= \frac{1}{8} \left[1 \cdot \begin{pmatrix} S_{1x} \\ S_{1y} \\ S_{1z} \end{pmatrix} + (-1) \cdot \begin{pmatrix} -S_{2x} \\ -S_{2y} \\ S_{2z} \end{pmatrix} + 1 \cdot \begin{pmatrix} -S_{2x} \\ S_{2y} \\ -S_{2z} \end{pmatrix} + (-1) \cdot \begin{pmatrix} S_{1x} \\ -S_{1y} \\ -S_{1z} \end{pmatrix} \right] \\
 &+ \frac{1}{8} \left[1 \cdot \begin{pmatrix} S_{1x} \\ S_{1y} \\ S_{1z} \end{pmatrix} + (-1) \cdot \begin{pmatrix} -S_{2x} \\ -S_{2y} \\ S_{2z} \end{pmatrix} + 1 \cdot \begin{pmatrix} -S_{2x} \\ S_{2y} \\ -S_{2z} \end{pmatrix} + (-1) \cdot \begin{pmatrix} S_{1x} \\ -S_{1y} \\ -S_{1z} \end{pmatrix} \right] \\
 &= \frac{1}{2} \left[\begin{pmatrix} 0 \\ S_{1y} \\ S_{1z} \end{pmatrix} + \begin{pmatrix} 0 \\ S_{2y} \\ -S_{2z} \end{pmatrix} \right] \tag{A.343}
 \end{aligned}$$

- $\Gamma^{\mathbf{k}_1,5}$ 8e

$$\begin{aligned}
 \psi_{1,1}^{\mathbf{k}_1,5} &= \frac{1}{8} \left[1 \cdot \begin{pmatrix} S_{1x} \\ S_{1y} \\ S_{1z} \end{pmatrix} + (-1) \cdot \begin{pmatrix} -S_{2x} \\ -S_{2y} \\ S_{2z} \end{pmatrix} + 1 \cdot \begin{pmatrix} -S_{1x} \\ S_{1y} \\ -S_{1z} \end{pmatrix} + (-1) \cdot \begin{pmatrix} S_{2x} \\ -S_{2y} \\ -S_{2z} \end{pmatrix} \right] \\
 &+ \frac{1}{8} \left[1 \cdot \begin{pmatrix} S_{3x} \\ S_{3y} \\ S_{3z} \end{pmatrix} + (-1) \cdot \begin{pmatrix} -S_{4x} \\ -S_{4y} \\ S_{4z} \end{pmatrix} + 1 \cdot \begin{pmatrix} -S_{3x} \\ S_{3y} \\ -S_{3z} \end{pmatrix} + (-1) \cdot \begin{pmatrix} S_{4x} \\ -S_{4y} \\ -S_{4z} \end{pmatrix} \right] \\
 &= \frac{1}{4} \left[\begin{pmatrix} 0 \\ S_{1y} \\ 0 \end{pmatrix} + \begin{pmatrix} 0 \\ S_{2y} \\ 0 \end{pmatrix} + \begin{pmatrix} 0 \\ S_{3y} \\ 0 \end{pmatrix} + \begin{pmatrix} 0 \\ S_{4y} \\ 0 \end{pmatrix} \right]. \tag{A.344}
 \end{aligned}$$

- $\Gamma^{\mathbf{k}_1,6}$ 4a

$$\begin{aligned}
 \psi_{1,1}^{\mathbf{k}_1,6} &= \frac{1}{8} \left[1 \cdot \begin{pmatrix} S_{1x} \\ S_{1y} \\ S_{1z} \end{pmatrix} + (-1) \cdot \begin{pmatrix} -S_{2x} \\ -S_{2y} \\ S_{2z} \end{pmatrix} + 1 \cdot \begin{pmatrix} -S_{2x} \\ S_{2y} \\ -S_{2z} \end{pmatrix} + (-1) \cdot \begin{pmatrix} S_{1x} \\ -S_{1y} \\ -S_{1z} \end{pmatrix} \right] \\
 &+ \frac{1}{8} \left[(-1) \cdot \begin{pmatrix} S_{1x} \\ S_{1y} \\ S_{1z} \end{pmatrix} + 1 \cdot \begin{pmatrix} -S_{2x} \\ -S_{2y} \\ S_{2z} \end{pmatrix} + (-1) \cdot \begin{pmatrix} -S_{2x} \\ S_{2y} \\ -S_{2z} \end{pmatrix} + 1 \cdot \begin{pmatrix} S_{1x} \\ -S_{1y} \\ -S_{1z} \end{pmatrix} \right] \\
 &= 0 \tag{A.345}
 \end{aligned}$$

As expected, because $\Gamma^{\mathbf{k}_1,6}$ is not contained in the decomposition of $\Gamma_{4a}^{\mathbf{k}_1}$.

- $\Gamma^{\mathbf{k}_1,6}$ 8e

$$\begin{aligned}
\psi_{1,1}^{\mathbf{k}_1,6} &= \frac{1}{8} \left[1 \cdot \begin{pmatrix} S_{1x} \\ S_{1y} \\ S_{1z} \end{pmatrix} + (-1) \cdot \begin{pmatrix} -S_{2x} \\ -S_{2y} \\ S_{2z} \end{pmatrix} + 1 \cdot \begin{pmatrix} -S_{1x} \\ S_{1y} \\ -S_{1z} \end{pmatrix} + (-1) \cdot \begin{pmatrix} S_{2x} \\ -S_{2y} \\ -S_{2z} \end{pmatrix} \right] \\
&\quad + \frac{1}{8} \left[(-1) \cdot \begin{pmatrix} S_{3x} \\ S_{3y} \\ S_{3z} \end{pmatrix} + 1 \cdot \begin{pmatrix} -S_{4x} \\ -S_{4y} \\ S_{4z} \end{pmatrix} + (-1) \cdot \begin{pmatrix} -S_{3x} \\ S_{3y} \\ -S_{3z} \end{pmatrix} + 1 \cdot \begin{pmatrix} S_{4x} \\ -S_{4y} \\ -S_{4z} \end{pmatrix} \right] \\
&= \frac{1}{4} \left[\begin{pmatrix} 0 \\ S_{1y} \\ 0 \end{pmatrix} + \begin{pmatrix} 0 \\ S_{2y} \\ 0 \end{pmatrix} + \begin{pmatrix} 0 \\ -S_{3y} \\ 0 \end{pmatrix} + \begin{pmatrix} 0 \\ -S_{4y} \\ 0 \end{pmatrix} \right]. \tag{A.346}
\end{aligned}$$

- $\Gamma^{\mathbf{k}_1,7}$ 4a

$$\begin{aligned}
\psi_{1,1}^{\mathbf{k}_1,7} &= \frac{1}{8} \left[1 \cdot \begin{pmatrix} S_{1x} \\ S_{1y} \\ S_{1z} \end{pmatrix} + (-1) \cdot \begin{pmatrix} -S_{2x} \\ -S_{2y} \\ S_{2z} \end{pmatrix} + (-1) \cdot \begin{pmatrix} -S_{2x} \\ S_{2y} \\ -S_{2z} \end{pmatrix} + 1 \cdot \begin{pmatrix} S_{1x} \\ -S_{1y} \\ -S_{1z} \end{pmatrix} \right] \\
&\quad + \frac{1}{8} \left[1 \cdot \begin{pmatrix} S_{1x} \\ S_{1y} \\ S_{1z} \end{pmatrix} + (-1) \cdot \begin{pmatrix} -S_{2x} \\ -S_{2y} \\ S_{2z} \end{pmatrix} + (-1) \cdot \begin{pmatrix} -S_{2x} \\ S_{2y} \\ -S_{2z} \end{pmatrix} + 1 \cdot \begin{pmatrix} S_{1x} \\ -S_{1y} \\ -S_{1z} \end{pmatrix} \right] \\
&= \frac{1}{2} \left[\begin{pmatrix} S_{1x} \\ 0 \\ 0 \end{pmatrix} + \begin{pmatrix} S_{2x} \\ 0 \\ 0 \end{pmatrix} \right] \tag{A.347}
\end{aligned}$$

- $\Gamma^{\mathbf{k}_1,7}$ 8e

$$\begin{aligned}
\psi_{1,1}^{\mathbf{k}_1,7} &= \frac{1}{8} \left[1 \cdot \begin{pmatrix} S_{1x} \\ S_{1y} \\ S_{1z} \end{pmatrix} + (-1) \cdot \begin{pmatrix} -S_{2x} \\ -S_{2y} \\ S_{2z} \end{pmatrix} + (-1) \cdot \begin{pmatrix} -S_{1x} \\ S_{1y} \\ -S_{1z} \end{pmatrix} + 1 \cdot \begin{pmatrix} S_{2x} \\ -S_{2y} \\ -S_{2z} \end{pmatrix} \right] \\
&\quad + \frac{1}{8} \left[1 \cdot \begin{pmatrix} S_{3x} \\ S_{3y} \\ S_{3z} \end{pmatrix} + (-1) \cdot \begin{pmatrix} -S_{4x} \\ -S_{4y} \\ S_{4z} \end{pmatrix} + (-1) \cdot \begin{pmatrix} -S_{3x} \\ S_{3y} \\ -S_{3z} \end{pmatrix} + 1 \cdot \begin{pmatrix} S_{4x} \\ -S_{4y} \\ -S_{4z} \end{pmatrix} \right] \\
&= \frac{1}{4} \left[\begin{pmatrix} S_{1x} \\ 0 \\ S_{1z} \end{pmatrix} + \begin{pmatrix} S_{2x} \\ 0 \\ -S_{2z} \end{pmatrix} + \begin{pmatrix} S_{3x} \\ 0 \\ S_{3z} \end{pmatrix} + \begin{pmatrix} S_{4x} \\ 0 \\ -S_{4z} \end{pmatrix} \right]. \tag{A.348}
\end{aligned}$$

- $\Gamma^{\mathbf{k}_1,8}$ 4a

$$\begin{aligned}
 \psi_{1,1}^{\mathbf{k}_1,8} &= \frac{1}{8} \left[1 \cdot \begin{pmatrix} S_{1x} \\ S_{1y} \\ S_{1z} \end{pmatrix} + (-1) \cdot \begin{pmatrix} -S_{2x} \\ -S_{2y} \\ S_{2z} \end{pmatrix} + (-1) \cdot \begin{pmatrix} -S_{2x} \\ S_{2y} \\ -S_{2z} \end{pmatrix} + 1 \cdot \begin{pmatrix} S_{1x} \\ -S_{1y} \\ -S_{1z} \end{pmatrix} \right] \\
 &+ \frac{1}{8} \left[(-1) \cdot \begin{pmatrix} S_{1x} \\ S_{1y} \\ S_{1z} \end{pmatrix} + 1 \cdot \begin{pmatrix} -S_{2x} \\ -S_{2y} \\ S_{2z} \end{pmatrix} + 1 \cdot \begin{pmatrix} -S_{2x} \\ S_{2y} \\ -S_{2z} \end{pmatrix} + (-1) \cdot \begin{pmatrix} S_{1x} \\ -S_{1y} \\ -S_{1z} \end{pmatrix} \right] \\
 &= 0
 \end{aligned} \tag{A.349}$$

As expected, because $\Gamma^{\mathbf{k}_1,8}$ is not contained in the decomposition of $\Gamma_{4a}^{\mathbf{k}_1}$.

- $\Gamma^{\mathbf{k}_1,8}$ 8e

$$\begin{aligned}
 \psi_{1,1}^{\mathbf{k}_1,8} &= \frac{1}{8} \left[1 \cdot \begin{pmatrix} S_{1x} \\ S_{1y} \\ S_{1z} \end{pmatrix} + (-1) \cdot \begin{pmatrix} -S_{2x} \\ -S_{2y} \\ S_{2z} \end{pmatrix} + (-1) \cdot \begin{pmatrix} -S_{1x} \\ S_{1y} \\ -S_{1z} \end{pmatrix} + 1 \cdot \begin{pmatrix} S_{2x} \\ -S_{2y} \\ -S_{2z} \end{pmatrix} \right] \\
 &+ \frac{1}{8} \left[(-1) \cdot \begin{pmatrix} S_{3x} \\ S_{3y} \\ S_{3z} \end{pmatrix} + 1 \cdot \begin{pmatrix} -S_{4x} \\ -S_{4y} \\ S_{4z} \end{pmatrix} + 1 \cdot \begin{pmatrix} -S_{3x} \\ S_{3y} \\ -S_{3z} \end{pmatrix} + (-1) \cdot \begin{pmatrix} S_{4x} \\ -S_{4y} \\ -S_{4z} \end{pmatrix} \right] \\
 &= \frac{1}{4} \left[\begin{pmatrix} S_{1x} \\ 0 \\ S_{1z} \end{pmatrix} + \begin{pmatrix} S_{2x} \\ 0 \\ -S_{2z} \end{pmatrix} + \begin{pmatrix} -S_{3x} \\ 0 \\ -S_{3z} \end{pmatrix} + \begin{pmatrix} -S_{4x} \\ 0 \\ S_{4z} \end{pmatrix} \right].
 \end{aligned} \tag{A.350}$$

2. $\mathbf{k}_2 = (k_{a^*}, 0, 0)$

- $\Gamma^{\mathbf{k}_2,1}$ 4a

$$\begin{aligned}
 \psi_{1,1}^{\mathbf{k}_2,1} &= \frac{1}{4} \left[1 \cdot \begin{pmatrix} S_{1x} \\ S_{1y} \\ S_{1z} \end{pmatrix} + 1 \cdot \begin{pmatrix} S_{1x} \\ -S_{1y} \\ -S_{1z} \end{pmatrix} + 1 \cdot \begin{pmatrix} -S_{2x} \\ -S_{2y} \\ S_{2z} \end{pmatrix} + 1 \cdot \begin{pmatrix} -S_{2x} \\ S_{2y} \\ -S_{2z} \end{pmatrix} \right] \\
 &= \frac{1}{2} \left[\begin{pmatrix} S_{1x} \\ 0 \\ 0 \end{pmatrix} + \begin{pmatrix} -S_{2x} \\ 0 \\ 0 \end{pmatrix} \right].
 \end{aligned} \tag{A.351}$$

- $\Gamma^{\mathbf{k}_2,1}$ 8e

$$\begin{aligned}\psi_{1,1}^{\mathbf{k}_2,1} &= \frac{1}{4} \left[1 \cdot \begin{pmatrix} S_{1x} \\ S_{1y} \\ S_{1z} \end{pmatrix} + 1 \cdot \begin{pmatrix} S_{2'x} \\ -S_{2'y} \\ -S_{2'z} \end{pmatrix} + 1 \cdot \begin{pmatrix} -S_{4x} \\ -S_{4y} \\ S_{4z} \end{pmatrix} + 1 \cdot \begin{pmatrix} -S_{3'x} \\ S_{3'y} \\ -S_{3'z} \end{pmatrix} \right] \\ &= \frac{1}{4} \left[\begin{pmatrix} S_{1x} \\ S_{1y} \\ S_{1z} \end{pmatrix} + \begin{pmatrix} S_{2'x} \\ -S_{2'y} \\ -S_{2'z} \end{pmatrix} + \begin{pmatrix} -S_{3'x} \\ S_{3'y} \\ -S_{3'z} \end{pmatrix} + \begin{pmatrix} -S_{4x} \\ -S_{4y} \\ S_{4z} \end{pmatrix} \right] \quad (\text{A.352})\end{aligned}$$

- $\Gamma^{\mathbf{k}_2,2}$ 4a

$$\begin{aligned}\psi_{1,1}^{\mathbf{k}_2,2} &= \frac{1}{4} \left[1 \cdot \begin{pmatrix} S_{1x} \\ S_{1y} \\ S_{1z} \end{pmatrix} + 1 \cdot \begin{pmatrix} S_{1x} \\ -S_{1y} \\ -S_{1z} \end{pmatrix} + (-1) \cdot \begin{pmatrix} -S_{2x} \\ -S_{2y} \\ S_{2z} \end{pmatrix} + (-1) \cdot \begin{pmatrix} -S_{2x} \\ S_{2y} \\ -S_{2z} \end{pmatrix} \right] \\ &= \frac{1}{2} \left[\begin{pmatrix} S_{1x} \\ 0 \\ 0 \end{pmatrix} + \begin{pmatrix} S_{2x} \\ 0 \\ 0 \end{pmatrix} \right]. \quad (\text{A.353})\end{aligned}$$

- $\Gamma^{\mathbf{k}_2,2}$ 8e

$$\begin{aligned}\psi_{1,1}^{\mathbf{k}_2,2} &= \frac{1}{4} \left[1 \cdot \begin{pmatrix} S_{1x} \\ S_{1y} \\ S_{1z} \end{pmatrix} + 1 \cdot \begin{pmatrix} S_{2'x} \\ -S_{2'y} \\ -S_{2'z} \end{pmatrix} + (-1) \cdot \begin{pmatrix} -S_{4x} \\ -S_{4y} \\ S_{4z} \end{pmatrix} + (-1) \cdot \begin{pmatrix} -S_{3'x} \\ S_{3'y} \\ -S_{3'z} \end{pmatrix} \right] \\ &= \frac{1}{4} \left[\begin{pmatrix} S_{1x} \\ S_{1y} \\ S_{1z} \end{pmatrix} + \begin{pmatrix} S_{2'x} \\ -S_{2'y} \\ -S_{2'z} \end{pmatrix} + \begin{pmatrix} S_{3'x} \\ -S_{3'y} \\ S_{3'z} \end{pmatrix} + \begin{pmatrix} S_{4x} \\ S_{4y} \\ -S_{4z} \end{pmatrix} \right] \quad (\text{A.354})\end{aligned}$$

- $\Gamma^{\mathbf{k}_2,3}$ 4a

$$\begin{aligned}
 \psi_{1,1}^{\mathbf{k}_2,3} &= \frac{1}{4} \left[1 \cdot \begin{pmatrix} S_{1x} \\ S_{1y} \\ S_{1z} \end{pmatrix} + (-1) \cdot \begin{pmatrix} S_{1x} \\ -S_{1y} \\ -S_{1z} \end{pmatrix} + 1 \cdot \begin{pmatrix} -S_{2x} \\ -S_{2y} \\ S_{2z} \end{pmatrix} + (-1) \cdot \begin{pmatrix} -S_{2x} \\ S_{2y} \\ -S_{2z} \end{pmatrix} \right] \\
 &= \frac{1}{2} \left[\begin{pmatrix} 0 \\ S_{1y} \\ S_{1z} \end{pmatrix} + \begin{pmatrix} 0 \\ -S_{2y} \\ S_{2z} \end{pmatrix} \right]. \tag{A.355}
 \end{aligned}$$

- $\Gamma^{\mathbf{k}_2,3}$ 8e

$$\begin{aligned}
 \psi_{1,1}^{\mathbf{k}_2,3} &= \frac{1}{4} \left[1 \cdot \begin{pmatrix} S_{1x} \\ S_{1y} \\ S_{1z} \end{pmatrix} + (-1) \cdot \begin{pmatrix} S_{2'x} \\ -S_{2'y} \\ -S_{2'z} \end{pmatrix} + 1 \cdot \begin{pmatrix} -S_{4x} \\ -S_{4y} \\ S_{4z} \end{pmatrix} + (-1) \cdot \begin{pmatrix} -S_{3'x} \\ S_{3'y} \\ -S_{3'z} \end{pmatrix} \right] \\
 &= \frac{1}{4} \left[\begin{pmatrix} S_{1x} \\ S_{1y} \\ S_{1z} \end{pmatrix} + \begin{pmatrix} -S_{2'x} \\ S_{2'y} \\ S_{2'z} \end{pmatrix} + \begin{pmatrix} S_{3'x} \\ -S_{3'y} \\ S_{3'z} \end{pmatrix} + \begin{pmatrix} -S_{4x} \\ -S_{4y} \\ S_{4z} \end{pmatrix} \right] \tag{A.356}
 \end{aligned}$$

- $\Gamma^{\mathbf{k}_2,4}$ 4a

$$\begin{aligned}
 \psi_{1,1}^{\mathbf{k}_2,4} &= \frac{1}{4} \left[1 \cdot \begin{pmatrix} S_{1x} \\ S_{1y} \\ S_{1z} \end{pmatrix} + (-1) \cdot \begin{pmatrix} S_{1x} \\ -S_{1y} \\ -S_{1z} \end{pmatrix} + (-1) \cdot \begin{pmatrix} -S_{2x} \\ -S_{2y} \\ S_{2z} \end{pmatrix} + 1 \cdot \begin{pmatrix} -S_{2x} \\ S_{2y} \\ -S_{2z} \end{pmatrix} \right] \\
 &= \frac{1}{2} \left[\begin{pmatrix} 0 \\ S_{1y} \\ S_{1z} \end{pmatrix} + \begin{pmatrix} 0 \\ S_{2y} \\ -S_{2z} \end{pmatrix} \right]. \tag{A.357}
 \end{aligned}$$

- $\Gamma^{\mathbf{k}_2,4}$ 8e

$$\begin{aligned}
 \psi_{1,1}^{\mathbf{k}_2,4} &= \frac{1}{4} \left[1 \cdot \begin{pmatrix} S_{1x} \\ S_{1y} \\ S_{1z} \end{pmatrix} + (-1) \cdot \begin{pmatrix} S_{2'x} \\ -S_{2'y} \\ -S_{2'z} \end{pmatrix} + (-1) \cdot \begin{pmatrix} -S_{4x} \\ -S_{4y} \\ S_{4z} \end{pmatrix} + 1 \cdot \begin{pmatrix} -S_{3'x} \\ S_{3'y} \\ -S_{3'z} \end{pmatrix} \right] \\
 &= \frac{1}{4} \left[\begin{pmatrix} S_{1x} \\ S_{1y} \\ S_{1z} \end{pmatrix} + \begin{pmatrix} -S_{2'x} \\ S_{2'y} \\ S_{2'z} \end{pmatrix} + \begin{pmatrix} -S_{3'x} \\ S_{3'y} \\ -S_{3'z} \end{pmatrix} + \begin{pmatrix} S_{4x} \\ S_{4y} \\ -S_{4z} \end{pmatrix} \right] \tag{A.358}
 \end{aligned}$$

3. $\mathbf{k}_3 = (0, k_{b^*}, 0)$

• $\Gamma^{\mathbf{k}_3,1}$ 4a

$$\begin{aligned}\psi_{1,1}^{\mathbf{k}_3,1} &= \frac{1}{4} \left[1 \cdot \begin{pmatrix} S_{1x} \\ S_{1y} \\ S_{1z} \end{pmatrix} + a \cdot \begin{pmatrix} -S_{2x} \\ S_{2y} \\ -S_{2z} \end{pmatrix} + (-a) \cdot \begin{pmatrix} -S_{2x} \\ -S_{2y} \\ S_{2z} \end{pmatrix} + (-1) \cdot \begin{pmatrix} S_{1x} \\ -S_{1y} \\ -S_{1z} \end{pmatrix} \right] \\ &= \frac{1}{2} \left[\begin{pmatrix} 0 \\ S_{1y} \\ S_{1z} \end{pmatrix} + \begin{pmatrix} 0 \\ aS_{2y} \\ -aS_{2z} \end{pmatrix} \right].\end{aligned}\tag{A.359}$$

• $\Gamma^{\mathbf{k}_3,1}$ o_1

$$\begin{aligned}\psi_{1,1}^{\mathbf{k}_3,1} &= \frac{1}{4} \left[1 \cdot \begin{pmatrix} S_{1x} \\ S_{1y} \\ S_{1z} \end{pmatrix} + a \cdot \begin{pmatrix} -S_{1^*x} \\ S_{1^*y} \\ -S_{1^*z} \end{pmatrix} + (-a) \cdot \begin{pmatrix} -S_{4x} \\ -S_{4y} \\ S_{4z} \end{pmatrix} + (-1) \cdot \begin{pmatrix} S_{4^*x} \\ -S_{4^*y} \\ -S_{4^*z} \end{pmatrix} \right] \\ &\equiv \frac{1}{4} \left[\begin{pmatrix} 0 \\ S_{1y} \\ 0 \end{pmatrix} + a \cdot \begin{pmatrix} 0 \\ S_{4y} \\ 0 \end{pmatrix} \right]\end{aligned}\tag{A.360}$$

• $\Gamma^{\mathbf{k}_3,1}$ o_2

$$\begin{aligned}\psi_{1,1}^{\mathbf{k}_3,1} &= \frac{1}{4} \left[1 \cdot \begin{pmatrix} S_{2x} \\ S_{2y} \\ S_{2z} \end{pmatrix} + a \cdot \begin{pmatrix} -S_{2^*x} \\ S_{2^*y} \\ -S_{2^*z} \end{pmatrix} + (-a) \cdot \begin{pmatrix} -S_{3x} \\ -S_{3y} \\ S_{3z} \end{pmatrix} + (-1) \cdot \begin{pmatrix} S_{3^*x} \\ -S_{3^*y} \\ -S_{3^*z} \end{pmatrix} \right] \\ &\equiv \frac{1}{4} \left[\begin{pmatrix} 0 \\ S_{2y} \\ 0 \end{pmatrix} + a \cdot \begin{pmatrix} 0 \\ S_{3y} \\ 0 \end{pmatrix} \right]\end{aligned}\tag{A.361}$$

• $\Gamma^{\mathbf{k}_3,2}$ 4a

$$\begin{aligned}\psi_{1,1}^{\mathbf{k}_3,2} &= \frac{1}{4} \left[1 \cdot \begin{pmatrix} S_{1x} \\ S_{1y} \\ S_{1z} \end{pmatrix} + a \cdot \begin{pmatrix} -S_{2x} \\ S_{2y} \\ -S_{2z} \end{pmatrix} + a \cdot \begin{pmatrix} -S_{2x} \\ -S_{2y} \\ S_{2z} \end{pmatrix} + 1 \cdot \begin{pmatrix} S_{1x} \\ -S_{1y} \\ -S_{1z} \end{pmatrix} \right] \\ &= \frac{1}{2} \left[\begin{pmatrix} S_{1x} \\ 0 \\ 0 \end{pmatrix} + a \cdot \begin{pmatrix} -S_{2x} \\ 0 \\ 0 \end{pmatrix} \right].\end{aligned}\tag{A.362}$$

- $\Gamma^{\mathbf{k}_3,2} o_1$

$$\begin{aligned}\psi_{1,1}^{\mathbf{k}_3,2} &= \frac{1}{4} \left[1 \cdot \begin{pmatrix} S_{1x} \\ S_{1y} \\ S_{1z} \end{pmatrix} + a \cdot \begin{pmatrix} -S_{1^*x} \\ S_{1^*y} \\ -S_{1^*z} \end{pmatrix} + a \cdot \begin{pmatrix} -S_{4x} \\ -S_{4y} \\ S_{4z} \end{pmatrix} + 1 \cdot \begin{pmatrix} S_{4^*x} \\ -S_{4^*y} \\ -S_{4^*z} \end{pmatrix} \right] \\ &\equiv \frac{1}{4} \left[\begin{pmatrix} 0 \\ S_{1y} \\ 0 \end{pmatrix} + a \cdot \begin{pmatrix} 0 \\ -S_{4y} \\ 0 \end{pmatrix} \right]\end{aligned}\quad (\text{A.363})$$

- $\Gamma^{\mathbf{k}_3,2} o_2$

$$\begin{aligned}\psi_{1,1}^{\mathbf{k}_3,2} &= \frac{1}{4} \left[1 \cdot \begin{pmatrix} S_{2x} \\ S_{2y} \\ S_{2z} \end{pmatrix} + a \cdot \begin{pmatrix} -S_{2^*x} \\ S_{2^*y} \\ -S_{2^*z} \end{pmatrix} + a \cdot \begin{pmatrix} -S_{3x} \\ -S_{3y} \\ S_{3z} \end{pmatrix} + 1 \cdot \begin{pmatrix} S_{3^*x} \\ -S_{3^*y} \\ -S_{3^*z} \end{pmatrix} \right] \\ &\equiv \frac{1}{4} \left[\begin{pmatrix} 0 \\ S_{2y} \\ 0 \end{pmatrix} + a \cdot \begin{pmatrix} 0 \\ -S_{3y} \\ 0 \end{pmatrix} \right]\end{aligned}\quad (\text{A.364})$$

- $\Gamma^{\mathbf{k}_3,3} 4a$

$$\begin{aligned}\psi_{1,1}^{\mathbf{k}_3,3} &= \frac{1}{4} \left[1 \cdot \begin{pmatrix} S_{1x} \\ S_{1y} \\ S_{1z} \end{pmatrix} + (-a) \cdot \begin{pmatrix} -S_{2x} \\ S_{2y} \\ -S_{2z} \end{pmatrix} + (-a) \cdot \begin{pmatrix} -S_{2x} \\ -S_{2y} \\ S_{2z} \end{pmatrix} + 1 \cdot \begin{pmatrix} S_{1x} \\ -S_{1y} \\ -S_{1z} \end{pmatrix} \right] \\ &= \frac{1}{2} \left[\begin{pmatrix} S_{1x} \\ 0 \\ 0 \end{pmatrix} + a \cdot \begin{pmatrix} S_{2x} \\ 0 \\ 0 \end{pmatrix} \right].\end{aligned}\quad (\text{A.365})$$

- $\Gamma^{\mathbf{k}_3,3} o_1$

$$\begin{aligned}\psi_{1,1}^{\mathbf{k}_3,3} &= \frac{1}{4} \left[1 \cdot \begin{pmatrix} S_{1x} \\ S_{1y} \\ S_{1z} \end{pmatrix} + (-a) \cdot \begin{pmatrix} -S_{1^*x} \\ S_{1^*y} \\ -S_{1^*z} \end{pmatrix} + (-a) \cdot \begin{pmatrix} -S_{4x} \\ -S_{4y} \\ S_{4z} \end{pmatrix} + 1 \cdot \begin{pmatrix} S_{4^*x} \\ -S_{4^*y} \\ -S_{4^*z} \end{pmatrix} \right] \\ &\equiv \frac{1}{4} \left[\begin{pmatrix} S_{1x} \\ 0 \\ S_{1z} \end{pmatrix} + a \cdot \begin{pmatrix} S_{4x} \\ 0 \\ -S_{4z} \end{pmatrix} \right]\end{aligned}\quad (\text{A.366})$$

- $\Gamma^{\mathbf{k}_3,3} o_2$

$$\begin{aligned}\psi_{1,1}^{\mathbf{k}_3,3} &= \frac{1}{4} \left[1 \cdot \begin{pmatrix} S_{2x} \\ S_{2y} \\ S_{2z} \end{pmatrix} + (-a) \cdot \begin{pmatrix} -S_{2^*x} \\ S_{2^*y} \\ -S_{2^*z} \end{pmatrix} + (-a) \cdot \begin{pmatrix} -S_{3x} \\ -S_{3y} \\ S_{3z} \end{pmatrix} + 1 \cdot \begin{pmatrix} S_{3^*x} \\ -S_{3^*y} \\ -S_{3^*z} \end{pmatrix} \right] \\ &\equiv \frac{1}{4} \left[\begin{pmatrix} S_{2x} \\ 0 \\ S_{2z} \end{pmatrix} + a \cdot \begin{pmatrix} S_{3x} \\ 0 \\ -S_{3z} \end{pmatrix} \right]\end{aligned}\quad (\text{A.367})$$

- $\Gamma^{\mathbf{k}_3,4} 4a$

$$\begin{aligned}\psi_{1,1}^{\mathbf{k}_3,4} &= \frac{1}{4} \left[1 \cdot \begin{pmatrix} S_{1x} \\ S_{1y} \\ S_{1z} \end{pmatrix} + (-a) \cdot \begin{pmatrix} -S_{2x} \\ S_{2y} \\ -S_{2z} \end{pmatrix} + a \cdot \begin{pmatrix} -S_{2x} \\ -S_{2y} \\ S_{2z} \end{pmatrix} + (-1) \cdot \begin{pmatrix} S_{1x} \\ -S_{1y} \\ -S_{1z} \end{pmatrix} \right] \\ &= \frac{1}{2} \left[\begin{pmatrix} 0 \\ S_{1y} \\ S_{1z} \end{pmatrix} + a \cdot \begin{pmatrix} 0 \\ -S_{2y} \\ S_{2z} \end{pmatrix} \right].\end{aligned}\quad (\text{A.368})$$

- $\Gamma^{\mathbf{k}_3,4} o_1$

$$\begin{aligned}\psi_{1,1}^{\mathbf{k}_3,4} &= \frac{1}{4} \left[1 \cdot \begin{pmatrix} S_{1x} \\ S_{1y} \\ S_{1z} \end{pmatrix} + (-a) \cdot \begin{pmatrix} -S_{1^*x} \\ S_{1^*y} \\ -S_{1^*z} \end{pmatrix} + a \cdot \begin{pmatrix} -S_{4x} \\ -S_{4y} \\ S_{4z} \end{pmatrix} + (-1) \cdot \begin{pmatrix} S_{4^*x} \\ -S_{4^*y} \\ -S_{4^*z} \end{pmatrix} \right] \\ &\equiv \frac{1}{4} \left[\begin{pmatrix} S_{1x} \\ 0 \\ S_{1z} \end{pmatrix} + a \cdot \begin{pmatrix} -S_{4x} \\ 0 \\ S_{4z} \end{pmatrix} \right]\end{aligned}\quad (\text{A.369})$$

- $\Gamma^{\mathbf{k}_3,4} o_2$

$$\begin{aligned}\psi_{1,1}^{\mathbf{k}_3,4} &= \frac{1}{4} \left[1 \cdot \begin{pmatrix} S_{2x} \\ S_{2y} \\ S_{2z} \end{pmatrix} + (-a) \cdot \begin{pmatrix} -S_{2^*x} \\ S_{2^*y} \\ -S_{2^*z} \end{pmatrix} + a \cdot \begin{pmatrix} -S_{3x} \\ -S_{3y} \\ S_{3z} \end{pmatrix} + (-1) \cdot \begin{pmatrix} S_{3^*x} \\ -S_{3^*y} \\ -S_{3^*z} \end{pmatrix} \right] \\ &\equiv \frac{1}{4} \left[\begin{pmatrix} S_{2x} \\ 0 \\ S_{2z} \end{pmatrix} + a \cdot \begin{pmatrix} -S_{3x} \\ 0 \\ S_{3z} \end{pmatrix} \right]\end{aligned}\quad (\text{A.370})$$

B. Ab initio calculations

B.1. Orbital exponents and contraction parameters

```
COBALT
S      6
  1      65902.2082570      0.14284614936E-02
  2      9895.3896027      0.10946072783E-01
  3      2251.4305789      0.54285953890E-01
  4      635.61097084      0.18885179079
  5      206.78820681      0.38301634994
  6      71.179242971      0.29443551266
S      3
  1      137.77268040      -0.10990221736
  2      16.118079243      0.64455537395
  3      6.6030327710      0.45116787924
S      3
  1      11.479915788      -0.22593846910
  2      1.8956426324      0.72231409008
  3      0.78466232067      0.44903812296
S      1
  1      0.98425774432E-01      1.0000000000
S      1
  1      0.35945741932E-01      1.0000000000
P      5
  1      843.64358575      0.93866097254E-02
  2      198.76386994      0.69880208716E-01
  3      62.854963098      0.27037070345
  4      22.562842280      0.52904786880
  5      8.3713209127      0.34357029579
P      3
  1      4.2858719800      0.34027999036
  2      1.6508041817      0.56693392384
```

B. *Ab initio* calculations

3		0.61834231096	0.23617979783
D	4		
1		42.927867612	0.28487788365E-01
2		11.942533053	0.15206951283
3		4.0046495664	0.37310913999
4		1.3413193804	0.47549837676
D	1		
1		0.40015009743	0.31346831424
P	1		
1		0.1413080	1.0000000
OXYGEN			
S	5		
1		2266.1767785	-0.53431809926E-02
2		340.87010191	-0.39890039230E-01
3		77.363135167	-0.17853911985
4		21.479644940	-0.46427684959
5		6.6589433124	-0.44309745172
S	1		
1		0.80975975668	1.0000000000
S	1		
1		0.25530772234	1.0000000000
P	3		
1		17.721504317	0.43394573193E-01
2		3.8635505440	0.23094120765
3		1.0480920883	0.51375311064
P	1		
1		0.27641544411	1.0000000000
D	1		
1		1.2000000	1.0000000

B.2. Calculation output

The output of the *ab initio* calculations of the respective clusters yield the energy levels and AO coefficients for all MOs. The only ones which are of interest are those corresponding to the Co3d levels and are enumerated from 40 to 44. Note that due to the fact that the basal oxygen ions are not situated on the principal axes, the notation for the $d_{x^2-y^2}$ and

d_{xy} orbitals are swapped.

B.2.1. Co_cO₆ cluster

				40	41	42	43	44
				-0.0841	-0.0839	-0.0708	-0.0249	-0.0186
				A	A	A	A	A
1	CO	1	S	0.000000	-0.001202	-0.001543	0.000000	0.000670
2	CO	1	S	0.000000	0.003502	0.004640	0.000000	-0.002024
3	CO	1	S	0.000000	-0.015930	-0.019763	0.000000	0.008595
4	CO	1	S	0.000000	0.029985	0.022824	0.000000	-0.010252
5	CO	1	S	0.000000	-0.005206	0.031640	0.000000	0.014739
6	CO	1	X	0.000000	0.000000	0.000000	0.000000	0.000000
7	CO	1	Y	0.000000	0.000000	0.000000	0.000000	0.000000
8	CO	1	Z	0.000000	0.000000	0.000000	0.000000	0.000000
9	CO	1	X	0.000000	0.000000	0.000000	0.000000	0.000000
10	CO	1	Y	0.000000	0.000000	0.000000	0.000000	0.000000
11	CO	1	Z	0.000000	0.000000	0.000000	0.000000	0.000000
12	CO	1	XX	0.000000	-0.446416	-0.410215	0.000000	-0.558921
13	CO	1	YY	0.000000	0.634797	0.447145	0.000000	-0.253285
14	CO	1	ZZ	0.000000	-0.188381	-0.036930	0.000000	0.812206
15	CO	1	XY	0.187740	0.000000	0.000000	0.811189	0.000000
16	CO	1	XZ	0.782321	0.000000	0.000000	-0.193384	0.000000
17	CO	1	YZ	0.000000	-0.474882	0.665148	0.000000	-0.086530
18	CO	1	XX	0.000000	-0.187813	-0.157990	0.000000	-0.212289
19	CO	1	YY	0.000000	0.261747	0.170377	0.000000	-0.095866
20	CO	1	ZZ	0.000000	-0.073934	-0.012386	0.000000	0.308155
21	CO	1	XY	0.074985	0.000000	0.000000	0.302748	0.000000
22	CO	1	XZ	0.333625	0.000000	0.000000	-0.074428	0.000000
23	CO	1	YZ	0.000000	-0.201296	0.259832	0.000000	-0.032902
24	CO	1	X	0.000000	0.000000	0.000000	0.000000	0.000000
25	CO	1	Y	0.000000	0.000000	0.000000	0.000000	0.000000
26	CO	1	Z	0.000000	0.000000	0.000000	0.000000	0.000000
27	O	6	S	0.000000	0.010356	-0.004846	0.000000	-0.030205
28	O	6	S	0.000000	0.028272	-0.012953	0.000000	-0.075858
29	O	6	S	0.000000	0.002361	-0.007466	0.000000	-0.035948
30	O	6	X	-0.085818	0.000000	0.000000	0.012209	0.000000

B. Ab initio calculations

31	0	6	Y	0.000000	0.033748	-0.041375	0.000000	0.021131
32	0	6	Z	0.000000	-0.022855	-0.007770	0.000000	0.103307
33	0	6	X	-0.069239	0.000000	0.000000	0.010512	0.000000
34	0	6	Y	0.000000	0.033462	-0.038286	0.000000	0.003621
35	0	6	Z	0.000000	-0.032234	0.000078	0.000000	0.129385
36	0	6	XX	0.000000	0.001134	-0.001429	0.000000	-0.003282
37	0	6	YY	0.000000	0.000149	0.002261	0.000000	-0.004046
38	0	6	ZZ	0.000000	-0.001284	-0.000833	0.000000	0.007328
39	0	6	XY	0.002352	0.000000	0.000000	0.000065	0.000000
40	0	6	XZ	-0.007180	0.000000	0.000000	0.001360	0.000000
41	0	6	YZ	0.000000	0.005359	-0.005163	0.000000	-0.002428
42	0	5	S	0.000000	0.010356	-0.004846	0.000000	-0.030205
43	0	5	S	0.000000	0.028272	-0.012953	0.000000	-0.075858
44	0	5	S	0.000000	0.002361	-0.007466	0.000000	-0.035948
45	0	5	X	0.085818	0.000000	0.000000	-0.012209	0.000000
46	0	5	Y	0.000000	-0.033748	0.041375	0.000000	-0.021131
47	0	5	Z	0.000000	0.022855	0.007770	0.000000	-0.103307
48	0	5	X	0.069239	0.000000	0.000000	-0.010512	0.000000
49	0	5	Y	0.000000	-0.033462	0.038286	0.000000	-0.003621
50	0	5	Z	0.000000	0.032234	-0.000078	0.000000	-0.129385
51	0	5	XX	0.000000	0.001134	-0.001429	0.000000	-0.003282
52	0	5	YY	0.000000	0.000149	0.002261	0.000000	-0.004046
53	0	5	ZZ	0.000000	-0.001284	-0.000833	0.000000	0.007328
54	0	5	XY	0.002352	0.000000	0.000000	0.000065	0.000000
55	0	5	XZ	-0.007180	0.000000	0.000000	0.001360	0.000000
56	0	5	YZ	0.000000	0.005359	-0.005163	0.000000	-0.002428
57	0	1	S	-0.009909	-0.005577	-0.004033	-0.024040	0.014589
58	0	1	S	-0.026101	-0.015635	-0.010565	-0.060037	0.036353
59	0	1	S	-0.005015	-0.001939	-0.006890	-0.023712	0.013828
60	0	1	X	0.011522	0.042932	0.009015	0.068525	-0.037102
61	0	1	Y	0.025065	-0.044311	-0.028404	0.058142	-0.043756
62	0	1	Z	-0.046446	0.037200	-0.022498	0.015846	-0.000711
63	0	1	X	0.019469	0.039741	0.010816	0.081394	-0.046210
64	0	1	Y	0.024294	-0.034741	-0.022386	0.060365	-0.044751
65	0	1	Z	-0.040873	0.028286	-0.019947	0.006582	0.003145
66	0	1	XX	0.000831	0.005453	0.002047	0.005716	-0.002601
67	0	1	YY	-0.001533	-0.002737	-0.002314	-0.002043	0.000555
68	0	1	ZZ	0.000702	-0.002716	0.000267	-0.003673	0.002047

69	0	1	XY	0.001593	-0.003013	-0.001967	0.004399	-0.003328
70	0	1	XZ	-0.005087	0.001694	-0.003378	-0.001113	0.001490
71	0	1	YZ	-0.002838	0.001785	-0.000014	-0.001395	0.001501
72	0	2	S	0.009909	-0.005577	-0.004033	0.024040	0.014589
73	0	2	S	0.026101	-0.015635	-0.010565	0.060037	0.036353
74	0	2	S	0.005015	-0.001939	-0.006890	0.023712	0.013828
75	0	2	X	-0.011522	0.042932	0.009015	-0.068525	-0.037102
76	0	2	Y	0.025065	0.044311	0.028404	0.058142	0.043756
77	0	2	Z	-0.046446	-0.037200	0.022498	0.015846	0.000711
78	0	2	X	-0.019469	0.039741	0.010816	-0.081394	-0.046210
79	0	2	Y	0.024294	0.034741	0.022386	0.060365	0.044751
80	0	2	Z	-0.040873	-0.028286	0.019947	0.006582	-0.003145
81	0	2	XX	-0.000831	0.005453	0.002047	-0.005716	-0.002601
82	0	2	YY	0.001533	-0.002737	-0.002314	0.002043	0.000555
83	0	2	ZZ	-0.000702	-0.002716	0.000267	0.003673	0.002047
84	0	2	XY	0.001593	0.003012	0.001967	0.004399	0.003328
85	0	2	XZ	-0.005087	-0.001694	0.003378	-0.001113	-0.001490
86	0	2	YZ	0.002838	0.001785	-0.000014	0.001395	0.001501
87	0	3	S	-0.009909	-0.005577	-0.004033	-0.024040	0.014589
88	0	3	S	-0.026101	-0.015635	-0.010565	-0.060037	0.036353
89	0	3	S	-0.005015	-0.001939	-0.006890	-0.023712	0.013828
90	0	3	X	-0.011522	-0.042932	-0.009015	-0.068525	0.037102
91	0	3	Y	-0.025065	0.044311	0.028404	-0.058142	0.043756
92	0	3	Z	0.046446	-0.037200	0.022498	-0.015846	0.000711
93	0	3	X	-0.019469	-0.039741	-0.010816	-0.081394	0.046210
94	0	3	Y	-0.024294	0.034741	0.022386	-0.060365	0.044751
95	0	3	Z	0.040873	-0.028286	0.019947	-0.006582	-0.003145
96	0	3	XX	0.000831	0.005453	0.002047	0.005716	-0.002601
97	0	3	YY	-0.001533	-0.002737	-0.002314	-0.002043	0.000555
98	0	3	ZZ	0.000702	-0.002716	0.000267	-0.003673	0.002047
99	0	3	XY	0.001593	-0.003013	-0.001967	0.004399	-0.003328
100	0	3	XZ	-0.005087	0.001694	-0.003378	-0.001113	0.001490
101	0	3	YZ	-0.002838	0.001785	-0.000014	-0.001395	0.001501
102	0	4	S	0.009909	-0.005577	-0.004033	0.024040	0.014589
103	0	4	S	0.026101	-0.015635	-0.010565	0.060037	0.036353
104	0	4	S	0.005015	-0.001939	-0.006890	0.023712	0.013828
105	0	4	X	0.011522	-0.042932	-0.009015	0.068525	0.037102
106	0	4	Y	-0.025065	-0.044311	-0.028404	-0.058142	-0.043756

B. *Ab initio* calculations

107	0	4	Z	0.046446	0.037200	-0.022498	-0.015846	-0.000711
108	0	4	X	0.019469	-0.039741	-0.010816	0.081394	0.046210
109	0	4	Y	-0.024294	-0.034741	-0.022386	-0.060365	-0.044751
110	0	4	Z	0.040873	0.028286	-0.019947	-0.006582	0.003145
111	0	4	XX	-0.000831	0.005453	0.002047	-0.005716	-0.002601
112	0	4	YY	0.001533	-0.002737	-0.002314	0.002043	0.000555
113	0	4	ZZ	-0.000702	-0.002716	0.000267	0.003673	0.002047
114	0	4	XY	0.001593	0.003012	0.001967	0.004399	0.003328
115	0	4	XZ	-0.005087	-0.001694	0.003378	-0.001113	-0.001490
116	0	4	YZ	0.002838	0.001785	-0.000014	0.001395	0.001501

B.2.2. Co_sO_6 cluster

				40	41	42	43	44
				-0.1048	-0.1016	-0.0908	-0.0451	-0.0400
				A	A	A	A	A
1	CO	2	S	0.000272	0.000000	-0.000039	-0.000112	0.000000
2	CO	2	S	-0.000731	0.000000	0.000346	0.000390	0.000000
3	CO	2	S	0.003880	0.000000	0.000440	-0.001230	0.000000
4	CO	2	S	-0.015267	0.000000	-0.017105	-0.001852	0.000000
5	CO	2	S	0.011406	0.000000	0.023079	-0.001440	0.000000
6	CO	2	X	0.000000	-0.002941	0.000000	0.000000	-0.001396
7	CO	2	Y	-0.001889	0.000000	-0.002439	0.000976	0.000000
8	CO	2	Z	0.000000	0.002594	0.000000	0.000000	-0.002539
9	CO	2	X	0.000000	0.009239	0.000000	0.000000	0.004371
10	CO	2	Y	0.005968	0.000000	0.007573	-0.003090	0.000000
11	CO	2	Z	0.000000	-0.008015	0.000000	0.000000	0.008132
12	CO	2	XX	0.723807	0.000000	0.254039	-0.264299	0.000000
13	CO	2	YY	-0.510175	0.000000	-0.358546	-0.534023	0.000000
14	CO	2	ZZ	-0.213632	0.000000	0.104508	0.798323	0.000000
15	CO	2	XY	0.000000	0.080192	0.000000	0.000000	0.830146
16	CO	2	XZ	-0.309196	0.000000	0.744489	-0.184840	0.000000
17	CO	2	YZ	0.000000	0.799100	0.000000	0.000000	-0.083985
18	CO	2	XX	0.305090	0.000000	0.099357	-0.096866	0.000000
19	CO	2	YY	-0.221375	0.000000	-0.138094	-0.203145	0.000000
20	CO	2	ZZ	-0.083715	0.000000	0.038737	0.300010	0.000000
21	CO	2	XY	0.000000	0.031715	0.000000	0.000000	0.315148

22	CO	2	XZ	-0.132497	0.000000	0.286345	-0.070200	0.000000
23	CO	2	YZ	0.000000	0.336276	0.000000	0.000000	-0.034257
24	CO	2	X	0.000000	-0.017696	0.000000	0.000000	0.006733
25	CO	2	Y	-0.019323	0.000000	-0.016902	-0.002695	0.000000
26	CO	2	Z	0.000000	0.015531	0.000000	0.000000	-0.027039
27	O	7	S	-0.010442	0.004032	-0.002069	0.014753	0.027566
28	O	7	S	-0.029257	0.009966	-0.005405	0.037008	0.070101
29	O	7	S	0.000959	0.003484	-0.000837	0.018103	0.030168
30	O	7	X	0.034368	0.033033	0.012573	0.046398	0.069628
31	O	7	Y	0.044668	-0.024279	0.029005	-0.022327	-0.044763
32	O	7	Z	-0.017993	-0.054331	0.043716	0.000640	0.013725
33	O	7	X	0.023815	0.032248	0.010261	0.051495	0.081432
34	O	7	Y	0.045522	-0.024284	0.025518	-0.037029	-0.071726
35	O	7	Z	-0.017812	-0.042720	0.033658	0.005463	0.022636
36	O	7	XX	-0.006161	-0.001587	-0.001761	-0.000893	0.000529
37	O	7	YY	0.006629	-0.001732	0.004375	-0.000860	-0.002363
38	O	7	ZZ	-0.000468	0.003319	-0.002614	0.001753	0.001834
39	O	7	XY	-0.000004	0.002372	-0.000412	0.003566	0.006461
40	O	7	XZ	0.000147	0.002110	-0.002288	-0.001603	-0.003221
41	O	7	YZ	-0.004595	-0.003674	0.003277	0.000537	0.002817
42	O	8	S	-0.010442	-0.004032	-0.002069	0.014753	-0.027566
43	O	8	S	-0.029257	-0.009966	-0.005405	0.037008	-0.070101
44	O	8	S	0.000959	-0.003484	-0.000837	0.018103	-0.030168
45	O	8	X	-0.034368	0.033033	-0.012573	-0.046398	0.069628
46	O	8	Y	0.044668	0.024279	0.029005	-0.022327	0.044763
47	O	8	Z	0.017993	-0.054331	-0.043716	-0.000640	0.013725
48	O	8	X	-0.023815	0.032248	-0.010261	-0.051495	0.081432
49	O	8	Y	0.045522	0.024284	0.025518	-0.037029	0.071726
50	O	8	Z	0.017812	-0.042720	-0.033658	-0.005463	0.022636
51	O	8	XX	-0.006161	0.001587	-0.001761	-0.000893	-0.000529
52	O	8	YY	0.006629	0.001732	0.004375	-0.000860	0.002363
53	O	8	ZZ	-0.000468	-0.003319	-0.002614	0.001753	-0.001834
54	O	8	XY	0.000004	0.002372	0.000412	-0.003566	0.006461
55	O	8	XZ	0.000147	-0.002110	-0.002288	-0.001603	0.003221
56	O	8	YZ	0.004595	-0.003674	-0.003277	-0.000537	0.002817
57	O	9	S	-0.005283	0.007690	-0.002138	0.013165	0.023125
58	O	9	S	-0.012889	0.020645	-0.005885	0.032852	0.057946
59	O	9	S	-0.007573	0.004982	-0.003273	0.012957	0.021555

B. *Ab initio* calculations

60	0	9	X	-0.036299	-0.020990	-0.020529	-0.050474	-0.072016
61	0	9	Y	-0.061723	0.005899	-0.004070	0.029384	0.065161
62	0	9	Z	0.039366	0.041042	-0.029375	-0.000898	-0.014257
63	0	9	X	-0.023966	-0.021699	-0.015204	-0.049345	-0.073809
64	0	9	Y	-0.056100	0.014701	-0.005893	0.037317	0.075745
65	0	9	Z	0.028604	0.034803	-0.025313	0.002998	-0.002651
66	0	9	XX	-0.003795	0.000680	-0.002067	-0.000756	0.000233
67	0	9	YY	0.005613	-0.000208	0.001303	-0.000787	-0.003147
68	0	9	ZZ	-0.001817	-0.000473	0.000763	0.001544	0.002914
69	0	9	XY	0.000374	0.000975	0.000512	0.002791	0.004731
70	0	9	XZ	0.001414	0.002771	-0.000925	0.001401	0.001456
71	0	9	YZ	-0.000234	-0.003246	0.003125	-0.001003	-0.001073
72	0	6	S	-0.005283	-0.007690	-0.002138	0.013165	-0.023125
73	0	6	S	-0.012889	-0.020645	-0.005885	0.032852	-0.057946
74	0	6	S	-0.007573	-0.004982	-0.003273	0.012957	-0.021555
75	0	6	X	0.036299	-0.020990	0.020529	0.050474	-0.072016
76	0	6	Y	-0.061723	-0.005899	-0.004070	0.029384	-0.065161
77	0	6	Z	-0.039366	0.041042	0.029375	0.000898	-0.014257
78	0	6	X	0.023966	-0.021699	0.015204	0.049345	-0.073809
79	0	6	Y	-0.056100	-0.014701	-0.005893	0.037317	-0.075745
80	0	6	Z	-0.028604	0.034803	0.025313	-0.002998	-0.002651
81	0	6	XX	-0.003795	-0.000680	-0.002067	-0.000756	-0.000233
82	0	6	YY	0.005613	0.000208	0.001303	-0.000787	0.003147
83	0	6	ZZ	-0.001817	0.000473	0.000763	0.001544	-0.002914
84	0	6	XY	-0.000374	0.000975	-0.000512	-0.002791	0.004731
85	0	6	XZ	0.001414	-0.002771	-0.000925	0.001401	-0.001456
86	0	6	YZ	0.000234	-0.003246	-0.003125	0.001003	-0.001073
87	0	10	S	0.011590	0.004184	-0.004681	-0.028931	0.001121
88	0	10	S	0.030499	0.011248	-0.012854	-0.072593	0.001460
89	0	10	S	0.005920	-0.000906	-0.002018	-0.028504	0.009182
90	0	10	X	0.026158	-0.000907	-0.041146	0.010272	0.002375
91	0	10	Y	0.002084	-0.086093	-0.000369	-0.019246	0.009178
92	0	10	Z	-0.029469	-0.025145	-0.010509	0.102197	0.000874
93	0	10	X	0.026450	0.001252	-0.036474	-0.004138	0.002832
94	0	10	Y	0.005015	-0.068989	0.000526	-0.017159	0.008114
95	0	10	Z	-0.037538	-0.024120	-0.005997	0.121023	-0.006096
96	0	10	XX	-0.000248	0.000566	0.003126	-0.003886	-0.000220
97	0	10	YY	0.001301	0.001766	-0.001490	-0.003107	-0.000137

98	0	10	ZZ	-0.001053	-0.002332	-0.001636	0.006993	0.000357
99	0	10	XY	-0.000632	0.003820	0.000585	0.001074	-0.000228
100	0	10	XZ	0.004839	0.001709	-0.004587	-0.004457	0.000322
101	0	10	YZ	-0.000034	-0.006465	-0.000006	-0.001793	0.000929
102	0	1	S	0.011590	-0.004184	-0.004681	-0.028931	-0.001121
103	0	1	S	0.030499	-0.011248	-0.012854	-0.072593	-0.001460
104	0	1	S	0.005920	0.000906	-0.002018	-0.028504	-0.009182
105	0	1	X	-0.026158	-0.000907	0.041146	-0.010272	0.002375
106	0	1	Y	0.002084	0.086093	-0.000369	-0.019246	-0.009178
107	0	1	Z	0.029469	-0.025145	0.010509	-0.102197	0.000874
108	0	1	X	-0.026450	0.001252	0.036474	0.004138	0.002832
109	0	1	Y	0.005015	0.068989	0.000526	-0.017159	-0.008114
110	0	1	Z	0.037538	-0.024120	0.005997	-0.121023	-0.006096
111	0	1	XX	-0.000248	-0.000566	0.003126	-0.003886	0.000220
112	0	1	YY	0.001301	-0.001766	-0.001490	-0.003107	0.000137
113	0	1	ZZ	-0.001053	0.002332	-0.001636	0.006993	-0.000357
114	0	1	XY	0.000632	0.003820	-0.000585	-0.001074	-0.000228
115	0	1	XZ	0.004839	-0.001709	-0.004587	-0.004457	-0.000322
116	0	1	YZ	0.000034	-0.006465	0.000006	0.001793	0.000929

Bibliography

- [1] H. FUESS, E. F. BERTAUT, R. PAUTHENET AND A. DURIF. Structure aux rayons X, neutrons et propriétés magnétiques des orthovanadates de nickel et de cobalt. *Acta Crystallogr., Sect. B: Struct. Sci* **26** 2036 (1970).
- [2] E. E. SAUERBREI, R. FAGGIANI AND C. CALVO. Refinement of the Crystal Structures of $\text{Co}_3\text{V}_2\text{O}_8$ and $\text{Ni}_3\text{V}_2\text{O}_8$. *Acta Crystallogr., Sect. B: Struct. Crystallogr. Cryst. Chem.* **29** 2304 (1973).
- [3] I. SYÔZI. Statistics of Kagomé Lattice. *Progr. Theoret. Phys.* **6** 306 (1951).
- [4] S. SACHDEV. Kagomé- and triangular-lattice Heisenberg antiferromagnets: Ordering from quantum fluctuations and quantum-disordered ground states with unconfined bosonic spinons. *Phys. Rev. B* **45** 12377 (1992).
- [5] P. SINDZINGRE, G. MISGUICH, C. LHUILLIER, B. BERNU, L. PIERRE, C. WALDTMANN AND H.-U. EVERTS. Magnetothermodynamics of the Spin- $\frac{1}{2}$ Kagomé Antiferromagnet. *Phys. Rev. Lett.* **84** 2953 (2000).
- [6] Y. CHEN, J. W. LYNN, Q. HUANG, F. M. WOODWARD, T. YILDIRIM, G. LAWES, A. P. RAMIREZ, N. ROGADO, R. J. CAVA, A. AHARONY, O. ENTIN-WOHLMAN AND A. B. HARRIS. Complex magnetic order in the kagomé staircase compound $\text{Co}_3\text{V}_2\text{O}_8$. *Phys. Rev. B* **74** 014430 (2006).
- [7] H. FUESS, R. MÜLLER, D. SCHWABE AND F. TASSET. Form factor measurement in ferromagnetic cobalt orthovanadate. *J. Phys. Col.* **C7** 253 (1982).
- [8] N. ROGADO, G. LAWES, D. A. HUSE, A. P. RAMIREZ AND R. J. CAVA. The Kagomé-staircase lattice: magnetic ordering in $\text{Ni}_3\text{V}_2\text{O}_8$ and $\text{Co}_3\text{V}_2\text{O}_8$. *Solid State Commun.* **124** 229 (2002).
- [9] N. ROGADO, M. K. HAAS, G. LAWES, D. A. HUSE, A. P. RAMIREZ AND R. J. CAVA. $\beta\text{-Cu}_3\text{V}_2\text{O}_8$: magnetic ordering in a spin- $\frac{1}{2}$ Kagomé-staircase lattice. *J. Phys.: Condens. Matter* **15** 907 (2003).

- [10] G. BALAKRISHNAN, O. A. PETRENKO, M. R. LEES AND D. M. K. PAUL. Single crystals of the anisotropic Kagomé staircase compounds $\text{Ni}_3\text{V}_2\text{O}_8$ and $\text{Co}_3\text{V}_2\text{O}_8$. *J. Phys.: Condens. Matter* **16** L347 (2004).
- [11] N. QURESHI. Magnetische Phasenübergänge und Strukturen der Orthooxovanadate $(\text{Co}_x\text{Ni}_{1-x})_3\text{V}_2\text{O}_8$. Master's thesis, University of Technology Darmstadt (2005).
- [12] R. SZYMCAK, M. BARAN, R. DIDUSZKO, J. FINK-FINOWICKI, M. GUTOWSKA, A. SZEWCZYK AND H. SZYMCAK. Magnetic field-induced transitions in geometrically frustrated $\text{Co}_3\text{V}_2\text{O}_8$ single crystal. *Phys. Rev. B* **73** 094425 (2006).
- [13] N. QURESHI, H. FUESS, H. EHRENBERG, T. C. HANSEN AND D. SCHWABE. Magnetic phase transitions and structures of $\text{Co}_3\text{V}_2\text{O}_8$. *Solid State Commun.* **142** 169 (2007).
- [14] Y. KOBAYASHI, Y. YASUI AND M. SATO. Magnetic and thermal properties of $\text{Co}_3\text{V}_2\text{O}_8$ and $\text{Ni}_3\text{V}_2\text{O}_8$. *J. Magn. Magn. Mater.* **310** 1160 (2007).
- [15] G. LAWES, M. KENZELMANN, N. ROGADO, K. H. KIM, G. A. JORGE, R. CAVA, A. A. AHARONY, O. ENTIN-WOHLMANN, A. B. HARRIS, T. YILDIRIM, Q. Z. HUANG, S. PARK, C. BROHOLM AND A. P. RAMIREZ. Competing Magnetic Phases on a Kagomé staircase. *Phys. Rev. Lett.* **93** 247201 (2004).
- [16] N. R. WILSON, O. A. PETRENKO AND G. BALAKRISHNAN. Magnetic phase diagrams of the Kagomé staircase compounds $\text{Co}_3\text{V}_2\text{O}_8$. *J. Phys.: Condens. Matter* **19** 145257 (2007).
- [17] E. MOROSAN, J. FLEITMAN, T. KLIMCZUK AND R. J. CAVA. Rich magnetic phase diagram of the kagome-staircase compound $\text{Mn}_3\text{V}_2\text{O}_8$. *Phys. Rev. B* **76** 144403 (2007).
- [18] N. R. WILSON, O. A. PETRENKO AND L. C. CHAPON. Magnetic phases in the Kagomé staircase compound $\text{Co}_3\text{V}_2\text{O}_8$ studied using powder neutron diffraction. *Phys. Rev. B* **75** 094432 (2007).
- [19] M. KENZELMANN, A. B. HARRIS, A. AHARONY, O. ENTIN-WOHLMAN, T. YILDIRIM, Q. HUANG, S. PARK, G. LAWES, C. BROHOLM, N. ROGADO, R. J. CAVA, K. H. KIM, G. JORGE AND A. P. RAMIREZ. Field dependence of magnetic ordering in Kagomé-staircase compound $\text{Ni}_3\text{V}_2\text{O}_8$. *Phys. Rev. B* **74** 014429 (2006).
- [20] T. LANCASTER, S. J. BLUNDELL, P. J. BAKER, D. PRABHAKARAN, W. HAYES AND F. L. PRATT. Kagome staircase compounds $\text{Ni}_3\text{V}_2\text{O}_8$ and $\text{Co}_3\text{V}_2\text{O}_8$ studied with implanted muons. *Phys. Rev. B* **75** 064427 (2007).

-
- [21] N. R. WILSON, O. A. PETRENKO, G. BALAKRISHNAN, P. MANUEL AND B. FAK. Magnetic excitations in the Kagomé staircase compounds. *J. Magn. Magn. Mater.* **310** 1334 (2007).
- [22] G. LAWES, A. B. HARRIS, T. KIMURA, N. ROGADO, R. J. CAVA, A. AHARONY, O. ENTIN-WOHLMAN, T. YILDIRIM, M. KENZELMANN, C. BROHOLM AND A. P. RAMIREZ. Magnetically Driven Ferroelectric Order in $\text{Ni}_3\text{V}_2\text{O}_8$. *Phys. Rev. Lett.* **95** 087205 (2005).
- [23] A. B. HARRIS, T. YILDIRIM, A. AHARONY AND O. ENTIN-WOHLMAN. Ferroelectricity induced by incommensurate magnetism. *Phys. Rev. B* **73** 184433 (2006).
- [24] R. C. RAI, J. CAO, S. BROWN, J. L. MUSFELDT, D. KASINATHAN, D. J. SINGH, G. LAWES, N. ROGADO, R. J. CAVA AND X. WEI. Optical properties and magnetic-field-induced phase transitions in the ferroelectric state of $\text{Ni}_3\text{V}_2\text{O}_8$: Experiments and first-principles calculations. *Phys. Rev. B* **76** 174414 (2007).
- [25] R. P. CHAUDHURY, F. YEN, C. R. DELA CRUZ, B. LORENZ, Y. Q. WANG, Y. Y. SUN AND C. W. CHU. Pressure-temperature phase diagram of multiferroic $\text{Ni}_3\text{V}_2\text{O}_8$. *Phys. Rev. B* **75** 012407 (2007).
- [26] B. ROESSLI AND P. BÖNI. Polarized Neutron Scattering. *In* Scattering and Inverse Scattering in Pure and Applied Science (Academic Press, New York, 2002).
- [27] P. J. BROWN. Polarized Neutron Diffraction. *Sci. Prog., Oxf.* **73** 213 (1989).
- [28] B. GILLON. La technique classique du rapport de flipping. Application aux aimants moléculaires et aux aimants photo-commutables. *In* Neutrons Polarisés, edited by N. KERNAVANOIS, E. RESSOUCHE, H. SCHOBER AND J. L. SOUBEYROUX, p. 13 (EDP Sciences, 2007).
- [29] M. J. COOPER, P. E. MIJNARENDS, N. SHIOTANI, N. SAKAI AND A. BANSIL, eds. X-ray Compton Scattering (Oxford University Press, 2004).
- [30] N. SAKAI. Magnetic Compton Scattering and Measurements of Momentum Distribution of Magnetic Electrons. *J. Appl. Cryst.* **29** 81 (1996).
- [31] P. PATTISON AND B. WILLIAMS. Fermi surface parameters from the Fourier analysis of Compton profiles. *Solid State Commun.* **20** 585 (1976).
- [32] P. PATTISON, W. WEYRICH AND B. WILLIAMS. Observation of ionic deformation and bonding from compton profiles. *Solid State Commun.* **21** 967 (1977).

- [33] R. SUZUKI, M. OSAWA, S. TANIGAWA, M. MATSUMOTO AND N. SHIOTANI. Positron Study of Electron Momentum Density and Fermi Surface in Titanium and Zirconium. *Journal of the Physical Society of Japan* **58** 3251 (1989).
- [34] Y. TANAKA, Y. SAKURAI, A. T. STEWART, N. SHIOTANI, P. E. MIJNARENDS, S. KAPRZYK AND A. BANSIL. Reconstructed three-dimensional electron momentum density in lithium: A Compton scattering study. *Phys. Rev. B* **63** 045120 (2001).
- [35] P. M. PLATZMAN AND N. TSOAR. Magnetic Scattering of X Rays from Electrons in Molecules and Solids. *Phys. Rev. B* **2** 3556 (1970).
- [36] A. KOIZUMI, S. MIYAKI, Y. KAKUTANI, H. KOIZUMI, N. HIRAOKA, K. MAKOSHI, N. SAKAI, K. HIROTA AND Y. MURAKAMI. Study of the e_g Orbitals in the Bilayer Manganite $\text{La}_{2-2x}\text{Sr}_{1+2x}\text{Mn}_2\text{O}_7$ by Using Magnetic Compton-Profile Measurement. *Phys. Rev. Lett.* **86** 5589 (2001).
- [37] T. INUI, Y. TANABE AND Y. ONODERA. Group Theory and Its Applications in Physics (Springer-Verlag, 1990).
- [38] R. BALLOU AND B. OULADDIAF. Representation Analysis of Magnetic Structures. *In Neutron Scattering from Magnetic Materials*, edited by T. CHATTERJI (Elsevier, 2006).
- [39] T. HAHN, ed. International Tables for Crystallography, Volume A: Space Group Symmetry (D. Reidel Publishing Company, 1983).
- [40] E. F. BERTAUT. Lattice Theory of Spin Configuration. *J. Appl. Phys. Suppl.* **33** 1138 (1962).
- [41] L. V. AZAROFF. Elements of X-ray Crystallography (McGraw-Hill, 1968).
- [42] C. G. DARWIN. The Theory of X-ray Reflection. *Phil. Mag.* **27** 315 (1914).
- [43] C. G. DARWIN. The Theory of X-ray Reflection. Part II. *Phil. Mag.* **27** 675 (1914).
- [44] P. P. EWALD. Zur Begründung der Kristalloptik. I. Dispersionstheorie. *Ann. Physik* **49** 1 (1916).
- [45] P. P. EWALD. Zur Begründung der Kristalloptik. II. Theorie der Reflexion und Brechung. *Ann. Physik* **49** 117 (1916).
- [46] P. P. EWALD. Zur Begründung der Kristalloptik. III. Die Kristalloptik der Röntgenstrahlen. *Ann. Physik* **54** 519 (1917).

-
- [47] M. VON LAUE. Die dynamische Theorie der Röntgenstrahlinterferenzen in neuer Form. *Ergeb. Exakt. Naturw.* **10** 133 (1931).
- [48] W. H. ZACHARIASEN. A General Theory of X-Ray Diffraction in Crystals. *Acta Crystallogr.* **23** 558 (1967).
- [49] J. C. MATTHEWMAN, P. THOMPSON AND P. J. BROWN. The Cambridge Crystallographic Subroutine Library. *J. Appl. Cryst.* **15** 167 (1982).
- [50] J. RODRÍGUEZ-CARVAJAL. Recent advances in magnetic structure determination by neutron powder diffraction. *Physica B* **192** 55 (1993).
- [51] P. J. BECKER AND P. COPPENS. Extinction within the Limit of Validity of the Darwin Transfer Equations. I. General Formalisms for Primary and Secondary Extinction and Their Application to Spherical Crystals. *Acta Crystallogr., Sect. A: Found. Crystallogr.* **30** 129 (1974).
- [52] P. J. BECKER AND P. COPPENS. Extinction within the Limit of Validity of the Darwin Transfer Equations. II. Refinement of Extinction in Spherical Crystals of SrFz and LiF. *Acta Crystallogr., Sect. A: Found. Crystallogr.* **30** 148 (1974).
- [53] P. J. BECKER AND P. COPPENS. Extinction within the Limit of Validity of the Darwin Transfer Equations. III. Non-Spherical Crystals and Anisotropy of Extinction. *Acta Crystallogr., Sect. A: Found. Crystallogr.* **31** 417 (1975).
- [54] M. BONNET, A. DELAPALME, P. BECKER AND H. FUESS. Polarized Neutron Diffraction - A Tool for Testing Extinction Models: Application to Yttrium Iron Garnet. *Acta Crystallogr., Sect. A: Found. Crystallogr.* **32** 946 (1976).
- [55] R. M. MOON, W. C. KOEHLER, J. W. CABLE AND H. R. CHILD. Distribution of Magnetic Moment in Metallic Gadolinium. *Phys. Rev. B* **5** 997 (1972).
- [56] G. M. SHELDRICK. A short history of *SHELX*. *Acta Crystallogr., Sect. A: Found. Crystallogr.* **64** 112 (2008).
- [57] A. C. LARSON. Extinction corrections. In *Crystallographic Computing*, edited by F. R. AHMED, S. R. HALL AND C. P. HUBER, pp. 291–294 (Copenhagen, Munksgaard, 1970).
- [58] J. C. SLATER. Atomic Shielding Constants. *Phys. Rev.* **36** 57 (1930).
- [59] S. F. BOYS. Electronic Wave Functions. I. A General Method of Calculation for the Stationary States of Any Molecular System. *Proc. R. Soc. London Ser. A* **200** 542 (1950).

- [60] J. S. BINKLEY, J. A. POPLE AND W. J. HEHRE. Self-Consistent Molecular Orbital Methods. 21. Small Split-Valence Basis Sets for First-row Elements. *J. Am. Chem. Soc.* **102** 939 (1980).
- [61] M. GORDON, J. S. BINKLEY, J. A. POPLE, W. J. PIETRO AND W. J. HEHRE. Self-Consistent Molecular Orbital Methods. 22. Small Split-Valence Basis Sets for Second-Row elements. *J. Am. Chem. Soc.* **104** 2797 (1982).
- [62] K. D. DOBBS AND W. J. HEHRE. Molecular orbital theory of the properties of inorganic and organometallic compounds 4. Extended basis sets for third-and fourth-row, main-group elements. *J. Comput. Chem.* **7** 359 (1986).
- [63] K. D. DOBBS AND W. J. HEHRE. Molecular orbital theory of the properties of inorganic and organometallic compounds 5. Extended basis sets for first-row transition metals. *J. Comput. Chem.* **8** 861 (1987).
- [64] K. D. DOBBS AND W. J. HEHRE. Molecular orbital theory of the properties of inorganic and organometallic compounds. 6. Extended basis sets for second-row transition metals. *J. Comput. Chem.* **8** 880 (1987).
- [65] A. SCHÄFER, C. HUBER AND R. AHLRICH. Fully optimized contracted Gaussian basis sets of triple zeta valence quality for atoms Li to Kr. *J. Chem. Phys.* **100** 5829 (1994).
- [66] M. W. SCHMIDT, K. K. BALDRIDGE, J. A. BOATZ, S. T. ELBERT, M. S. GORDON, J. H. JENSEN, S. KOSEKI, N. MATSUNAGA, K.A.NGUYEN, S. J. SU, T. L. WINDUS, M. DUPUIS AND J. A. MONTGOMERY. General Atomic and Molecular Electronic Structure System. *J. Comput. Chem.* **14** 1347 (1993).
- [67] M. S. GORDON AND M. W. SCHMIDT. Advances in electronic structure theory: GAMESS a decade later. *In* Theory and Applications of Computational Chemistry, the first forty years, edited by C. E. DYKSTRA, G. FRENKING, K. S. KIM AND G. E. SCUSERIA, p. 1167 (Elsevier, Amsterdam, 2005).
- [68] A. V. NEMUKHIN, B. L. GRIGORENKO AND A. A. GRANOVSKY. Molecular modeling by using the PC GAMESS program: From diatomic molecules to enzymes. *Moscow Univ. Chem. Bull.* **45** 75 (2004).
- [69] A. D. BECKE. Density-functional thermochemistry. III. The role of exact exchange. *J. Chem. Phys.* **98** 5648 (1993).
- [70] C. LEE, W. YANG AND R. G. PARR. Development of the Colle-Salvetti correlation-energy formula into a functional of the electron density. *Phys. Rev. B* **37** 785 (1988).

-
- [71] B. MIEHLICH, A. SAVIN, H. STOLL AND H. PREUSS. Results obtained with the correlation energy density functionals of Becke and Lee, Yang and Parr. *Chem. Phys. Lett.* **157** 200 (1989).
- [72] P. J. STEPHENS, F. J. DEVLIN, C. F. CHABALOWSKI AND M. J. FRISCH. Ab Initio Calculation of Vibrational Absorption and Circular Dichroism Spectra Using Density Functional Force Fields. *J. Phys. Chem.* **98** 11623 (1994).
- [73] A. SCHÄFER, H. HORN AND R. AHLRICHS. Fully optimized contracted Gaussian basis sets for atoms Li to Kr. *J. Chem. Phys.* **97** 2571 (1992).
- [74] M. S. GORDON, M. A. FREITAG, P. BANDYOPADHYAY, J. H. JENSEN, V. KAIRYS AND W. J. STEVENS. The Effective Fragment Potential Method: a QM-based MM approach to modeling environmental effects in chemistry. *J. Phys. Chem. A* **105** 293 (2001).
- [75] E. RADZHAVOV AND M. KIRM. Triplet luminescence of cadmium centres in alkaline-earth fluoride crystals. *J. Phys.: Condens. Matter* **17** 5821 (2005).
- [76] J. L. PASCUAL, J. SCHAMPS, Z. BARANDIARÁN AND L. SEIJO. Large anomalies due to insufficiency of Madelung embedding in *ab initio* calculations of 4f-5d and 4f-6s excitations of lanthanides in ionic crystals: The BaF₂:Ce³⁺ crystal. *Phys. Rev. B* **74** 104105 (2006).
- [77] Z. BARANDIARÁN AND L. SEIJO. The *ab initio* model potential representation of the crystalline environment. Theoretical study of the local distortion on NaCl:Cu⁺. *J. Chem. Phys.* **89** 5739 (1988).
- [78] J. L. PASCUAL, L. SEIJO AND Z. BARANDIARÁN. *Ab initio* model potential study of environmental effects on the Jahn-Teller parameters of Cu²⁺ and Ag²⁺ impurities in MgO, CaO, and SrO hosts. *J. Chem. Phys.* **98** 9715 (1993).
- [79] W. J. STEVENS AND M. KRAUSS. Relativistic compact effective potentials and efficient, shared-exponent basis sets for the third-, fourth-, and fifth-row atoms. *Can. J. Chem.* **70** 612 (1992).
- [80] WOLFRAM RESEARCH, INC. Mathematica Edition: Version 5.0 (Wolfram Research, Inc., 2003).
- [81] M. ZBIRI, N. QURESHI, M. R. JOHNSON, H. FUESS AND H. EHRENBERG. to be published (2008).
- [82] F. BIGGS, L. B. MENDELSON AND J. B. MANN. Hartree Fock Compton profiles for the elements. *At. Data Nucl. Data Tables* **16** 201 (1975).

- [83] E. ŻUKOWSKI. The processing of experimental data. *In* X-ray Compton Scattering, edited by M. J. COOPER, P. E. MIJNARENDS, N. SHIOTANI, N. SAKAI AND A. BANSIL, p. 133 (Oxford University Press, 2004).
- [84] E. J. LISHER AND J. B. FORSYTH. Analytical approximations to form factors. *Acta Crystallogr., Sect. A: Found. Crystallogr.* **27** 545 (1971).
- [85] W. J. HEHRE, R. DITCHFIELD AND J. A. POPLE. Self-Consistent Molecular Orbital Methods. XII. Further Extensions of Gaussian-Type Basis Sets for Use in Molecular Orbital Studies of Organic Molecules. *J. Chem. Phys.* **56** 2257 (1972).
- [86] V. RASSOLOV, J. A. POPLE, M. RATNER AND T. L. WINDUS. 6-31G* basis set for atoms K through Zn. *J. Chem. Phys.* **109** 1223 (1998).
- [87] W. J. STEVENS, H. BASCH AND M. KRAUSS. Compact effective potentials and efficient shared-exponent basis sets for the first- and second-row atoms. *J. Chem. Phys.* **81** 6026 (1984).
- [88] P. FUENTEALBA, L. V. SZENTPALY, H. PREUSS AND H. STOLL. Pseudopotential calculations for alkaline-earth atoms. *J. Phys. B* **18** 1287 (1985).
- [89] G. IGEL-MANN, H. STOLL AND H. PREUSS. Pseudopotentials for main group elements (IIIa through VIIa). *Mol. Phys.* **65** 1321 (1988).
- [90] P. L. WANG, P. E. WERNER AND A. G. NORD. Cation distribution studies of Mg, Co and Ni orthovanadate solid solutions. *Z. Kristallogr.* **198** 271 (1992).
- [91] J. C. LASHLEY, M. F. HUNDLEY, A. MIGLIORI, J. L. SARRAO, P. G. PAGLIUSO, T. W. DARLING, M. JAIME, J. C. COOLEY, W. L. HULTS, L. MORALES, D. J. THOMA, J. L. SMITH, J. BOERIO-GOATES, B. F. WOODFIELD, G. R. STEWART, R. A. FISHER AND N. E. PHILLIPS. Critical examination of heat capacity measurements made on a Quantum Design physical property measurement system. *Cryogenics* **43** 369 (2003).
- [92] H. V. LÖHNEYSSEN, M. SIECK, O. STOCKERT AND M. WAFFENSCHMIDT. Investigation of non-Fermi-liquid behavior in CeCu_{6-x}Au_x. *Physica B* **223&224** 471 (1996).
- [93] I. DZYALOSHINSKI. A thermodynamic theory of "weak" ferromagnetism of antiferromagnetics. *J. Phys. Chem. Solids* **4** 241 (1958).
- [94] T. MORIYA. Anisotropic Superexchange Interaction and Weak Ferromagnetism. *Phys. Rev.* **120** 91 (1960).

- [95] M. J. FREISER. Thermal Variation of the Pitch of Helical Spin Configurations. *Phys. Rev.* **123** 2003 (1961).
- [96] W. MARSHALL AND R. STUART. Theory of Transition Ion Complexes. *Phys. Rev.* **123** 2048 (1961).
- [97] V. C. RAKHEECHA AND N. S. SATYA MURTHY. Spin-transfer due to covalency for the tetrahedral-site Fe^{3+} ions in Fe_3O_4 . *J. Phys. C: Solid State Phys.* **11** 4389 (1978).

Lebenslauf

Persönliche Daten

Name	Qureshi
Vorname	Navid
Nationalität	französisch
Geburtsdatum	25. März 1981
Geburtsort	Rüsselsheim
Familienstand	ledig

Schulausbildung

1987 - 1991	Grundschule, Pestalozzischule Raunheim
1991 - 2000	Gymnasium, Max-Planck-Schule Rüsselsheim

Hochschulausbildung

2000 - 2005	Studium der Materialwissenschaften an der Technischen Universität Darmstadt
-------------	---

Praktische Tätigkeiten

08/2004 - 11/2004	Betriebs- und Vertiefungspraktikum am Institut Laue-Langevin in Grenoble
-------------------	--

Publikationen

N. Qureshi, H. Fuess, H. Ehrenberg, T. C. Hansen, C. Ritter, K. Prokes, A. Podlesnyak and D. Schwabe.

Magnetic properties of the Kagomé mixed compounds $(\text{Co}_x\text{Ni}_{1-x})_3\text{V}_2\text{O}_8$.
Phys. Rev. B **74** 212407 (2006).

N. Qureshi, H. Fuess, H. Ehrenberg, T. C. Hansen and D. Schwabe.

Magnetic phase transitions and structures of $\text{Co}_3\text{V}_2\text{O}_8$.
Solid State Commun. **142** 169 (2007).

N. Qureshi, H. Fuess, H. Ehrenberg, T. C. Hansen, C. Ritter, P. Adelman, C. Meingast, T. Wolf, Q. Zhang and W. Knafo.

The magnetic composition-temperature phase diagram of the kagome mixed system $(\text{Co}_x\text{Ni}_{1-x})_3\text{V}_2\text{O}_8$.
J. Phys.: Condens. Matter **20** 095219 (2008).

N. Qureshi, H. Fuess, H. Ehrenberg, T. C. Hansen, C. Ritter, T. Wolf, C. Meingast, Q. Zhang, W. Knafo and H. von Löhneysen.

Magnetic structure of the kagome mixed compound $(\text{Co}_{0.5}\text{Ni}_{0.5})_3\text{V}_2\text{O}_8$.
J. Phys.: Condens. Matter **20** 235228 (2008).

N. Qureshi, M. Zbiri, J. Rodríguez-Carvajal, A. Stunault, E. Ressouche, T. C. Hansen, M. T. Fernández-Díaz, M. R. Johnson, H. Fuess, H. Ehrenberg, Y. Sakurai, M. Itou, B. Gillon, Th. Wolf, J. A. Rodríguez-Velamazán, J. Sánchez-Montero.

Experimental magnetic form factors in $\text{Co}_3\text{V}_2\text{O}_8$: A combined study of *ab initio* calculations, magnetic Compton scattering, and polarized neutron diffraction.
Phys. Rev. B **79** 094417 (2009).

Navid Qureshi
Klopstockstraße 20
65479 Raunheim

Eidesstattliche Erklärung

Ich erkläre hiermit an Eides Statt, dass ich meine Dissertation selbständig und nur mit den angegebenen Hilfsmitteln angefertigt habe.

Navid Qureshi

Erklärung

Ich erkläre hiermit, noch keinen Promotionsversuch unternommen zu haben.

Navid Qureshi